LBL-16176
c.2

Lawrence Berkeley Laboratory

UNIVERSITY OF CALIFORNIA

RECEIVED
NOV 2 6 1983
LBL LIBRARY

Materials & Molecular Research Division

MASS TRANSFER AT GAS EVOLVING SURFACES IN ELECTROLYSIS

D.W. Dees* and C.W. Tobias
(*Ph.D. Thesis)

September 1983

TWO-WEEK LOAN COPY
This is a Library Circulating Copy which may be borrowed for two weeks. For a personal retention copy, call Tech. Info. Division, Ext. 6782.

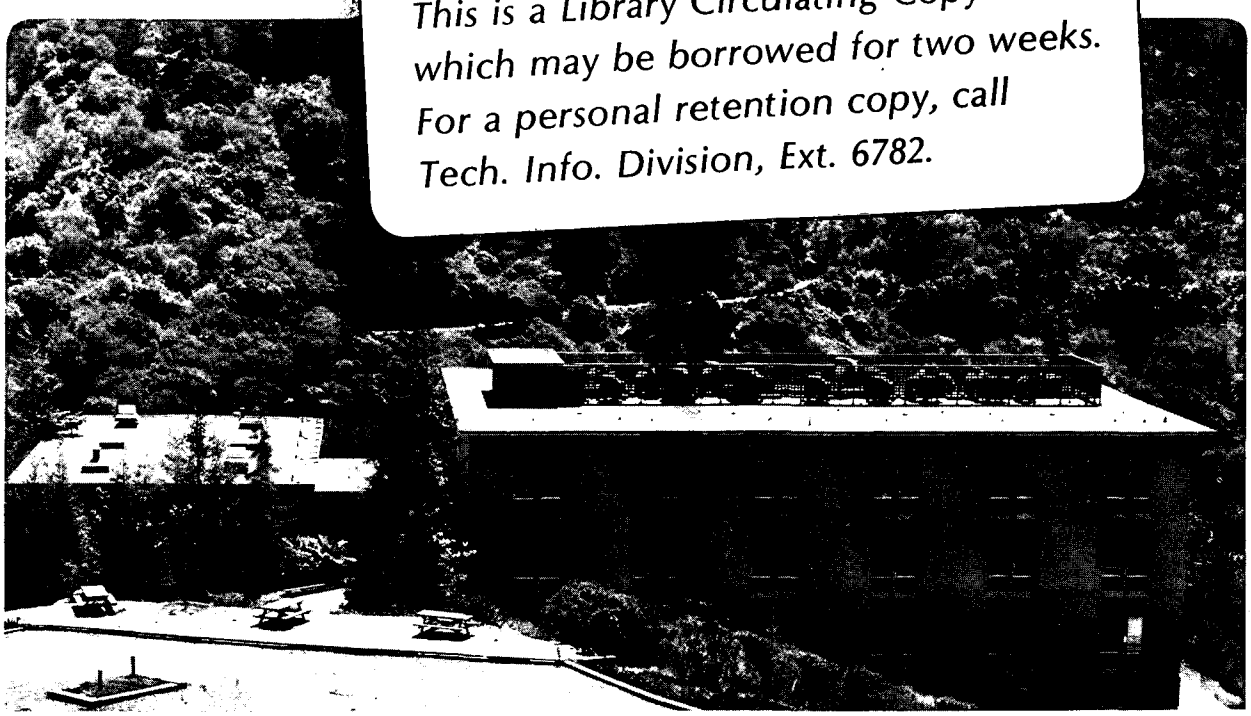

LBL-16176
c.2

Prepared for the U.S. Department of Energy under Contract DE-AC03-76SF00098

DISCLAIMER

This document was prepared as an account of work sponsored by the United States Government. While this document is believed to contain correct information, neither the United States Government nor any agency thereof, nor the Regents of the University of California, nor any of their employees, makes any warranty, express or implied, or assumes any legal responsibility for the accuracy, completeness, or usefulness of any information, apparatus, product, or process disclosed, or represents that its use would not infringe privately owned rights. Reference herein to any specific commercial product, process, or service by its trade name, trademark, manufacturer, or otherwise, does not necessarily constitute or imply its endorsement, recommendation, or favoring by the United States Government or any agency thereof, or the Regents of the University of California. The views and opinions of authors expressed herein do not necessarily state or reflect those of the United States Government or any agency thereof or the Regents of the University of California.

LBL-16176

MASS TRANSFER AT GAS EVOLVING SURFACES IN ELECTROLYSIS

Dennis W. Dees

(Ph.D. Thesis)

with

Charles W. Tobias

Materials and Molecular Research Division
Lawrence Berkeley Laboratory
and Department of Chemical Engineering
University of California
Berkeley, CA 94720

This work was supported by the Assistant Secretary of Conservation and Renewable Energy, Office of Energy Systems Research, Energy Storage Division of U. S. Department of Energy under Contract DE-AC03-76SF00098

TABLE OF CONTENTS

	Page
ABSTRACT	vii
DEDICATION	ix
ACKNOWLEDGEMENTS	xi
1. INTRODUCTION	1
1.1 Purpose of the Study	1
1.2 Practical Applications	1
1.3 Gas Evolution, A Qualitative Description	3
1.4 Literature Review of Mass Transfer at Gas-Evolving Surfaces	7
1.5 Scope of Study	15
1.6 Limiting Current Technique on Segmented Electrodes	16
1.7 Nomenclature	19
2. EXPERIMENTAL	21
2.1 Method	21
2.2 Mass-Transfer Studies with Multi-Electrode Cell	25
2.2.1 Electrochemical Cell	25
2.2.2 Instrumentation	25
2.2.3 Results and Discussion	31
2.3 Initial Mass-Transfer Studies with Micro-Mosaic Electrode	34
2.3.1 Description of Micro-Mosaic Electrode	34
2.3.2 Description of Micro-Mosaic Electrode Cells	37
2.3.3 Instrumentation	45
2.3.4 Results and Discussion	49

Page

2.4 Mass-Transfer Studies with the Micro-Mosaic Electrode Coupled to a Data Acquisition and Control System 57

2.4.1 Description of Data Acquisition and Control System 57

2.4.2 Results and Discussion 69

Free-Convection Studies. 70

Limiting Current Studies During Bubble Growth. . 81

Limiting Current Studies After Ceasing Bubble Growth 88

General Comments on Bubble Disengagement and Coalescence Studies. 92

Bubble Disengagement Studies 93

Simultaneous Bubble Coalescence and Disengagement Studies. 109

2.5 Stability of Micro-Mosaic Electrodes. 122

2.6 Mass-Transfer Studies with a Replica of the Micro-Mosaic Electrode. 132

2.6.1 Description of the Replica of the Micro-Mosaic Electrode 132

2.6.2 Method and Instrumentation 135

2.6.3 Results and Discussion 137

2.7 Nomenclature. 145

Page

3. THEORETICAL CONSIDERATIONS 146

3.1 Relevant Transport Equations. 146

Nomenclature. 150

3.2 Equilibrium Shape of a Bubble Attached to a Horizontal Surface. 152

Nomenclature. 160

3.3 Mass Transport to a Horizontal Surface Near an Ascending Fluid Sphere. 161

Nomenclature. 178

3.4 Mass Transport in a Wedge 181

Nomenclature. 195

3.5 Transport Equations for Free Convection Mass Transfer to a Horizontal Surface 197

Nomenclature. 206

4. CONCLUSIONS. 208

4.1 General Remarks 208

4.2 Effect of Macroconvection on Bubble Phenomena 210

4.3 Effect of Size on the Disengagement of a Bubble 212

4.4 Effect of Size on the Coalescence of Two Bubbles. . . . 213

4.5 Concluding Remarks. 214

Nomenclature 215

Page

APPENDIX A 216

APPENDIX B 220

APPENDIX C 225

APPENDIX D 233

APPENDIX E 241

APPENDIX F 248

APPENDIX G 273

APPENDIX H 276

APPENDIX I 288

REFERENCES 293

MASS TRANSFER AT GAS EVOLVING SURFACES IN ELECTROLYSIS

Dennis Wayne Dees

Materials and Molecular Research Division
Lawrence Berkeley Laboratory
and Department of Chemical Engineering
University of California
Berkeley, CA 94720

ABSTRACT

A novel micro-mosaic electrode was developed to resolve time-dependent, mass-transfer distribution in the close vicinity of bubble phenomena. The electrode, prepared on a silicon wafer using integrated circuit manufacturing technology, consists of a 10 by 10 matrix of coplanar, electrically isolated, square platinum segments on 100 micron centers, surrounded by a relatively large buffer segment. A computer actuated data acquisition and control system was assembled and the software developed to monitor the current to each of the segments and control the potential of selected segments.

The utility of the electrode to examine interfacial mass transport phenomena which have characteristic lengths as small as 100 microns has been clearly demonstrated. The effect of a single hydrogen bubble

disengagement and of the coalescence of two bubbles, on the limiting current of the reduction of ferric to ferrous ion was measured using the micro-mosaic electrode in a horizontal: facing-up orientation. In the absence of gas evolution, large regular fluctuations in the limiting current to the segments with a period of 29 seconds were observed. This periodic behavior is attributed to free convection: a cellular fluid motion moving across the electrode with a velocity of 40 microns/second. It was found that the mass-transfer enhancement due to bubble disengagement is small when compared to that due to coalescence. Increases in the mass-transfer rate of more than an order of magnitude over the free convection limiting current were observed for the coalescence phenomena.

Two theoretical models were developed to account for the observed effect of a bubble disengagement on the mass transfer-rate to the surface. Numerical solutions of the convective diffusion equation were obtained for the flow generated by an ascending fluid sphere near a horizontal surface and for the flow in the wedge formed by the electrode and the bubble in the region near the collapse of the bubble contact area. The models correctly predict the observed direction of the initial change in the limiting current beneath a separating and ascending bubble.

DEDICATION

This thesis is dedicated to my parents:

David and Joann

ACKNOWLEDGEMENTS

First and foremost I wish to thank Professor Charles W. Tobias for providing me with a superior electrochemical research environment to work in and also for giving me the appropriate amount of support and guidance.

I want to express my gratitude to the Hewlett Packard Company for making their personnel and facilities available for the fabrication of the micro-mosaic electrodes. I want to especially thank Pat Castro for committing the resources of the Hewlett Packard Company to build the electrodes when the project was little more than an idea. Harold Levie took a genuine interest in the project and his work on the design of the micro-mosaic electrode proved invaluable to the success of the project. Also the work of David Liu who followed through with the fabrication of the devices and Greg Peterschmidt who assisted me in the digitizing of the mask patterns is greatly appreciated.

I will always be indebted to Larry Galovich for his work on the design and construction of the electrochemical cells which he built for me. He is truly a man of many talents whom I am proud to call a friend.

Many thanks are due to Professor Radke and Professor Greif for reviewing this manuscript. Thanks are also due to Gina Whitney who has had to bear the brunt of my writing.

In my 21 years of school I have had a large number of teachers and have sat through hundreds of hours of lectures, but a small number of instructors have had a particularly strong influence on me along this path that I have chosen. These are Michael Moore, Paul Harris, Sam Porter, Alan Morgan, Professor Richard Alkire, and Professor John Newman.

There have been many friends and acquaintances of mine who have been a joy for me to know and work with in my years at Berkeley. Although they are too numerous to mention individually, I would like to acknowledge the people in the Tobias-Muller and Newman research groups and the congregation of the Trinity United Methodist Church. Some people who have been very special to me are Corinne Coughanowr, Tom and Joni Buttke, Ellen Pawlikowski, Andrew Kindler, and John Dukovic. I also want to remember Mike Matlosz who has been a good friend since the "late 50's." I consider it a privilege to have been able to play basketball on the Chemwipes intramural team and with a great group of people on Saturday mornings.

This work was supported by the Assistant Secretary of Conservation and Renewable Energy, Office of Energy Systems Research, Energy Storage Division of U. S. Department of Energy under Contract DE-AC03-76SF00098.

1. INTRODUCTION

1.1 Purpose of the Study

As with all processes occuring at gas-evolving surfaces, the mass transfer is quite complicated and little understood. While the enhancement of the average rate of mass transfer at gas-evolving surfaces has been extensively studied (9-26), virtually nothing is known about the relative contribution of the various individual bubble phenomena.

It is the purpose of this investigation to obtain quantitative measurements of the effect of individual bubble phenomena on the rate of mass transfer. A novel micro-mosaic electrode was conceived for the study and was built by Hewlett Packard Company. The unique properties of the electrode permitted individual bubble phenomena to be controlled and their effect on the rate of mass transfer monitored.

1.2 Practical Applications

Gas evolution is one of the most common types of electrosynthesis reactions; a gas is evolved in many industrially important electrochemical processes. The importance of gas-evolving electrodes to industry was a major impetus in performing this study. Although a complete listing of all the industrial processes is beyond the scope of this survey, some of the more significant processes will be noted. Extensive reviews of the various processes can be found in recent literature (1,2).

Of the many industrial processes involving the evolution of a gas, the production of chlorine is the best known. Sales of chlorine in the U. S. are expected to reach 1.25 billion dollars in 1983 (3). Chlorine is almost exclusively produced by the electrolysis of aqueous solutions of NaCl, KCl, or HCl.

High purity hydrogen is produced by the electrolysis of water. The electrochemical production of hydrogen is limited to regions where power is relatively inexpensive, but it does account for a significant portion of the hydrogen produced. Commercial electrolyzers capable of generating 40,000 m^3 of hydrogen per hour are in operation.

Gas evolution generally occurs at the counter electrode in the electrowinning of metals. The generation of oxygen is the most frequent anodic reaction in aqueous systems, while in molten salt systems the production of chlorine or carbon dioxide may alternatively be the main reaction. The production of aluminum is almost exclusively done electrochemically.

Certain advanced rechargeable battery systems employ electrode reactions that involve gas evolution on charging (4). Among these the H_2/NiO(OH) and Zn/Cl_2 batteries are the most significant. In some batteries a gas is evolved as an unwanted side reaction, such as the Ni-Zn and Pb-acid batteries.

Electrochemically generated gas bubble streams are used in flotation processes, because of the characteristically small bubble size available by the method.

This is only a small sample of the industrially important electrochemical systems in which gases are evolved. New processes are continually being added to this list. The production of hydrogen in photo-voltaic electrochemical cells is one such example.

1.3 Gas Evolution, A Qualitative Description

An understanding of the mass-transfer enhancement effect at gas-evolving electrodes should be based on knowledge of the bubble dynamics at the electrode. The bubble dynamics are obscured by the small size of the bubbles (10-100 μm) and their density near the electrode. The rate at which bubble phenomena occur further complicates the situation. Bubble behavior can be observed through an optical microscope using a high speed movie camera (5). Then by correlating the observations of gas-evolving electrodes with physical parameters, such as gas evolution rate, fluid flow rate (6), electrode substrate, and electrolyte composition (7), a description of the bubble layer can be developed.

Before describing gas evolution in the steady-state, it will be instructive to examine the process during the initiation of electrolysis. This is done by polarizing an inert electrode into a voltage range where gas molecules are generated at the electrode as a result of an electrochemical reaction. The molecules diffuse into the electrolyte and a supersaturated layer next to the electrode quickly develops as a result of the relatively low solubility of the gas in the electrolyte. Gas bubbles are nucleated on the electrode and grow through diffusion. As an example the concentration profile of dissolved hydrogen near a cathode before and after the nucleation of

bubbles is shown in Figures 1.3.1 and 1.3.2 respectively. They eventually reach a size where they touch other neighboring bubbles and coalescence starts to occur. The bubbles continue to grow by diffusion and coalescence until the hydraulic and buoyancy forces exceed surface tension forces. They then disengage from the surface and rise. At current densities of about 500 mA/cm^2, it takes less than a second for a steady-state to be achieved (7).

The phenomena occuring during the steady-state evolution of gas include all of those in the transient period. The process is further complicated by the bubbles rising in the bulk electrolyte. Bubbles in the bulk coalesce with bubbles on the surface, and also with other bubbles in the bulk, as they rise along vertical electrodes. Because of the cell geometry, bubbles in the bulk do not coalesce with bubbles on the surface on horizontal electrodes, but in both cases the rising bubbles in the bulk do generate a flow of electrolyte. The rising bubbles drag fluid with them, which generates a circulating flow. This flow can have a profound effect on the bubble dynamics both in the bulk and on the surface.

All observable quantities such as characteristic bubble size and shape in the bulk and on the surface, rate of coalescence, and gas hold-up at the electrode are influenced by physical forces. One of the strongest and most obvious is the effect of buoyancy on each bubble. Surface tension effects are just as important and are generally much more system dependent; they are strongly affected by electrolyte composition, the presence of surfactants, electrode substrate, and polarization. Drag forces on the bubbles from the flow

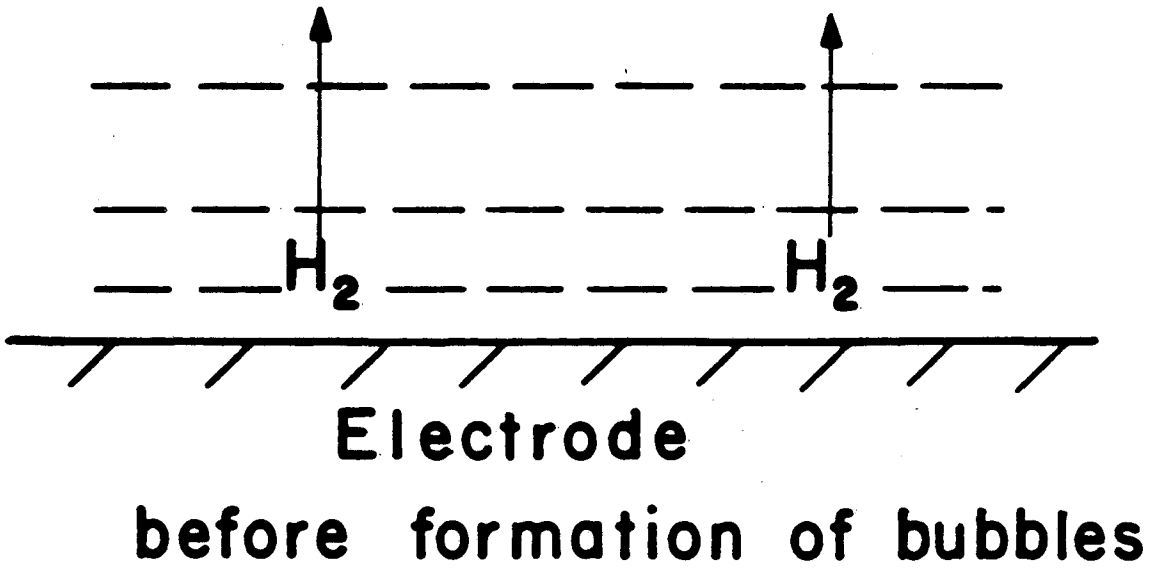

XBL 704-882

Figure 1.3.1 Hydrogen concentration distribution before the formation of bubbles.

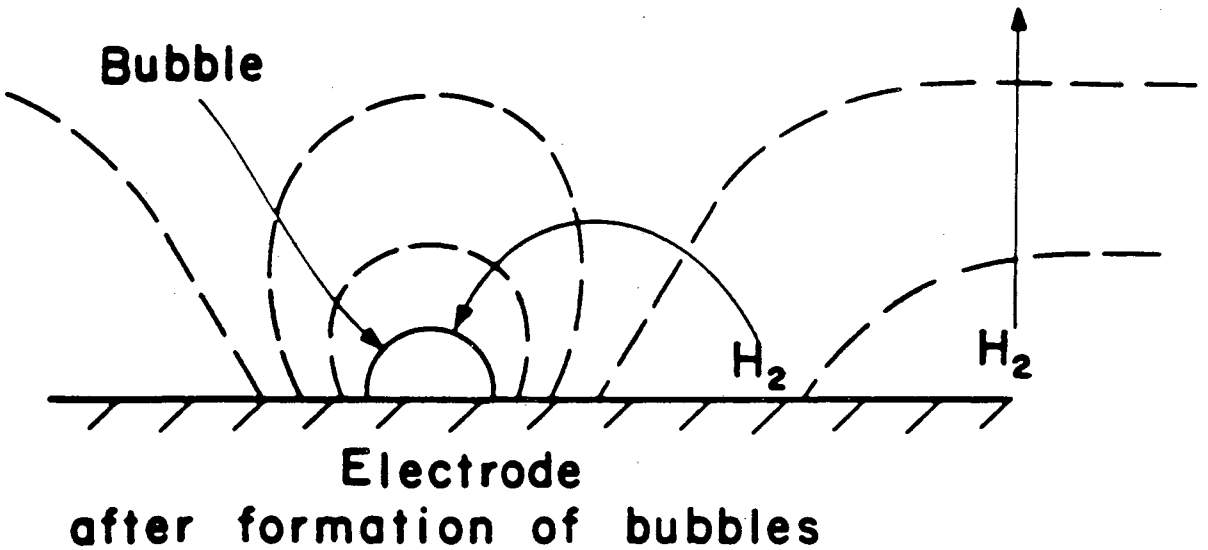

XBL 704-881

Figure 1.3.2 Hydrogen concentration distribution after the formation of bubbles.

of electrolyte are significant in many situations. The fluid flow due to gas evolution is generally broken down into two types; microscopic flows, which are generated by individual bubble phenomena and occur within a few bubble diameters of the phenomenon, and macroscopic flows which are a result of the rising swarm of bubbles. There is also the possibility of having an externally driven flow, as in a forced convection flow cell. These flows generally are not independent and do not linearly combine. The manner in which all these forces interact to determine the behavior of the gas evolving electrode is not well understood and impossible to predict with any accuracy.

The vehicle of the mass-transfer enhancement at gas-evolving electrodes is the fluid flow generated at the electrode. This flow serves to "mix" the electrolyte and thereby increases the mass transfer rate at the electrode. The enhancement effect can be compared to that of mass transfer in forced convection. The mass transfer rate to an inert electrode where hydrogen is evolved at 1.0 A/cm^2 is equivalent to the mass-transfer rate in a 2 cm gap flow channel with a Reynold's number of 100,000 or a rotating disk spinning at 8,000 rpm (35). It is evident that gas evolution provides an extremely effective stirring mechanism.

1.4 Literature Review of Mass Transfer at Gas-Evolving Surfaces

The mass-transfer enhancement at gas-evolving electrodes was recognized as early as 1924 by Foerster (8). Ibl (9) was one of the first investigators to attempt to quantify this effect in 1963. It has been the subject of a great deal of research since about 1970.

There are certain similarities between nearly all the mass-transfer studies performed on gas evolving electrodes. An indicator ion is added to a well-supported electrolyte. The electrode is then polarized into a voltage range where a gas is evolved and the indicator ion is discharged under mass transfer limited conditions (i.e., at limiting current). The rate of reaction of the indicator ion is determined as a function of gas evolution rate, under different experimental conditions.

The mass-transfer rate (N) is usually correlated in the form of a mass transfer coefficient (k) or a Nernst boundary layer thickness (δ),

$$N = k\ (C_B - C_I) = D\ \frac{(C_B - C_I)}{\delta} \qquad (1.4.1)$$

$$k = D/\delta \qquad (1.4.2)$$

where C_B and C_I are the bulk and interface concentrations of the indicator ion, and D is its diffusion coefficient. The use of a dimensionless Sherwood number (L/δ) is also employed. The gas evolution rate is generally presented as a current density (i) or a volumetric flux (v):

$$v = \frac{M_W}{\rho}\ \frac{i}{nF} \qquad (1.4.3)$$

where M_W and ρ is the molecular weight and density of the gas being evolved. The number of electrons being transferred in the production of the gas is given by n and F is Faradays constant. Since volumetric flux has the same dimensions as velocity, the Reynolds number (vL/ν) is sometimes used to correlate the gas evolution rate.

Since the gas-evolving reaction and the indicator-ion reaction occur together, the total reaction rate of one must be determined. This could be done by measuring the total volume of gas produced, but that tends to be inaccurate. The most popular method is to use one component of a redox couple for the indicator ion and measure the change in concentration of one ion after electrolyzing for a set time. Care must be taken to avoid too large a concentration change as well as the possibility of the reverse reaction occuring at the counter electrode. Both methods suffer from not being able to determine the area over which the redox reaction occurs. Ibl et al. (10) used the ferric-ferrous ion pair (Fe^{+3}/Fe^{+2}) for studying hydrogen evolution. Janssen and Hoogland originally employed the cerric-cerrous couple (Ce^{+4}/Ce^{+3}) (11) to study hydrogen, oxygen, and chlorine evolution, and later switched to the ferricynanide-ferrocynanide couple ($Fe(CN)_6^{-3}/Fe(CN)_6^{-4}$) (12) for oxygen evolution. Alternative methods include the use of radioactive indicator ions that are deposited. The amount of deposit is determined by a Geiger counter. $^{203}Hg^{+2}$ was employed by Rousar et al. (13) to study hydrogen evolution. Alkire and Lu (14) measured the amount of copper deposited to determine the reaction rate of Cu^{+2} at a hydrogen-evolving electrode.

The design of the gas-evolving electrode can have a significant effect on the mass-transfer enhancement. Several different electrode geometries have been studied. A great deal of the work has been done on planar electrodes, oriented either horizontally or vertically. Gas evolving screen electrodes (15) and expanded-mesh, gas-diverting

electrodes (60) have also been studied. Not only electrode geometry, but also substrate material should influence the mass-transfer enhancement.

Vertical, gas-evolving electrodes are extensively used in electrochemical cells and have been studied by several investigators. One of the most extensive studies was performed by Janssen and Hoogland (11). Platinum foils of different lengths (1-16 mm) were used to study the evolution of hydrogen, oxygen, and chlorine in acid. Current densities of the gas-evolving reaction (i_G)were varied over two orders of magnitude (10 - 1000 mA/cm^2). Boundary layer thicknesses less than 5 μm were obtained at the high current densities. The results generally followed relation 1.4.4.

$$\delta \propto i_G^{\beta}, \qquad (1.4.4)$$

where β was -0.5 for hydrogen and -0.25 for oxygen. There was some deviation from this relation at current densities greater than about 200 mA/cm^2 where the current exhibited a greater influence on the bounding layer thickness (i.e., $|\beta|$ increased). The proportionality constant varied with the gas evolved and also the length of the electrode. The boundary layer thickness was found to increase with the length of the electrode, at constant current density. In a similar work done by Venczel (16), no dependence on electrode height was found. A more recent study by Alkire and Lu (14) was conducted on hydrogen evolution at a verticle copper electrode. They were able to perform a more detailed study with a segmented electrode. Included in their work are the effects of electrode orientation, separation gap size, and

non-uniformity of the current distribution. Their results indicate that the local mass transfer coefficient increases with electrode length. The different substrate material (Cu) and/or the larger electrode length (2-12 cm) could be responsible to the direct contradiction to previous work (11). The overall mass transfer coefficient for the 12 cm electrode is very similar to the earlier work by Janssen and Hoogland (11) on the smaller electrodes. The role of surface roughness was studied by Fouad et al. (17).

Nearly all the mass-transfer studies conducted on horizontal, gas-evolving electrodes have been carried out by Janssen and his associates (12, 18, 19, 20). The evolution of hydrogen and oxygen was studied in alkaline and acid solutions. The boundary layer thickness followed relation 1.4.4, except for oxygen evolution in an alkaline solution. In that case β goes through a transition at a current density of about 30 mA/cm^2. Values of β in relation 1.4.4 vary from -0.36 to -0.87. It was found that for oxygen evolution, orientation of the electrode (horizontal or vertical), had little effect on the mass-transfer rate. Effects of surface material and roughness, temperature, and pressure were examined. A stationary disk electrode with multiple rings was used to elucidate the enhancement effect of the microscopic and macroscopic flows at the electrode (see Section 1.3). Hydrogen and oxygen was evolved at the disk and the boundary layer thickness was determined on the rings. The boundary layer thickness was found to be an order of magnitude less at the disk, as compared to the inner most ring.

Gas-evolution studies conducted on systems with a forced flow of electrolyte are numerous. Rousar (13) measured the mass-transfer enhancement in a rectangular flow channel at relatively low hydrogen evolution current densities (1 - 10 mA/cm^2). Hamzah and Kuhn (21) also studied the mass transfer in a flow cell, as well as in a cylindrical concentric cell. The usefulness of a rotating ring electrode for mass transfer studies at gas-evolving electrodes was demonstrated by Kodija and Nakic (22,23).

Theoretical models of the mass-transfer enhancement at gas-evolving surfaces attempt to describe either the effect of the microconvection or the macroconvection at the electrode. Models of the microconvection generated by individual bubble phenomena have been developed with the assumption that the effect of one bubble phenomenon override the rest. There have been some attempts at developing relations that combine the microconvection and macroconvection models.

Ibl (10) was one of the first investigators to attempt to model the mass transfer at gas evolving surfaces. His model is based on the assumption that the enhancement effect is due to the disengagement of the bubbles. Further, it is assumed that the separation of a bubble forms a void that is filled by solution from the bulk. In this way the gas bubbles accelerate the mass transfer by perodic destruction of the diffusion layer. With these assumptions, the Nernst boundary layer thickness is given by Equation 1.4.5.

$$\delta = \sqrt{\frac{D\pi R}{6v(1-\theta)}}, \qquad (1.4.5)$$

where θ is the fractional surface coverage of the bubbles and R is their radius.

In an attempt to improve on Ibl's displacement model, Rousar and Cezner (24) examined two limiting cases of surface coverage. In the first case the bubbles occupy only a fraction of the surface area and the current density of the reacting species (i_R) is related to the current density of the gas (i_G) by:

$$\frac{s_R\ i_R\ n_G\ (\pi\ D_R)^{1/2}}{n_R\ D_R\ C_{R,B}\ \overline{V}_G} \times \frac{2}{3} = \frac{1}{\gamma}\ i_G^{2/3}\ , \qquad (1.4.6)$$

where the subscript R refers to the reacting species and the subscript G refers to the gas. $\overline{V}_G$ and γ are the molar volume and bubble growth constant of the gas. The second case, in which the bubbles occupy the entire surface is given by Equation 1.4.7.

$$\frac{s_R\ i_R\ (\pi\ D_R)^{1/2}}{2\ F\ n_R\ D_R\ C_{R,B}} = \frac{\gamma}{R_K}\ i_G^{1/3} \qquad (1.4.7)$$

Following Ibl's work, Janssen and van Stralen (20) developed a model for the mass transfer enhancement as a result of the coalescence of bubbles on the surface. It is assumed that a void above a surface area of $\pi\ f\ R_c^2$ is generated by a coalescence. This void volume is filled with solution from the bulk, thus generating a mechanism for mass transfer enhancement. Their result for the boundary layer thickness is given by Equation 1.4.8.

$$\delta = 0.6\ f\ R_c^{-1/2}\ \eta^{-1/2}\ D^{1/2}\ \nu^{-1/2}. \qquad (1.4.8)$$

where η is the bubble density on the surface.

Stephen and Vogt (25) propose a model based on the convection generated by the growth of a bubble. It is assumed that as a bubble grows a radial flow is generated, which enhances the mass transfer. Further it is assumed that the enhancement effect is represented by a mass transfer boundary layer correlation for a flat plate. Several different correlations are presented depending on which mass transfer boundary layer correlation and geometry are used.

A model of the mass-transfer enhancement at a horizontal surface, due to the macroconvection generated by the bubble swarm as it rises, was developed by Janssen (19). It is based on a mass-transfer correlation for free-convection turbulent flow at a horizontal surface. A phase averaged density difference was used in the correlation to develop relation 1.4.9.

$$\delta \propto \left(\frac{\nu D u}{z g v}\right)^{1/3}, \tag{1.4.9}$$

where z and u are the drag coefficient and terminal velocity of the bubbles and g is the acceleration due to gravity. A similar model is presented by Ibl (26) for gas-sparged electrodes.

At a gas-evolving surface the mass-transfer rate is the result of a combination of microconvective and macroconvective effects. Beck (27) proposed that these effects could be combined linearly according to Equation 1.4.10.

$$k_0 = k_{MA} + k_{MI}. \tag{1.4.10}$$

Alternatively Vogt (28) proposed Equation 1.4.11.

$$k_0 = k_{MA}\left[1 + \left(\frac{k_{MI}}{k_{MA}}\right)^2\right]^{1/2}. \tag{1.4.11}$$

Nearly all the theoretical models can be reduced to the form of relation 1.4.4. The values of β from these models vary from -1/3 to -2/3. Therefore it is likely that some experimental data can be found, that fit one of the correlations quite well. In fact all the correlations give an estimate of the mass-transfer rate accurate within an order of magnitude. It is evident that more sophisticated modeling is required to obtain more accurate predictions of the mass transfer at gas-evolving surfaces.

There has been virtually no experimental work done on the effect of individual bubble phenomena on mass transfer. Some investigators have examined the mechanics of bubble phenomena. Westwater and associates (28,29) looked at the growth process of single bubbles. The equilibrium size of a bubble upon disengagement was examined by Kabanow and Frumkin (30). The growth and disengagement of single bubbles at relatively high, gas-evolution rates was investigated by Darby and Haque (31). A general review of the theoretical work on the dynamics of single bubble phenomena was presented by Cheh (32).

The need for more sophisticated models of the mass transfer at gas-evolving surfaces and the lack of experimental work on which to base these models has prompted the present work.

1.5 Scope of Study

An experimental program was developed by which the mass-transfer enhancement of individual bubble phenomena could be studied. This not only included the design and construction of a special experimental apparatus, but also the development of a feasible experimental procedure. The system is capable of examining phenomena on an electrode

oriented either horizontally or vertically. Mass-transfer enhancements caused by a single bubble disengagement and by the coalescence of two bubbles were measured.

The utility of the system to perform other electrochemical studies was demonstrated. Spacial changes in the current, over distances as short as 100 μm, for the transient, local free-convection mass transfer to a horizontal surface were measured. The system was originally designed to monitor the transient current distribution on a surface, but can also be used to study potential distributions with only minor changes in the monitoring scheme.

A substantial amount of theoretical work was performed to explain some of the experimental results. Mathematical models of a single bubble disengagement were developed. One model describes the events associated with the ascension of a bubble and the other is useful for the actual disengagement process. Attempts were also made to model the free-convection mass transfer to a horizontal surface.

1.6 Limiting Current Technique on Segmented Electrodes

Electrochemical methods have been extensively used to measure mass-transfer rates since the early 1950's. Numerous reviews have been written on the theoretical and experimental aspects of the limiting current method (33,34,35).

Qualitatively the limiting current technique is easily described. If only one electrochemical reaction occurs at an electrode, then the flux of reacting ions to the surface of the electrode is proportional to the current to the electrode. By polarizing the electrode to a

potential where the reaction is mass transfer limited, the current (i.e., limiting current) will be proportional to the rate of mass transfer to the electrode. Theoretically one must have an infinite overpotential to drive the surface concentration of the reacting ion to zero and create a mass transfer limited reaction. Fortunately the limiting current is reached in some cases, for all practical purposes, at only moderately high overpotentials before any other reaction occurs. Since a current can be measured easily and accurately the limiting current method is an effective technique for determining mass-transfer rates at a surface.

A large excess of non-reacting ions is often added to the electrolyte (i.e., well-supported electrolyte) to eliminate the effect of the electric field on the reacting ion. This is consequence of nearly all the charge being carried by the non-reacting ions.

When a detailed description of the current distribution on an electrode is desired a segmented electrode is often used. The electrode is sectioned into individual electrically isolated segments. Each segment is insulated from the other segments and a separate current collector is attached to each. The choice of size and shape of the segments is based on the phenomena to be studied. For example the characteristic length of the segment and of the phenomena under study should be of the same order. The separation between the segments must be minimized, in order to insure that the electrode will simulate a continuous surface. By polarizing the individual segments to the same potential and monitoring the current to each segment, the current distribution on the electrode is obtained.

Local, mass-transfer rates can be measured by employing the limiting current technique on a segmented electrode. This has proven to be a powerful method.

1.7 Nomenclature

C: Concentration, moles cm^{-3}.

D: Diffusion coefficient, cm^2 sec^{-1}.

f: Fraction of πR_c^2 that forms a void on the surface following coalescence.

F: Faraday constant, 96,487 C $equiv.^{-1}$.

g: Acceleration due to gravity, cm sec^{-2}.

i: Current density A cm^{-2}

k: Mass transfer coefficient, cm sec^{-1}.

L: Characteristic length, cm.

M_w: Molecular weight, g $mole^{-1}$.

n: Electrons transferred in reaction; equiv $mole^{-1}$.

N: Molar flux, moles cm^{-2} sec^{-1}.

R: Bubble radius, cm.

s: Stoichiometric coefficient.

u: Terminal velocity of rising bubbles, cm sec^{-1}.

v: Volumetric flux, cm sec^{-1}.

$\overline{V}$: Molar volume, cm^3 $mole^{-1}$.

z: Drag coefficient (i.e. the ratio between the volume of liquid transported upwards by rising bubbles and the volume of the rising bubbles).

Greek Letters

β: Correlation constant.

γ: Bubble growth constant, $cm^{5/3}\ sec^{-1/3}\ A^{-1/3}$.

δ: Nearnst boundary layer thickness, cm.

η: Bubble density on electrode surface, cm^{-2}.

θ: Fractional coverage of surface by bubbles.

ν: Kinematic viscosity of liquid, $cm^2\ sec^{-1}$.

ρ: Density, $g\ cm^{-3}$.

Subscripts

B: Denotes bulk property.

C: Denotes property of coalescence.

G: Denotes property of gas.

I: Denotes interface property.

K: Denotes bubble quantity at breakoff.

MA: Denotes macroconvection property.

MI: Denotes microconvection property.

O: Denotes overall property.

R: Denotes property of indicator ion.

2. EXPERIMENTAL

2.1 Method

The limiting current technique was used to measure the local, mass-transfer enhancement effect of individual bubble phenomena. A single bubble disengagement and coalescence of two bubbles, both on a horizontal surface, were studied. These studies were conducted with a multi-electrode cell and the micro-mosaic electrode.

The reduction of ferric ion ($Fe^{+3} + e^- \rightarrow Fe^{+2}$) was used as an indicator ion reaction. Ferric sulphate was added to a well-supported aqueous electrolyte (0.05 M $Fe_2(SO_4)_3$; 1.0 M $H_2\ SO_4$). All chemicals were analytical reagent grade. The water used was from a reverse-osmosis unit that was passed through a Culligan Cartridge Water Treatment System, which included an organic trap, deionizer, and micro-filter. The specific resistance of the water was always greater than 10 megohm-cm. The electrolyte was sparged with nitrogen for at least 30 minutes to reduce the oxygen concentration.

The working and counter electrodes in all cells were made of platinum. A separator was not necessary and was not used. A mercurous sulphate reference electrode fabricated by Radiometer (K601) served as the reference electrode. The reference electrode was connected to the cell by a Luggin capillary (36). A ground glass junction was placed in the tube between the capillary and the reference electrode.

The working electrode consisted of multiple segments. The multi-electrode cell, although segmented, did not simulate a continuous surface. The micro-mosaic electrode was a true segmented electrode.

All segments on the working electrode were initially cathodically polarized into the limiting current region for the reduction of the indicator ion and just above the potential for hydrogen evolution. A value of -550 mV referred to the reference electrode was used in the experiments. The onset of hydrogen evolution occurred at about -625 mV, which gave a 75 mV cushion.

A single bubble was generated by reducing the potential of a single segment into the hydrogen evolution region. The ability to generate single bubbles was critical in controlling the individual bubble phenomena. The micro-mosaic electrode was much more efficient at generating single bubbles than the multi-electrode cell. A potential reduction of 200-300 mV between the bubble segment and the other working electrode segments was needed to nucleate and grow a single bubble. As the bubble grew on a segment of the micro-mosaic electrode, the IR drop to the segment increased as its active area decreased. Thus a higher potential difference was required during the latter stages of growth to maintain the optimal current to the segment. The optimal current for bubble growth on a segment of the micro-mosaic electrode was 15 μA. It was 1-5 μA for the multi-electrode cell, according to the condition of the segment.

The bubble phenomena were generated by the controlled growth of the bubbles. For a single bubble disengagement, a bubble was nucleated and grown until it disengaged from the surface. Two bubbles were nucleated on separate segments and were grown until they coalesced in the coalescence studies.

Observations of the electrode were made with a microscope during the experiments. Magnifications of 20X-50X were used. The eye-piece on the microscope was calibrated to allow for the determination of the bubble size.

A special stand was used with the micro-mosaic electrode cell to allow the electrode surface to be leveled. A standard bubble level was used for this task.

The temperature was not controlled during an experiment. A Cole Parmer digital thermometer (8502-20) was used to measure the temperature following the completion of an experiment.

The current to the segments on which the only reaction occurring was the reduction of the indicator ion was measured as an individual bubble phenomenon took place. Since the indicator ion reaction was at limiting current, the change in the current to the segments was a result of a change in the mass transport rate. In this manner the local change in the mass transfer rate was determined. A schematic of the reactions occurring on the working and counter electrodes is given in Figure 2.2.1.

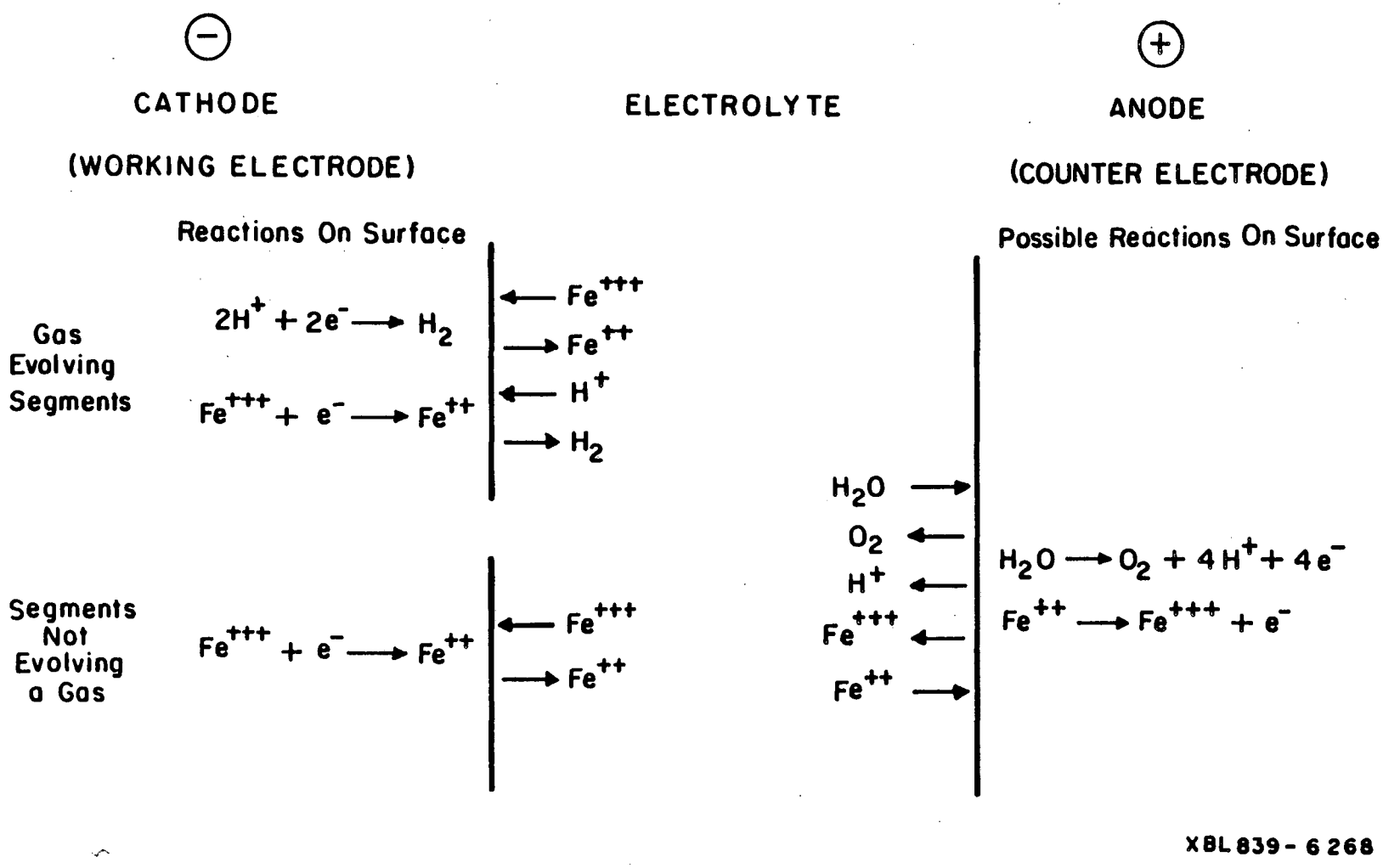

Figure 2.2.1 Schematic of electrode reactions in electrochemical cell.

2.2 Mass Transfer Studies with Multi-Electrode Cell

2.2.1 Electrochemical Cell

The multi-electrode cell, shown in Fig. 2.2.1.1, is a special electrochemical cell, which was constructed by Cheh (32). The cell, which was not originally designed to perform mass transfer studies, was modified somewhat for this work. The top was removed to allow for the placement of a Luggin capillary in the cell for a reference electrode. A platinum wire, which was positioned in one corner of the cell, was used as the counter electrode.

The working electrode, shown in Fig. 2.2.1.2, consists of a matrix of circular micro-minature electrodes. It was fabricated by embedding fine platinum wires in an epoxy base, then cutting the epoxy and wires along a plane perpendicular to the wires. There are 19 wires in the matrix each with a diameter of 125 μm (0.005 in.). A schematic of the pattern of the electrode segments is given in Fig. 2.2.1.3. The electrode was polished with 1.0 μm diamond paste and was oriented horizontally during experiments.

2.2.2 Instrumentation

Instrumentation capable of controlling the apparatus and monitoring the current to an individual electrode segment was assembled. A diagram of the system is given in Fig. 2.2.2.1.

The experimental method required the use of a potentiostat with the ability to control two separate working electrode potentials simultaneously. A Pine (RDE3) potentiostat/galvanostat performed this task. One working electrode connection (K1) was made to a bus bar.

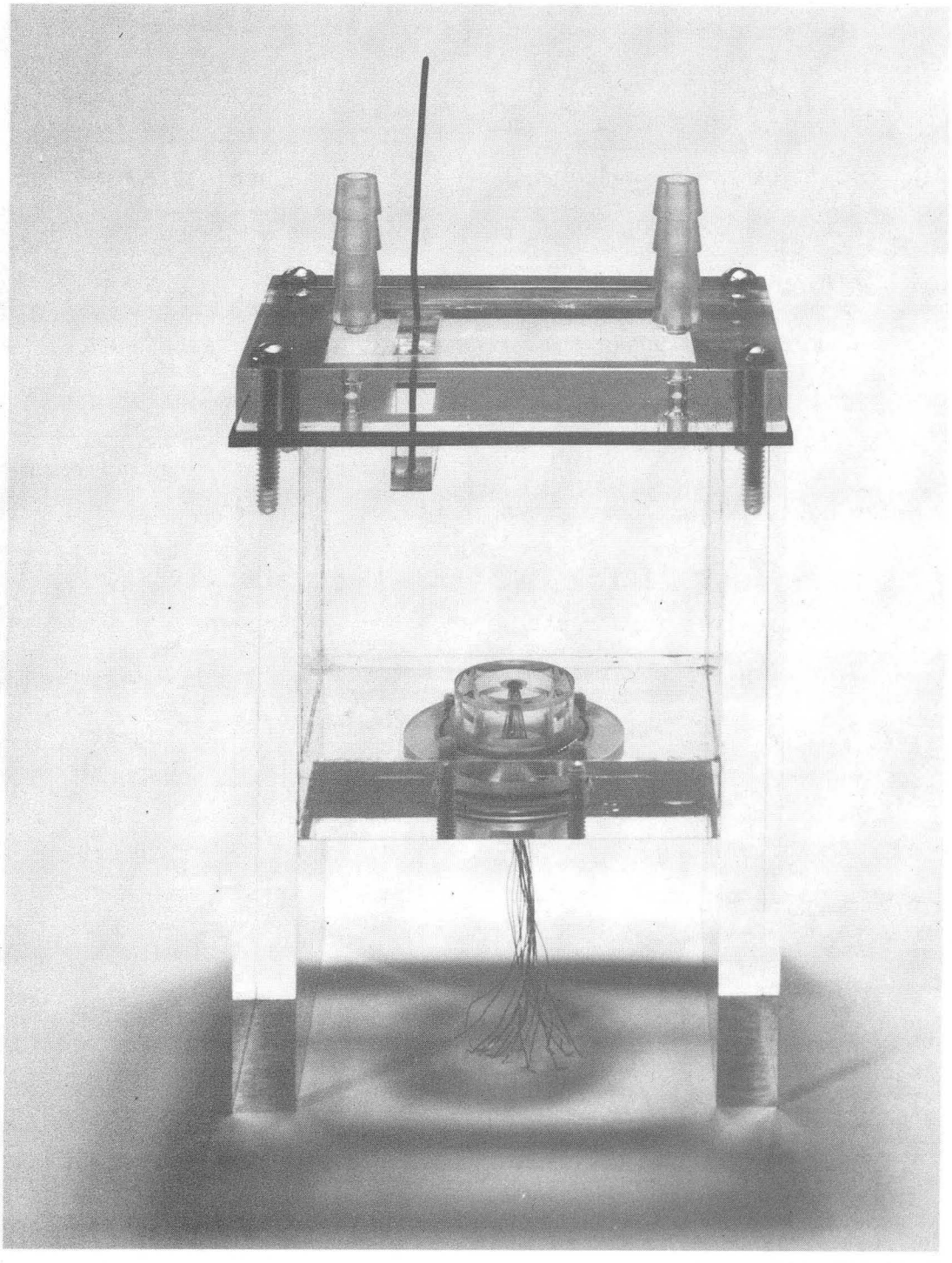

CBB 808-9197

Figure 2.2.1.1 Multi-electrode cell.

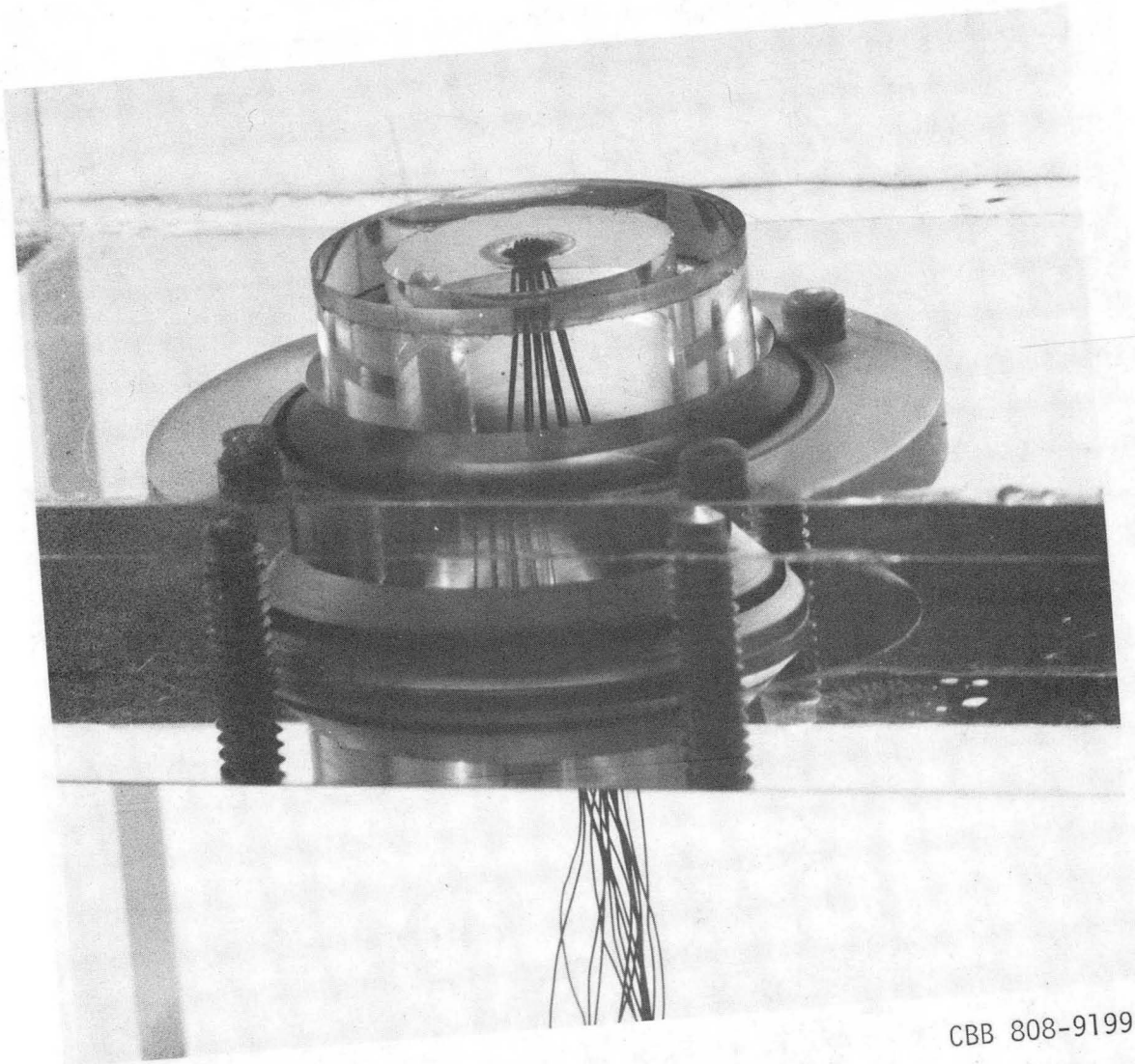

Figure 2.2.1.2 Working electrode in multi-electrode cell.

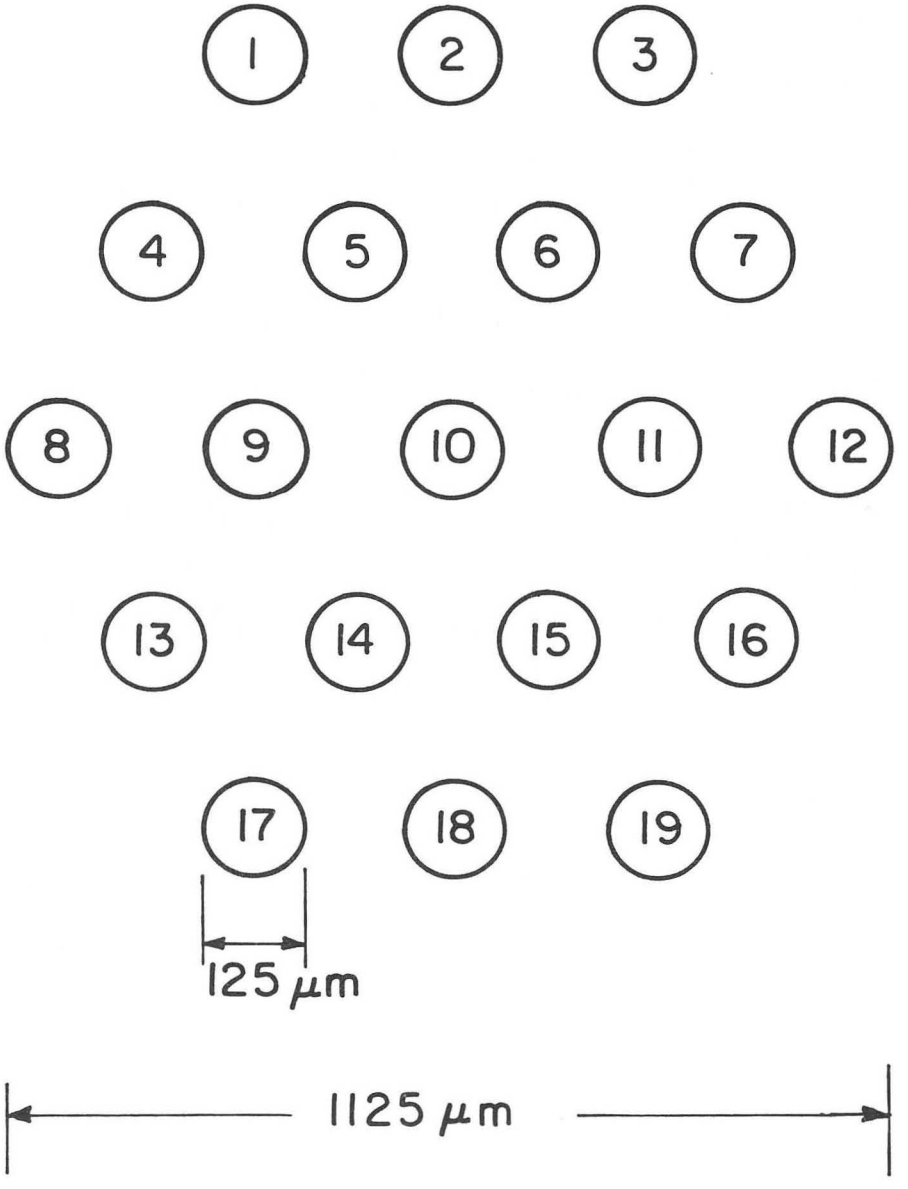

XBL 838-6133

Figure 2.2.1.3 Schematic of the working electrode.

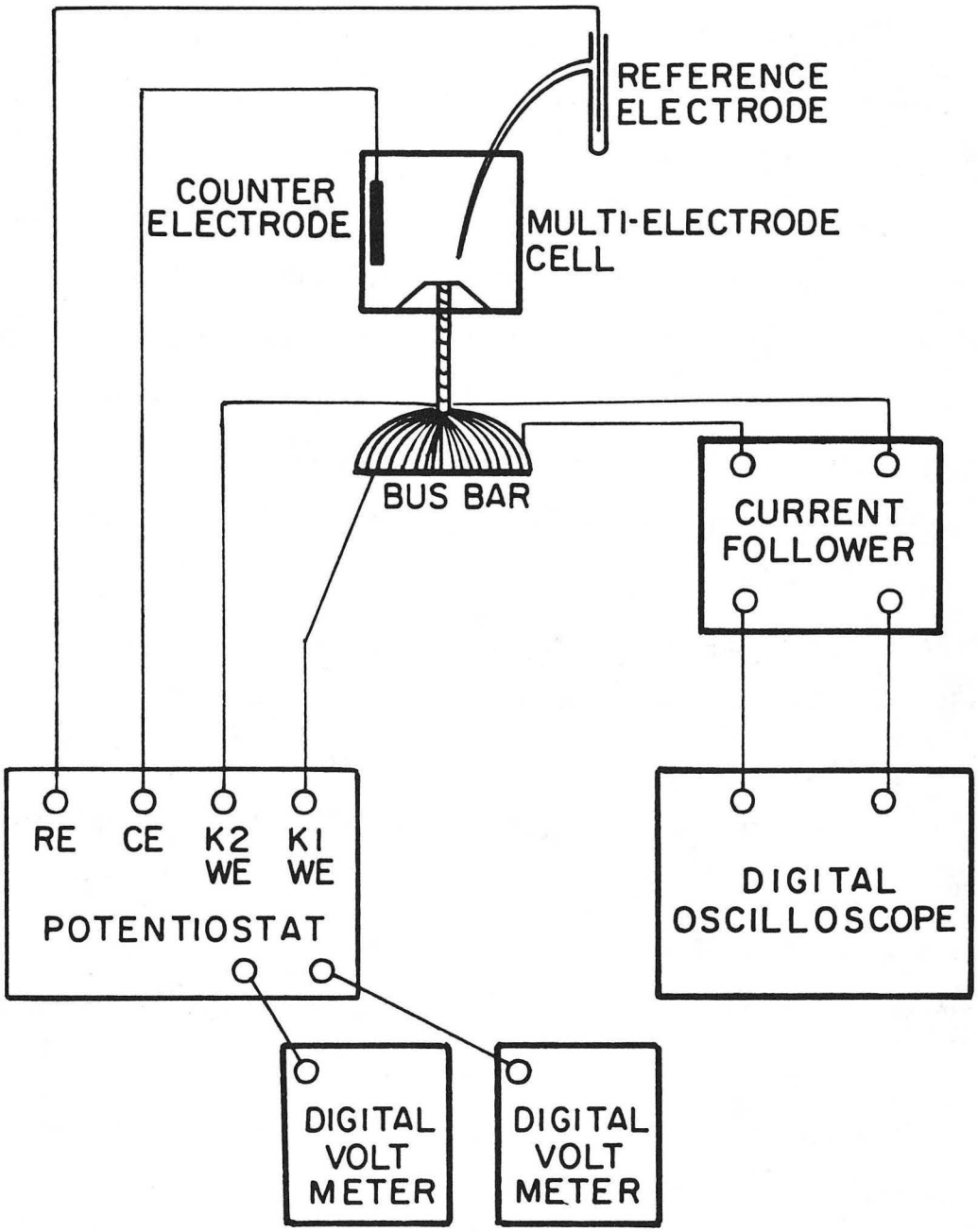

XBL 836-5933

Figure 2.2.2.1 Instrumentation for the multi-electrode cell.

All the electrode segments of the multi-electrode cell were connected to the bus bar through a set of color coded wires, except the segments where gas was to be evolved. The color code for the wires is given in Appendix A, along with certain precautions that should be taken with the potentiostat. The electrodes at which gas was evolved were connected to the other working electrode connection (K2) on the potentiostat. The reference and counter electrodes were also connected appropriately to the potentiostat. The current to each of the two working electrode connections was monitored with a set of Keithley digital multimeters (173A) through the current followers in the potentiostat.

Measuring the change in current to a single segment was made possible by the use of a current follower placed in the line between the electrode segment and the bus bar. The current follower was basically a battery-powered operational amplifier that converted the current to a voltage signal which was proportional to the current. It was designed and built by the electronic shop in the College of Chemistry at the University of California, Berkeley (DWG 961 A1). A more detailed description of the device is given in Appendix A.

The characteristics of the voltage signal which was monitored made it necessary to use a digital oscilloscope. During the bubble growth period, which lasted from 20 minutes to an hour, the current to the monitored segment and thus the voltage to the oscilloscope would remain relatively constant. A transient change in the current lasting only a

few seconds would occur as a result of the bubble phenomenon. The transient was captured using the mid-signal triggering capability on a Nicolet digital oscilloscope (1090A).

2.2.3 Results and Discussion

The mass transfer enhancement due to a single bubble disengagement and the coalescence of two bubbles was measured with the multi-electrode cell. The experimental method used is described in Section 2.1. Increases in current of over 35% were observed. The maximum current change was reached in approximately 40 milliseconds and decayed in a few seconds, following the occurrence of the phenomena.

Generating single large bubbles was not too difficult, but it was found that other bubbles, which were orders of magnitude smaller, were also nucleated. These smaller bubbles would coalesce with the large bubble and shake it slightly. The vibrations produced were only minor when compared to the effect of the phenomena being studied and did not affect the results significantly. The coalescence of the small bubbles with the large one did serve as a mode of growth for the large bubble. Also it was found that some of the electrode segments were better for growing bubbles than others.

Selected results from the bubble disengagement studies are given in Table 2.2.3.1. The relative position of the electrode segments is indicated by the number, which corresponds to the numbered segments in Fig. 2.2.1.3. It was observed that the bubble size upon disengagement was much larger than when a swarm of bubbles is produced. This is generally attributed to the lack of macroconvection and bubble-bubble

Table 2.2.3.1 Disengagement Studies With Multi-Electrode Cell

BUBBLE DIAMETER AT TIME OF SEPARATION	ELECTRODE AT WHICH BUBBLE WAS GENERATED	% CHANGE IN CURRENT	ELECTRODE AT WHICH CURRENT WAS MONITORED
1.2 MM	10	38.3	19
1.2 MM	1	12.2	19

Table 2.2.3.2 Coalescence Studies With Multi-Electrode Cell.

BUBBLE DIAMETER AT TIME OF COALESCENCE	ELECTRODE AT WHICH BUBBLE WAS GENERATED	% CHANGE IN CURRENT	ELECTRODE AT WHICH CURRENT WAS MONITORED
200 Micron 150 Micron	4 5	13.2	6
200 Micron 150 Micron	4 5	3.2	1
500 Micron 500 Micron	4 6	32.0	5

interactions for the single bubble. Indeed the size of the bubble was quite fortunate. Otherwise the mass-transfer enhancement could not be studied with the multi-electrode cell. It can be seen that the mass-transfer enhancement effect is about 12% near the edge of a single bubble during disengagement. The drop from 38% under the bubble indicates that the effect is localized. If the bubble had been much smaller (10 - 100 μm), the effect would not have been measurable on the adjacent electrode segment. The enhancement was quite significant within one bubble diameter of the disengagement.

The results of the coalescence studies are presented in Table 2.2.3.2. By comparing the first two sets of coalescence data, it is seen that there was a much greater enhancement effect along the axis of coalescence than a direction perpendicular to it. This would be expected since the bubble movement occurs mostly along the axis of coalescence. It was observed that the greatest enhancement occurred between the two bubbles as can be seen from the last entry of the table.

By comparing the results of the disengagement and coalescence studies, certain similarities can be seen. The enhancement effect of both phenomena are localized to one or two bubbles diameters of the phenomena. This indicates that both phenomena can have a significant effect on the mass transfer at gas-evolving surfaces.

These experimental results were considered in the design of the micro-mosaic electrode, which was used to study the mass-transfer enhancement effects further.

2.3 Initial Mass-transfer Studies with Micro-Mosaic Electrode

2.3.1 Description of Micro-Mosaic Electrode

The micro-mosaic electrode was designed to study individual bubble phenomena. It was prepared by Hewlett Packard Co. using integrated circuit technology. The novel electrode serves as the core of the system developed to measure the effect on the mass-transfer rate of individual bubble phenomena.

The electrode, shown in Fig. 2.3.1.1, was fabricated on a 7.6 cm. (3 inch) silicon wafer. The actual active electrode area is the 0.5 cm x 0.5 cm. platinum square at the center of the wafer. The lines extending radially from the electrode are aluminum current conductors that carry the current to the individual electrode segments. The conductors are connected to a set of bonding pads which are laid out in a square pattern near the edge of the wafer. The larger conductors carry the current to the relatively large buffer segment of the electrode.

A magnified view of the center portion of the wafer is shown in Fig. 2.3.1.2. The 1.0 mm x 1.0 mm segmented portion at the center of the micro-mosaic electrode can be seen. The segmented portion is surrounded by a relatively large buffer segment, which together makes up the total electrode area. The buffer segment was added to eliminate edge effects.

The 10 x 10 matrix of square platinum segments along with 12 specially positioned segments, shown in Fig. 2.3.1.3, make up the segmented portion of the micro-mosaic electrode. The segments in the matrix are on 100 micron centers. The maximum number of segments in

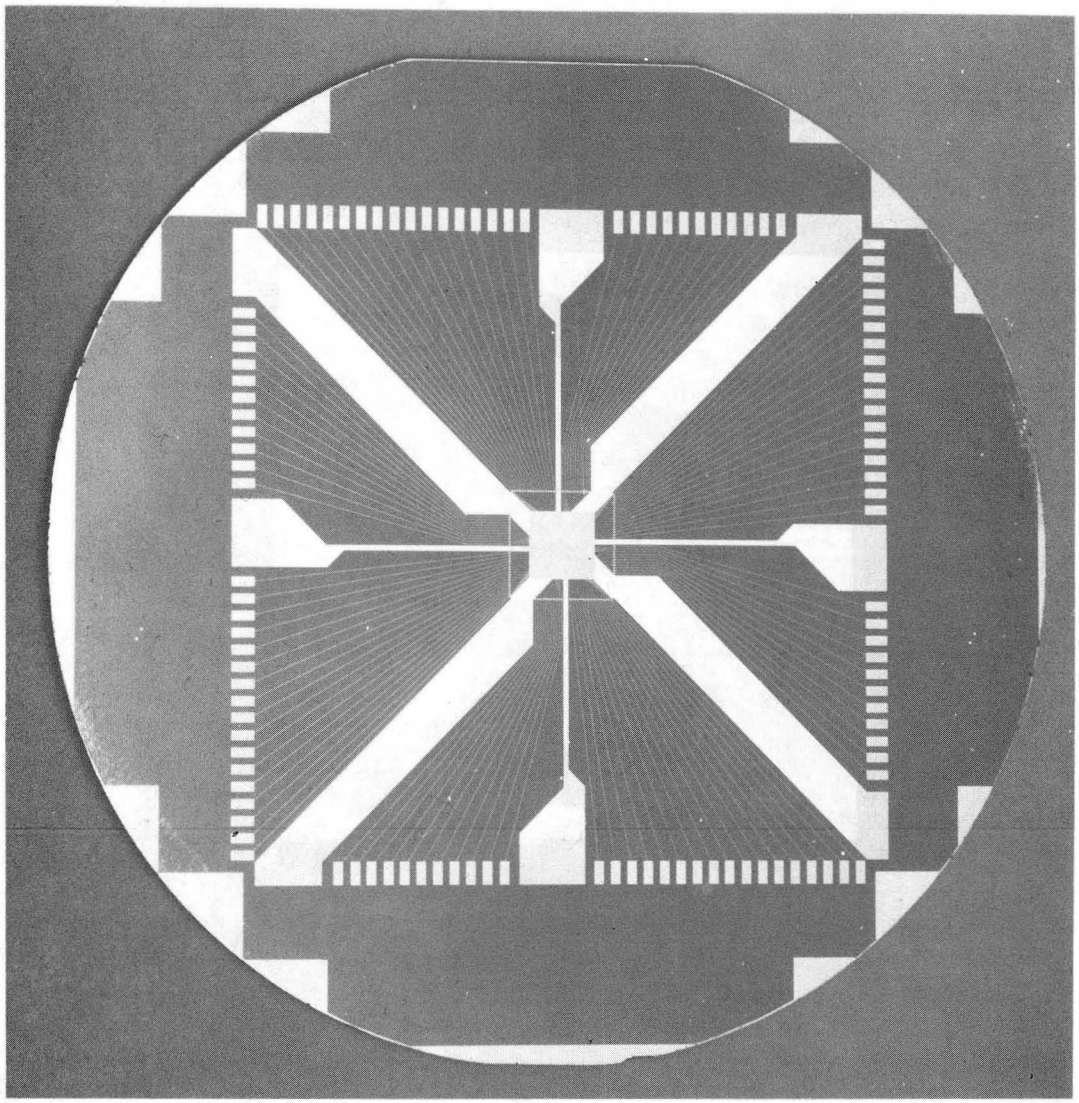

CBB 809-1993

Figure 2.3.1.1 Micro-mosaic electrode.

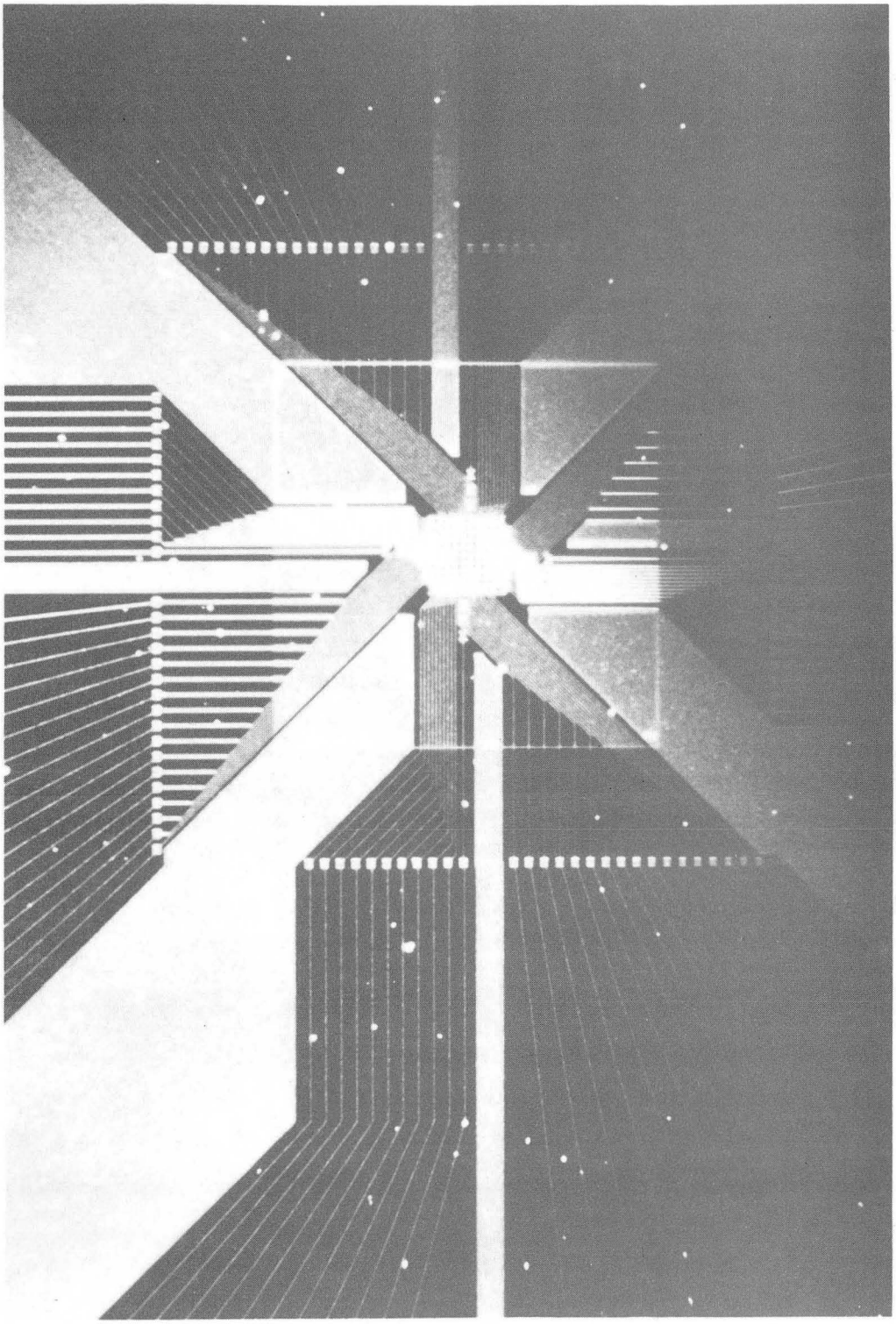

CBB 827-6359

Figure 2.3.1.2 Magnified view of micro-mosaic electrode.

the matrix is limited by the area needed for the current conductors to the segments. For certain long range bubble studies, a larger matrix was needed. Specially positioned segments were included in the design of the electrode to permit these long range studies. A closer view of the individual segments can be seen in Fig. 2.3.1.4. Each segment is 98 micron on a side, with a 2 micron gap between adjacent segments.

The separate layers of material that comprise the micro-mosaic electrode are shown in Fig. 2.3.1.5. An oxide was thermally grown on the wafer and then covered by a nitride layer to form a non-conducting base, upon which the electrode was built. The silicon dioxide layer between the aluminum conducting layer and the platinum electrode layer protects the aluminum layer from the electrolyte. It also serves to isolate each segment from the other segments. Holes were etched in the oxide to allow for electrical contact between the platinum and aluminum layers. The oxide layer extends to the inner edge of the outer square of bonding pads. Adherence of the platinum layer to the oxide was an anticipated problem. A relatively thin chromium layer was placed between the platinum and the oxide to improve adherence.

A detailed description of the process steps involved in fabricating the micro-mosaic electrode is given in Appendix B.

2.3.2 Description of Micro-Mosaic Electrode Cells

Two electrochemical cells were constructed to accommodate the micro-mosaic electrode. Both cells are made of lucite and are of similar design, except that one uses the electrode oriented horizontally and the other vertically.

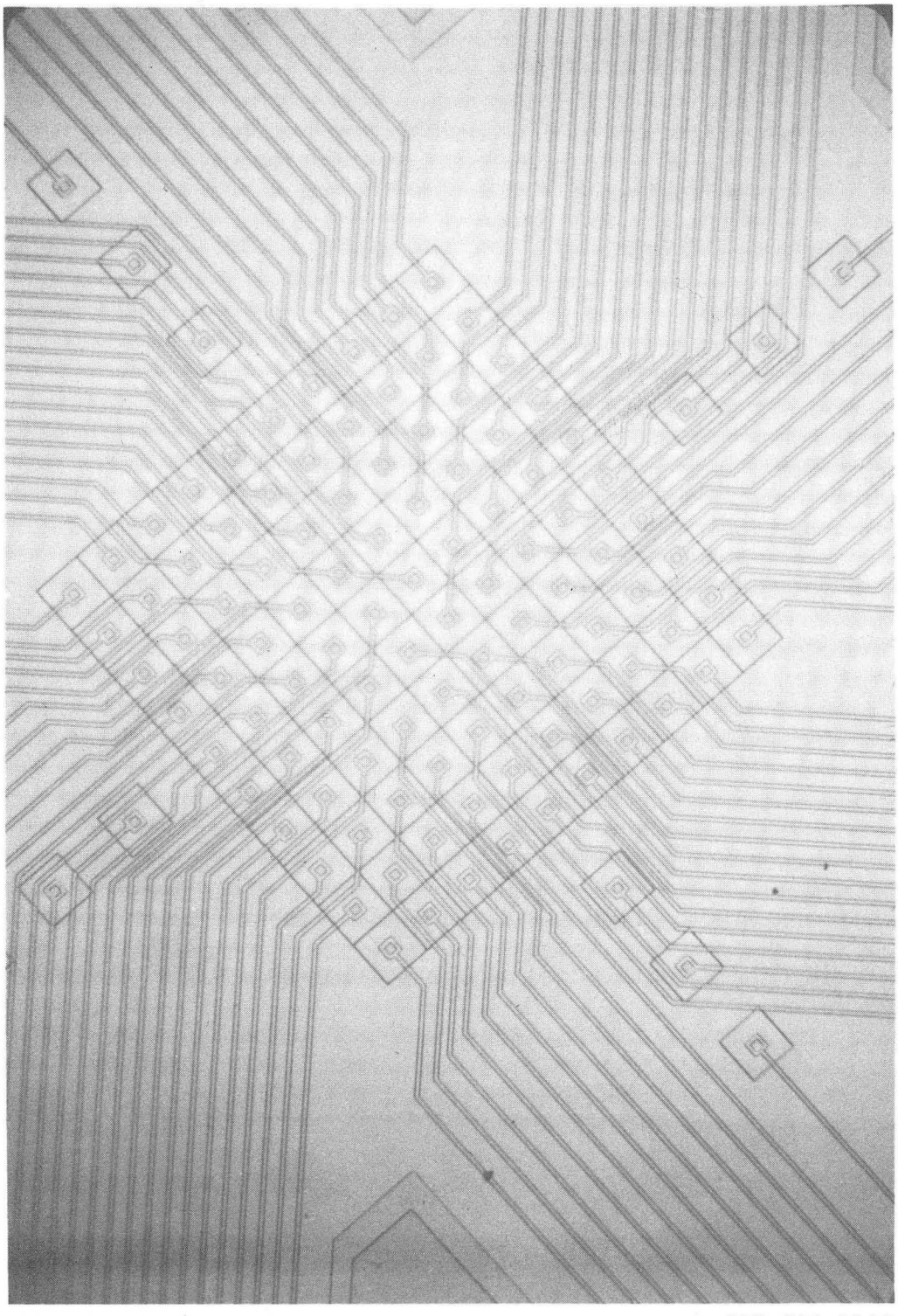

CBB 809-1146

Figure 2.3.1.3 Segmented portion of micro-mosaic electrode.

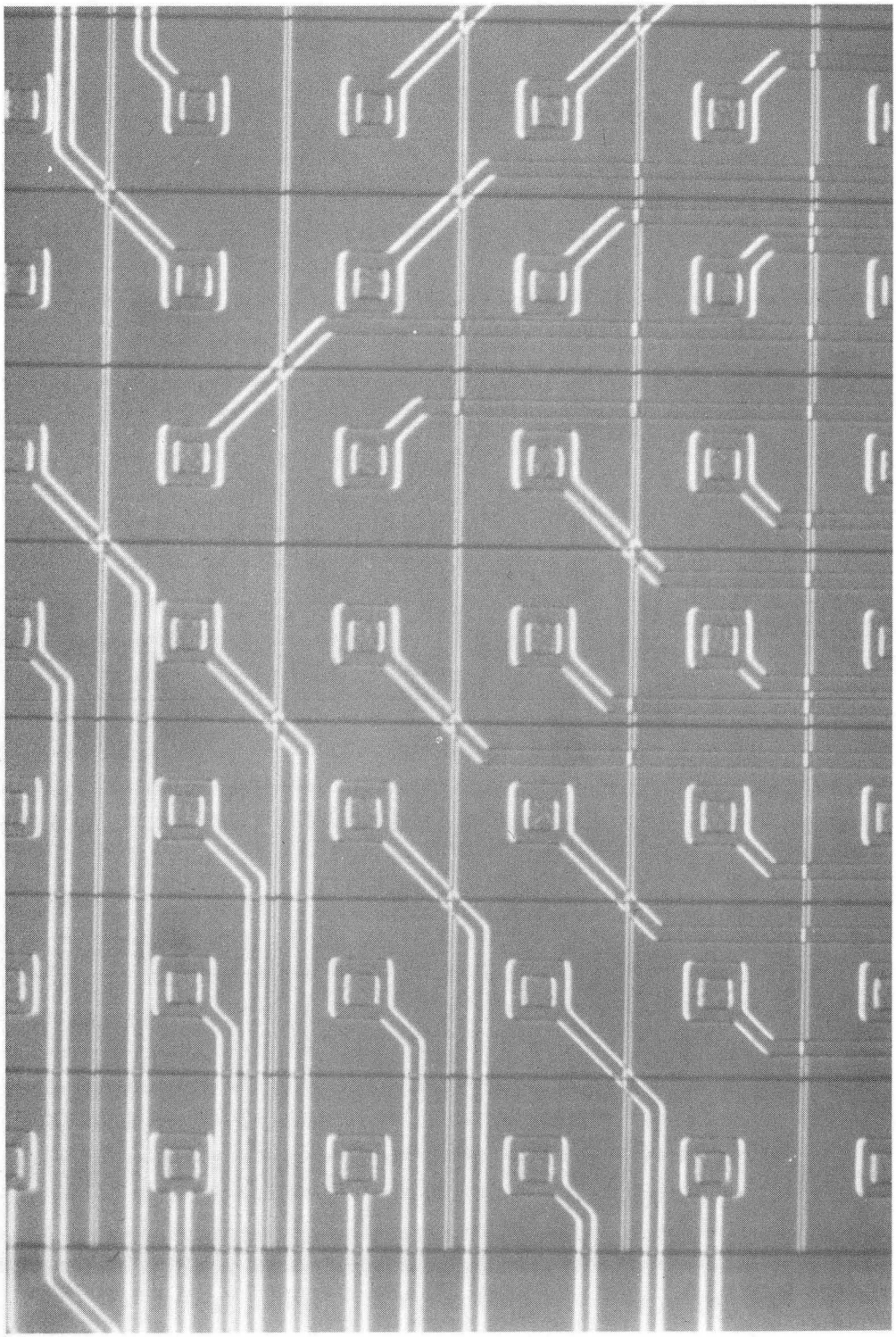

CBB 809-1148

Figure 2.3.1.4 Segments in micro-mosaic electrode.

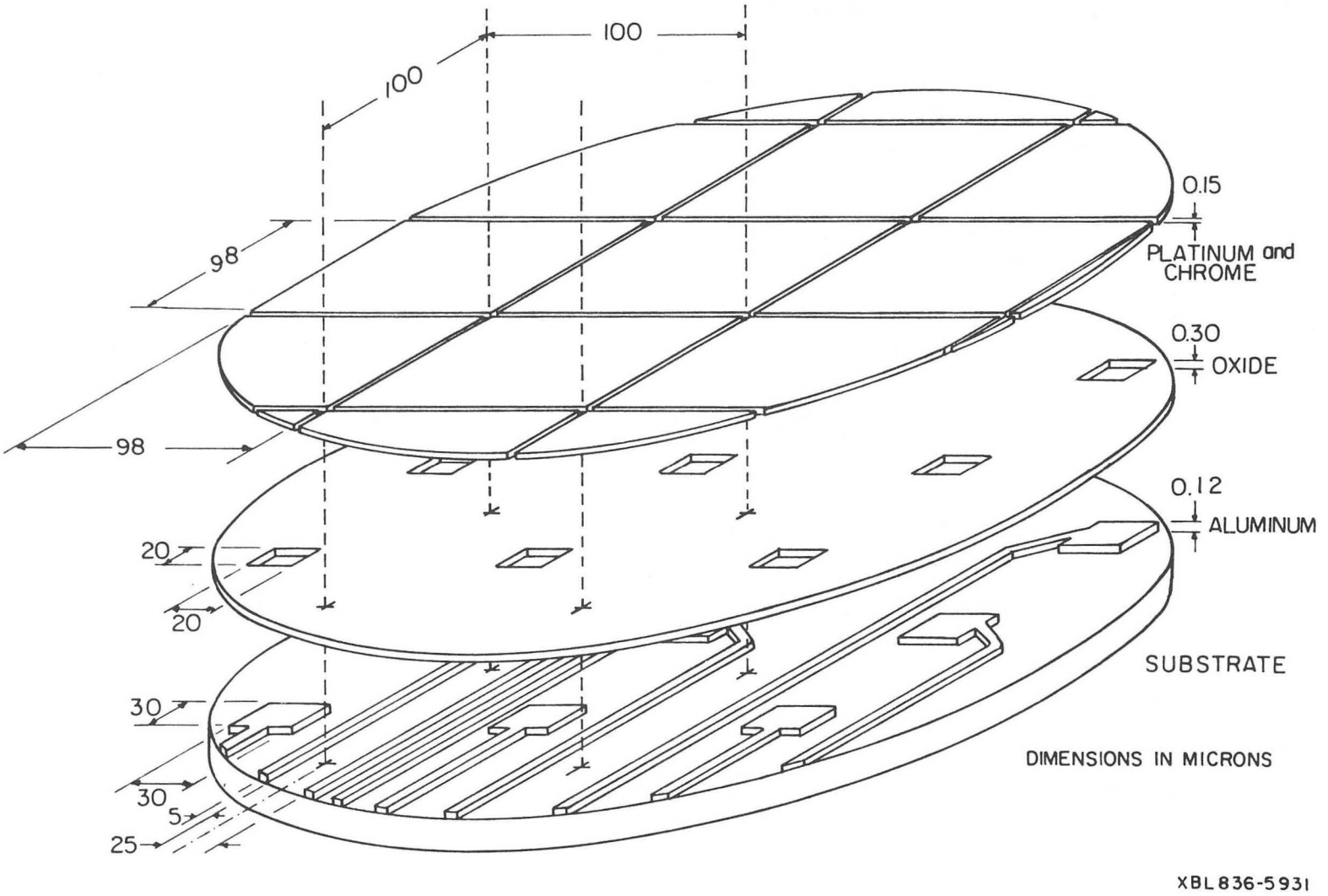

Figure 2.3.1.5 Exploded view of micro-mosaic electrode.

The electrochemical cell designed to accommodate the horizontally oriented micro-mosaic electrode is shown in Fig. 2.3.2.1. Connections to the micro-mosaic electrode are made through the printed circuit board. The actual cell is the cube in the center of the apparatus, which is 2.5 cm. (1 inch) on each side. Electrolyte is added and removed through either of the two vents in the top of the cell. The thermistor for the digital thermometer can also be lowered into the electrolyte through one of these ports. A reference electrode capillary was built into the cell; its connection is on one of the side walls of the cell. There are two counter electrodes on opposing side walls of the cell. The total counter electrode area is 2.0 cm^2, which is eight times the working electrode area. The window at the top of the cell, shown in Fig. 2.3.2.2, is used to view the micro-mosaic electrode, located at the bottom of the cell, during experiments.

The printed circuit board is connected to the micro-mosaic electrode via a set of Zebra connectors (Series 7000) made by Tecknit Corporation. The pattern on the printed circuit board is shown in Fig. 2.3.2.3. The conductors on the printed circuit board are terminated in a pattern that exactly matches the pattern of the bonding pads. In this manner they overlap when properly aligned. Four Zebra connectors are placed into slots in special holders built by the miniature tin plated copper contact pads on both sides of the on the bottom of the printed circuit board. Connections to the micro-mosaic electrode are made by pressing the board and the electrode together with the connectors in between. This is possible Zebra connectors.

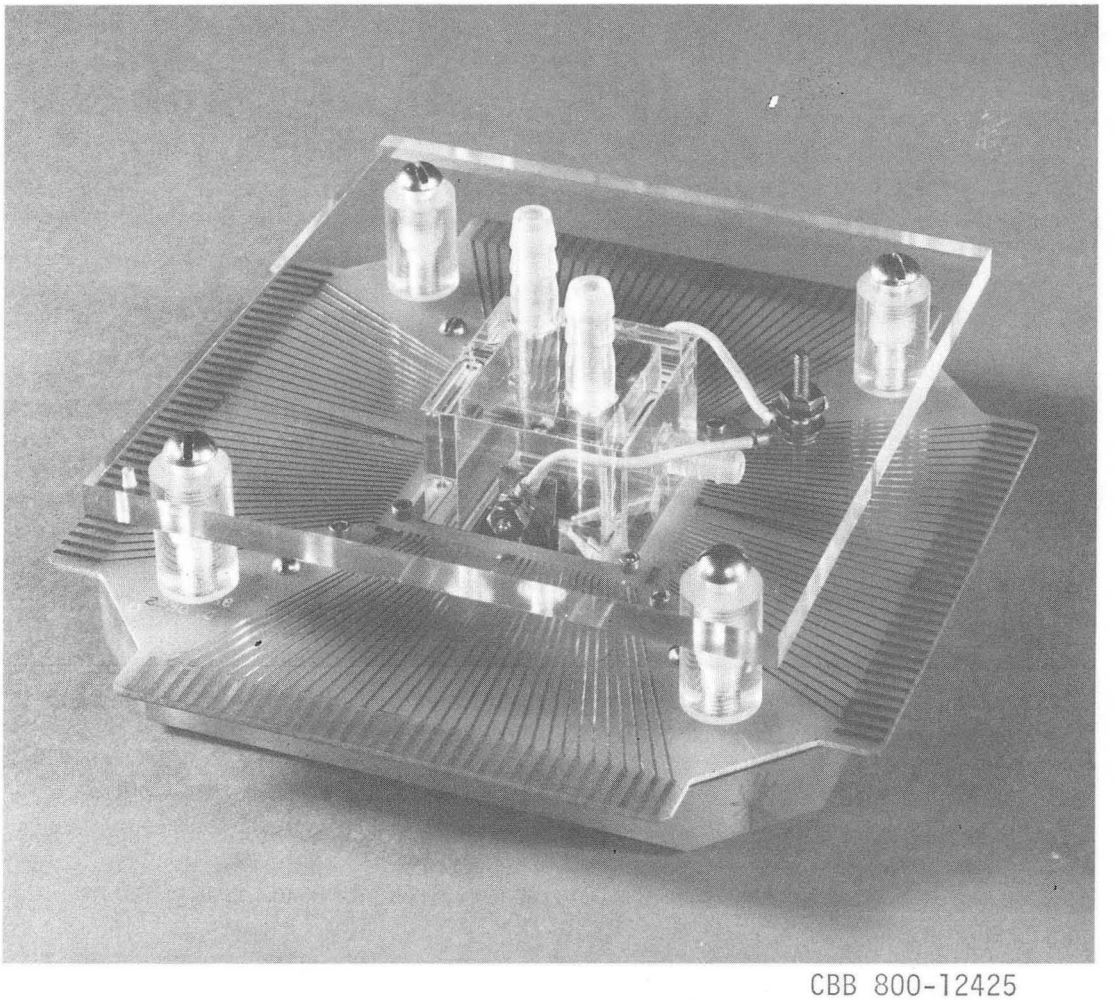

CBB 800-12425

Figure 2.3.2.1 Micro-mosaic electrode electrochemical cell with horizontal electrode orientation.

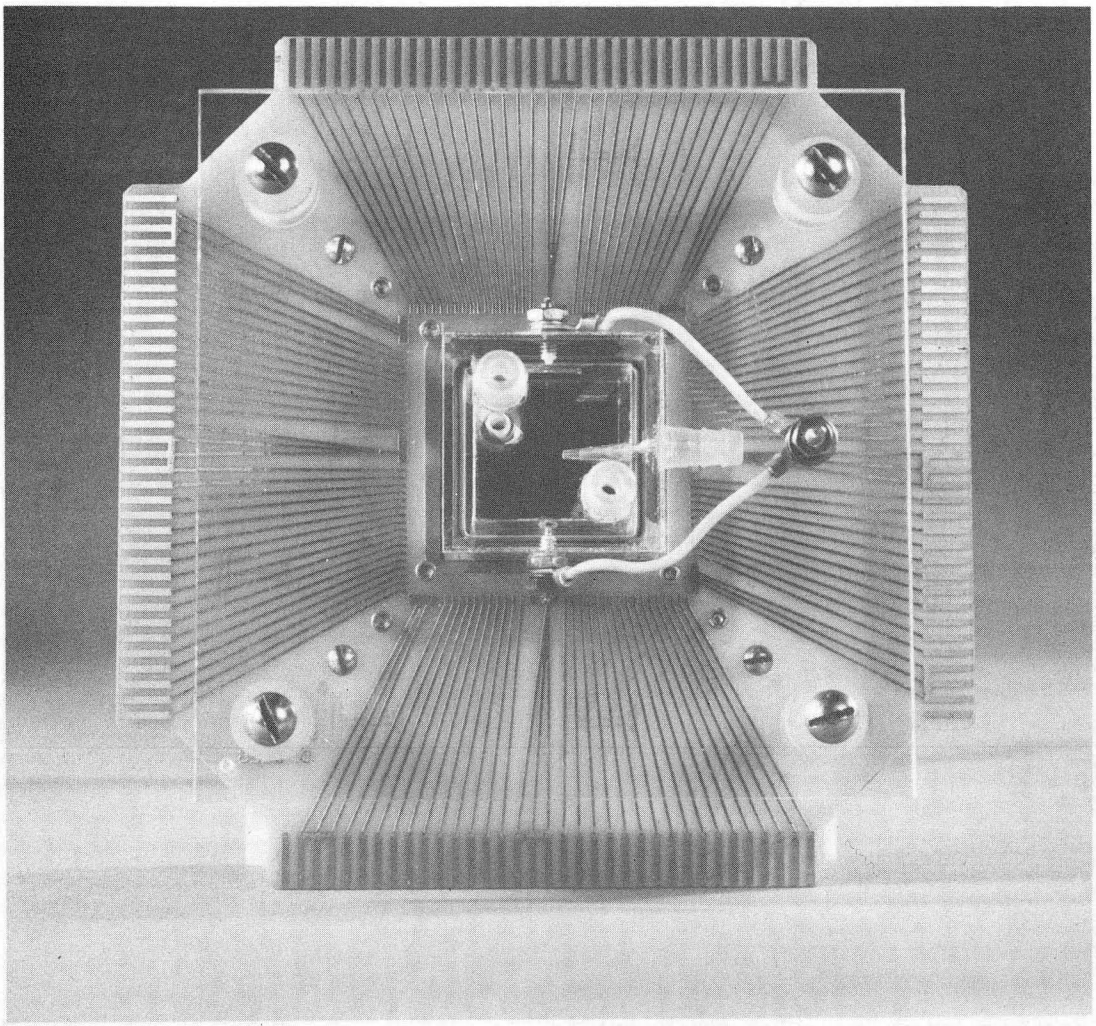

CBB 800-12427

Figure 2.3.2.2 Top view of electrochemical cell.

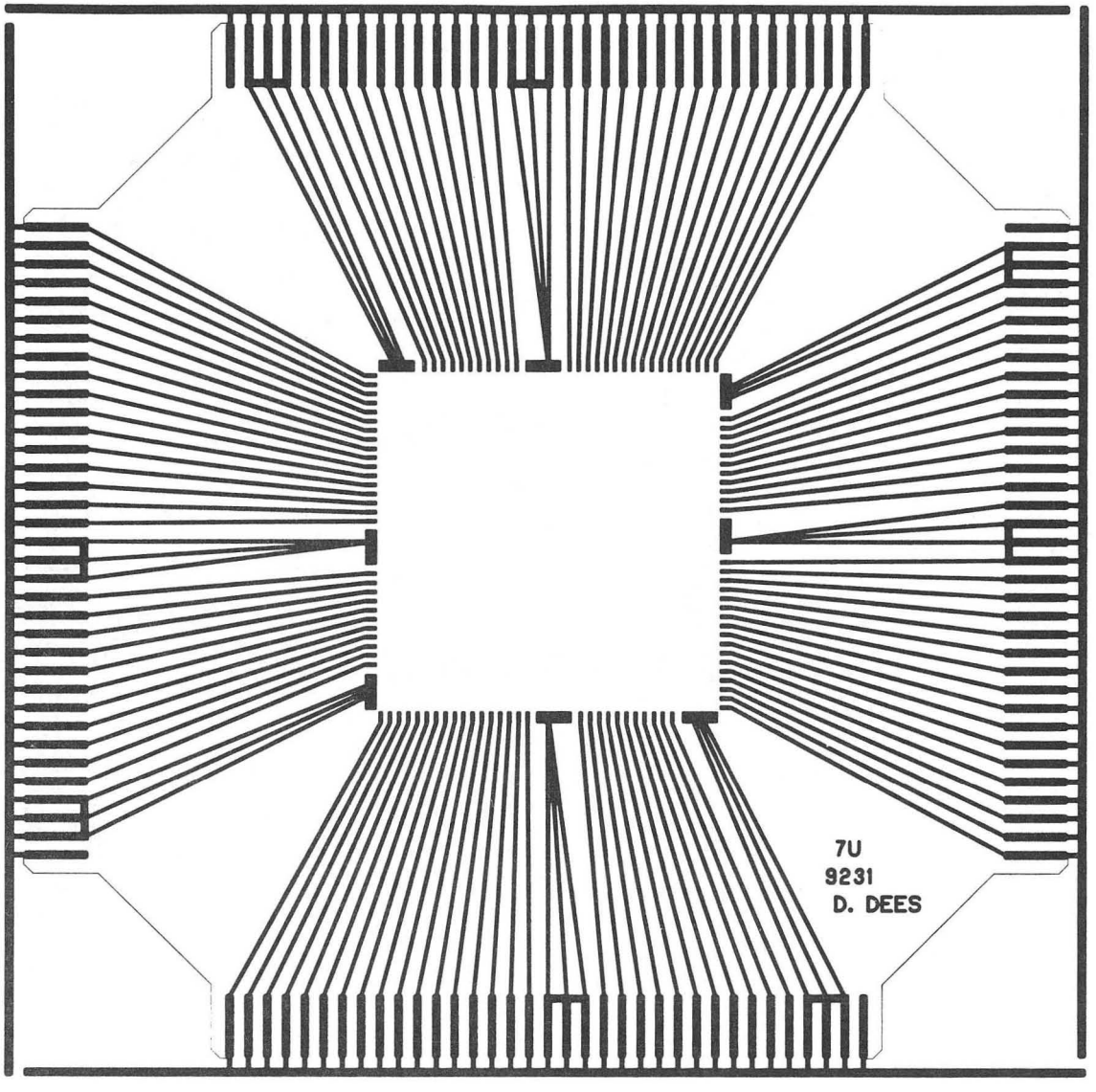

XBL 837-10675

Figure 2.3.2.3 Pattern for printed circuit board.

Connections from the outside world are made with standard printed circuit board connectors (CCC 600-121-66).

A disassembled view of the electrochemical cell is given in Fig. 2.3.2.4. Assembling of the cell is accomplished by first placing the micro-mosaic electrode in its 12.7 cm (5 in.) base. The base serves to house and protect the electrode. Next the Zebra connectors are placed in their holders, then the printed circuit board is fastened onto the base. The spacers are then attached to the base, followed by the placement of the actual cell. The cell is sealed to the micro-mosaic electrode with a Viton O-ring (70 Duro, 2-028).

The electrochemical cell made to be oriented vertically, shown in Fig. 2.3.2.5, has only a few design differences from the other cell. The cell is thinner and the counter electrodes are smaller. The thinner cell design and the depression in the side opposite the electrode allows for a much higher magnification of the electrode during experiments. The vents and filler tubes are displaced to be out of the way while observations are being made. A disassembled view of the cell is given in Fig. 2.3.2.6. It can be seen that the base and printed circuit board are for all practical purposes the same, while the actual cell and the spacers are considerably different.

2.3.3 Instrumentation

The instrumentation for the early mass-transfer studies with the micro-mosaic electrode was basically the same as was used in the mass-transfer studies with the multi-electrode cell (see Section 2.2.2). Some changes and improvements on the original system were made.

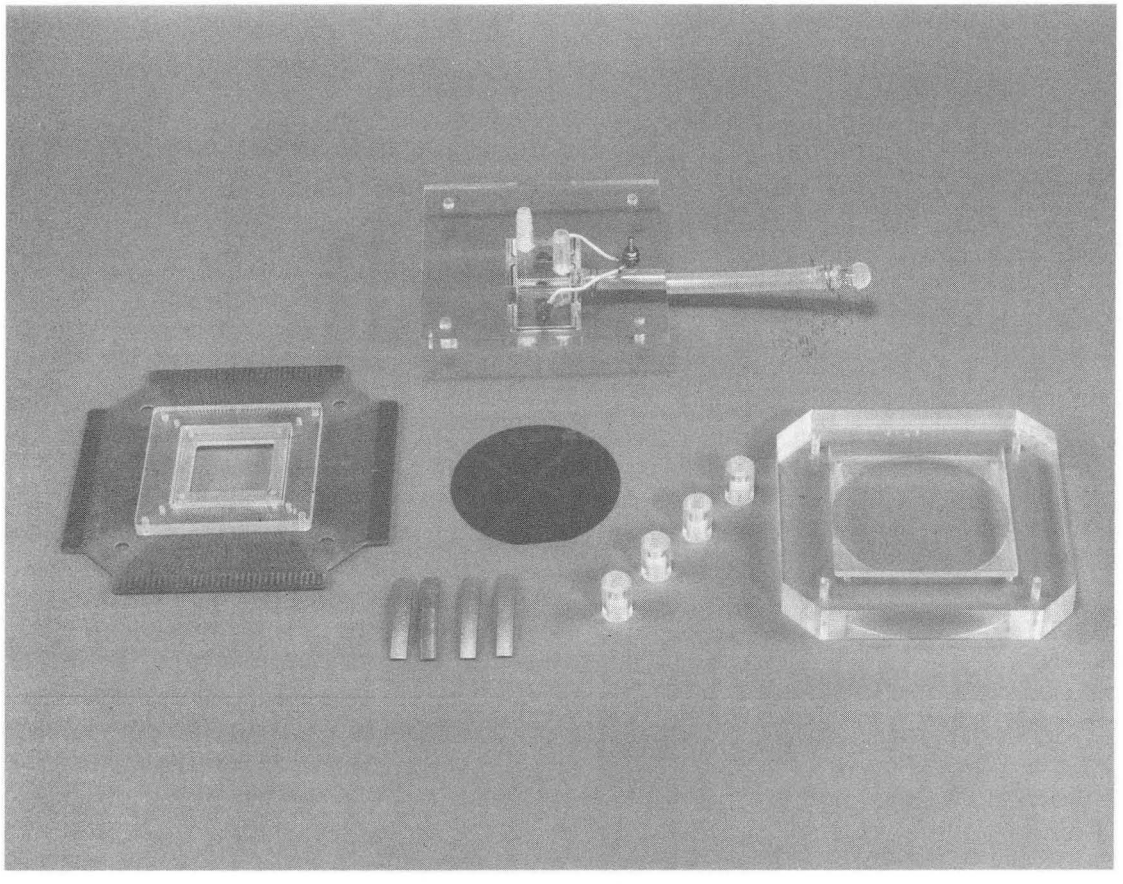

CBB 823-28

Figure 2.3.2.4 Disassembled view of electrochemical cell.

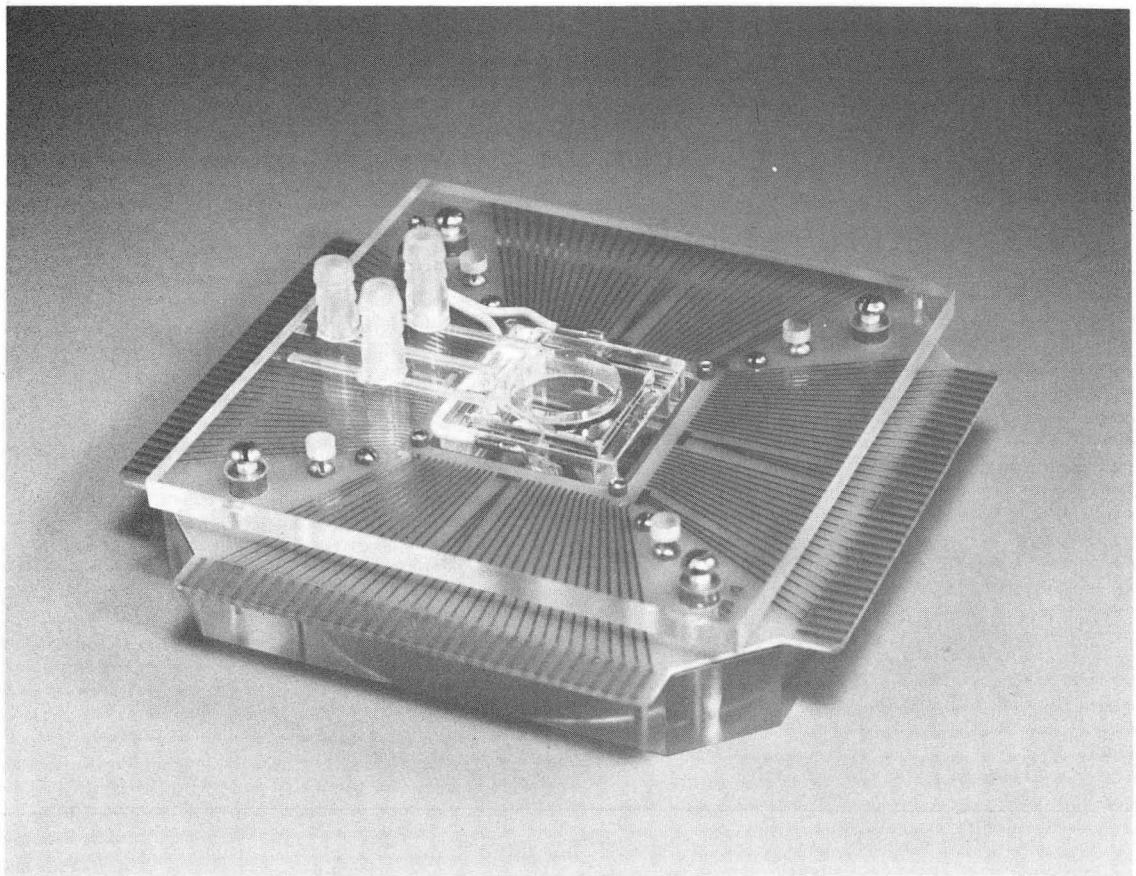

CBB 823-02076

Figure 2.3.2.5 Micro-mosaic electrode electrochemical cell with vertical electrode orientation.

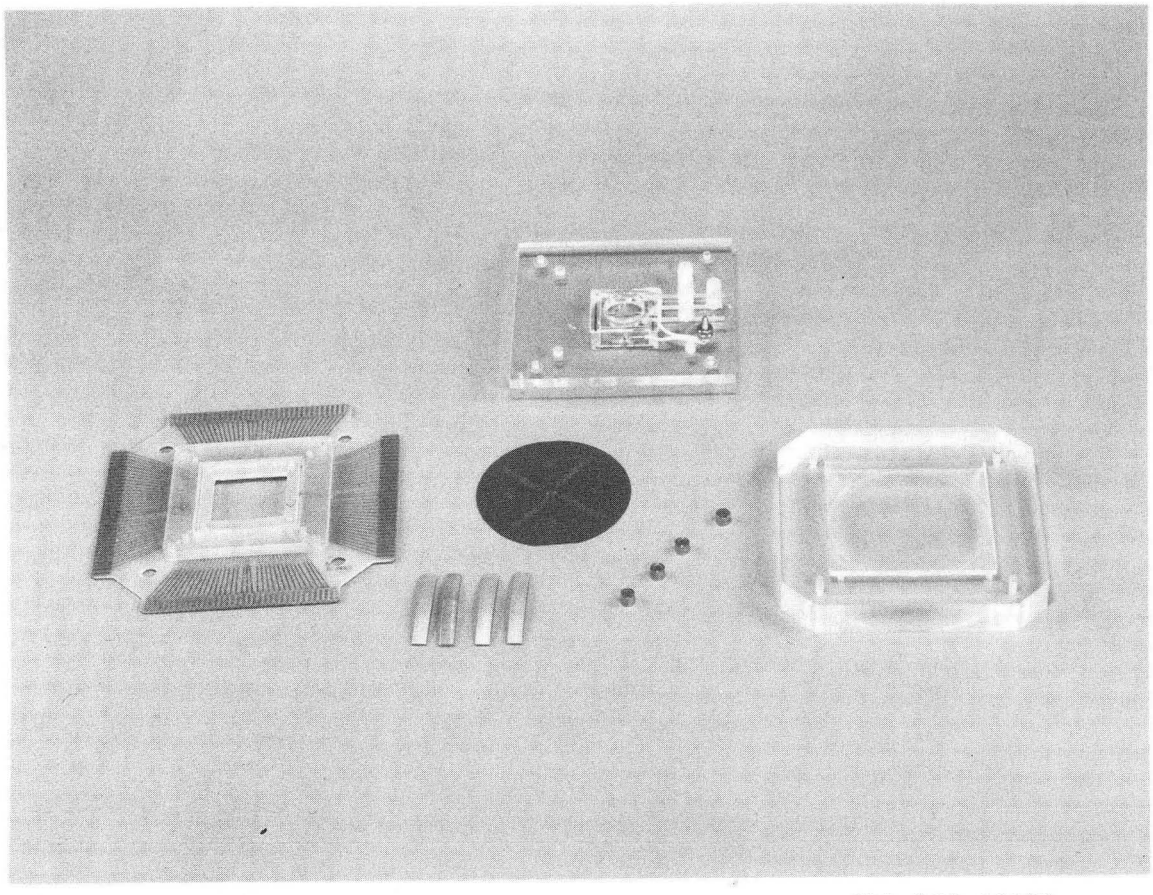

CBB 823-02078

Figure 2.3.2.6 Disassembled view of electrochemical cell.

Instead of 19 electrode connections, there were 112 connections, along with the buffer segment connections, which were made to the bus bar. As with the multi-electrode cell, all the connections were color coded. The color code is given in Appendix C.

Like in the multi-electrode cell, the change in the current to only one segment was monitored at a time. The current to a single segment of the micro-mosaic electrode was generally smaller than the current to one of the electrodes in the multi-electrode cell. For this reason the current follower had to be modified for use with the micro-mosaic electrode (see Appendix C).

A Hewlett Packard desktop computer (9825T) was interfaced with the digital oscilloscope, for the purpose of storing data from the oscilloscope. A program was written for the computer which will transfer the data from the oscilloscope and store it on magnetic tape. The program will also retrieve data from the tape and plot the data on a Hewlett Packard digital plotter (9862A), which was also interfaced to the computer. A second program was developed, which will obtain data from the tape and plot it against the inverse square root of time. These programs, along with some general oscilloscope data transfer and plotting routines, are listed in Appendix D.

2.3.4 Results and Discussion

A series of experiments was conducted with the micro-mosaic electrode in the cell oriented horizontally. Initial experiments were performed without any gas evolution on the electrode in order to characterize the system. Following these experiments, the effect of a single bubble disengagement on the rate of mass transfer to the electrode was studied.

As mentioned earlier, a segmented electrode simulates a continuous surface but consists of discrete segments. One method of determining whether the micro-mosaic electrode acts as a true segmented electrode is to observe its behavior upon the application of a cathodic potential step to the electrode. If the potential step is into the limiting current range for the reduction of ferric ions and above the potential for the onset of hydrogen evolution, the current to the electrode and to each individual segment should follow the Cottrell equation (36). This equation relates the current to the time elasped after the potential step;

$$I = n F A C_B \sqrt{\frac{D}{\pi t}} \qquad (2.3.4.1)$$

This equation represents the rate of unsteady state diffusion to a surface from a semi-infinite stagnant electrolyte. The current to each segment and to the entire electrode should decrease inversely proportional to the square root of time after the potential step if the micro-mosaic electrode acts as a continuous surface. Furthermore the diffusion coefficient determined from the current to a segment and the current to the entire electrode should agree.

The current to the entire electrode after a potential step is given in Fig. 2.3.4.1 (A), and in Fig. 2.3.4.1 (B) the current is plotted against the inverse square root of time. As predicted by Equation 2.3.4.1 the line in Fig. 2.3.4.1 (B) is straight and extrapolates to zero at infinite time. The diffusion coefficient for for the ferric ion was determined from Fig. 2.3.4.1 (B) is 4.58 x 10^{-6} cm^2/sec. This value can be compared to 5.4 x 10^{-6} cm^2/sec,

reported by Ibl et al. (10), and 4.22 x 10^{-6} cm^2/sec determined by Alkire and Gould (39).

The current to an individual segment following a potential step was measured for several segments of the micro-mosaic electrode. A typical example is given in Fig. 2.3.4.2 (A). A plot of the current versus the inverse square root of time is given in Fig. 2.3.4.2 (B). As in the case of the entire electrode current, a linear relationship is found that can be extrapolated through zero. The average diffusion coefficient determined from the results of the individual segment experiments is 4.21 x 10^{-6} cm^2/sec. This agrees with the value obtained from the entire electrode current to within 8%. The micro-mosaic electrode does appear to simulate a continuous surface.

The micro-mosaic electrode conductors that are connected to the discrete segments have a finite resistance. The resistance introduces a potential drop in each one of the conductors. The resistance for each of the conductors was measured. The average resistance was 0.6 Kohm. Each individual conductor varied from the average by not more than 0.1 Kohm, according to its length and pattern. This at first may seem to be a large resistance, but it must be remembered that the current in the conductor is of the order of 0.1 μA to 10μA. The potential drop for 1 μA would be 0.6 mV, which is quite reasonable for mass transfer studies.

All currents are presented as currents rather than current densities. To convert the current to a segment in microamps to a current density in milliamps per square centimeter, one has to multiply the

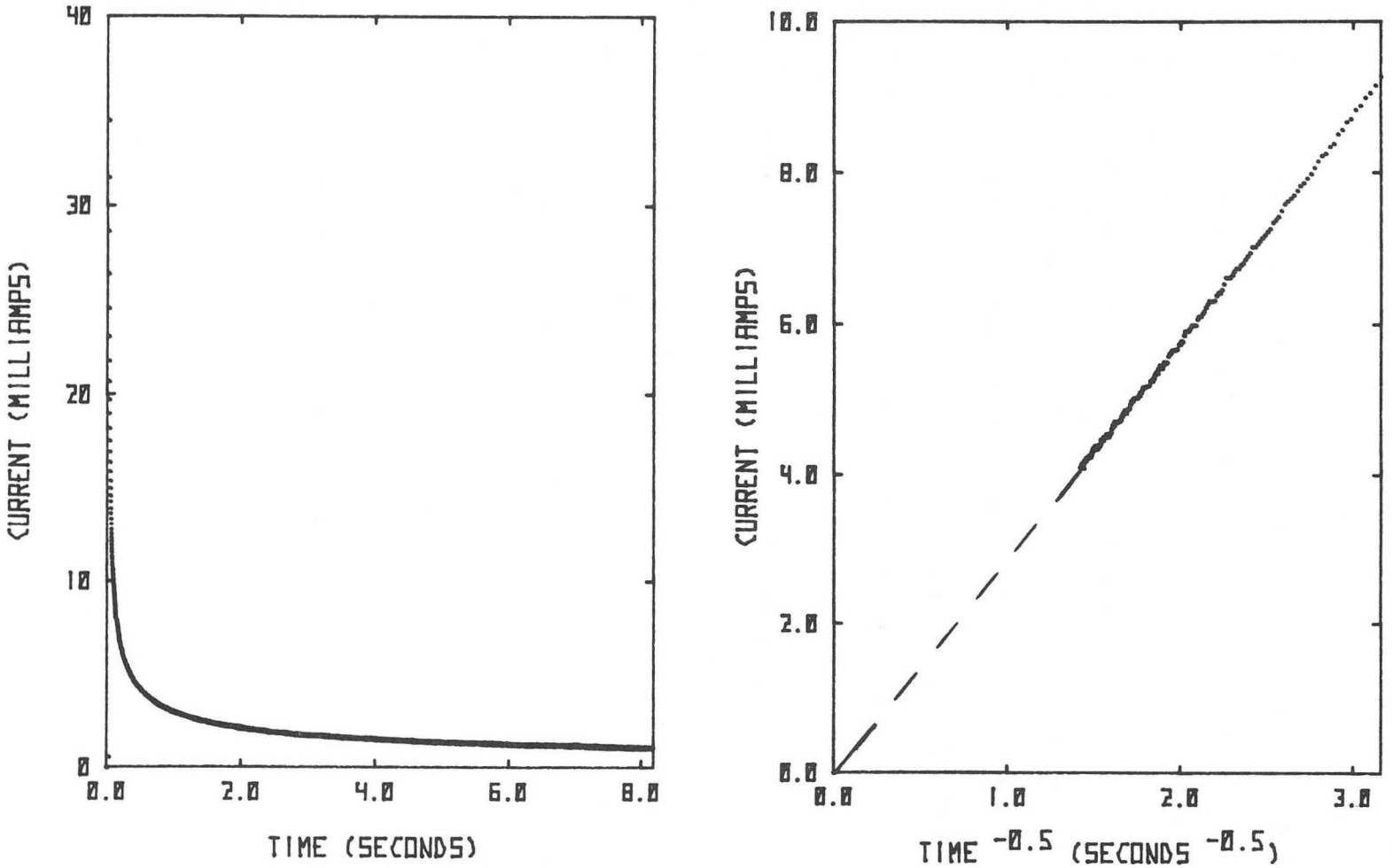

XBL 836-10386

Figure 2.3.4.1 Potential step limiting current to the entire electrode; (A) Time on abscissa; (B) Inverse square root of time on abscissa.

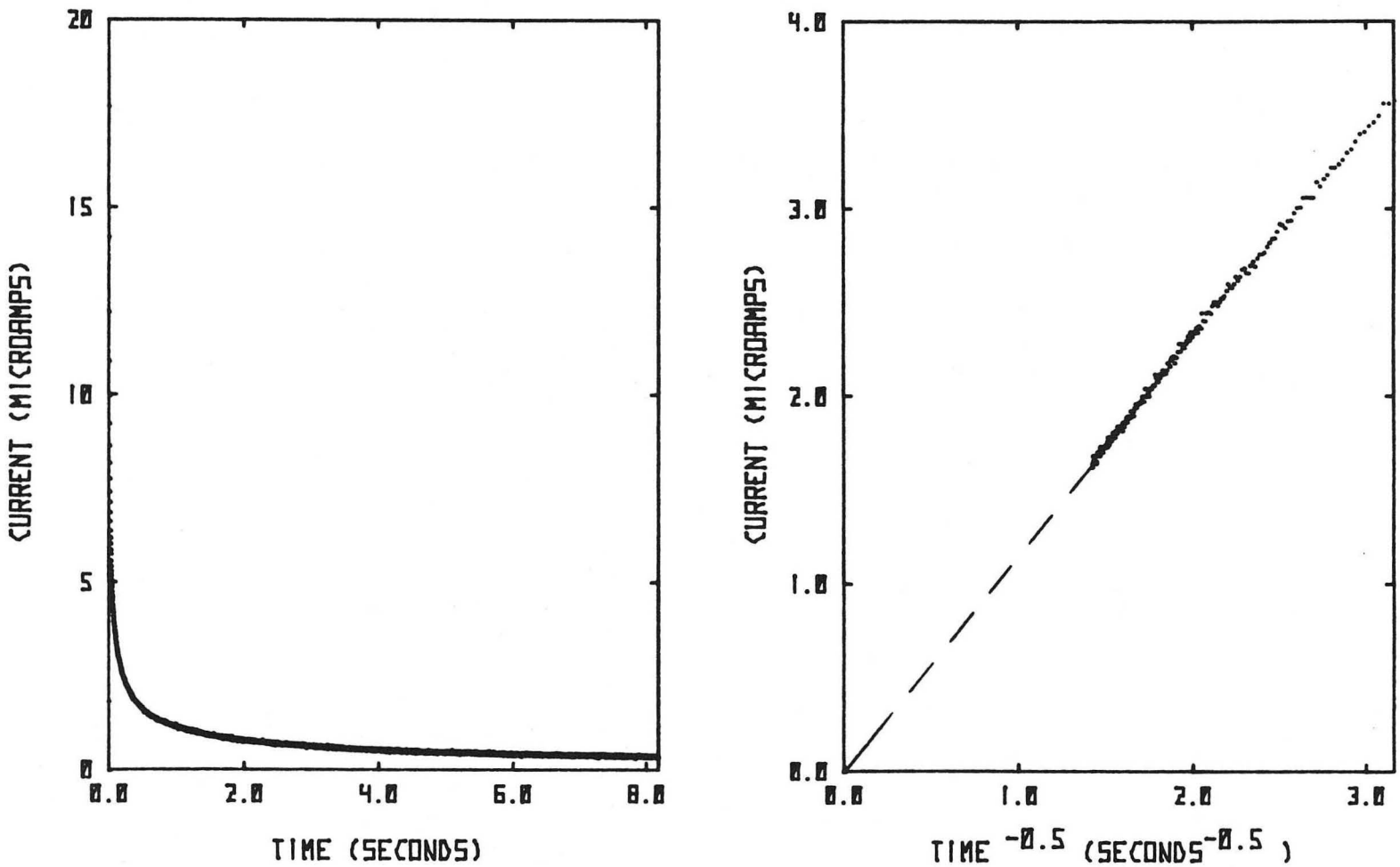

XBL 836-10387

Figure 2.3.4.2 Potential step limiting current to a single segment; (A) Time on abscissa; (B) Inverse square root of time on abscissa.

value by ten. Multiplying the total electrode current in milliamps by four converts the value into milliamps per square centimeter.

In all the following graphs of current versus time the value of time equal to zero has no real significance. During the experiments current was passed for several minutes while the growth of a bubble was taking place or a steady state was being approached. Time equal to zero only indicates the beginning of data acquisition.

Bubble growth for disengagement studies could take as much as thirty minutes. During this time the primary source of mass transfer is free convection generated by a density gradient next to the electrode; which results from the reduction of ferric ions. More accurately the density gradient is generated by a decrease in the sulfate ion concentration next to the electrode as a result of electroneutrality in the solution.

In an attempt to characterize the steady-state free convection, the current to a segment and the current to an entire electrode was measured in the absence of any gas evolution. The current to a segment is given in Fig. 2.3.4.3(A). There is a periodic variation in the current, with a period of about 25 seconds. The average current is approximately 0.29 μA and the peak-to-peak height is 0.24 μA. The current to the entire electrode, shown in Fig. 2.3.4.3(B), is also periodic. Its period is 27 seconds, which is about the same as the period for the current to a segment, but the relative magnitude of the fluctuations is much less. The peak-to-peak height is 0.026 mA with an average current of 0.78 mA.

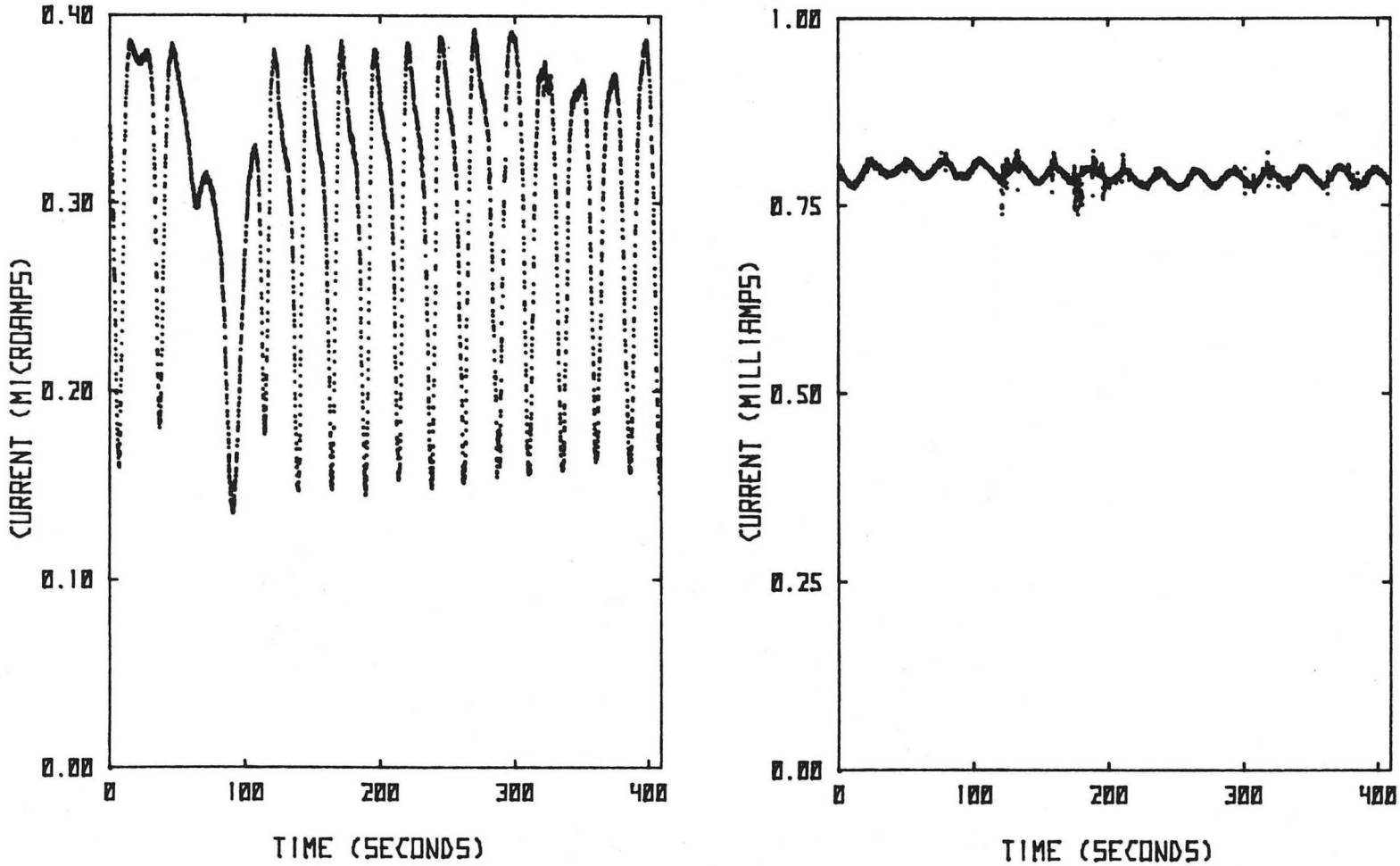

XBL 836-10385

Figure 2.3.4.3 Free convection limiting current; (A) Current to a single segment; (B) Current to the entire electrode.

The regular large, fluctuations in the free-convection limiting current were not anticipated. Small fluctuations in the limiting current to a horizontal electrode have been mentioned by Wragg (40), without explanation. From the relative magnitude of the fluctuations in the current to a segment and the current to the entire electrode, it is apparent that some mechanism for averaging the electrode current is taking place.

The ferric ions in the electrolyte were not replenished during an experiment. Therefore the bulk concentration decreased during the experiment. The rate of decrease can be estimated from the average current to the electrode. With a total current of 0.78 mA and an electrolyte volume of 12 ml, the rate of decrease was 0.03% per minute. Therefore during a 30 minute experiment there would be less than a 1% change in the bulk concentration.

The change in current to segments at various distances from the center of a bubble disengagement was obtained. Since only one segment was monitored during a bubble disengagement, several experiments were run to obtain a distribution. The results of these studies are given in Figs. 2.3.4.4-6. The diameter of the bubbles upon disengagement was approximately 1.5 mm. The relative size and position of the bubble upon disengagement is depicted by the diagram of the segmented portion of the micro-mosaic electrode. Also, the segment at which the current was monitored is indicated on the diagram by a blackened square. It should be noted that all segments monitored are well under the bubble.

The current to a segment 224 microns from the center of a bubble disengagement is given in Fig. 2.3.4.4. An increase in current of about 20% was observed. The rise time is approximately 0.2 seconds. This is much longer than the rise time of a few milliseconds for the studies with the multi-electrode cell.

At a segment 316 microns from the center of a buble disengagement, shown in Fig. 2.3.4.5, there is no increase at all. Instead there is a decrease in the current. It should be mentioned here that only increases in the current were observed with the multi-electrode cell.

The change in current 400 microns from the center of a bubble disengagement was obtained for two bubble disengagements. The results are given in Fig. 2.3.4.6. There is a slight increase in the current before the decrease that goes well below the initial value. The shape of the curves is similar, although their initial values are quite different. The difference in initial values of the current is a result of the fluctuations in the free convection background current.

Generally the results for the buble disengagement studies with the multi-electrode cell are significantly different from those obtained with the micro-mosaic electrode. The overall enhancement effect is much less for the micro-mosaic electrode. Indeed, a decrease in the current was noted for some segments.

2.4 Mass-Transfer Studies with the Micro-Mosaic Electrode Coupled to a Data Acquisition and Control System.

2.4.1 Description of Data Acquisition and Control System

A data acquisition and control system was assembled and the software developed for the micro-mosaic electrode cell. The system is

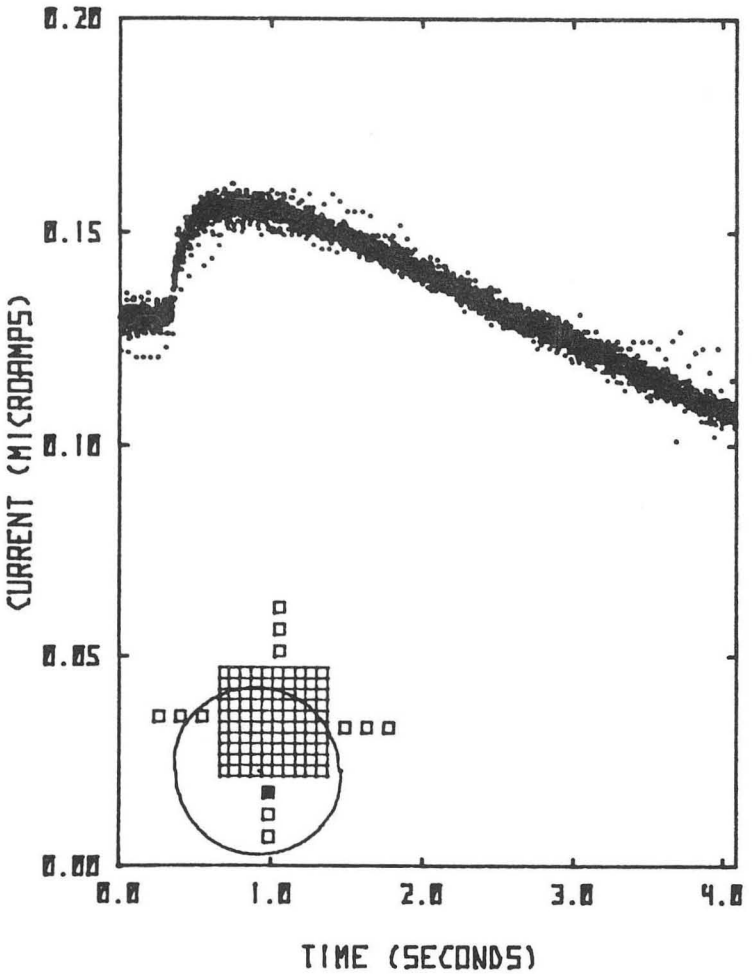

Figure 2.3.4.4 Limiting current to a segment 224 microns from the center of a 1.53 mm diameter bubble disengagement.

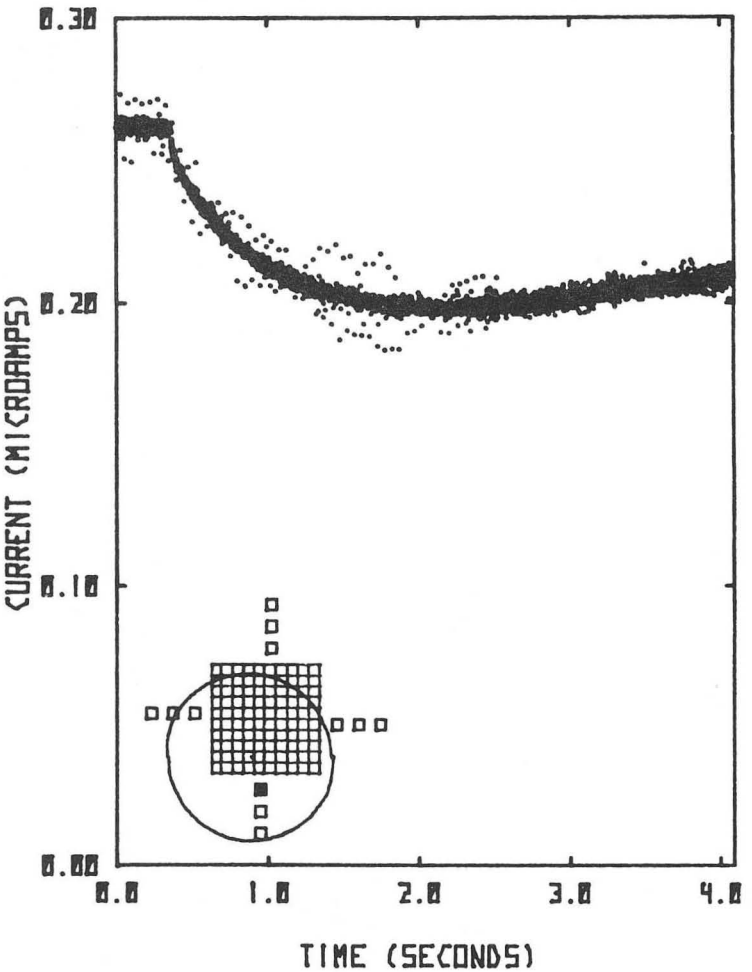

XBL 836-10383

Figure 2.3.4.5 Limiting current to a segment 316 microns from the center of a 1.53 mm diameter bubble disengagement.

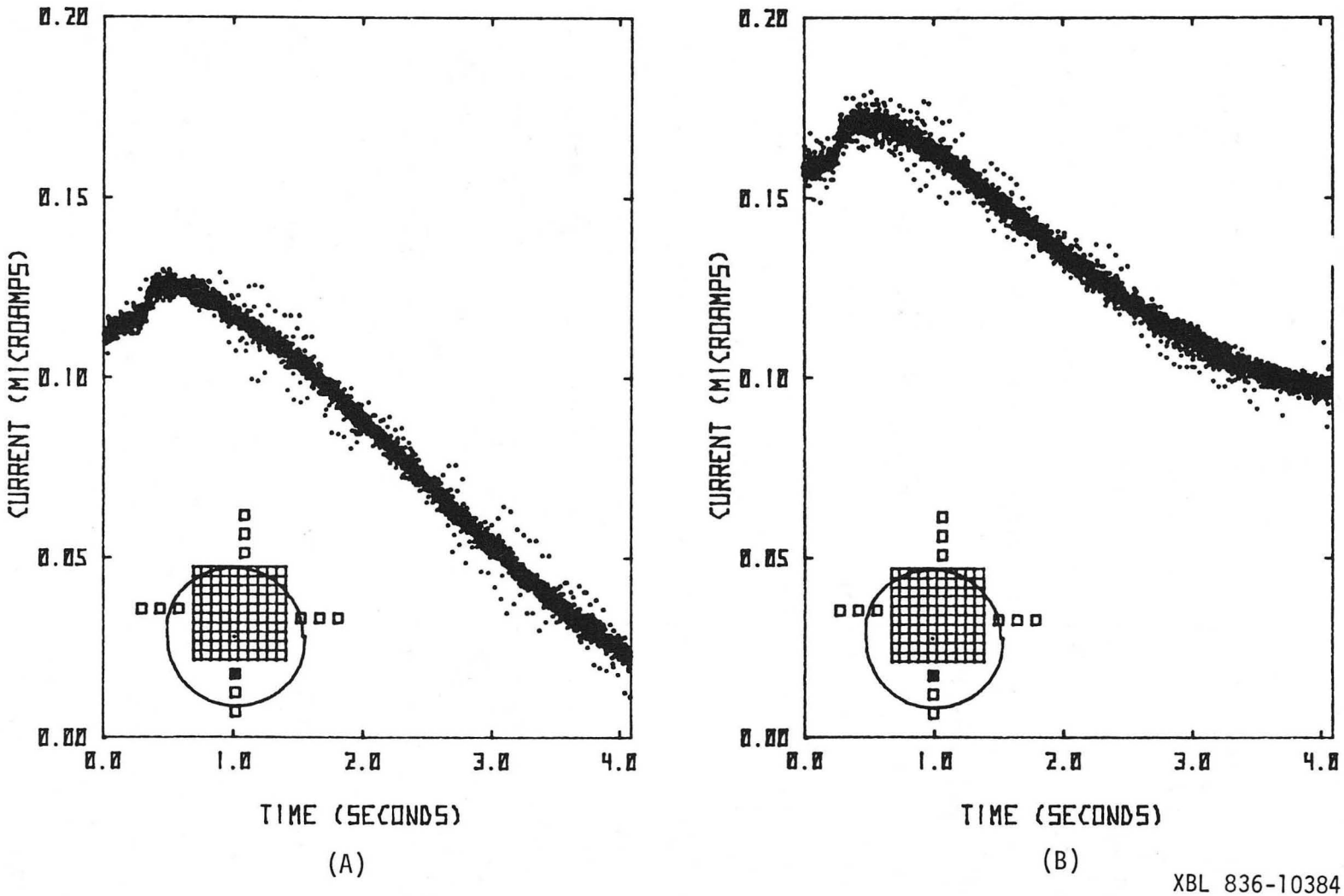

XBL 836-10384

Figure 2.3.4.6 Limiting current to a segment 400 microns from the center of a 1.485 mm diameter bubble disengagement; (A) & (B) are results from identical experiments.

capable of monitoring the current to each individual electrode segment. It also can control the growth of single or multiple bubbles during experimentation. A schematic of the entire system is given in Fig. 2.4.1.1 and the physical layout is shown in Fig. 2.4.1.2.

Connections to the individual segments of the micro-mosaic electrode cell, shown in Fig. 2.4.1.3, are made in a manner similar to those in early experiments performed with the micro-mosaic electrode and are described in Appendix C. From the electrochemical cell, the connector cables lead into a junction box. Inside the junction box, there are 10 terminal strips with 12 screw connections on each strip. The terminal strip connections are attached via a set of multi-conductor cables, to the current inputs of a 120 channel current follower. There are also two bus bars inside the box. The bus bars are connected to the two working electrode connections of the potentiostat. The wires leading from the buffer segment on the micro-mosaic electrode are attached to one bus bar. The wires connected to the segments where bubbles were to be grown are attached to the other bus bar. Each of the remaining wires leading from the other segments is attached to a connector on one of the terminal strips. All the wires are color coded and the connections are numbered. These are given in Appendix E.

Two different potentiostats were used for the experiments. A Pine potentiostat, which is described in Section 2.2.2, was used for the experiments in which bubbles were generated. A Princeton Applied Research potentiostat (173) was used in the experiments in which only a single, working-electrode potential was needed.

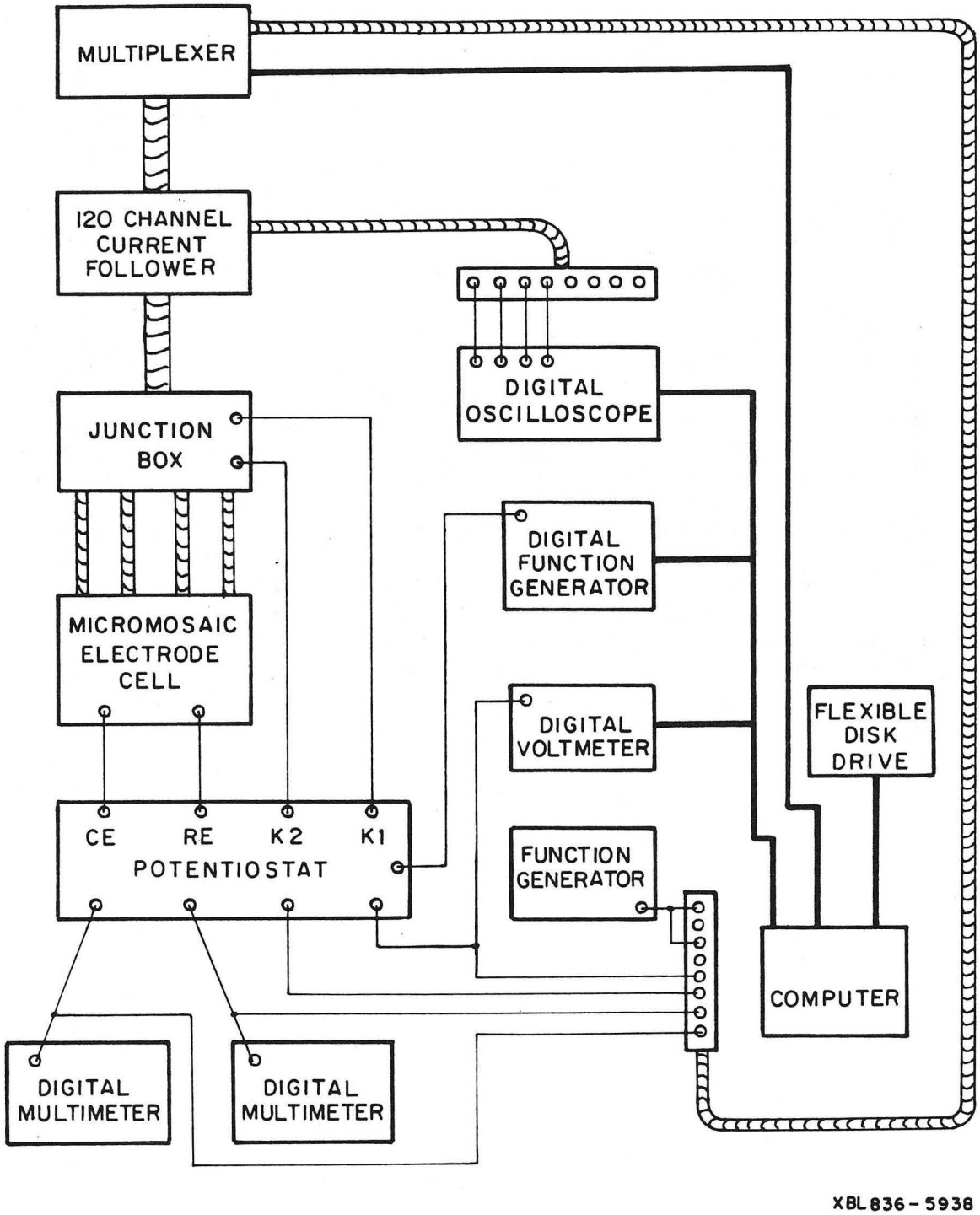

Figure 2.4.1.1 Instrumentation for data acquisition and control system.

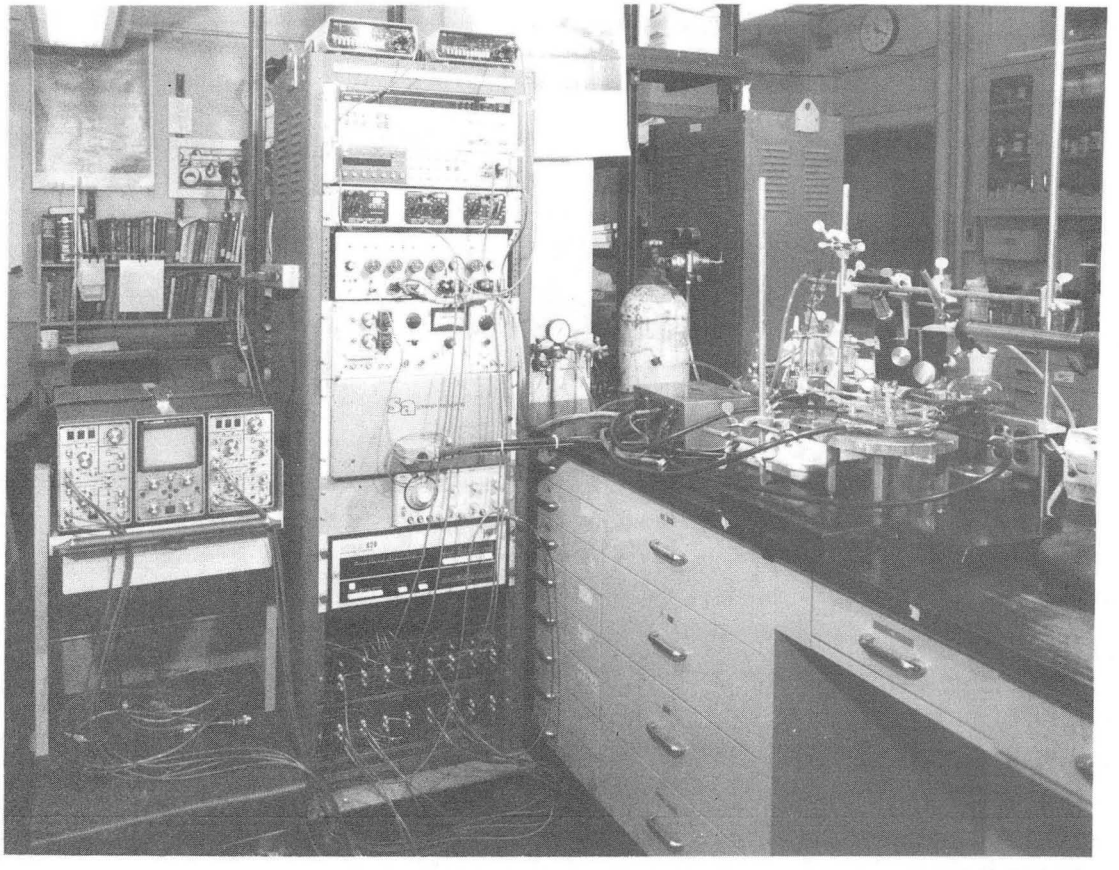

CBB 820-09963

Figure 2.4.1.2 Data acquisition and control system for micro-mosaic electrode cell.

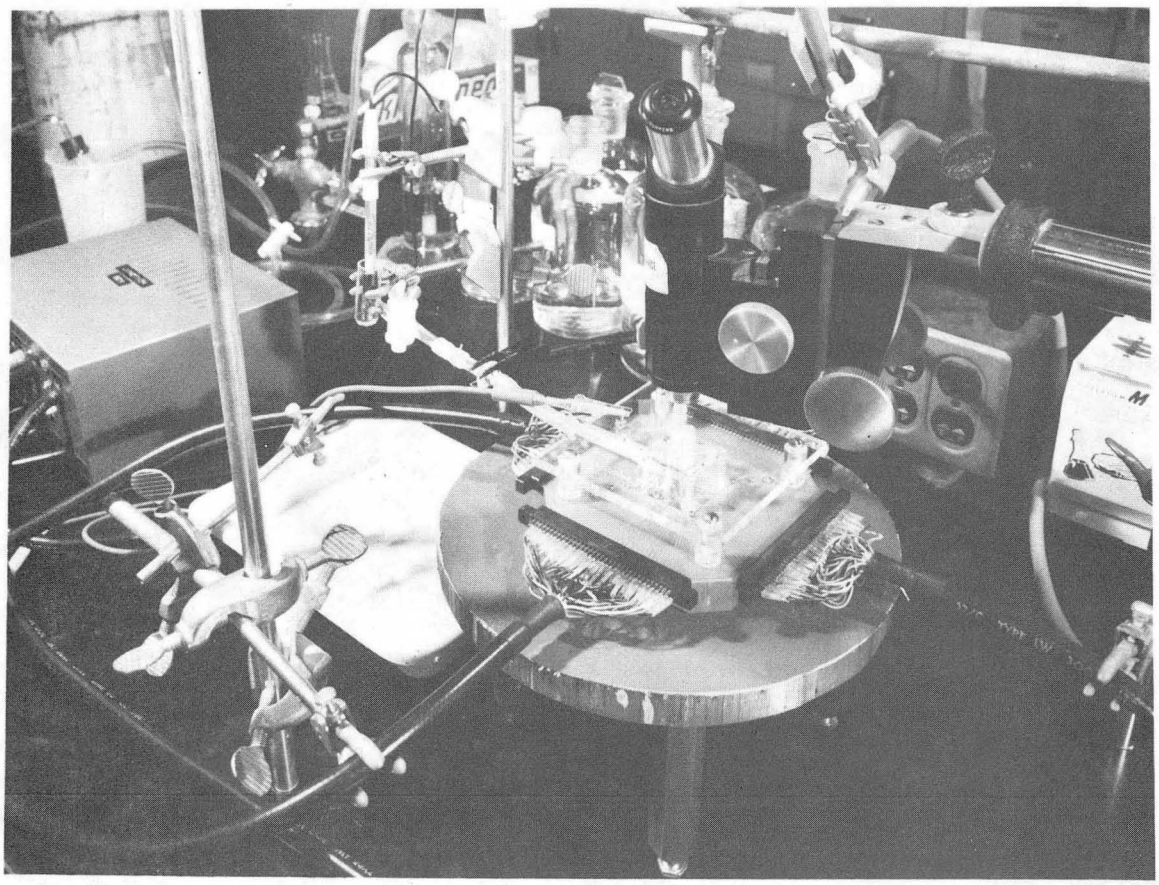

CBB 820-09965

Figure 2.4.1.3 Micro-mosaic electrode cell connected to the junction box for the data acquisition and control system.

The 120-channel current follower was designed specifically for use with the micro-mosaic electrode. It was designed and built by Scribner Associates, according to the requirements of the micro-mosaic electrode. The common of the system can be floated away from ground, but for the experiments it was connected to the ground of the potentiostat. The current-to-voltage conversion for each channel during the experiments was 1.0 μA/volt. This can be changed to 0.1 μA/volt. Further details on the multi-channel current follower are in the instruction manual.

All the voltage outputs from the 120-channel current follower were connected to a Neff Series 400 multiplexer (System 620). The number of multiplexer input analog channels can be adjusted from 16 to 256 by units of 16. This is done by adding 16 channel multiplexer cards to the system. Eight cards with 10 Hz filters on the inputs (620450) were used during the experiments, giving a total of 128 available channels. A single card with direct inputs (620451) is also available for use with the multiplexer. The eight channels, not attached to the current follower, are connected to a set of BNC connectors. Two of these channels were used for timing function inputs. Four more were used to monitor each of the working electrodes' current and potential on the potentiostat. The sampling rate of the multiplexer can be set between 1.25 kHz and 10 kHz. The gain can be adjusted from 5 mV to 10.24 volts full-scale. The data are transferred over a digital interface to a computer. The computer also controls

the total number of channels scanned along with the gain. More information on the multiplexer and also a description of how the system can be altered according to experimental needs is in Appendix E.

Eight of the current-follower outputs are attached to BNC connectors as well as to the multiplexer. The connectors can be used to monitor the current to a particular segment by an external device. A Nicolet digital oscilloscope (4094) was used to monitor four segments during experiments. After completion of the experiment, the data were transferred to a computer through a digital interface bus. The digital oscilloscope was used in the same manner as described for the earlier experiments. Besides its capability to obtain data much faster, it also served as a check for the multiplexer.

A triangular wave voltage function was supplied to two multiplexer channels by an Interstate Electronics Corporation Series 70 function generator (F77). The frequency of the wave was set to generate two complete waveforms in the total amount of time data was saved by the computer. The amplitude was set to be less than the full-scale voltage on the multiplexer. The computer used the waveform as a clock for the other data obtained from the multiplexer.

The total current to the segments where bubbles were grown was monitored with a Hewlett Packard digital voltmeter (3455A) attached to the potentiostat. The voltage was monitored by the computer, through a digital interface bus, in the experiments where bubble growth was controlled. Two Keithley digital multimeters (173A) were attached to the potentiostat to monitor the current to and potential of the buffer segment of the micro-mosaic electrode.

The analog signal from a Hewlett Packard digital function generator (3325A) was connected to the summing potential input of the working electrode on the potentiostat used for bubble growth. The function generator was used as a digital-to-analog (D/A) converter allowing the computer to control bubble growth.

The heart of the system, a Hewlett Packard desktop computer (9825T) is pictured in Fig. 2.4.1.4. Special attention should be paid to the "hard-working" author at the keyboard. The computer serves as a controller on an interface bus (HP-IB). The digital oscilloscope, digital voltmeter, and digital function generator are controlled by it. There is another interface for the multiplexer and one for the Hewlett Packard flexible disk drive (9885M). The Hewlett Packard digital plotter (9862A) is interfaced to the computer during data retrieval and plotting.

During an experiment, data acquisition by the multiplexer is initiated from the keyboard of the computer. The data are then stored in a memory buffer on the computer. When the buffer is loaded, the data are discarded until the computer is directed to save it. The computer can be directed to save the data from the keyboard or an internal trigger. The internal trigger is set by a sudden change in the current to segments where gas is being evolved. Once triggered, the amount of data saved by the computer is optional. If the memory of the computer is to be loaded only once, then data are saved starting one half second before triggering plus data taken thereafter up to a total of about 3 to 30 seconds depending on the scan rate set on the multiplexer. If the memory of the computer is to be loaded multiple

CBB 820-9967

Figure 2.4.1.4 Computer, digital plotter, and flexible disk drive for the data acquisition and control system.

times, the data are loaded onto a flexible disk after which the computer stores more data. This process is continued until data are saved for a set length of time. It should be noted that data are not saved while the computer is loading the memory onto a flexible disk, which takes a few seconds.

Control of the bubble growth is accomplished by the computer through the digital voltmeter and function generator. The current to the segments where gas is being evolved was kept at set value with a proportional-derivative-integral (PID) control loop (38) programmed on the computer. The controlled variable is the voltage diference between the segments where gas is evolved and the other segments. For a voltage difference less than a set value, the voltage is set according to the following function of time:

$$V = k_c \left[I + \tau_D \frac{dI}{dt} + 1/\tau_I \int_0^t I dt \right] + V_S .$$

If the voltage difference needed to maintain the constant current is greater than a set maximum value, the maximum value is used. If there is a sudden change in the current, greater than a set value, the voltage difference is set to zero. The difference can be set to zero from the keyboard of the computer also.

A "hard-copy" of the experimental results can be obtained through the digital plotter. The current to a segment can be plotted as a function of time for a given segment or position on the electrode at a

set time. The current can also be plotted against the sequence number in which the data was taken.

A listing and a more complete description of the computer program is given in Appendix F. More details on the system can be found in Appendix E.

2.4.2 Results and Discussion

The data acquisition and control system was used to extend the early studies with the micro-mosaic electrode and to investigate other bubble phenomena. All studies were conducted with the electrode oriented horizontally.

The data acquisition system is capable of producing an immense amount of data. It would not be possible or even desirable to include in this work all the data obtained. The results from the experiments have been examined and only selected typical and/or especially interesting data are included here. Generally data are presented in the form of a graph of the current to a segment versus time. The segment for which the data were obtained is indicated by numbering the curve on the graph, according to a numbering system described in Appendix C. The size and position of bubbles on the electrode are given in separate figures for the studies on bubble phenomena. The segment in the first row and first column of the matrix of segments (i.e., segment number [1,1]) is in the upper left hand corner of the diagrams. Rows then go across the page and columns go down the page.

It should be noted that the ordinate on the graphs of current versus time has only positive values on some graphs and both positive and negative values on others. Generally only positive values will appear on the ordinate. For these graphs a positive value indicates a cathodic current. On graphs with both positive and negative values, a cathodic current is negative and a positive value indicates an anodic current.

Free-Convection Studies

The fluctuations in the free-convection limiting current to the segments were studied further. Upon repeative experiments it was observed that the current to any given segment would fluctuate with a very regular pattern during some experiments and in others exhibited no detectable pattern. Indeed the fluctuations would almost disappear at times. This irregular fluctuation in the current will be referred to as chaotic behavior. This fact made understanding the physics of the phenomena next to the electrode quite difficult.

A comparison of the regular fluctuations in the current to various segments for different experiments revealed that the fluctuations varied in shape. The current curves can be placed in one of two different classifications, either a symmetric or an asymmetric-form. A curve belonging to each classification is shown in Fig. 2.4.2.1. The asymmetric fluctuations are much more common than the symmetric fluctuations. Generally the symmetric fluctuations occurred near a region on the electrode where chaotic behavior was prevalent.

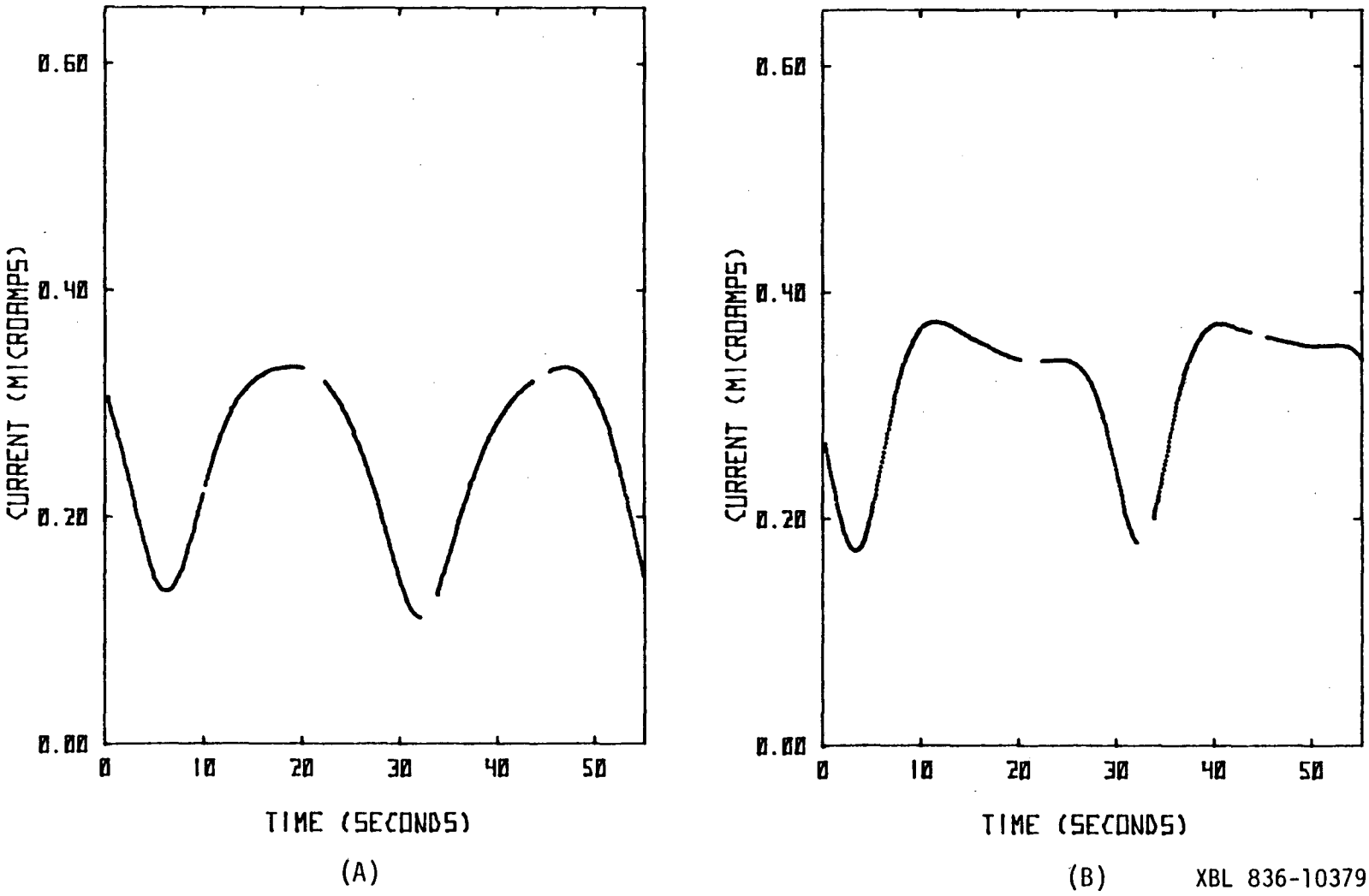

Figure 2.4.2.1 Free convection limiting current to a segment; (A) Symmetric curve shape; (B) Asymmetric curve shape.

The period of the regular fluctuations in the current to various segments is relatively constant with an average value of 28.8 seconds. Nearly all the periods measured are within two seconds of the average. Although the period of the fluctuations remains constant, the fluctuations of neighboring segments are not in phase with each other. An example is given in Fig. 2.4.2.2. In this figure the current to a segment is compared to the current to two other adjacent segments. It is seen that the current to each of the adjacent segments is out of phase with the other segment, but that the amount of phase difference is dependent on the relative position of the segments on the surface.

In one of the free convection experiments there were regular fluctuations in the current to all the segments. The phase difference in seconds was measured for all the segments relative to one segment. The fluctuations in the current to one segment which was chosen as a basis were ahead of the other segments in the matrix. The phase difference is reported as seconds of phase lag behind the one segment. The results for two rows in the matrix of segments is given in Fig. 2.4.3.3(A). The two rows plotted contain the segments of the least and greatest phase lag. An almost linear relationship between the phase lag and the column distance is apparent. It is even more instructive to see the results plotted as lines of constant phase lag over the surface formed by the matrix of segments, shown in Fig. 2.4.3.3(B). The lines of constant phase lag are plotted every two seconds; the arrow points in the direction of increasing

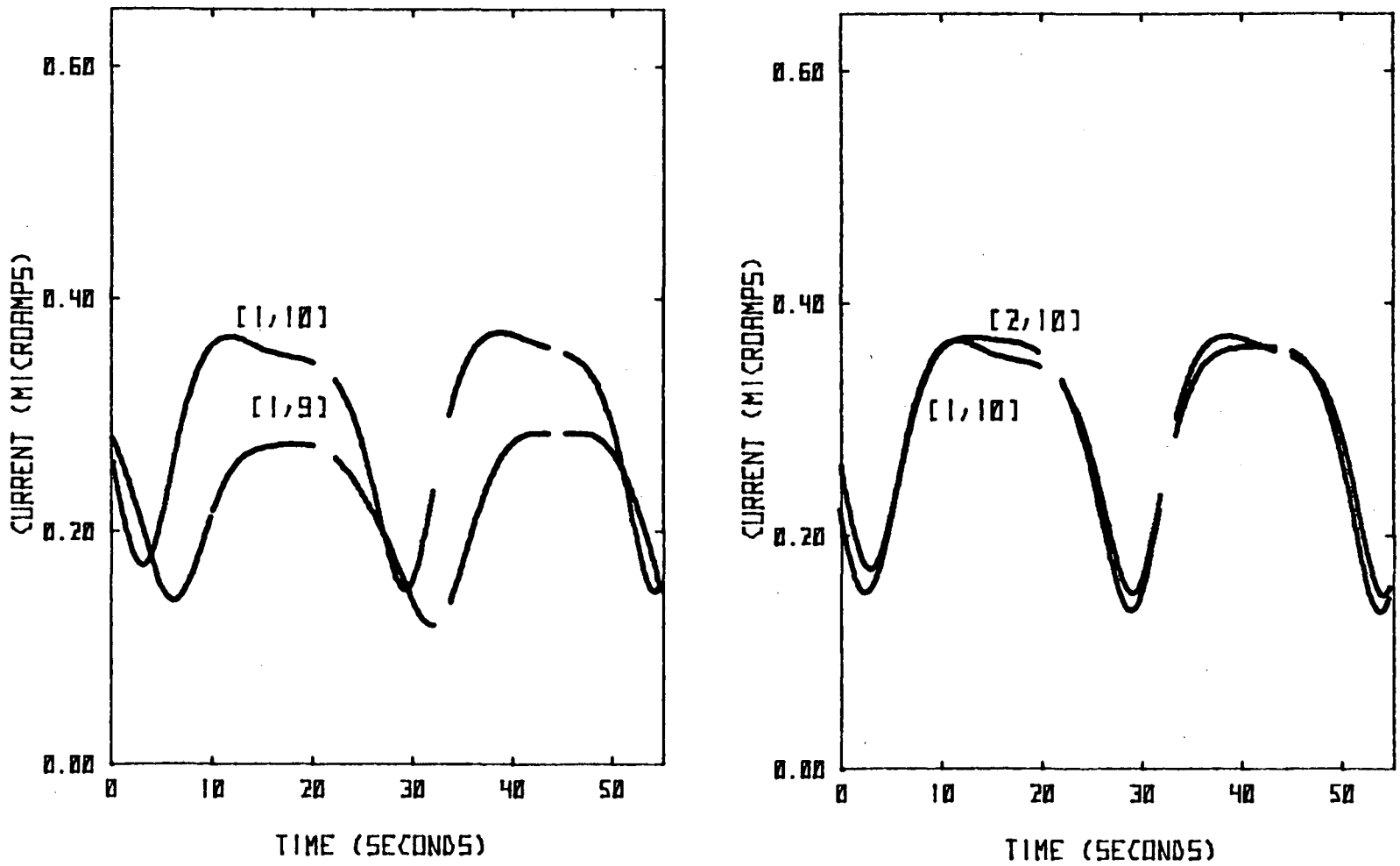

XBL 836-10377

Figure 2.4.2.2 Free convection limiting currents to adjacent segments; (A) & (B) are both results from the same experiment.

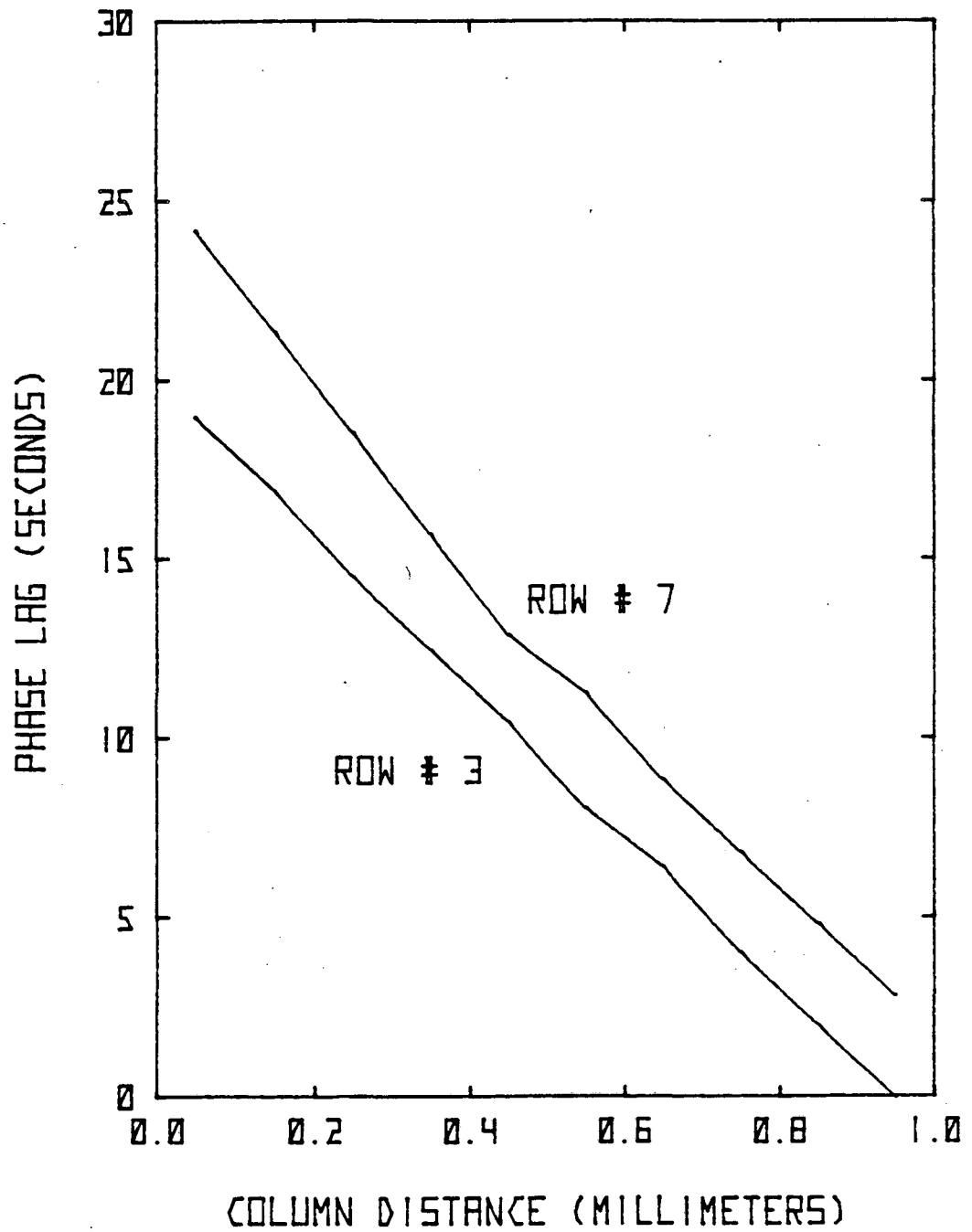

XBL 836-10461

Figure 2.4.2.3 (A) Phase lag of the fluctuations in the free convection limiting current to segments.

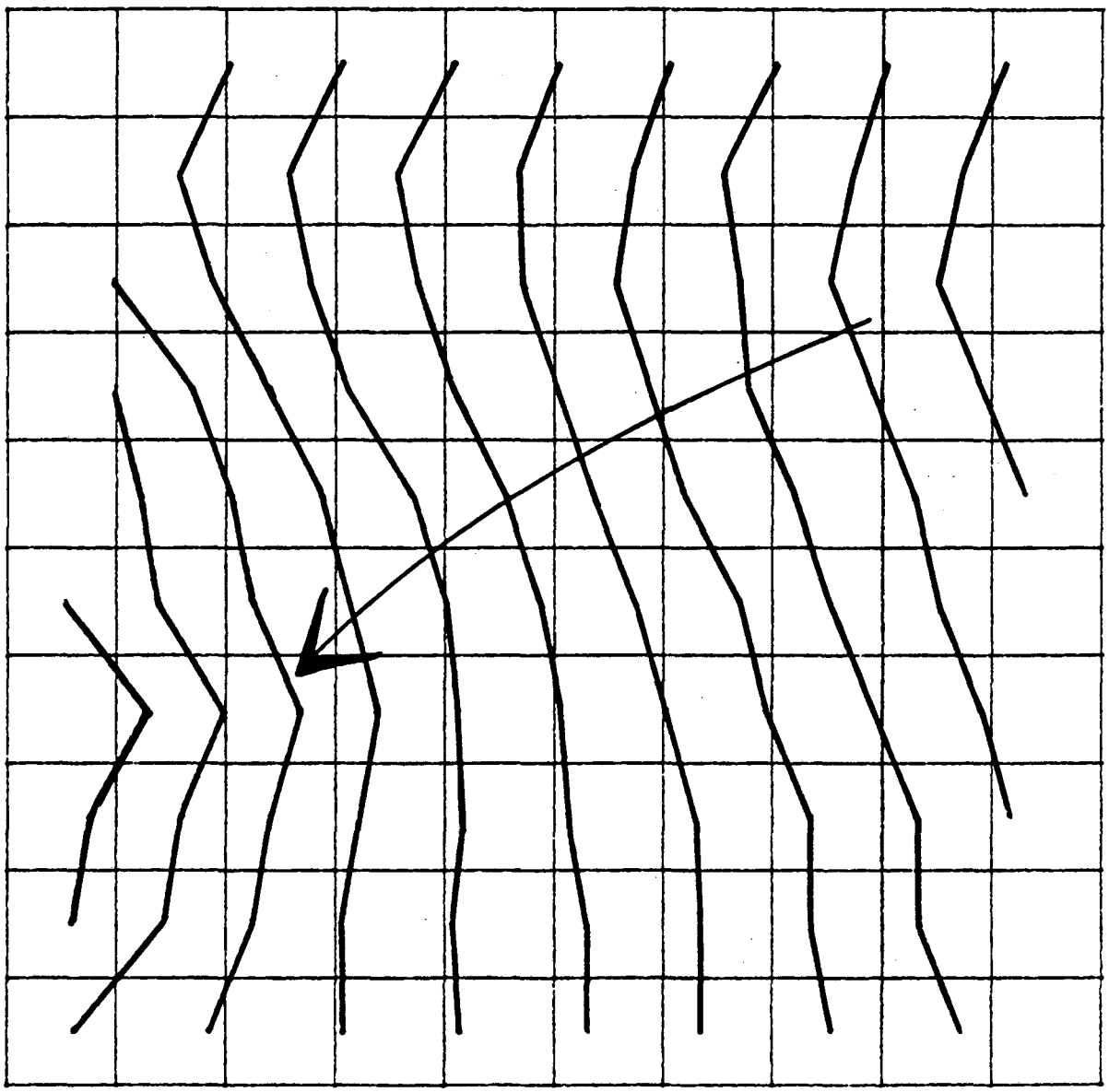

XBL 838-6114

Figure 2.4.2.3 (B) Lines of constant phase lag of the fluctuations in the free convection limiting current to the matrix segments; lines are plotted every two seconds with arrow indicating direction of increasing phase lag.

phase lag. This plot indicates that there is some regular fluid flow across the face of the electrode. Furthermore, from the distance between the lines of constant phase lag a velocity could be determined of 40 μm/sec.

The periodicity in the regular fluctuations in the current to a segment indicates a repetitive, fluid-flow pattern next to the electrode. The size of this characteristic, fluid-flow pattern can be estimated from the period of the fluctuations and the velocity at which it travels across the surface. By multiplying the average velocity of the fluid-flow pattern by its average period, one obtains a characteristic length of 1.1 mm.

The results of one of the free convection experiments exhibited a chaotic behavior of the current to segments in a region several hundred microns wide in the middle of the matrix of segments. Regular fluctuations in the current to segments were observed on either side of the chaotic region. Comparing the fluctuations in the current to two segments on one side of the region to two segments on the other side is quite revealing. An example of this is given in Fig. 2.4.2.4. By noticing the relative position of the segments and also their phase difference, it is clear that the fluid flow pattern moving across the surface is traveling in opposite directions towards the chaotic region on opposing sides of the region. A sample for comparison of the current to segments which bridge the region of chaotic behavior is given in Fig. 2.4.2.5. The current to segments in a row next to the

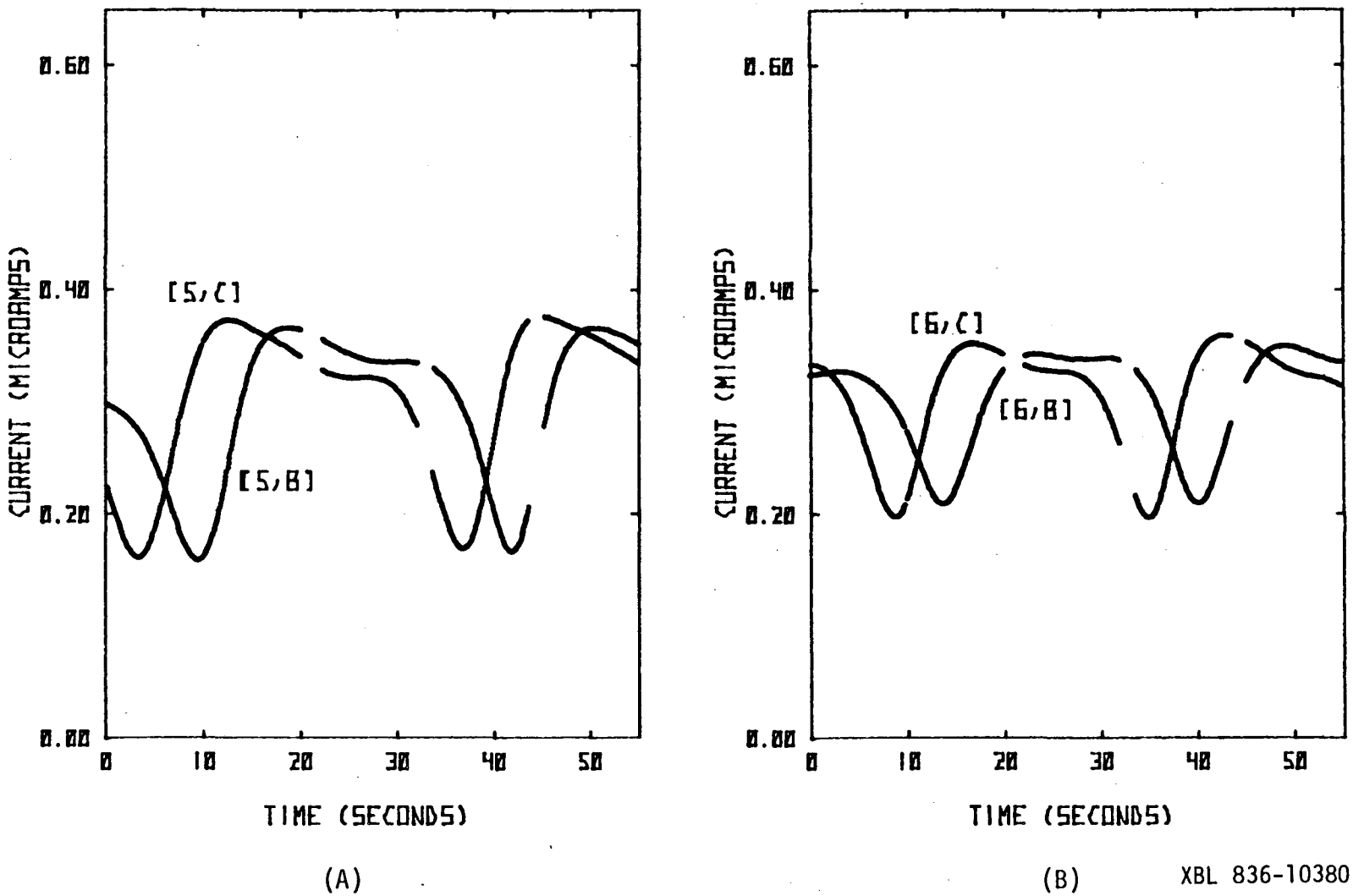

Figure 2.4.2.4 Free convection limiting current to segments; (A) & (B) are results from the same experiment.

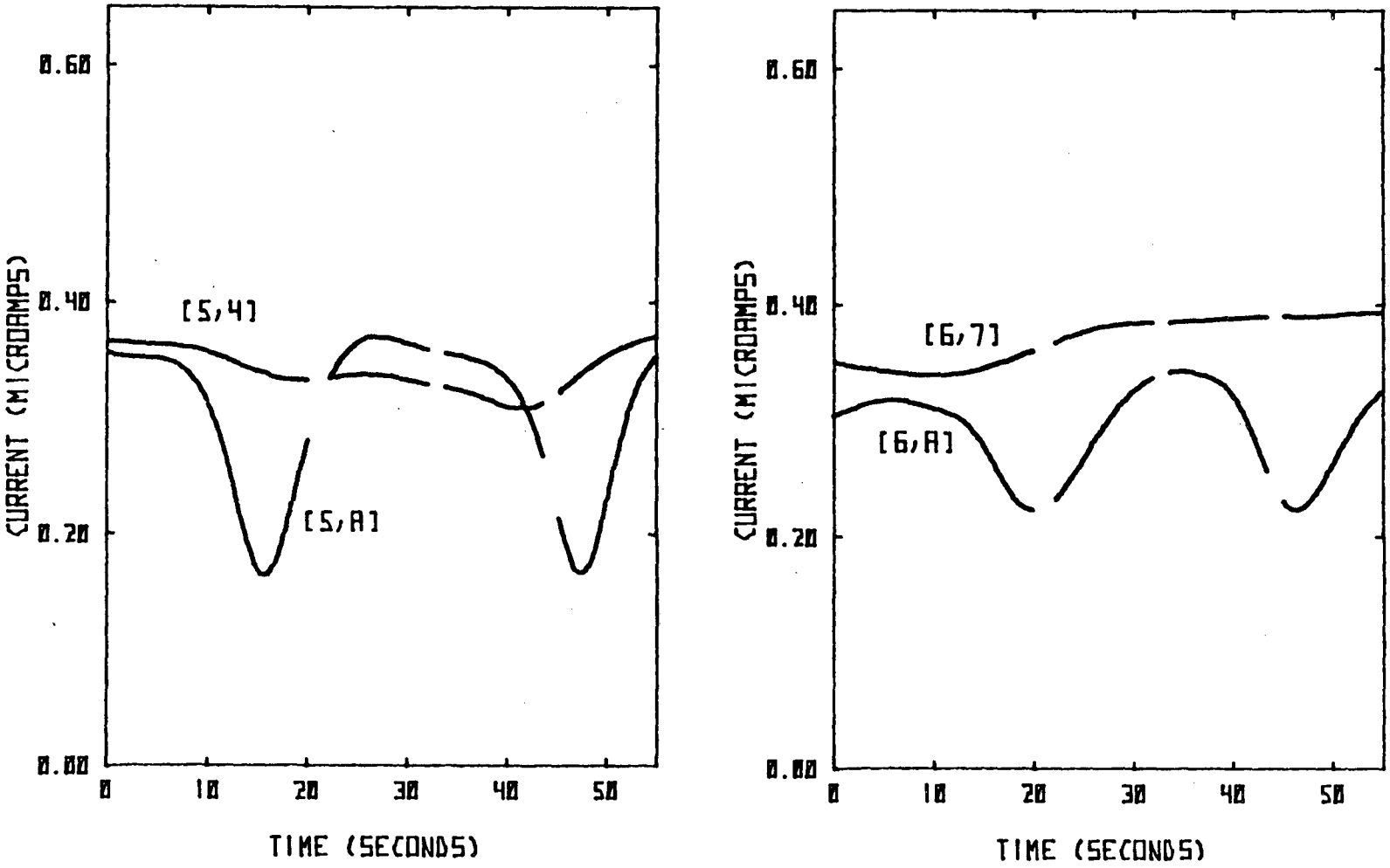

XBL 836-10381

Figure 2.4.2.5 Free convection limiting current to segments; (A) & (B) are results from the same experiment.

region of chaotic behavior indicates a smooth transition of the flow traveling in opposite directions. This is shown in Fig. 2.4.2.6. Generally the chaotic behavior is much more prevalent than the smooth transition, but both do occur.

Making further conclusions about the free-convection flow from the experimental results of these limiting current studies would be too speculative at this stage. However; by comparing this work to previous studies of free convection at horizontal surfaces, some postulates about the fluid flow can be made. One of the most extensive and earliest studies of free-convection mass transfer at horizontal surfaces was performed by Fenech (41), (42). Using an oblong rectangular electrode that could be considered infinite in one dimension and finite in the other, which was embedded in a coplanar insulating wall, several conclusions were made about the nature of the fluid flow above the electrode when edge effects are important. Basically the flow could be broken down into two types; a cellular flow occuring next to the electrode and a larger secondary circulating flow in the bulk electrolyte. Furthermore it was observed that the cellular flow was affected by the secondary flow within a few centimeters of the edge of the electrode. In the absence of any edge effects only a cellular flow, called Benard cells (43), would be expected. A plume flow (43) would develop from a point source (i.e., a situation where only edge effects are present). Therefore the combination of these flows over a finite electrode would seem reasonable.

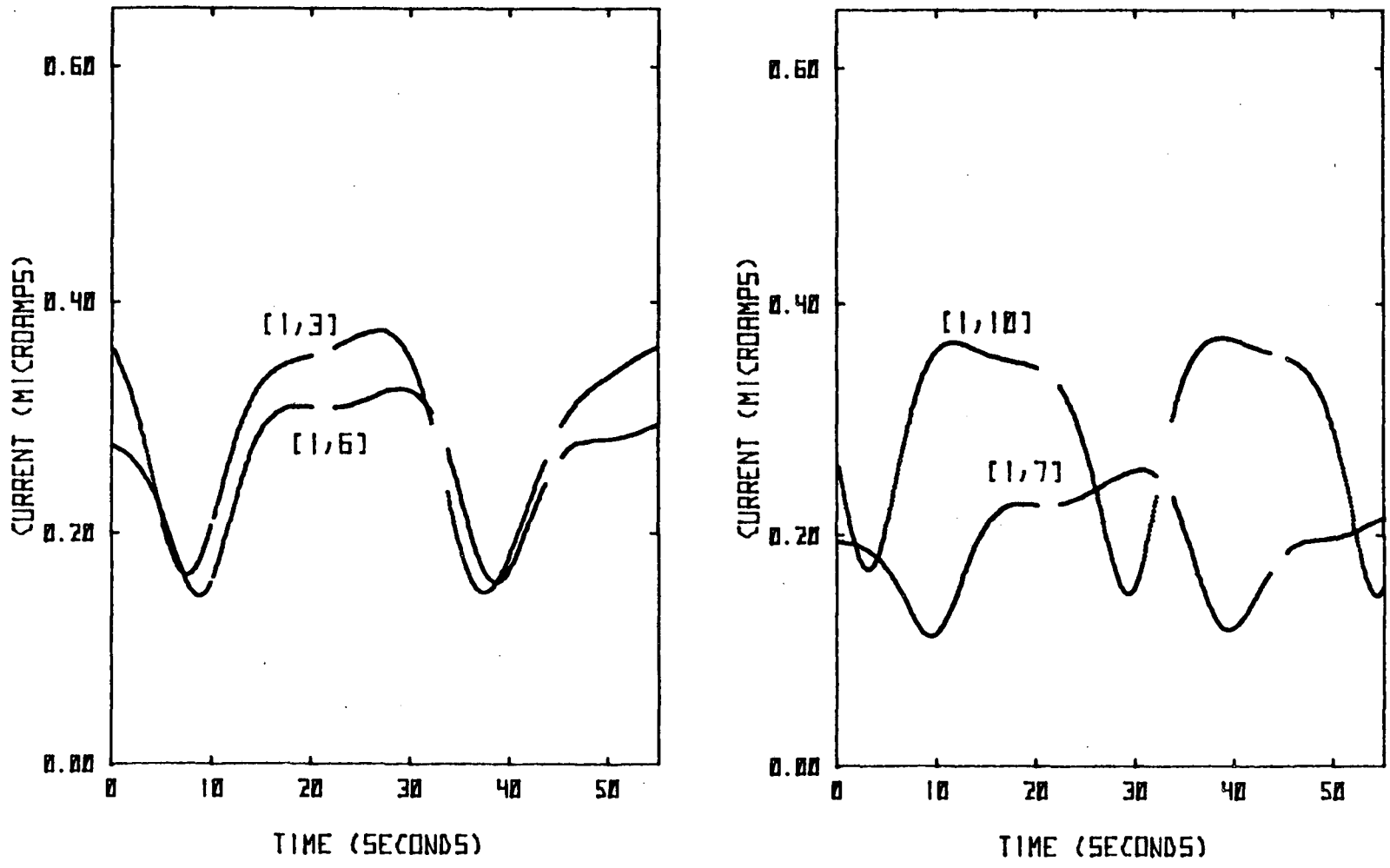

XBL 836-10378

Figure 2.4.2.6 Free convection limiting current to segments; (A) & (B) are results from the same experiment.

The micro-mosaic electrode is the two dimensional analogy to Fenech's electrode in that edge effects occur across the electrode as a result the electrode being finite in both dimensions. The secondary (plume) flow for the two cases was hypothesized by French (42) and is shown in the top two schematics of Fig. 2.4.2.7. The predicted flow for four sides is also shown. The pattern of the resulting cellular flow cannot be determined, but it does appear to be occuring and traveling across the surface at about 40 μm/sec. Furthermore the characteristic length in one dimension is about one millimeter.

Limiting Current Studies During Bubble Growth

The limiting current distribution surrounding a bubble during growth was measured. The data was obtained over a 20 second period after the bubble had been growing for several minutes. The bubble had attained a diameter of 0.9 mm, which did not change significantly during the data acquisition period. The relative size and position of the bubble on the electrode is depicted in Fig. 2.4.2.8.

The current to a segment 900 microns from the center of the bubble is shown in Fig. 2.4.2.9 (A). This segment is 450 microns away from the edge of the bubble. The curve exhibits the "normal" free convection limiting current. Closer to the edge of the bubble, smaller amplitude fluctuations in the current are observed. This is seen in Fig. 2.4.2.9 (B). Whether the decrease in amplitude can be attributed to the presence of the bubble cannot be determined.

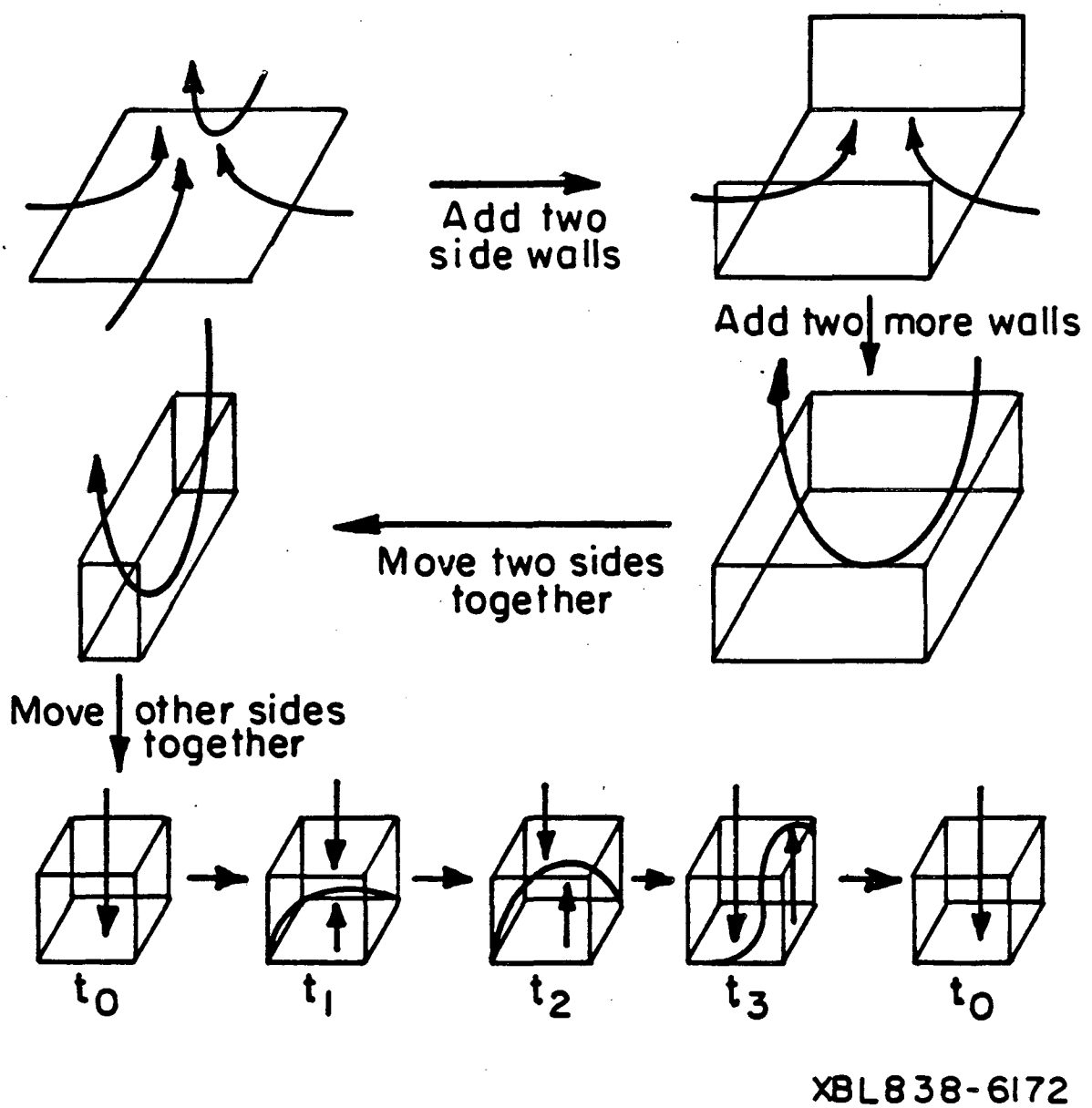

Figure 2.4.2.7 Summary of hypothesized secondary natural convection.

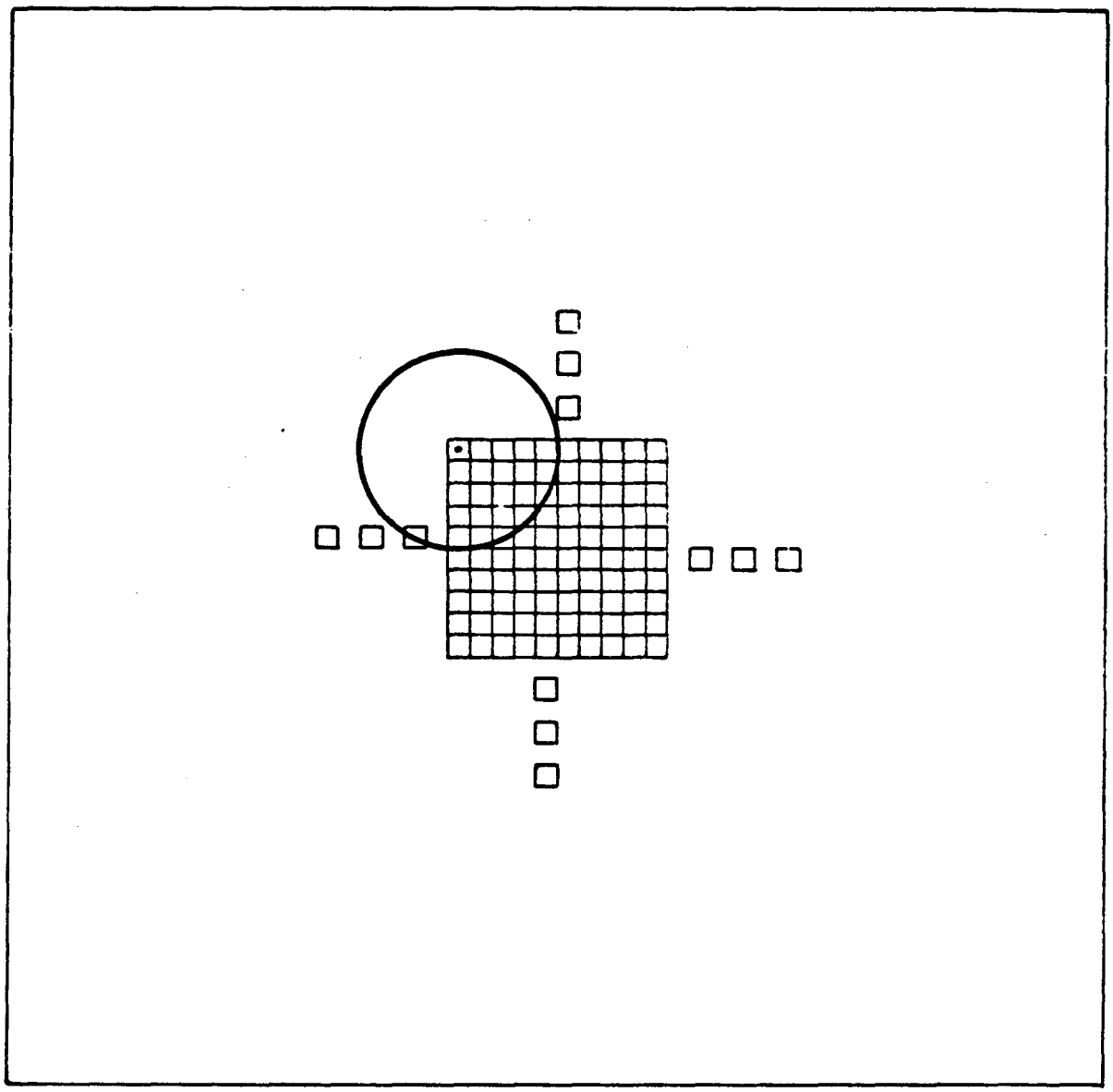

XBL838-6103

Figure 2.4.2.8 Schematic of the micro-mosaic electrode showing the perimeter of the bubble on the surface.

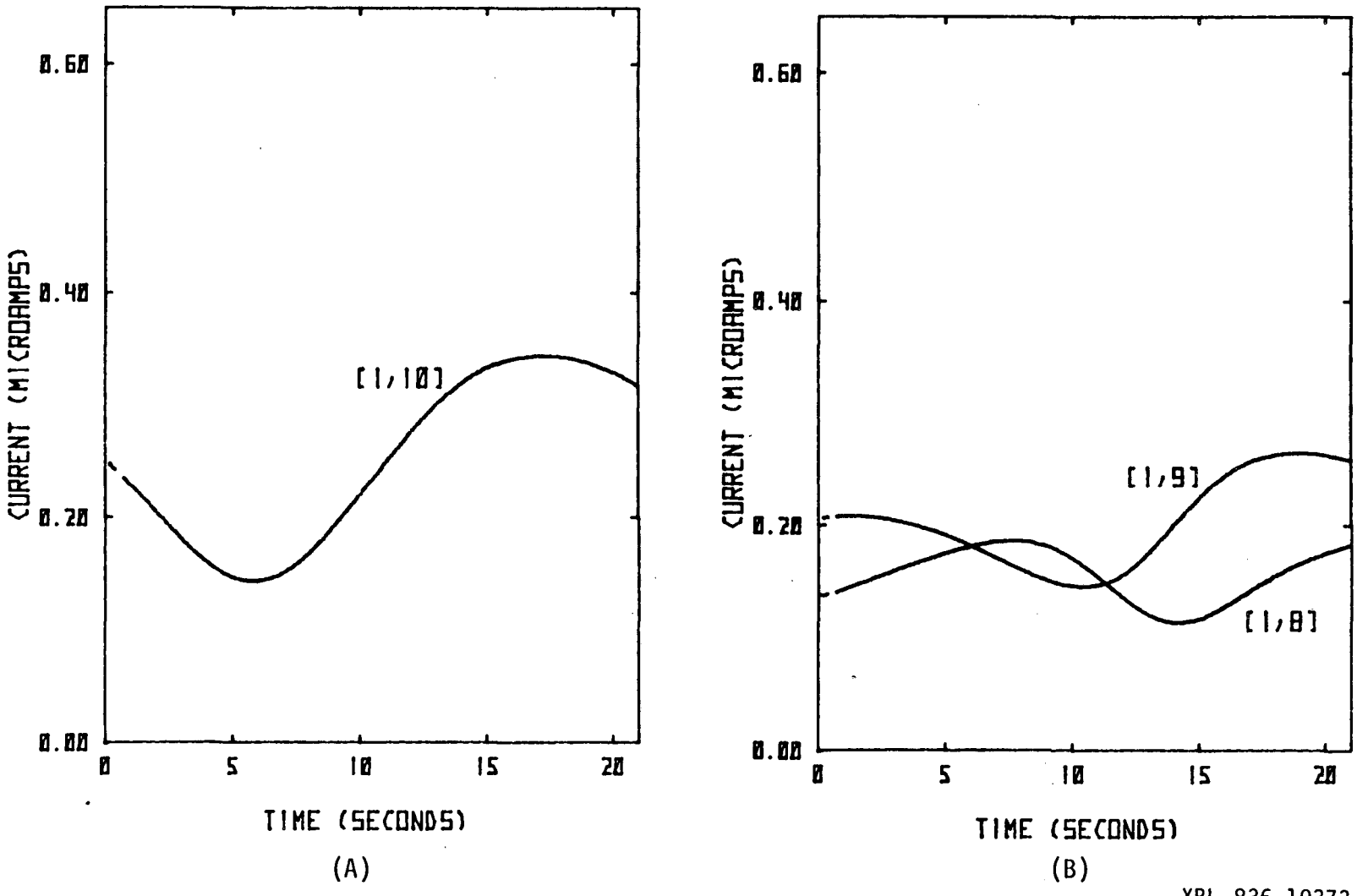

XBL 836-10373

Figure 2.4.2.9 Limiting current to segments during the growth of bubble; (A) & (B) segments are not under the bubble.

A clear transition occurs in the current to segments within 200 microns of the edge of the bubble. This is shown in Fig. 2.4.2.10 (A). The period of the fluctuations increases dramatically. The current to a segment just under the edge of the bubble is given in Fig. 2.4.2.10 (B). The larger period fluctuations seem to be quite stable at this segment. The transition in the current must parallel a transition in the free convection surrounding the bubble. Examining the current to segments well under the bubble, shown in Fig. 2.4.2.11, reveals the same large period fluctuations. A decrease in the amplitude is also evident. This is likely a result of the bubble hindering fluid flow near its base.

It is clear that the bubble has a significant effect on the free convection surrounding it. This effect appears to be limited to about one diameter from the center of the bubble. There is no reason to believe that this effect is symmetric around the bubble. In fact the nature of the free convection pointed out earlier indicates that the current distribution is asymmetric. Also the hydraulic forces on the bubble from the free convection would be asymmetric.

It was found that segments having a side or corner adjacent to a segment on which a bubble was growing had a net anodic current. An example of this is given in Fig. 2.4.2.12. The anodic current can result from a combination of two factors. The hydrogen generated at the one segment reaches the other segments and is oxidized. Another possibility in that the potential difference between the segments causes the less cathodic segments to act as bi-polar electrodes.

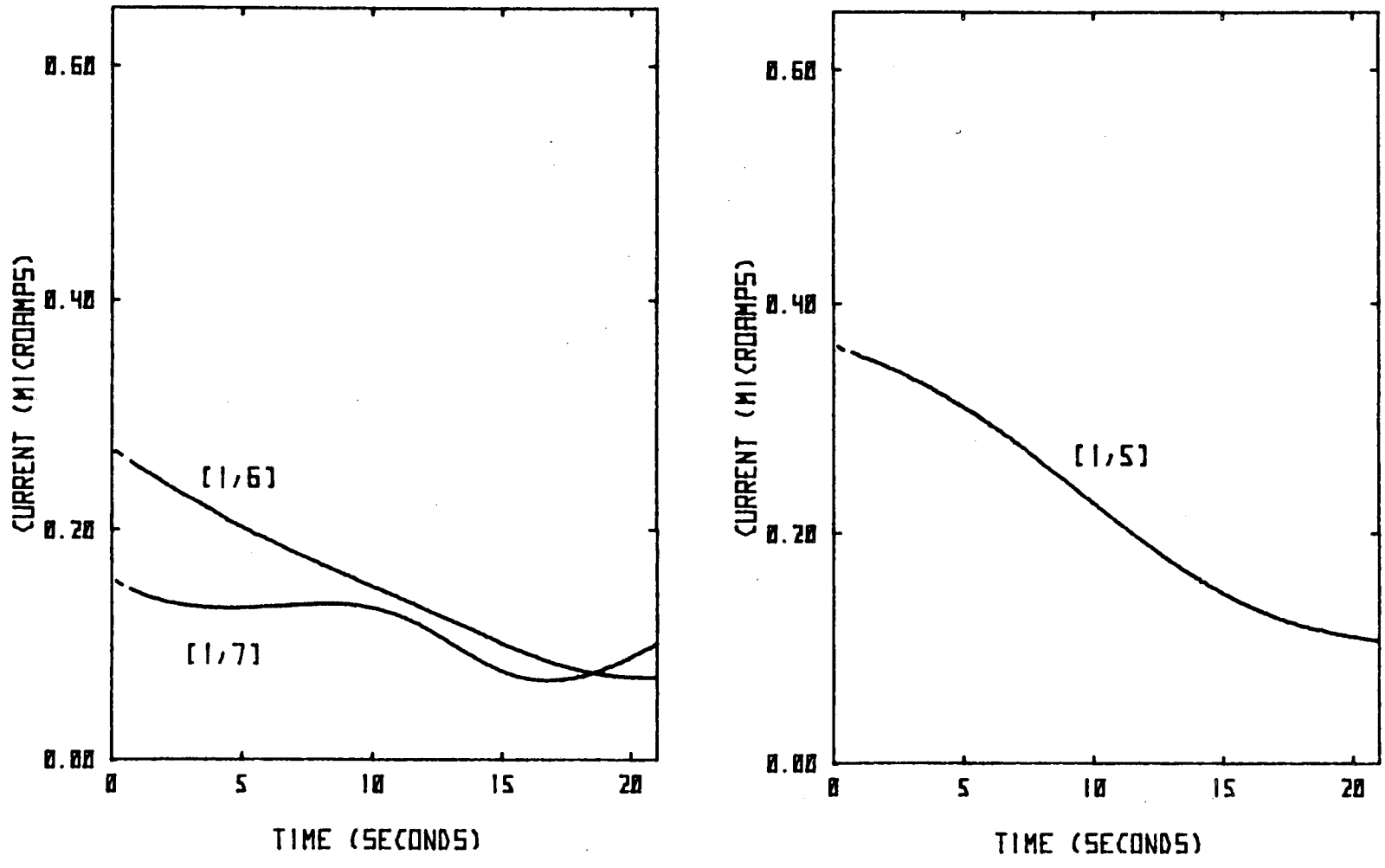

XBL 836-10374

Figure 2.4.2.10 Limiting current to segments during the growth of a bubble; (A) Segments in the transition region; (B) Segment under the outer edge of the bubble.

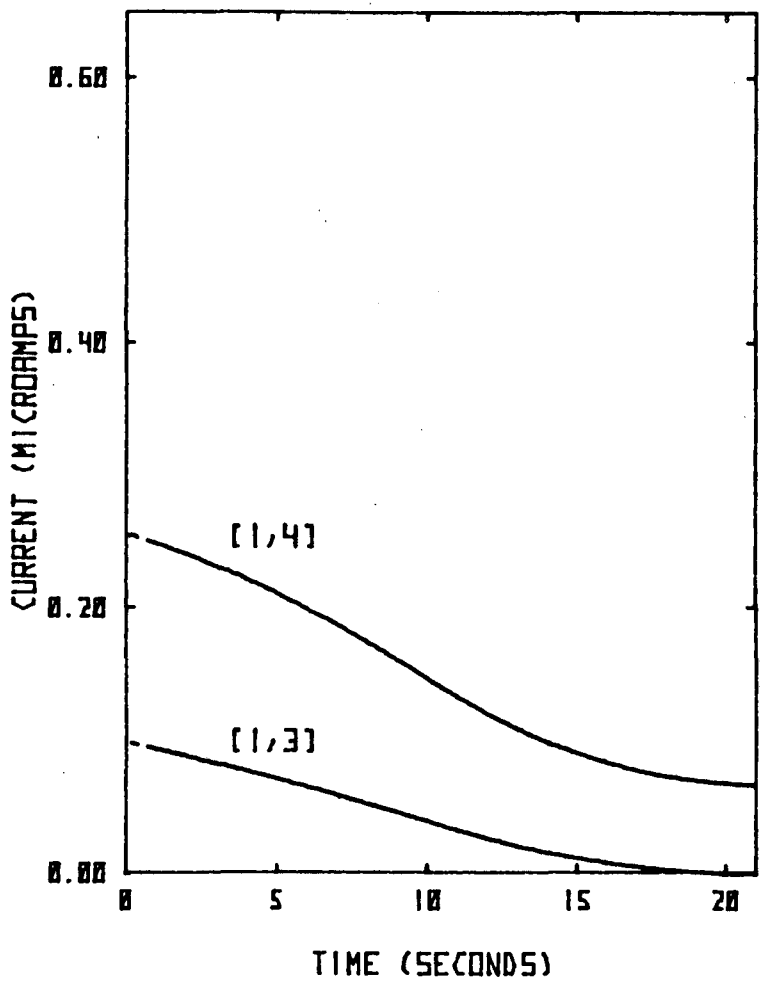

Figure 2.4.2.11 Limiting current to segments well under a bubble during its growth.

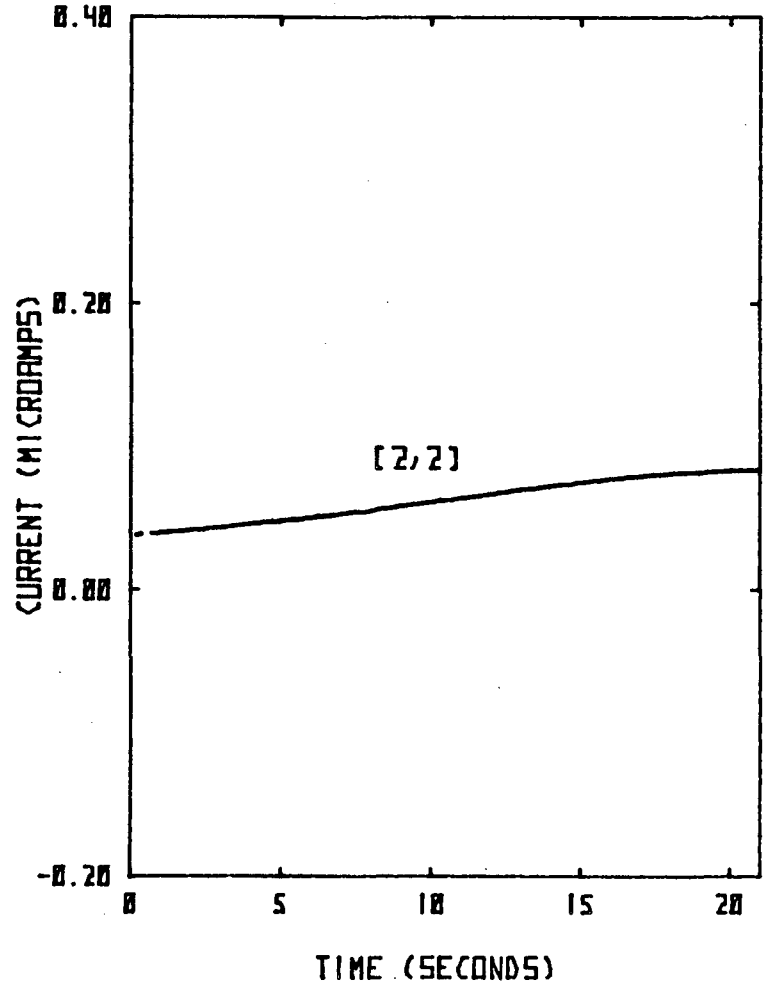

XBL 836-10375

Figure 2.4.2.12 Current to a segment which has a corner adjacent to a bubble growth segment.

Limiting Current Studies After Ceasing Bubble Growth

The current to the segment at which a bubble is being grown is shown in Fig. 2.4.2.13 (A). What happens to the current of a bubble growth segment when the potential difference is suddenly changed to zero is shown in Fig. 2.4.2.13 (B). The step change in the potential occurs a half second after the beginning of data acquisition. It should be noted that there is a small anodic current after the step change. This could perhaps be attributed to hydrogen being oxidized at the electrode.

It is quite instructive to examine the current to segments surrounding the segment at which a bubble is growing when the potential difference is set to zero. The effect on a segment with one of its sides adjacent to a bubble growth segment is given in Fig. 2.4.2.14 (A). The sudden drop in the current indicates that the segment was acting as a bi-polar electrode. Since an anodic current persists after the drop, it can be concluded that hydrogen is being oxidized at this segment also. Similar behavior, shown in Fig. 2.4.2.14 (B), is exhibited by the segments with a corner adjacent to a bubble growth segment, with the difference that the current after the change is cathodic. This indicates that not as much hydrogen reaches these segments, as could be expected. There is no effect on any of the segments not adjacent to a bubble growth segment. Some sample current curves at various distances from the bubble growth segment are given in Fig. 2.4.2.15.

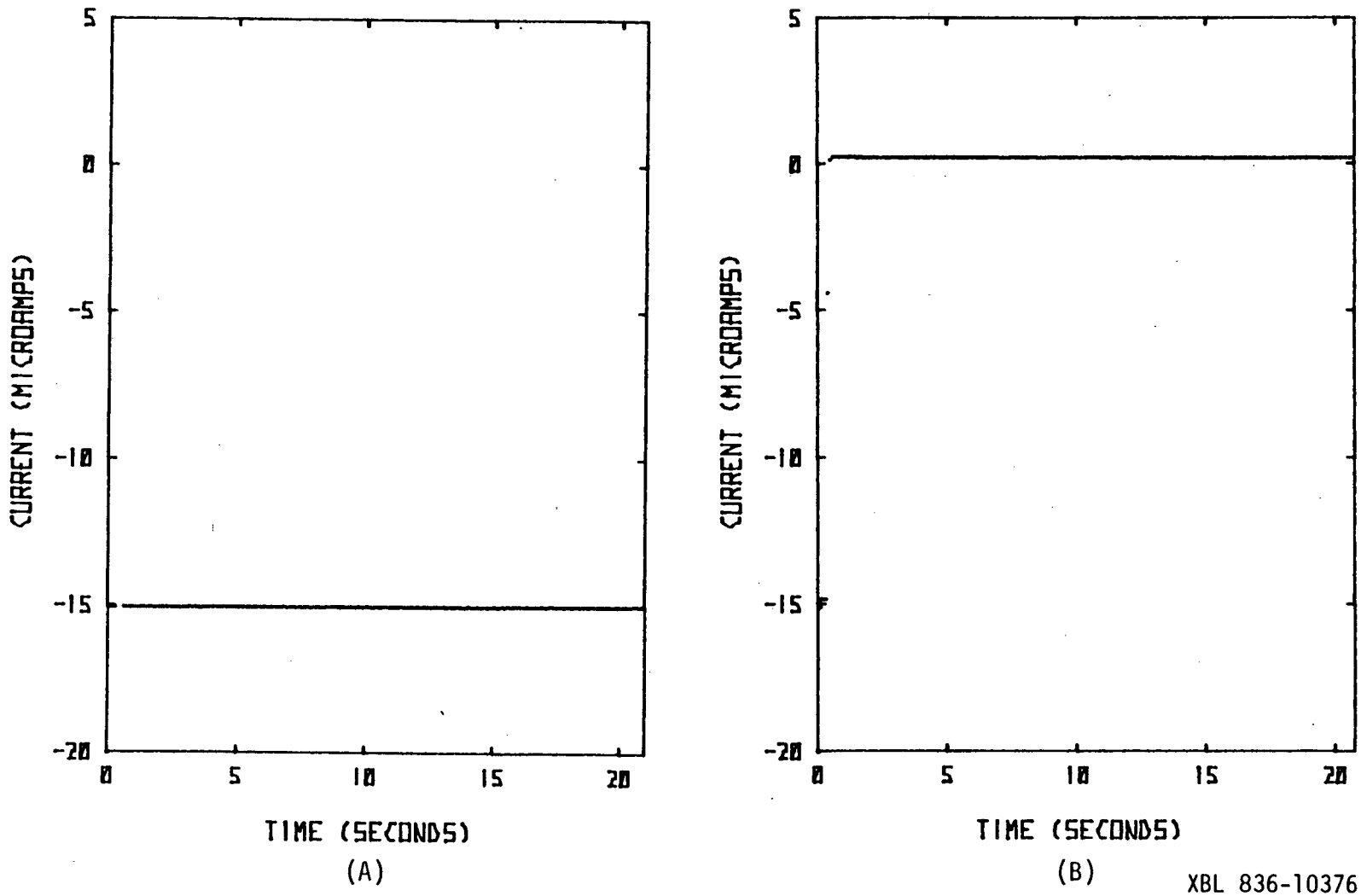

Figure 2.4.2.13 Current to a segment at which a bubble is growing; (A) Current is controlled at 15 microamps; (B) Potential difference is set to zero after 0.5 seconds.

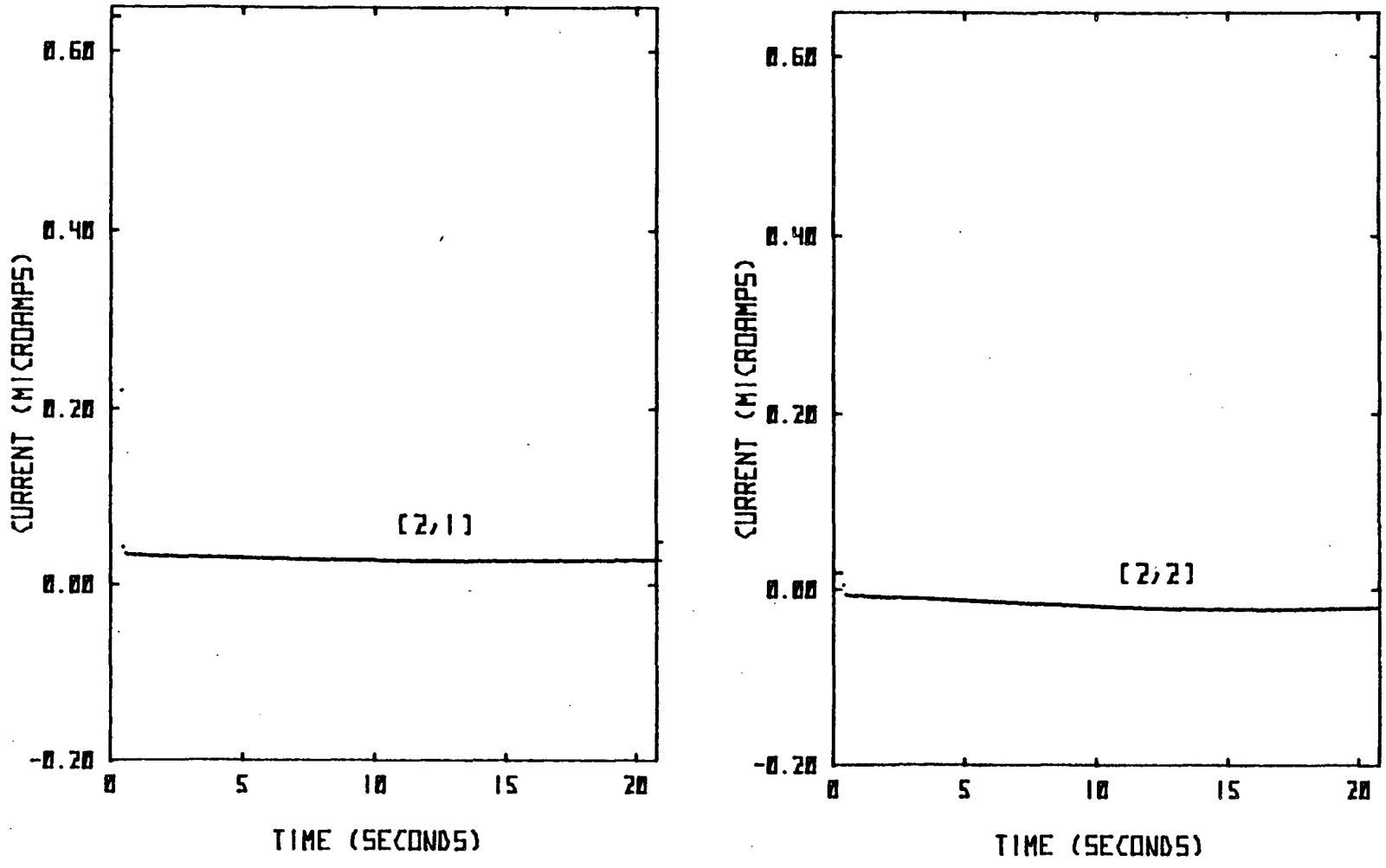

(A) (B) XBL 836-10371

Figure 2.4.2.14 Cureent to a segment adjacent to a bubble growth segment; potential difference is set to zero after 0.5 seconds; (A) Side adjacent; (B) Corner adjacent.

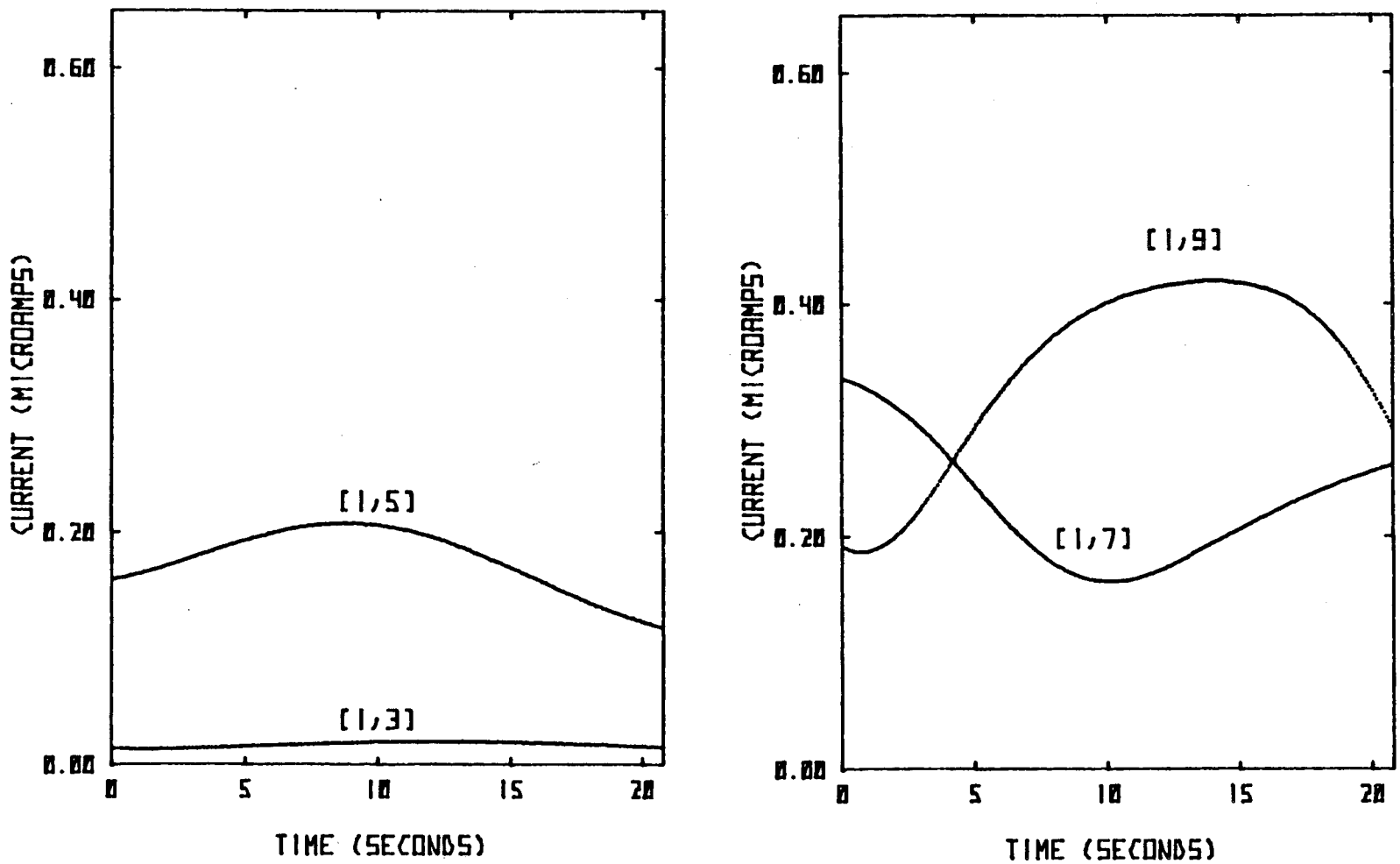

XBL 836-10372

Figure 2.4.2.15 Limiting current to segments with a bubble on the electrode; potential difference is set to zero after 0.5 seconds; (A) Segments under the bubble; (B) Segments not under the bubble.

General Comments on Bubble Disengagement and Coalescence Studies

The effect of a bubble disengagement on the rate of mass transfer to an electrode was studied further. The coalescence of two bubbles and disengagement of the resulting single bubble was also studied. Efforts were made to just study coalescence, but these were not successful, because disengagement from the surface was essentially simultaneous with the coalescence phenomena. The studies include both long and short time experiments.

Before discussing the experimental results it will be helpful to review some basic facts about the effect of laminar fluid flow on the rate of mass transfer to a surface. For any effect whatsoever on the mass transfer rate, the flow must occur in a region of varying concentration, which for aqueous systems generally implies the flow should be near the electrode (i.e., < 1 mm from the surface). The fluid flow near the electrode can be separated into two velocity components; one parallel to the electrode and one perpendicular to it. Flow parallel to the electrode only generates a change in the mass transfer rate to the electrode if there exists a concentration gradient parallel to the electrode. A concentration gradient parallel to the electrode implies a non-uniform limiting current distribution. A well known example of this case is the mass transfer to a flat plate in laminar flow. Flow perpendicular towards an electrode increases the rate of mass transfer if the concentration of the reacting species decreases next to the electrode. Likewise flow perpendicular away from the electrode

will decrease the rate of mass transfer for the same concentration gradient. Generally one can say that a flow will increase the rate of mass transfer if the local concentration of the reacting species is increased by the movement of fluid.

Bubble Disengagement Studies

The results of one experiment from the bubble disengagement studies yielded most interesting results compared to all the other experiments. These results will be used to illustrate the short time effect of a bubble disengagement. The results are typical of what was observed in the other studies and are also in agreement with the results of the earlier work with the micro-mosaic electrode. The diameter of the bubble at the time of disengagement was 1.53 mm. The relative size and position of the bubble is depicted in Fig. 2.4.2.16.

The net anodic currents to the segments adjacent to the bubble growth segment were measured. This usually prevents obtaining any reasonable mass transfer data from these segments; however in this experiment the bubble did not disengage until approximately a half second after the data acquisition was triggered. Since the potential difference is set to zero at the time that the data acquisition is triggered, the current to the segments adjacent to the bubble growth segment was cathodic for a half second before the bubble disengagement. An example of the current to a segment adjacent to the bubble growth segment is given in Fig. 2.4.2.17 (A). An increase in the cathodic current at disengagement is observed.

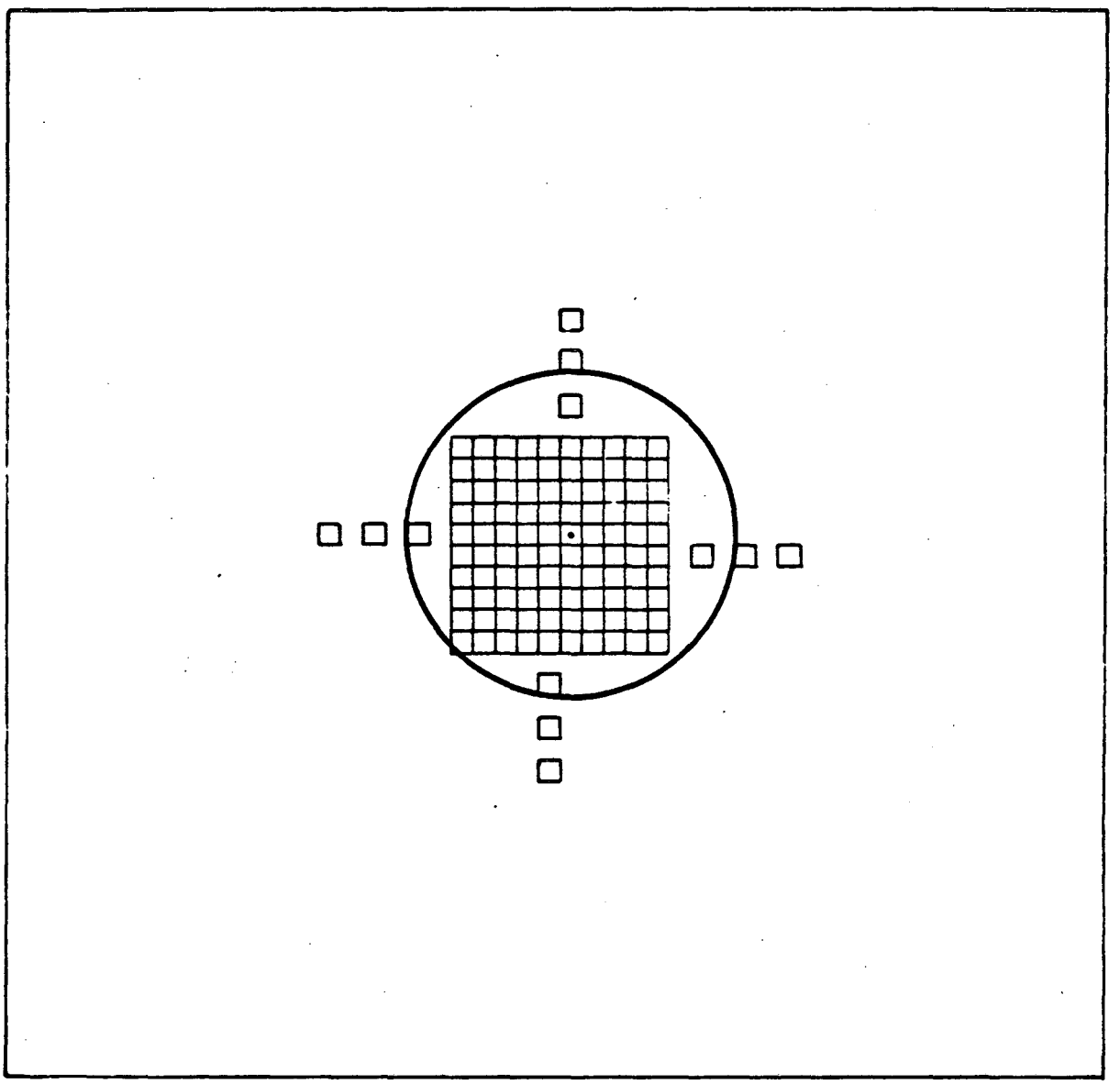

XBL 838-6107

Figure 2.4.2.16 Schematic of the micro-mosaic electrode showing the perimeter of the bubble at the time of disengagement.

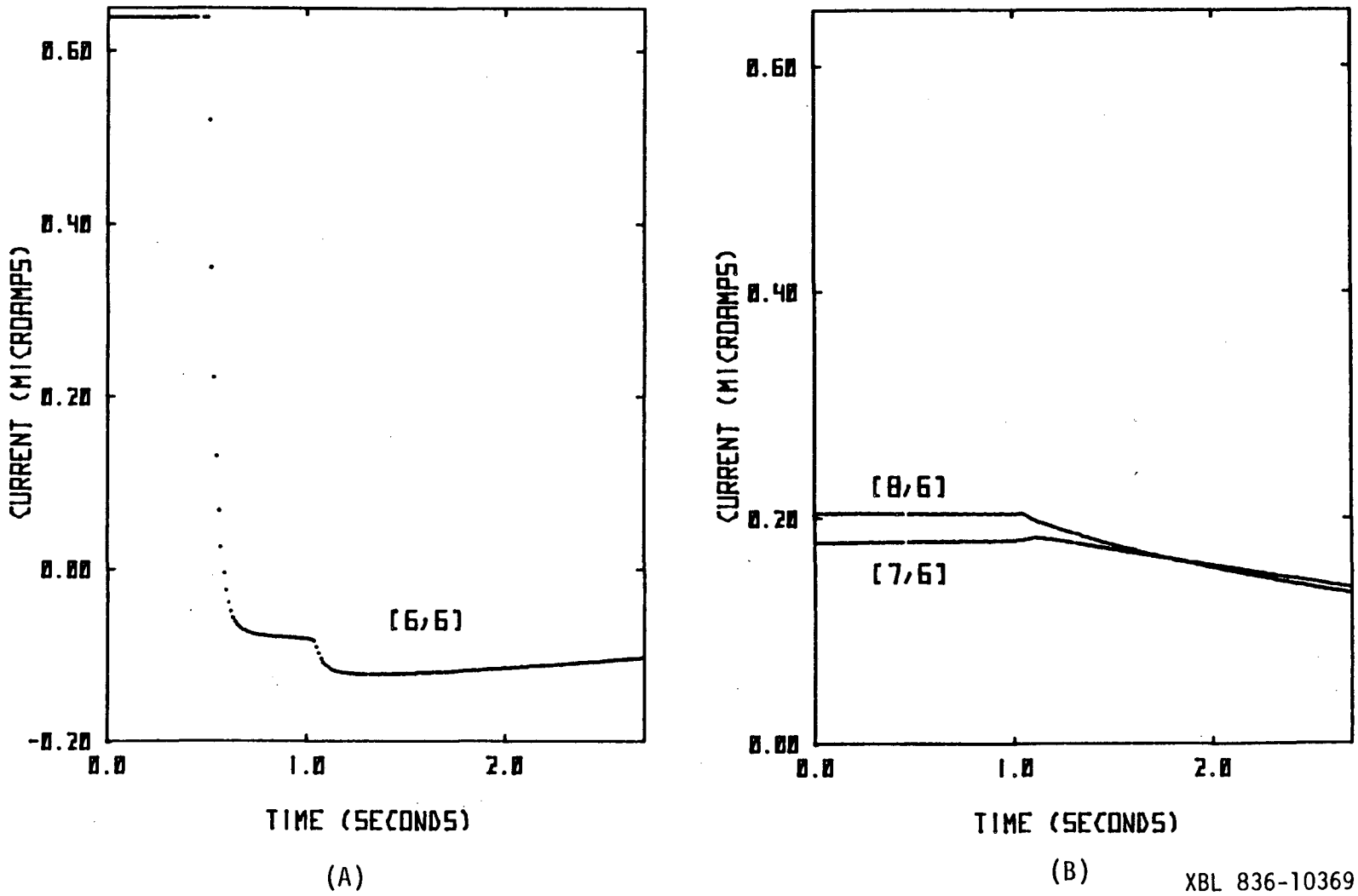

Figure 2.4.2.17 Limiting current to segments before and after the disengagement of a bubble.

Examining the changes in the current to segments farther away from the center of the bubble, a general pattern can be seen in the initial direction of the change in the current at the time of disengagement. Within 200 microns of the center of the bubble, a small absolute increase in the current is observed. At distances greater than 200 microns, but still well under the edge of the bubble, the current is seen to decrease. Near and past the perimeter of the bubble a more substantial increase in the current to segments is observed. This pattern is shown by examining Figs. 2.4.2.17, 2.4.2.18, and 2.4.2.19 (A). The segments represented in these Figures form a line that extends radially from the center of the bubble. The same general pattern is observed in the current to segments on the opposite side of the bubble. These results are given in Figs. 2.4.2.19 (B) and 2.4.2.20. It should be noted that the behavior is generally consistent even though the current before the event may be different. An example of this can be seen by comparing Figs. 2.4.2.17 (B) and 2.4.2.20 (A). The time constant for all the initial changes in the current is of the order of 0.1 seconds.

While the pattern of the initial direction of the change in the current to segments surrounding the bubble is general, it is not universal. Segments can be found which will deviate from this pattern. An example is given in Figs. 2.4.2.21 and 2.4.2.22 (B). These segments form a line extending radially from the center of the bubble along a diagonal. It can easily be seen that the increase in the current at the time of the event occurs past the 200 micron radius

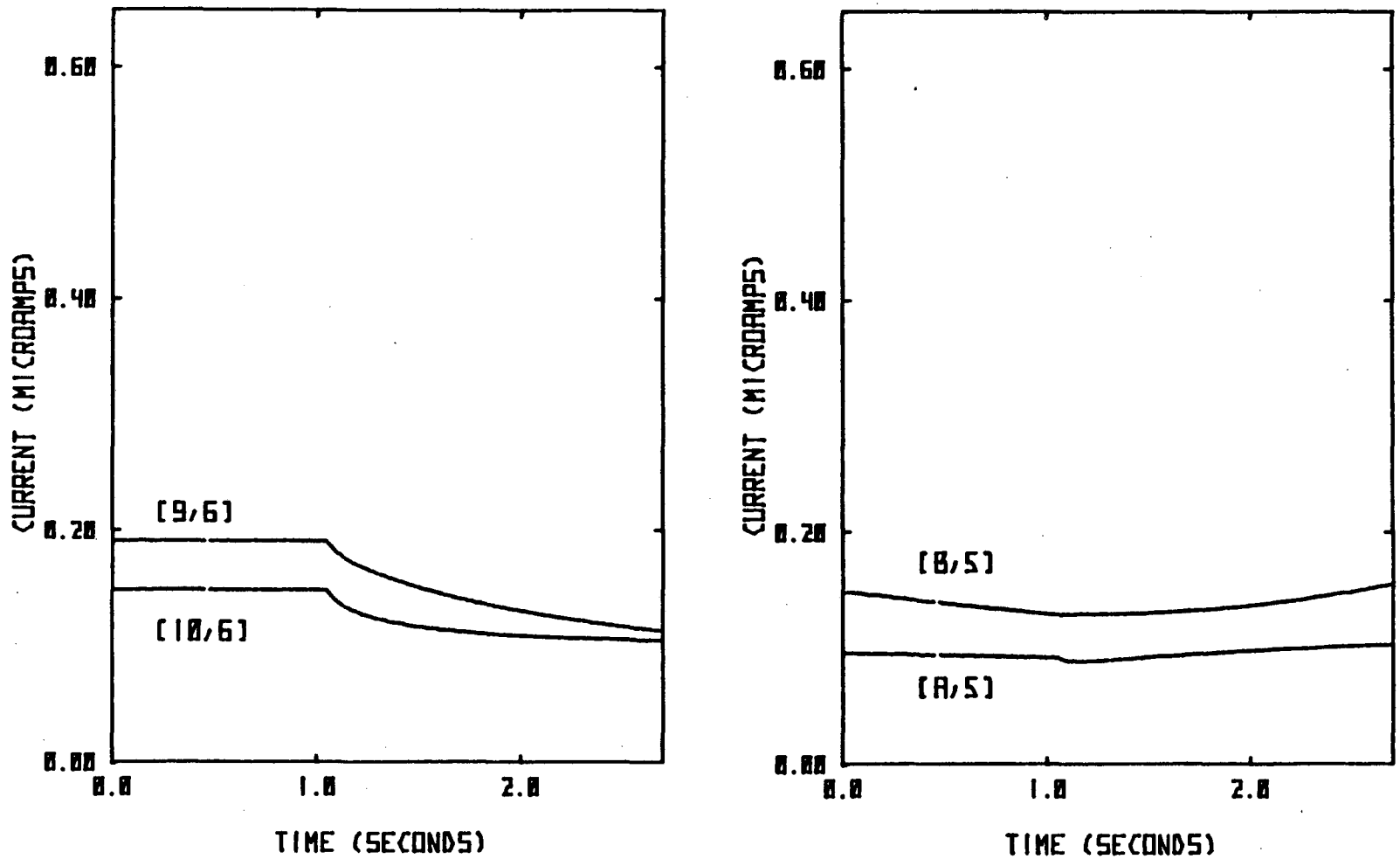

XBL 836-10367

Figure 2.4.2.18 Limiting current to segments before and after the disengagement of a bubble.

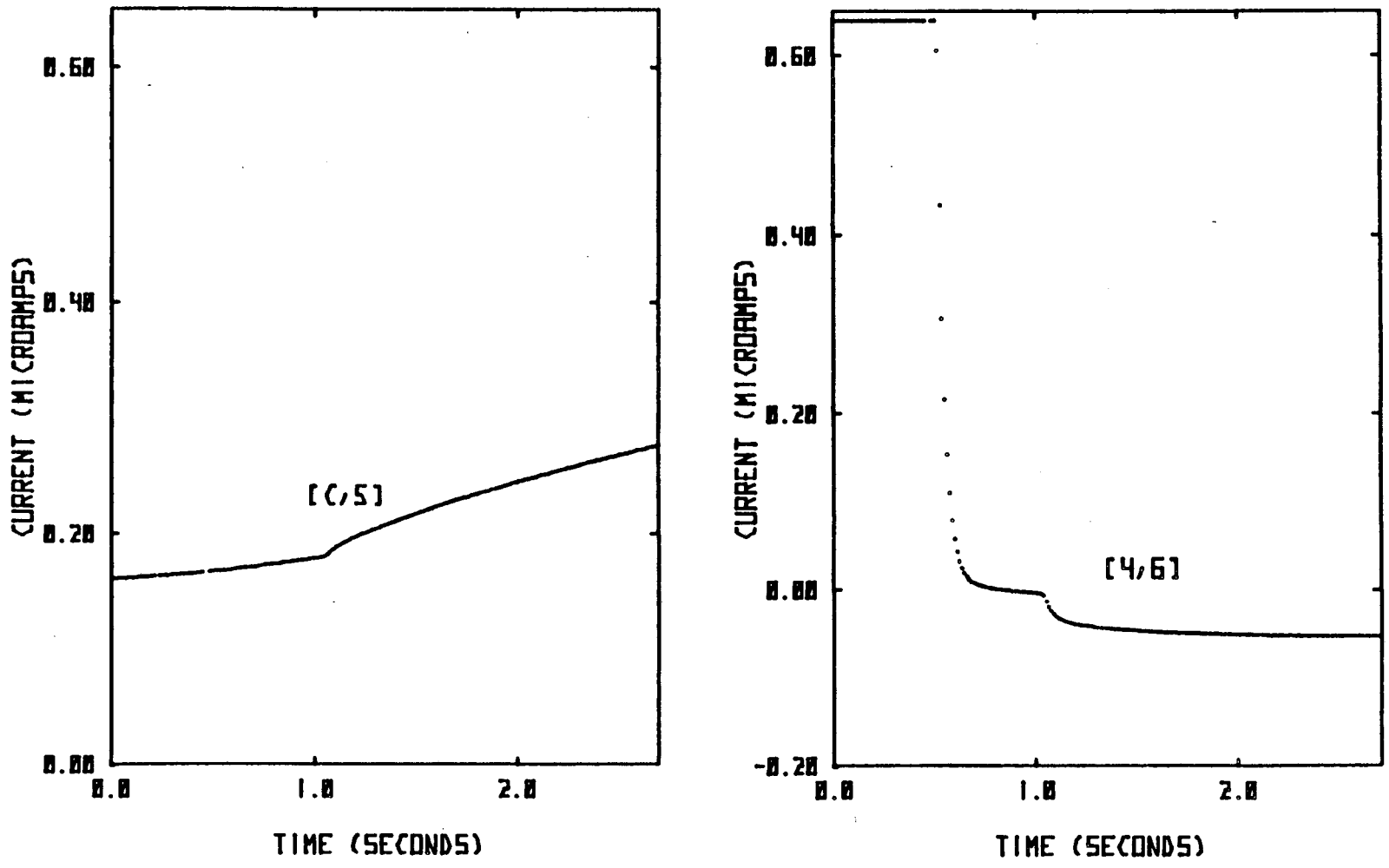

XBL 836-10370

Figure 2.4.2.19 Limiting current to a segment before and after the disengagement of a bubble.

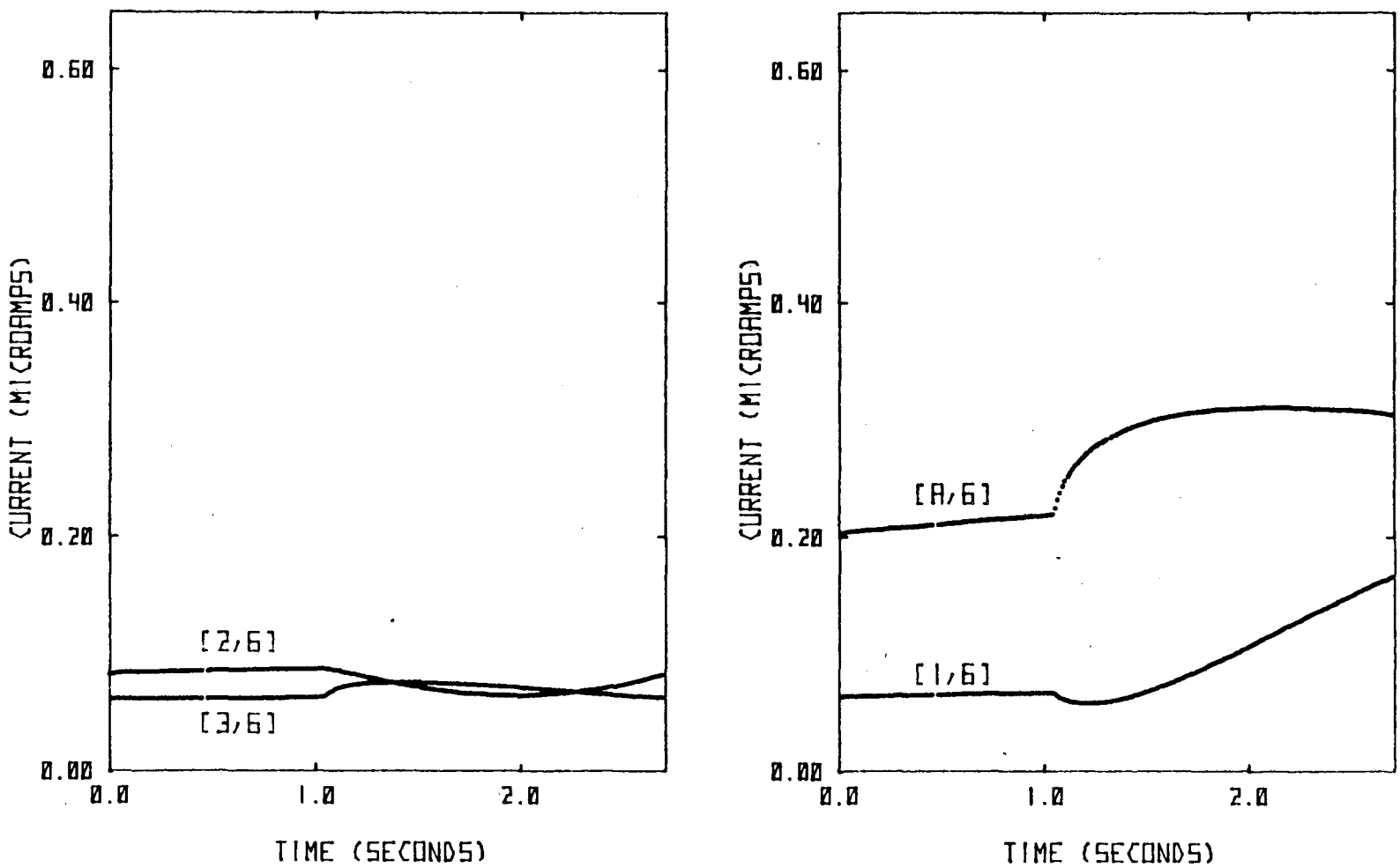

XBL 836-10366

Figure 2.4.2.20 Limiting current to segments before and after the disengagement of a bubble.

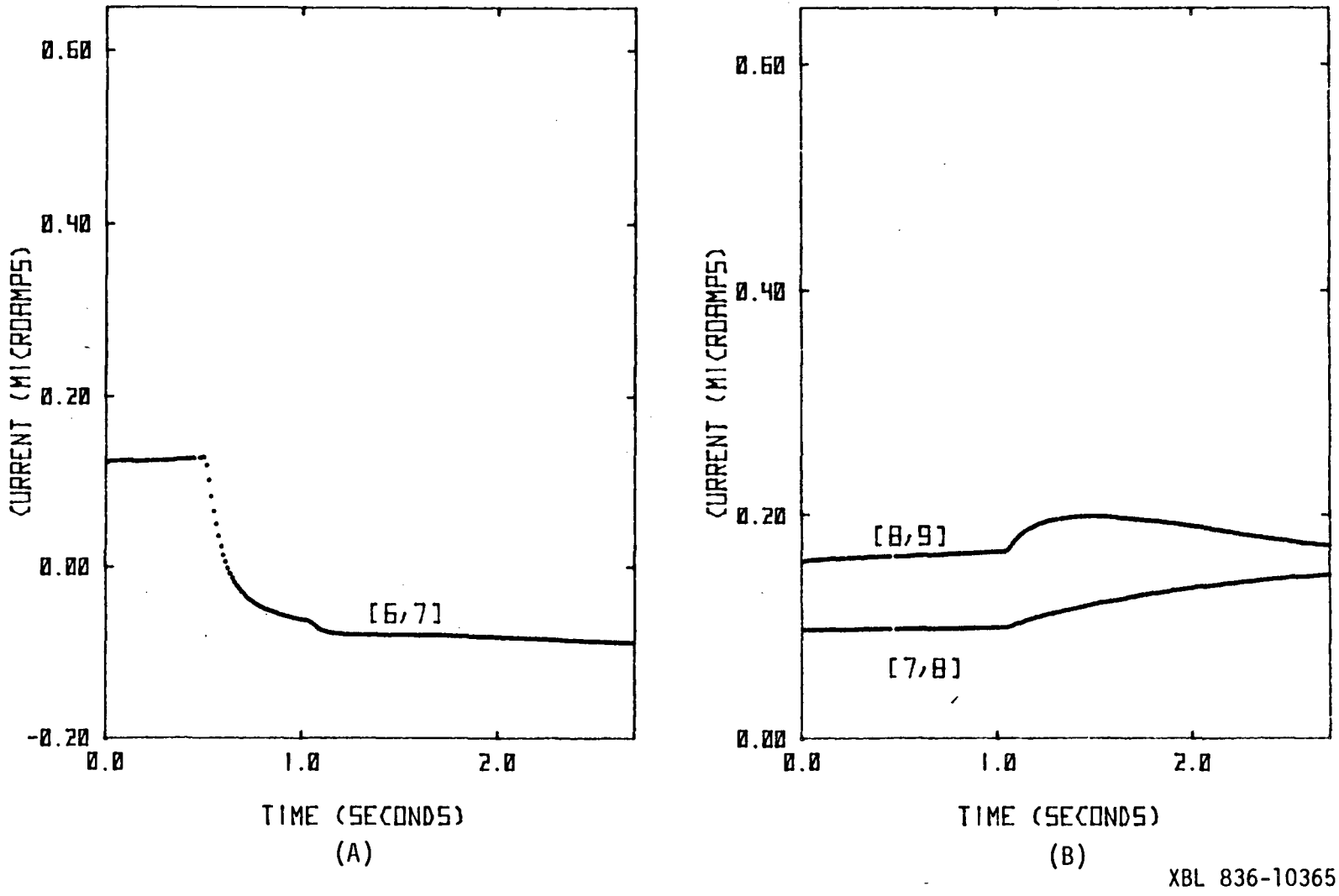

XBL 836-10365

Figure 2.4.2.21 Limiting current to segments before and after the disengagement of a bubble.

previously reported. Generally the deviations from the pattern for segments well under the bubble are few and do not occur over a larger area. This can be seen from Fig. 2.4.2.22 (A) in which an initial decrease in the current occurs at a segment adjacent to one at which the current increases. The deviations that do occur are usually found near or past the perimeter of the bubble. An example of this is given in Fig. 2.4.2.23.

It was pointed out earlier that the limiting current to the segments during bubble growth is governed by free convection. It is safe to assume that at long times after the bubble disengagement the current to segments is also governed by free convection. The abrupt change in the current to the segments surrounding the bubble at the time of its disengagement indicates that the convection generated by the bubble dominates the free convection. This is also indicated by the general pattern of the direction of change in the current. There seems to be no consistent pattern in the change of current to the segments after the first few tenths of seconds following the beginning of the event. This can be seen by comparing the current curves from segments [2,6] and [1,6] in Figs. 2.4.2.20 to segments [8,6] and [9,6] in Figs. 2.4.2.17 (B) and 2.4.2.18 (A). From other work (44) done in this laboratory, the time required for a single bubble of this size to disengage and rise to a height of one bubble diameter above the electrode is less than a tenth of a second. Therefore one would not expect that the convection generated by the bubble disengagement to be important for longer than a few tenths of seconds. Further it is

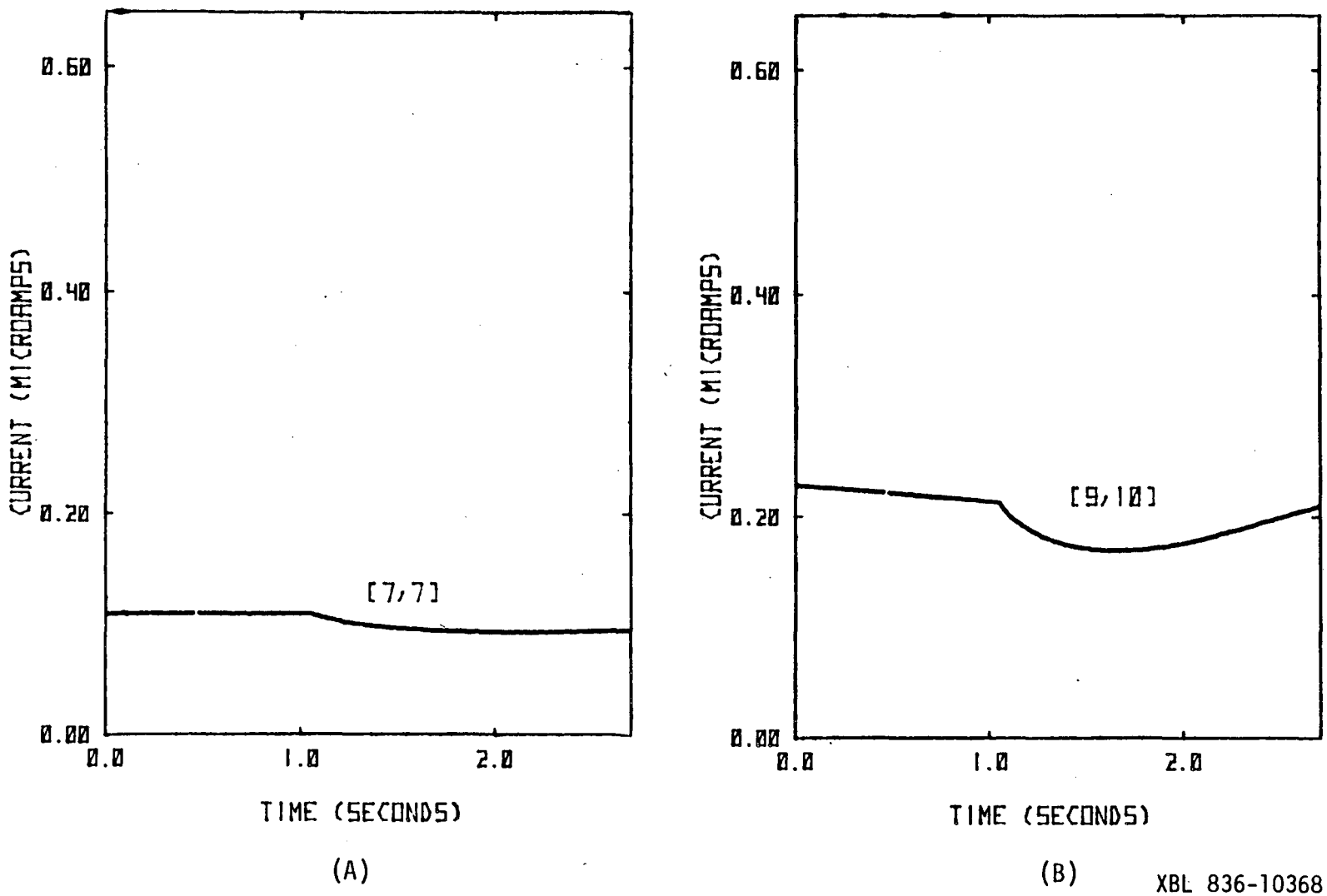

XBL 836-10368

Figure 2.4.2.22 Limiting current to a segment before and after the disengagement of a bubble.

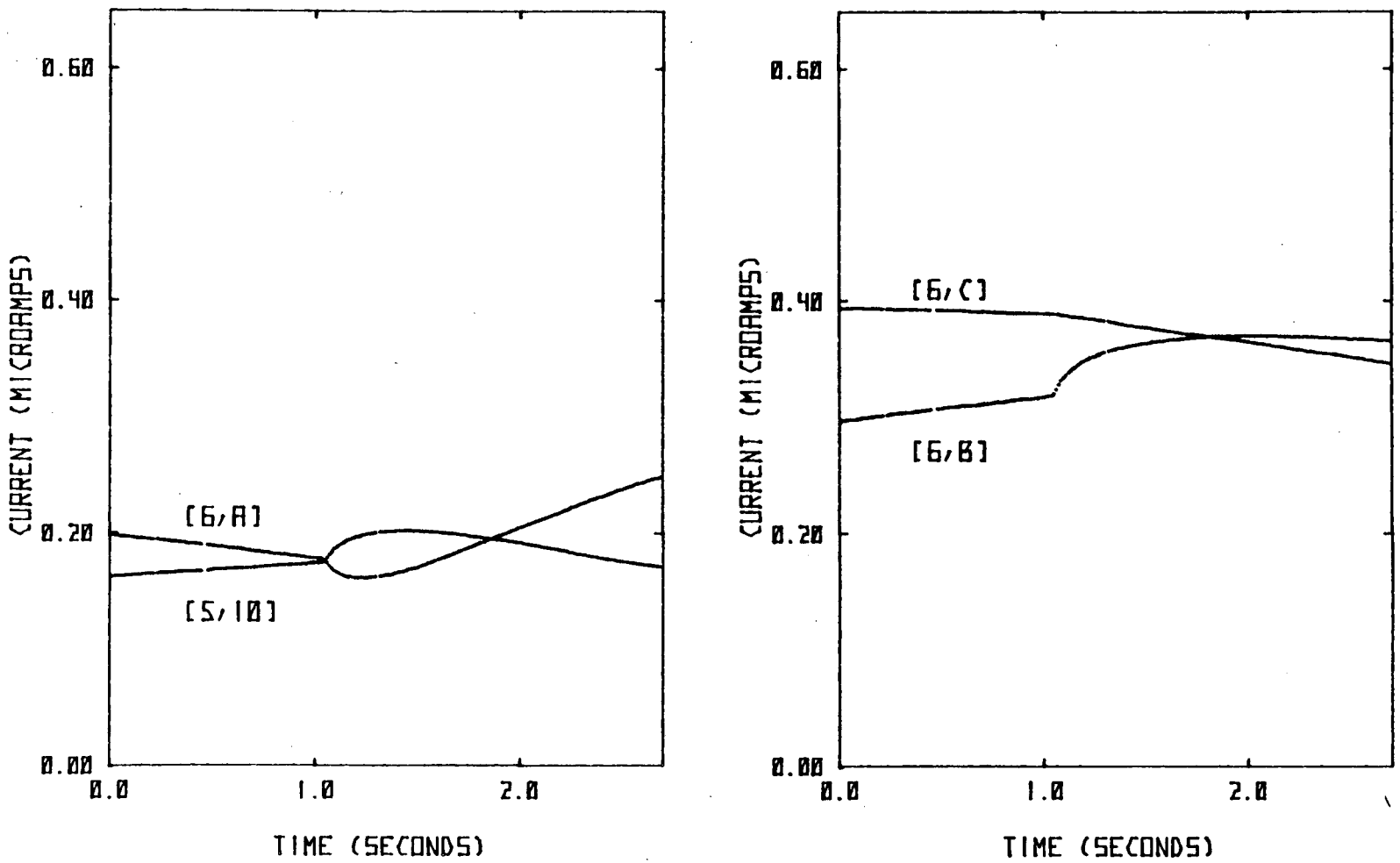

(A) (B) XBL 836-10364

Figure 2.4.2.23 Limiting current to segments before and after the disengagement of a bubble.

reasonable to believe that after this time the free convection is at least as important as the convection generated by the bubble disengagement.

It will be instructive to look at long time disengagement studies to examine free convection being reestablished after the bubble disengagement. The results from the disengagement of a 1.2 mm diameter bubble will be used to illustrate this. The relative size and position of the bubble on the micro-mosaic electrode at the time of disengagement is depicted in Fig. 2.4.2.24.

The trend in the direction of change in the current to segments caused by a bubble disengagement is usually maintained from one to three seconds. At that time the current fluctuates a local maximum or minimum. Following this, the current fluctuations relatively slowly and unpredictably for about 10 to 15 seconds. An illustration of this behavior is given in Fig. 2.4.2.25. The bubble disengaged 0.3 seconds before time equal to zero on the graph. An initial increase and decrease in the current is shown. After the 10-15 second period, the now familiar free convection limiting current pattern resumes. The complete cycle is exhibited in Fig. 2.4.2.26.

Bringing together all the observations of the current to segments before and after the bubble disengagement, the effect on the mass transfer rate to the surface can be described. As the bubble grows the limiting current is governed by free convection. When the hydraulic and buoyancy forces exceed the surface tension forces, the bubble starts to rise and its contact area collapses. The convection

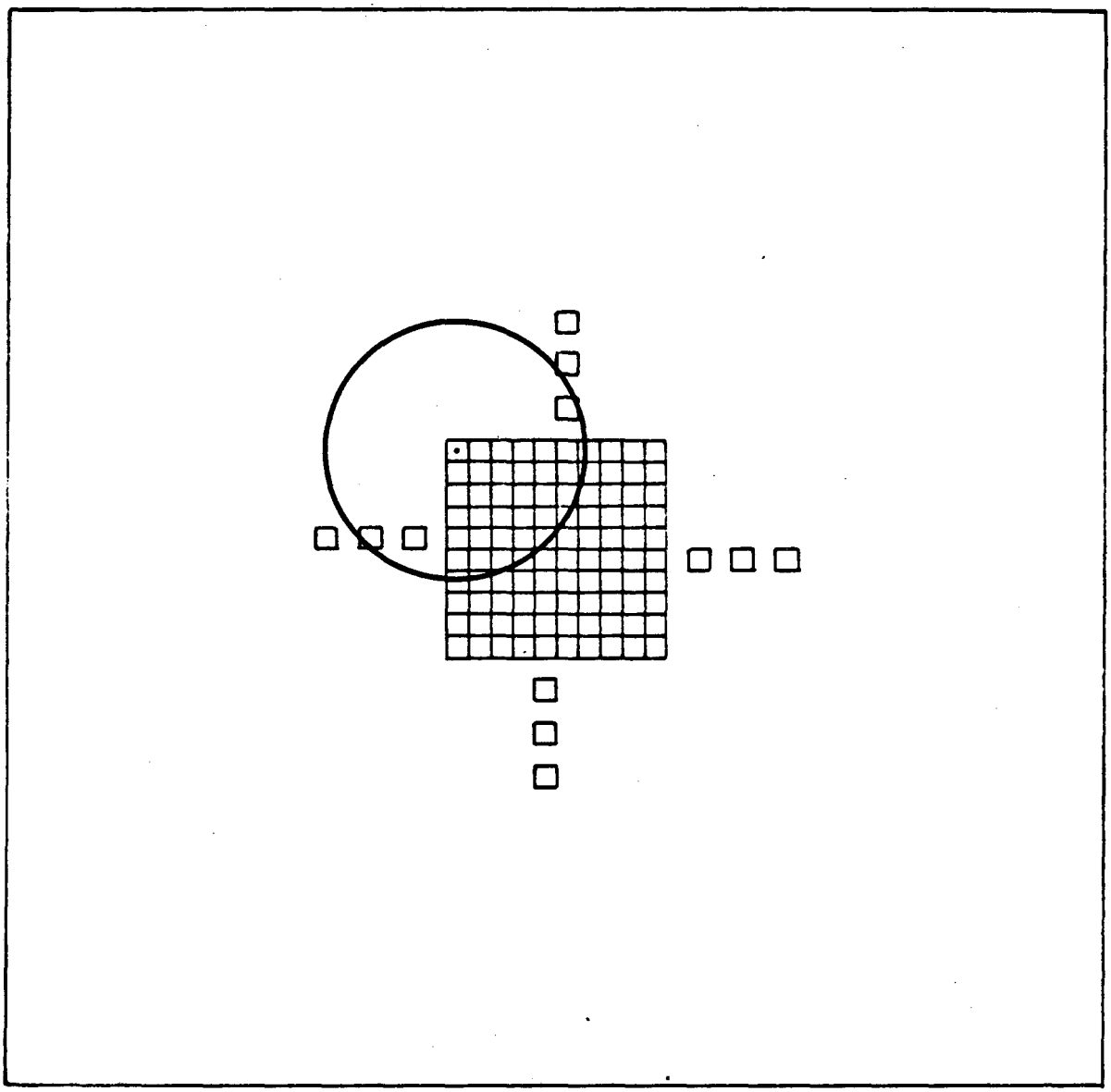

XBL 838-6106

Figure 2.4.2.24 Schematic of the micro-mosaic electrode showing the perimeter of a bubble at the time of disengagement.

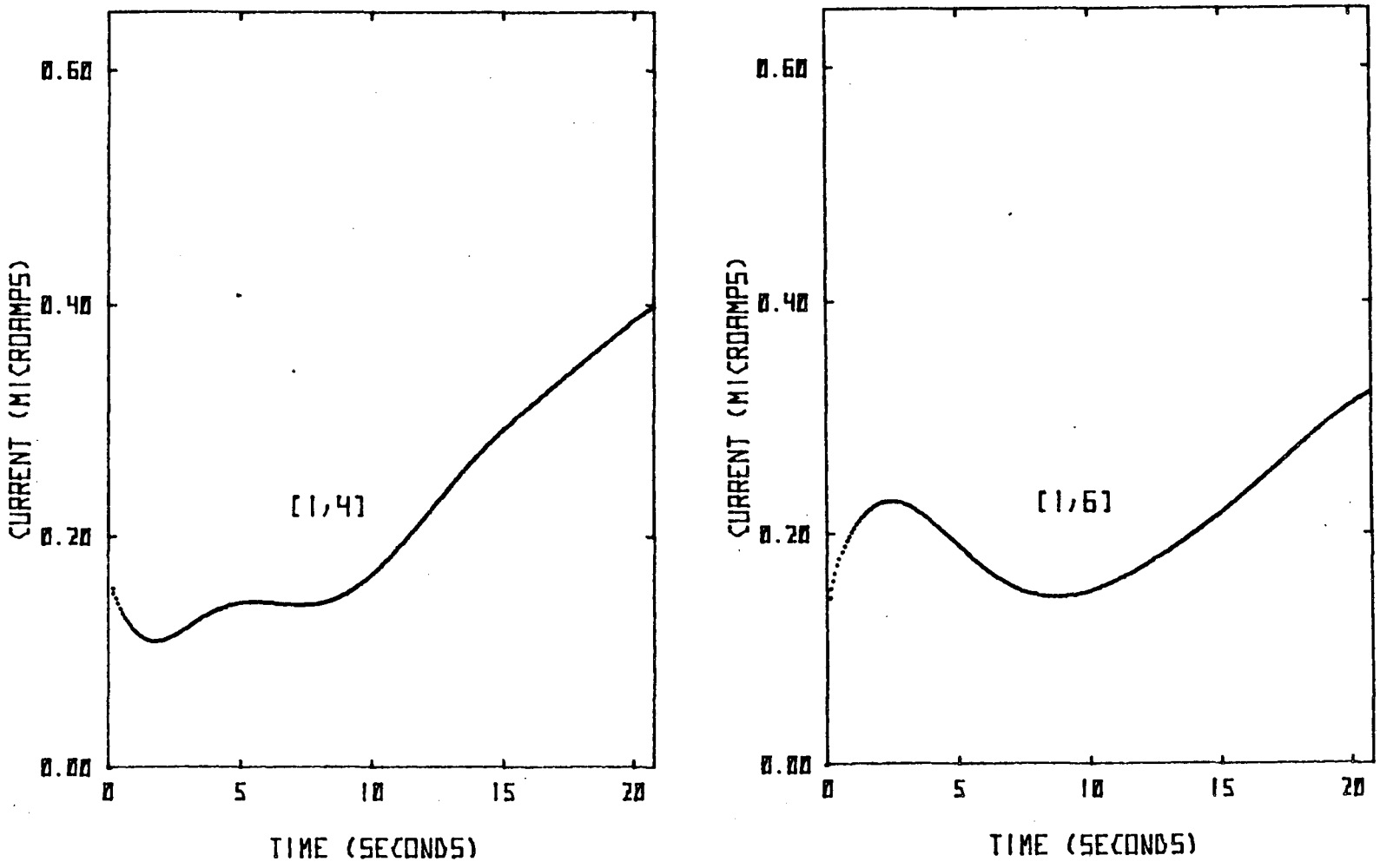

XBL 836-10469

Figure 2.4.2.25 Limiting current to a segment beginning 0.3 sec after the disengagement of a bubble

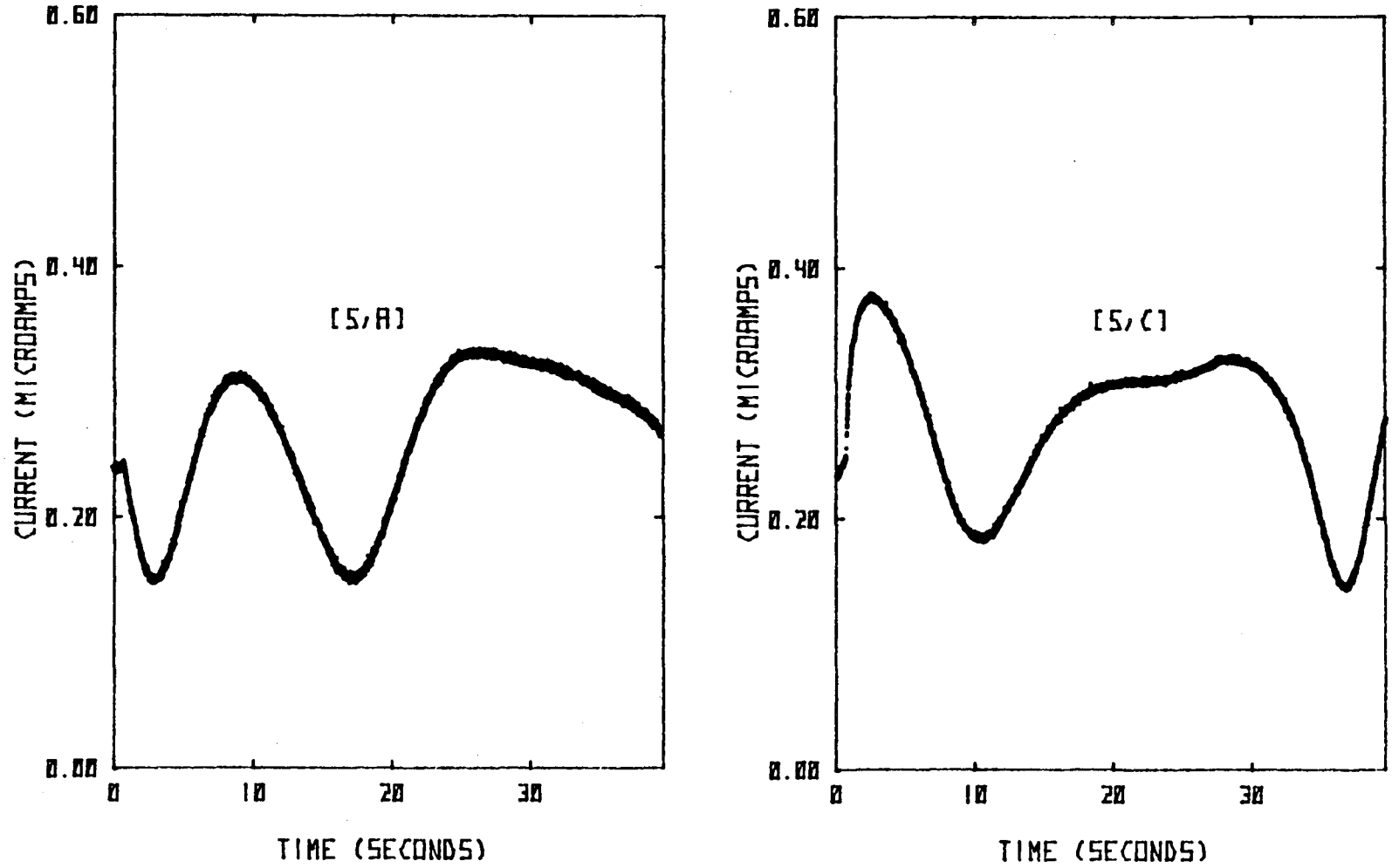

XBL 836-10470

Figure 2.4.2.26 Limiting current to a segment before and after the disengagement of a bubble.

generated by the disengagement and rising of the bubble causes an abrupt change in the current. After a few tenths of seconds, the bubble is several diameters away from the surface. Then the flow generated by the bubble has little effect on the rate of mass transfer to the surface and free convection starts to dominate again. One to three seconds after the bubble disengagement free convection governs the limiting current, but another 10-15 seconds is required to establish a steady state.

The direction of the abrupt change in the current when the bubble disengages can be explained by the flow generated by the bubble. As the bubble pulls loose from the electrode and rises, fluid is drawn up with the bubble. The void generated by the rising bubble and fluid is filled by an inward radial flow. Therefore under the bubble the direction of flow is inward and upward. Providing that the radial concentration gradients are not too great, there is a net decrease in the current as a result of the upward flow. Near the collapse of the contact area, the inward flow is turned down toward the electrode resulting in an increase in the current. Near and past the edge of the bubble, a recirculation flow occurs. The recirculation flow is basically a downward and inward movement of the fluid, which causes an increase in the current.

Variations in the current from the general pattern can occur for several reasons. An asymmetric collapse of the contact area could affect the flow significantly. This could induce some horizontal movement of the bubble upon release, which would affect the flow

also. Both these phenomena have been observed in this laboratory (44). An unusually large radial concentration gradient near the electrode could affect the change in current. This would most likely occur near the center of the bubble and in the free-convection transition region around the edge of the bubble.

The overall effect of the microconvection, generated by a bubble disengagement, on the local mass transfer rate to a horizontal electrode is relatively small. Even considering the rate of disengagement that is obtained on a gas-evolving electrode, a significant increase would not be expected. In fact a net decrease in the mass transfer rate could result from the disengagements.

Simultaneous Bubble Coalescence and Disengagement Studies

In contrast to the disengagement events, a significant increase in the rate of mass transfer was observed for simultaneous coalescence and disengagement of bubbles. Order of magnitude increases in the current to segments are not uncommon. An example of this is given in Fig. 2.4.2.29 (A) where the relative size and position of the bubbles before coalescence is depicted in Fig. 2.4.2.27. The largest increases in the current were observed between the bubbles along the line of coalesence, but increases in the current were observed on nearly all the segments surrounding the bubbles.

The change in the current to the segments between two coalescing bubbles can be seen by examining the results from the coalescence and disengagement of a 0.495 mm diameter bubble and a 0.540 mm diameter bubble. The relative size and position of the bubbles on the

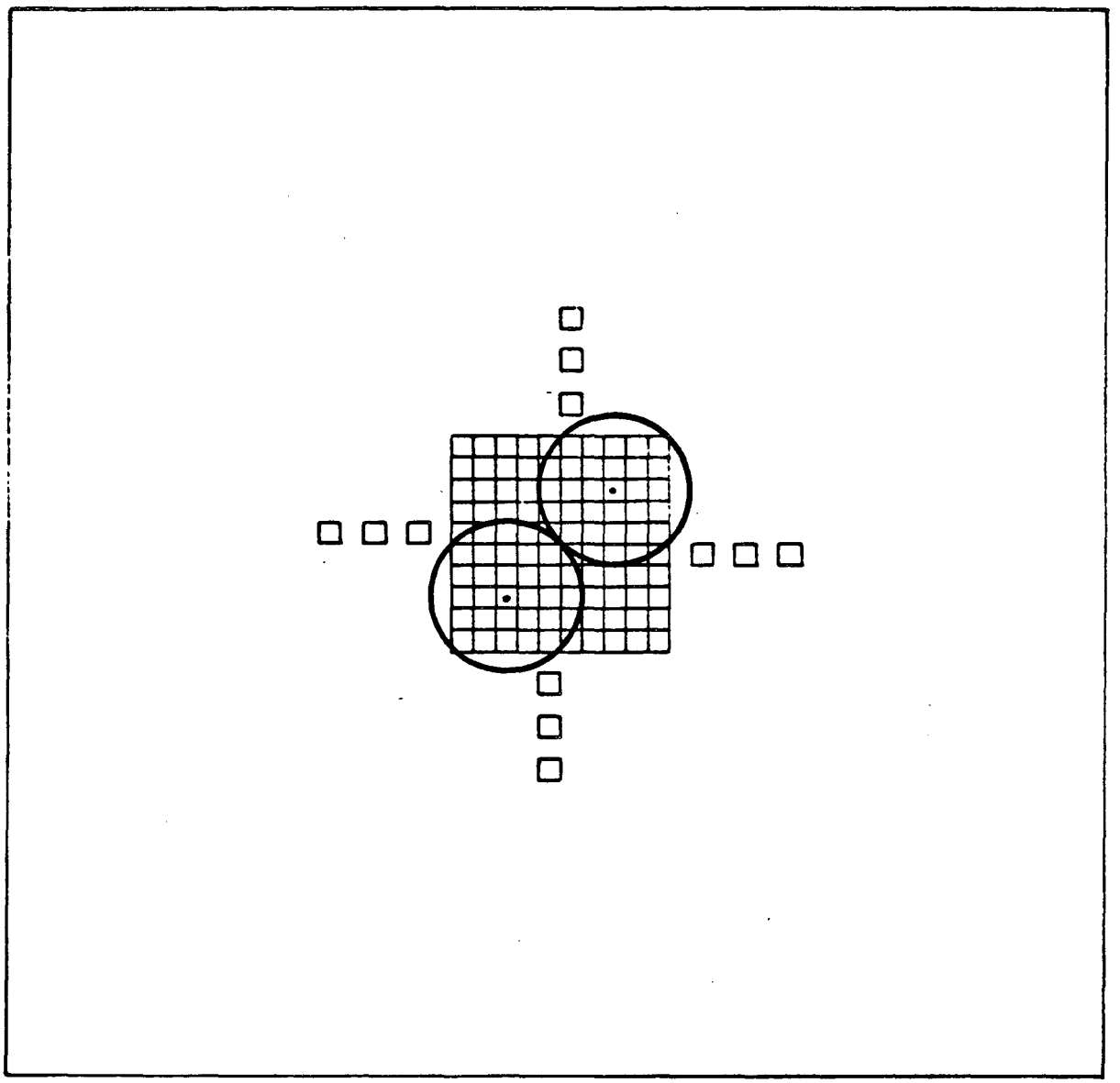

XBL 838-6102

Figure 2.4.2.27 Schematic of the micro-mosaic electrode showing the perimeter of the bubbles at the time of the event.

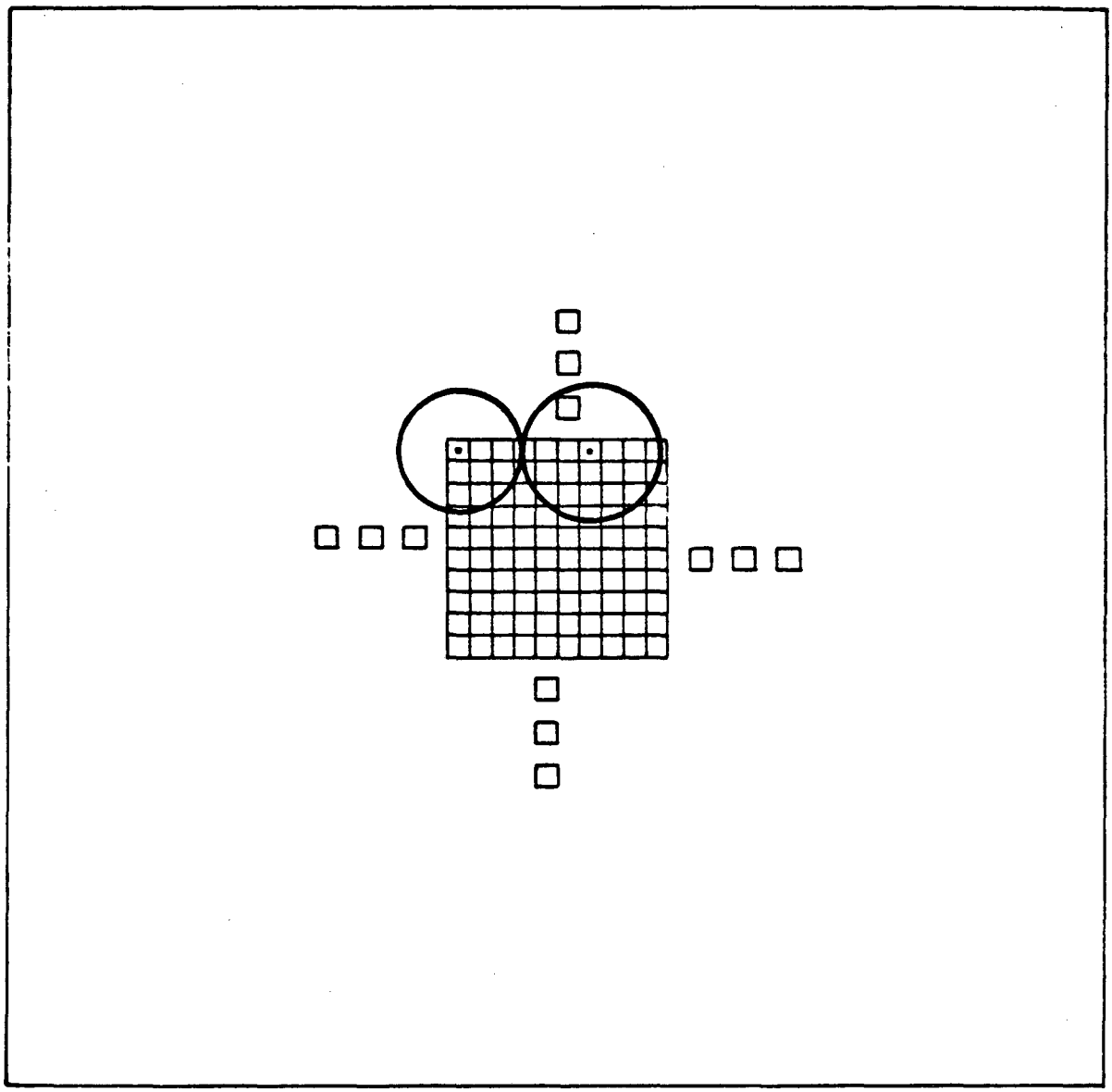

XBL 838-6101

Figure 2.4.2.28 Schematic of the micro-mosaic electrode showing the perimeter of the bubbles at the time of the event.

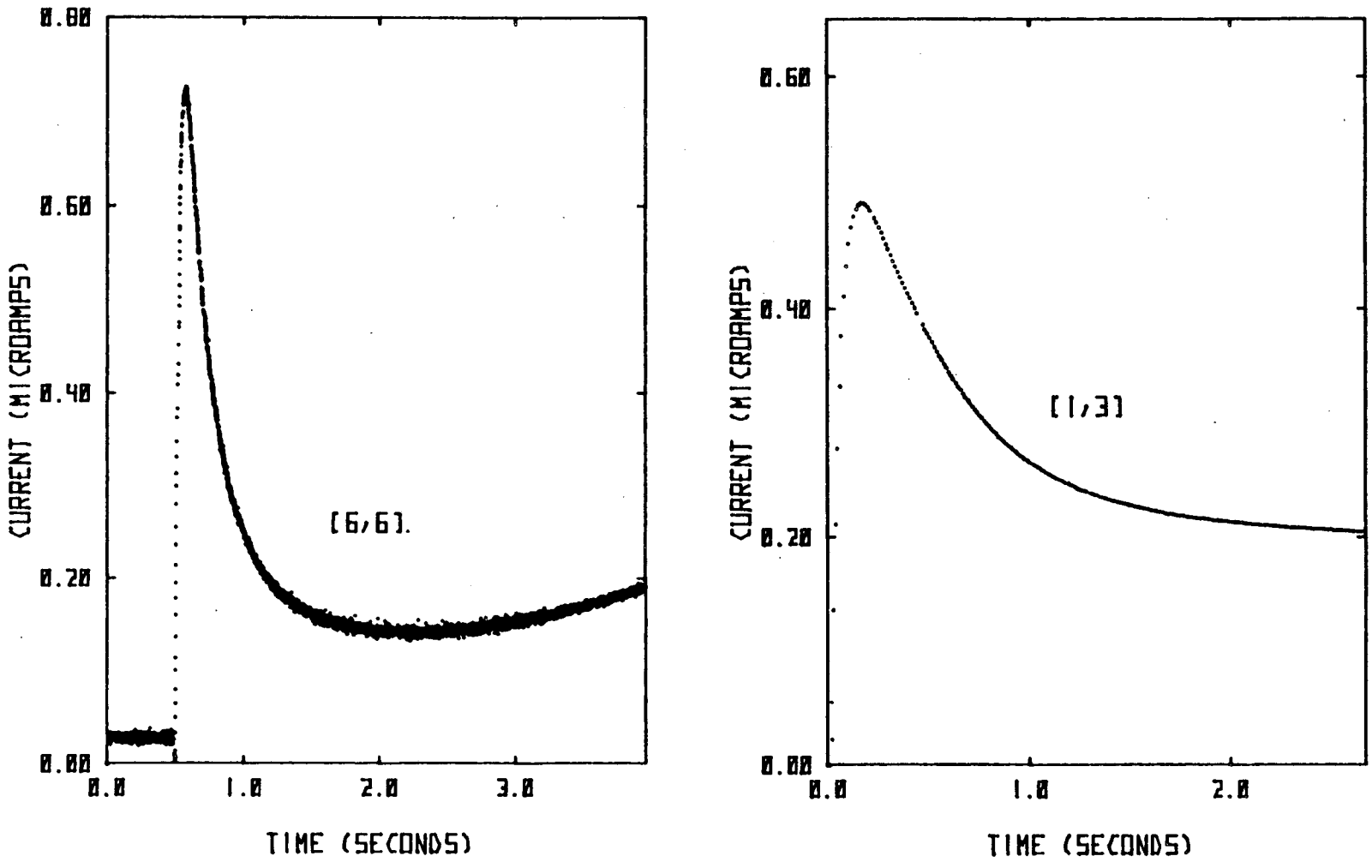

XBL 836-10474

Figure 2.4.2.29 Limiting current to a segment; (A) before and after the event; (B) beginning 0.2 sec after the event.

micro-mosaic electrode is shown in Fig. 2.4.2.28. Data were obtained approximately 0.1 seconds after the start of coalescence.

The current to the segments that are located on the axis of coalescence is given in Figs. 2.4.2.29 (B) and 2.4.2.30. Significant increases in the current are observed in all cases. The largest peak in the current exceeded the maximum value set on the multiplexer. The increase in the current is large enough and rapid enough that some distortion, from the 10 Hz filters on the multiplexer inputs, could have occurred. This would tend to decrease and round-off the maximum. The maximum occurs at different times for various segments, but always within less than 0.2 seconds after zero time.

The current to segments located between the two bubbles that fall on a line perpendicular to the axis of coalescence is given in Figs. 2.4.2.30 (B), 2.4.2.31, and 2.4.2.32. Two general trends can be observed: the height of the peak generally decreases and the peak occurs sooner the larger the distance from the line of coalescence. These trends are easily seen in Figs. 2.4.2.30 (B) and 2.4.2.31, but are obscured in the curves in Fig. 2.4.2.32 (A) since the peaks were not obtained. There seems to be very little effect 500 to 600 microns away from the line of coalescence, as can be seen in Fig. 2.4.2.32 (B).

When two bubbles coalesce, the fluid between them is squeezed out in all directions. Under and between the two bubbles there is a significant flow toward the electrode, which results in the observed peak in the current to segments located in a narrow region between the bubbles. For approximately equal size bubbles, the region is widest in

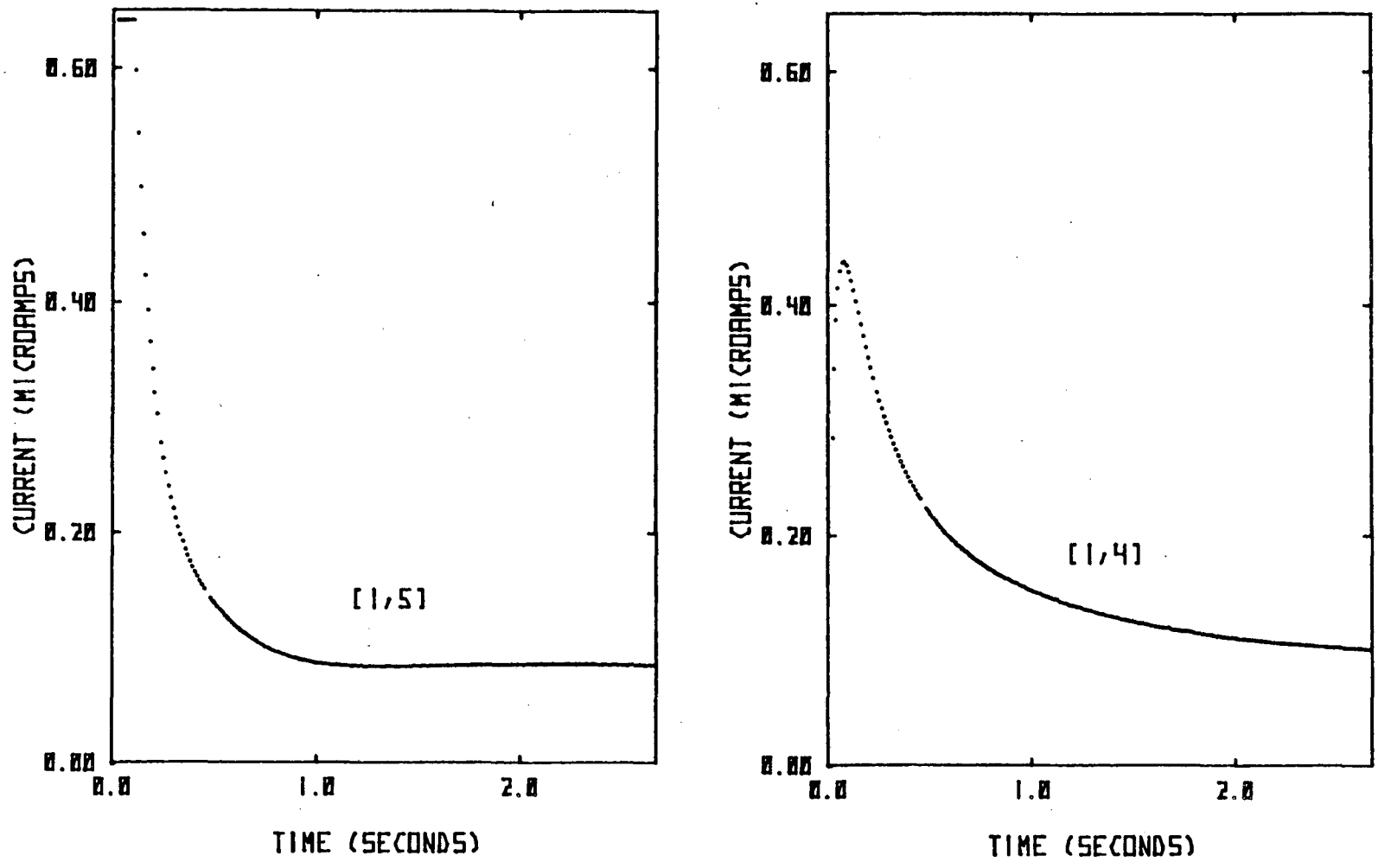

XBL 836-10473

Figure 2.4.2.30 Limiting current to a segment beginning 0.1 sec after the event.

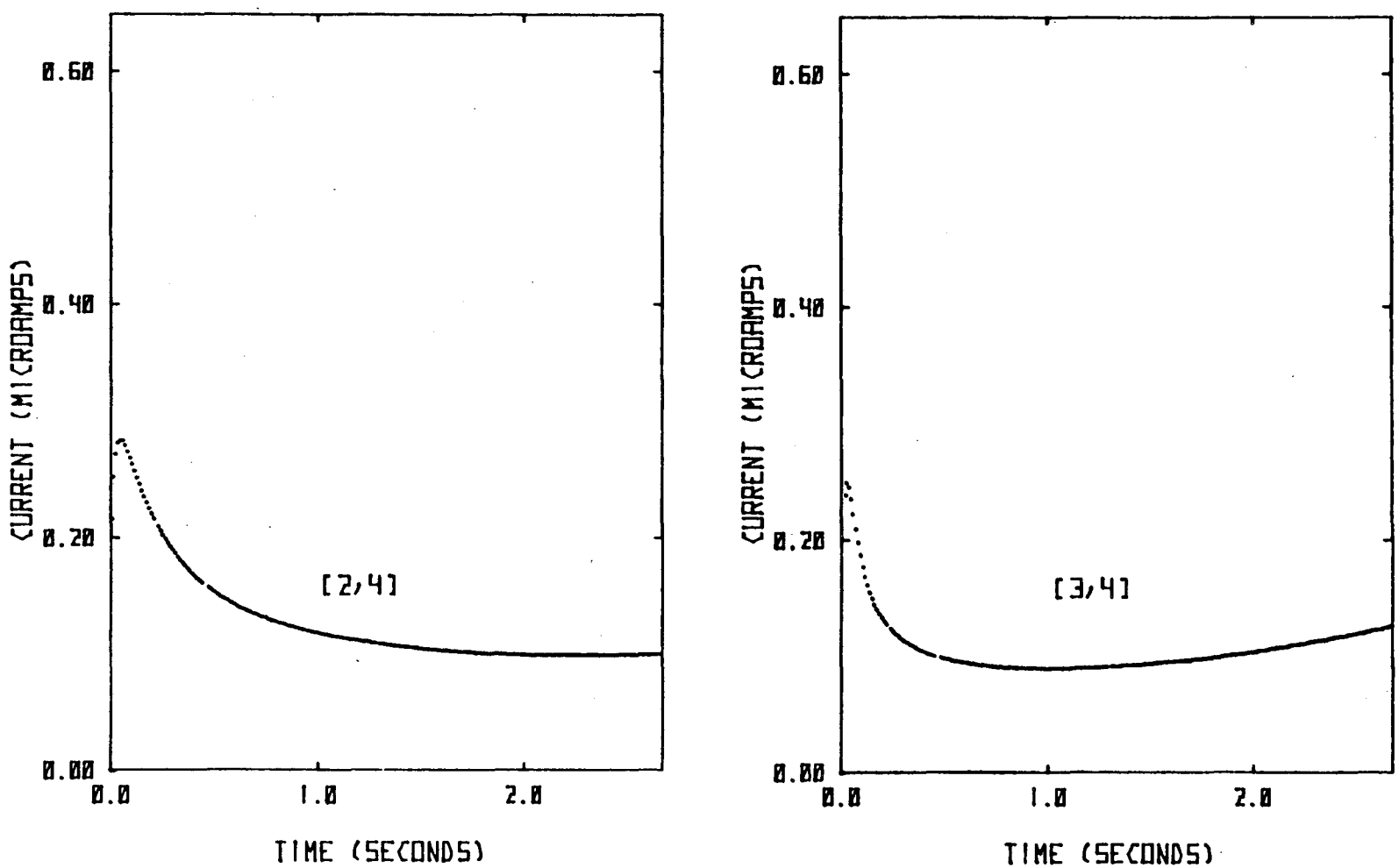

XBL 836-10475

Figure 2.4.2.31 Limiting current to a segment beginning 0.1 sec after the event.

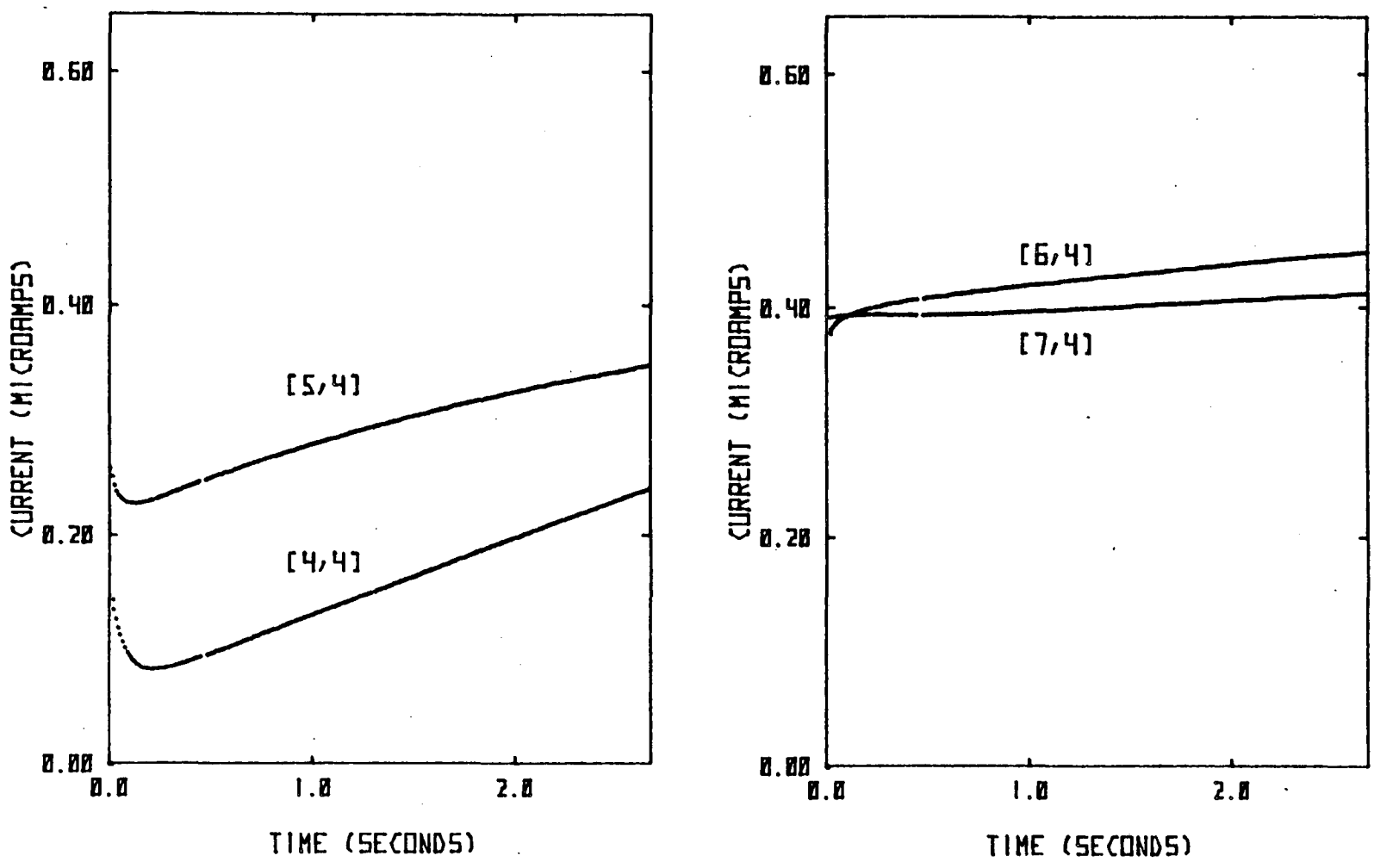

XBL 836-10476

Figure 2.4.2.32 Limiting current to segments beginning 0.1 seconds after the event.

the center. This would be expected from the movements of the bubbles during the occurrence of the event.

Increases in the current are observed outside the narrow region between the bubbles. These increases are not as intense and they occur over seconds rather than within tenths of seconds. This behavior can be seen in the results from the coalescence and disengagement of a 0.945 mm diameter bubble and a 0.765 mm diameter bubble. The relative size and position of the bubbles on the electrode is shown in Fig. 2.4.2.33. The initial current before the event was not obtained. The data begins 0.31 seconds after the start of the event.

Because the first 0.31 seconds of the current to the segments after the event was not obtained, it is difficult to make conclusions from the results. However some general observations can be made. Increases in the current are observed for segments located under the bubbles. This can be seen by examining the current to segments under the 0.945 mm diameter bubble given in Figs. 2.4.2.34 (A), 2.4.2.35, and 2.4.2.36 (A). There appears to be only a small increase and sometimes a decrease in the current to segments located past the edge of the bubbles, as can be seen in Figs. 2.4.2.34 (B) and 2.4.2.36 (B). Of the segments past the edge of the bubbles, the ones located nearest the wake created by the coalescence seem to be affected the most. This seems to be generally true of the segments located under the bubbles also. The wake formed by the bubbles during coalescence should be behind the bubbles and along the axis of coalescence.

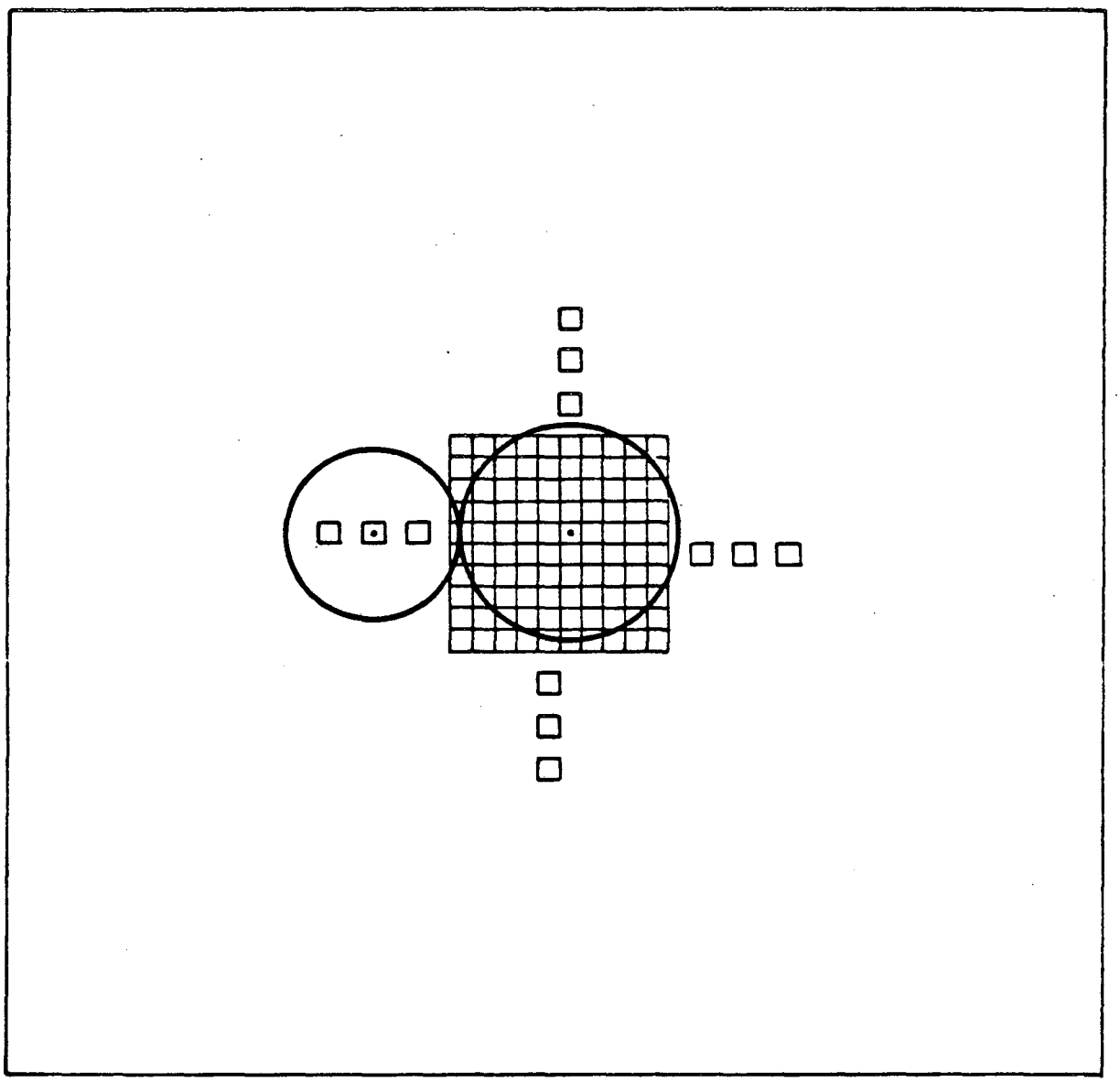

XBL838-6105

Figure 2.4.2.33 Schematic of the micro-mosaic electrode showing the perimeter of the bubbles at the time of the event.

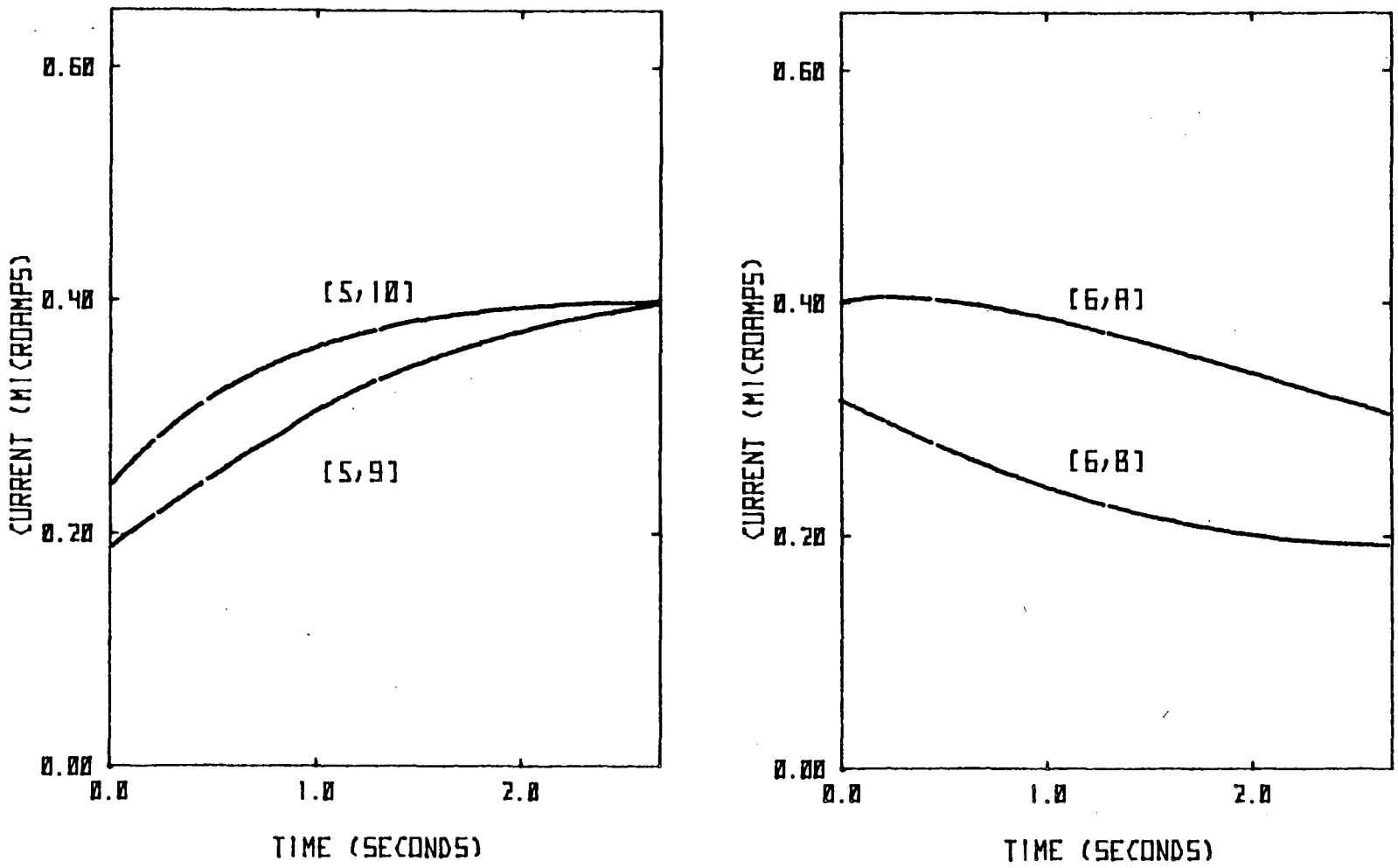

XBL 836-10479

Figure 2.4.2.34 Limiting current to segments beginning 0.31 sec after the event.

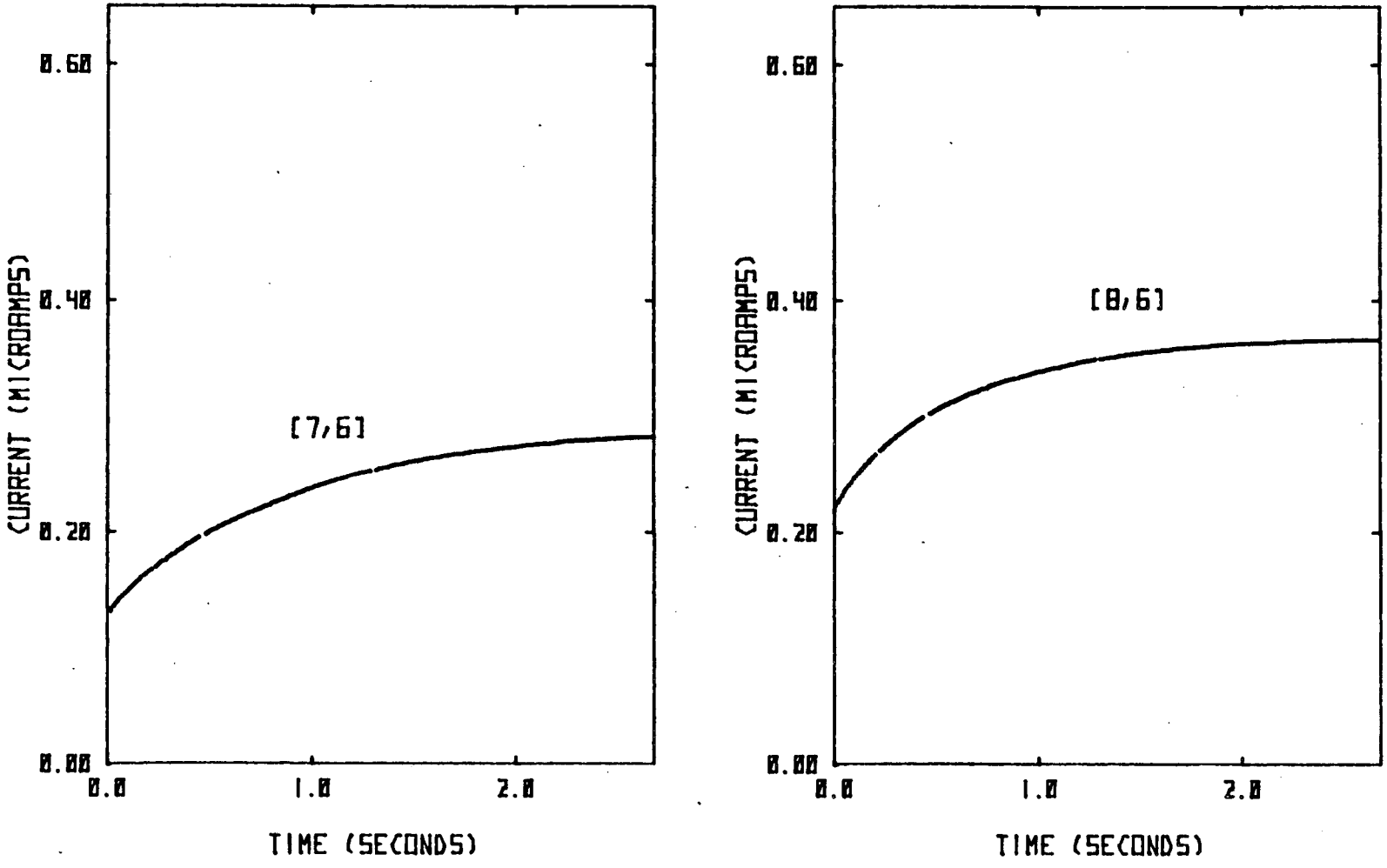

XBL 836-10477

Figure 2.4.2.35 Limiting current to a segment beginning 0.31 sec after the event.

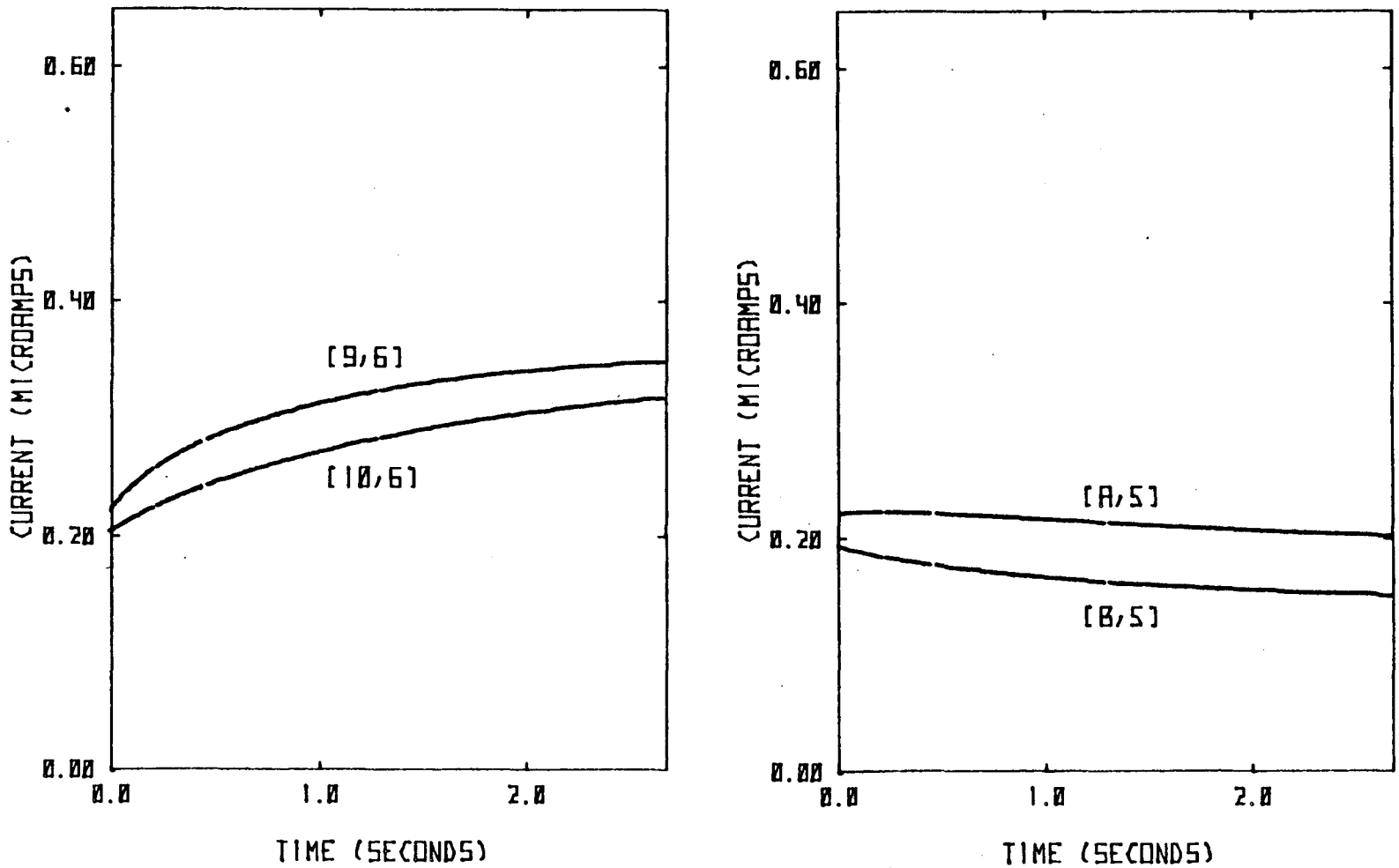

XBL 836-10478

Figure 2.4.2.36 Limiting current to segments beginning 0.31 sec after the event.

The long time studies of the simultaneous coalescence and disengagement reveals a behavior similar to that observed in the long time disengagement studies. A sample of the current to two segments after the beginning of the event is given in Fig. 2.4.2.37 where the relative size and position of the bubbles is given in Fig. 2.4.2.28. Some information after the event was lost, but it was less than a few tenths of a second of data. After a few seconds the current is governed by free convection, but another 10 to 15 seconds are required to obtain a normal stable pattern.

Significant increases have been observed in the rate of mass transfer to the surface as a result of the microconvection generated by the simultaneous coalescence and disengagement of the two bubbles. The relatively small increases observed from the disengagement studies and the area on the electrode exhibiting the greatest enhancement effect indicates that the substantial increases can be attributed to coalescence events. Therefore, considering the frequency of coalescence on a gas evolving surface (20), coalescence induced fluid motion provides a very effective mechanism for mass transfer enhancement to a surface.

2.5 Stability of Micro-Mosaic Electrodes

Although the micro-mosaic electrode has proven to be a very effective experimental device for studying bubble phenomena, it is unfortunately not indestructable. The micro-mosaic electrode is susceptible to physical erosion and chemical corrosion when it is exposed to the experimental environment. This severely limits the useful lifetime of the electrode.

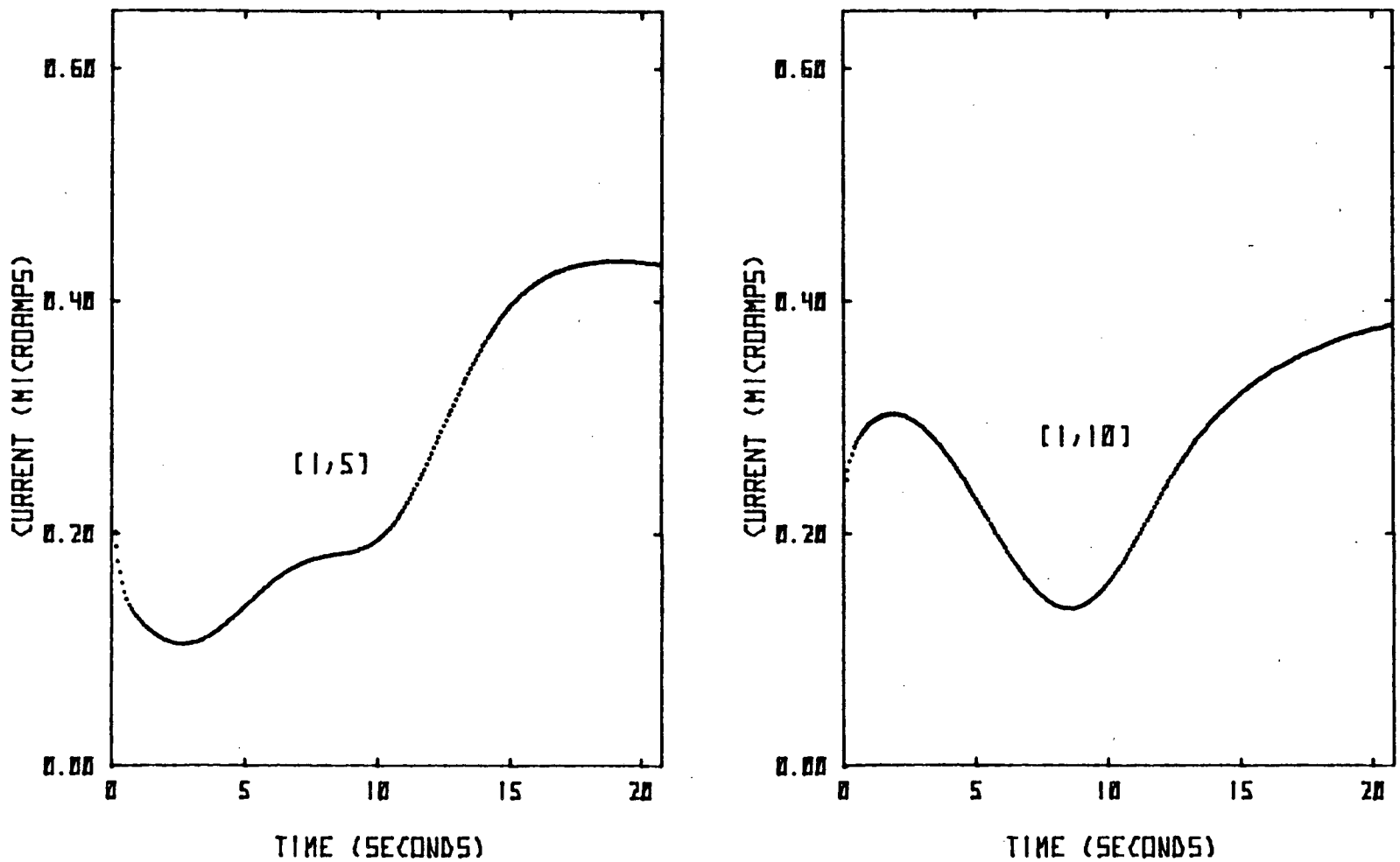

XBL 836-10468

Figure 2.4.2.37 Limiting current to a segment beginning less than 0.3 sec after the event.

Adhesion of the platinum to the oxide is a major problem. Even the chromium layer that was added does not prevent this. Any fluid flow exerts a net force on the elements of the electrode which erodes the platinum away. It has been observed that a bubble will pull loose the bubble growth segment upon disengaging from the electrode. This does not always occur, but after enough bubbles (i.e., approximately 4 to 6) the segment will be affected. The results of the erosion can be seen in Fig. 2.5.1. A missing segment in the lower right hand corner is quite visible. Gouges in the surface are also apparent. The darker segments can be seen better in Fig. 2.5.2. The segments are darker as a result of having less platinum on the surface. Erosion is apparent from the microscopic roughness of the segments and its rounded
corners.

The aluminum is subject to corrosion when it comes into contact with the electrolyte. This occurs as a result of the erosion of the platinum. Pin hole defects in the oxide layer can also expose aluminum. The rate of corrosion is relatively slow, requiring days of exposure to have a significant effect. The rate would be enhanced by adding chloride ions to electrolyte, so this should be avoided.

A series of 29 experiments were conducted over a 24 hour period. The micro-mosaic electrode used in the experiments was originally new. The experiments were conducted at approximately equal intervals and the electrode was exposed to the electrolyte during all the 24 hours. Initially ten segments on the electrode were defective. The rate at which segments stopped passing current can be seen in Fig. 2.5.3.

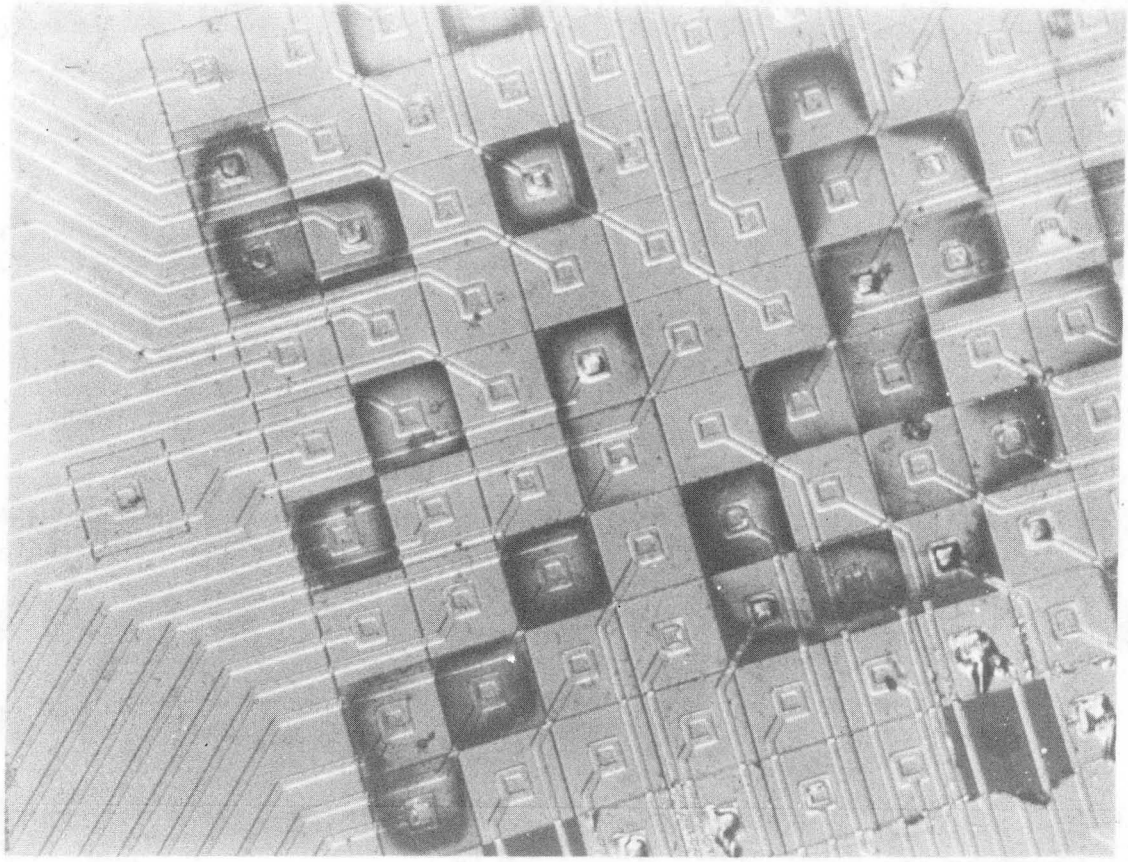

CBB 823-02040

Figure 2.5.1 Segmented portion of an "old" micro-mosaic electrode.

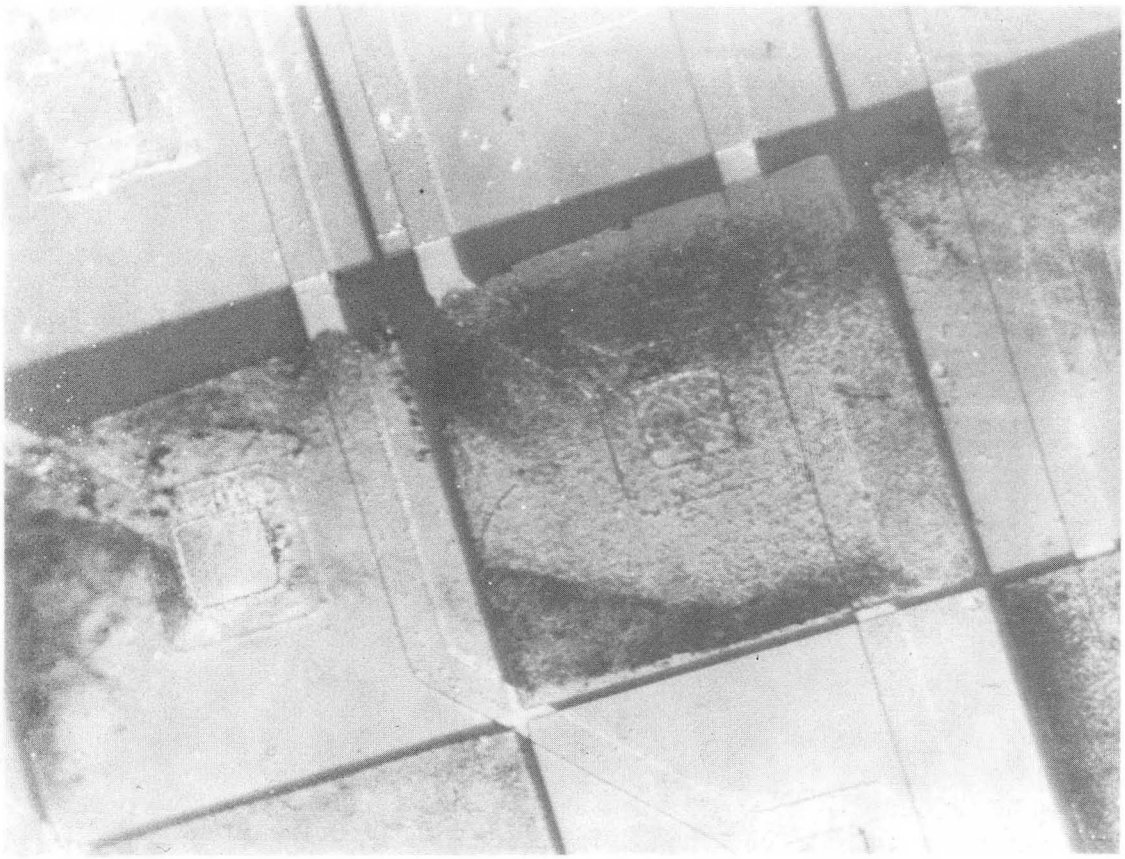

CBB 823-02038

Figure 2.5.2 Segments of an "old" micro-mosaic electrode.

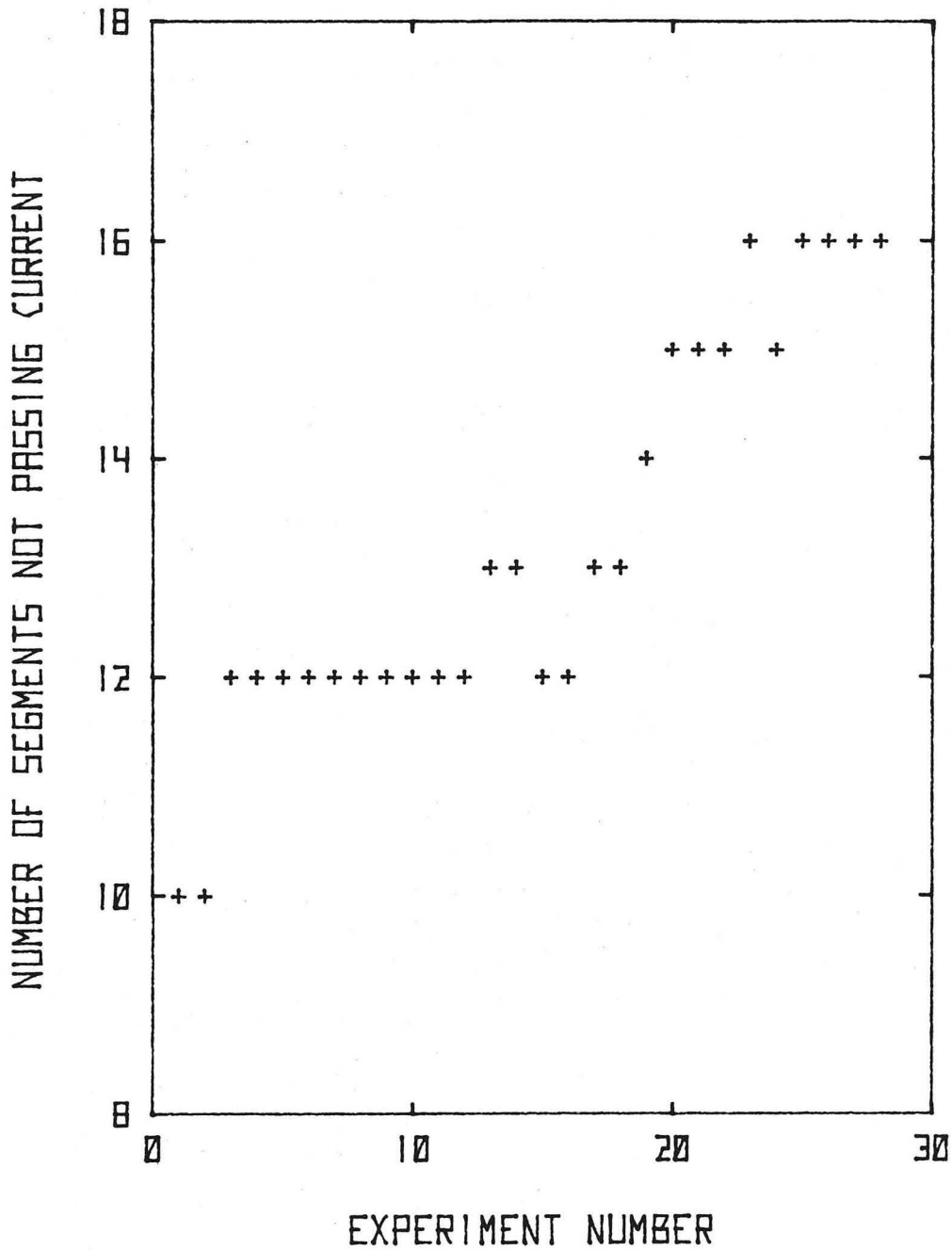

XBL 836-10462

Figure 2.5.3 Number of defective segments during experimentation over a 24 hour period.

Of even greater importance is the fact that the electrode will degrade in the cell after it has been used. This occurs whether there is air, deionized water, or electrolyte above the electrode. The degradation is not visible or necessarily permanent, but electrode segments do stop working. The source of this degradation was not determined. Both X-Ray Flouresence and Scanning Auger Microscopy were used to examine the elemental composition of the surface, without success. It was observed that the wetting characteristics of the oxide would change after it had been exposed to the electrolyte. Whether this is relevant to the problem was not determined.

The current to segments surrounding a defective segment was examined during bubble disengagements to determine the effect of the defective segments on the experimental results. The effect of a single bad segment is given in Fig. 2.5.4 (A), while the effect of two bad segments next to each other is shown in Fig. 2.5.4 (B). The relative size and position of the bubble on the micro-mosaic electrode at the time of disengagement is shown in Fig. 2.4.2.16. The inward fluid flow parallel to the electrode generated by the bubble disengagement can significantly enhance the mass transfer rate when an unusually large radial concentration gradient is created by defective segments. This is the reason for the significant mass transfer enhancement effect observed for a bubble disengagement with the multi-electrode cell.

The defective segments only affected the current to neighboring segments. Probably the ultimate example of this can be seen in Fig. 2.5.6 where the relative size and position of the bubble at disengagement is given in Fig. 2.5.5. Nearly all the micro-mosaic

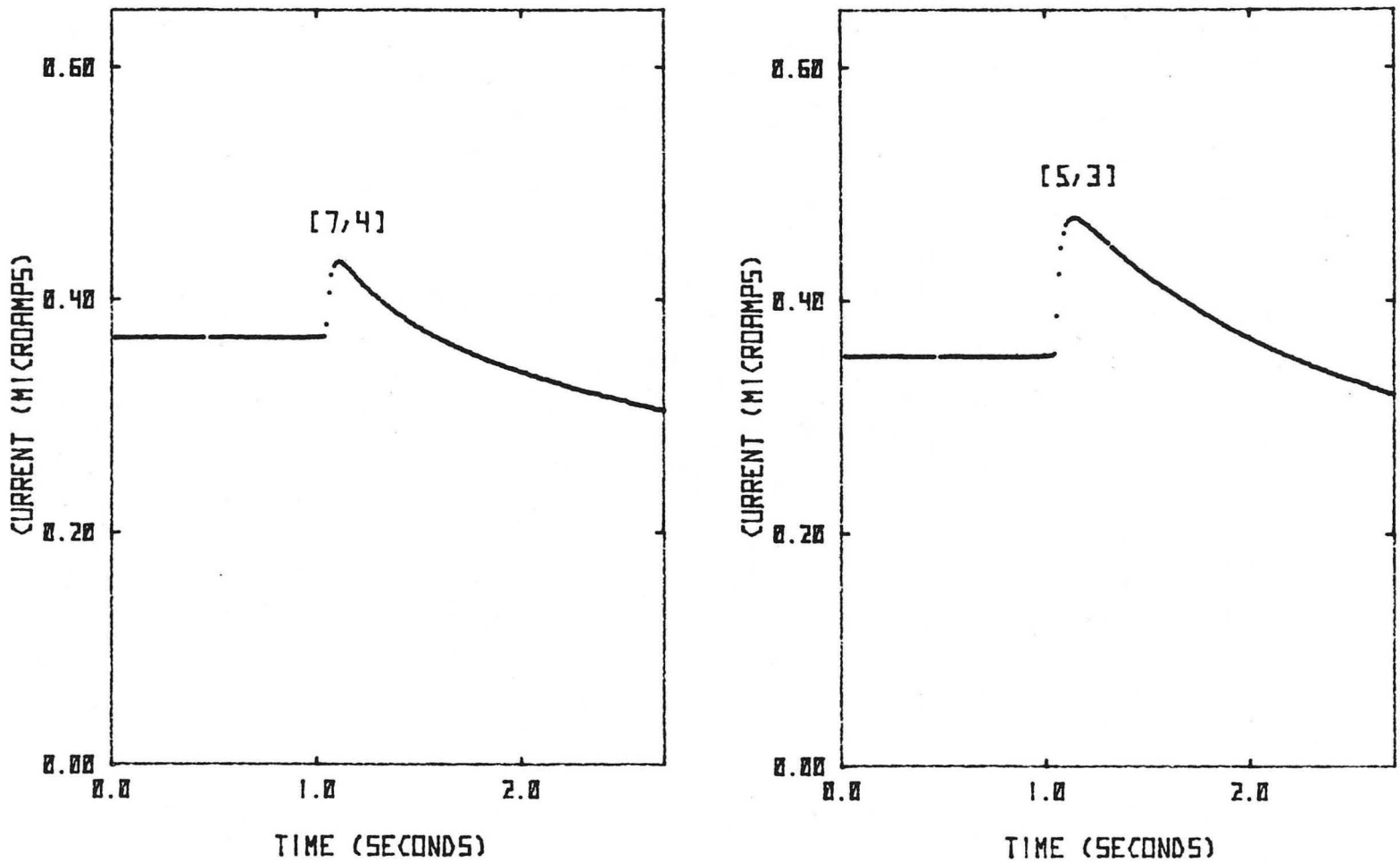

XBL 836-10471

Figure 2.5.4 Limiting current to a segment before and after the disengagement of a bubble; (A) near one defective segment; (B) near two defective segments.

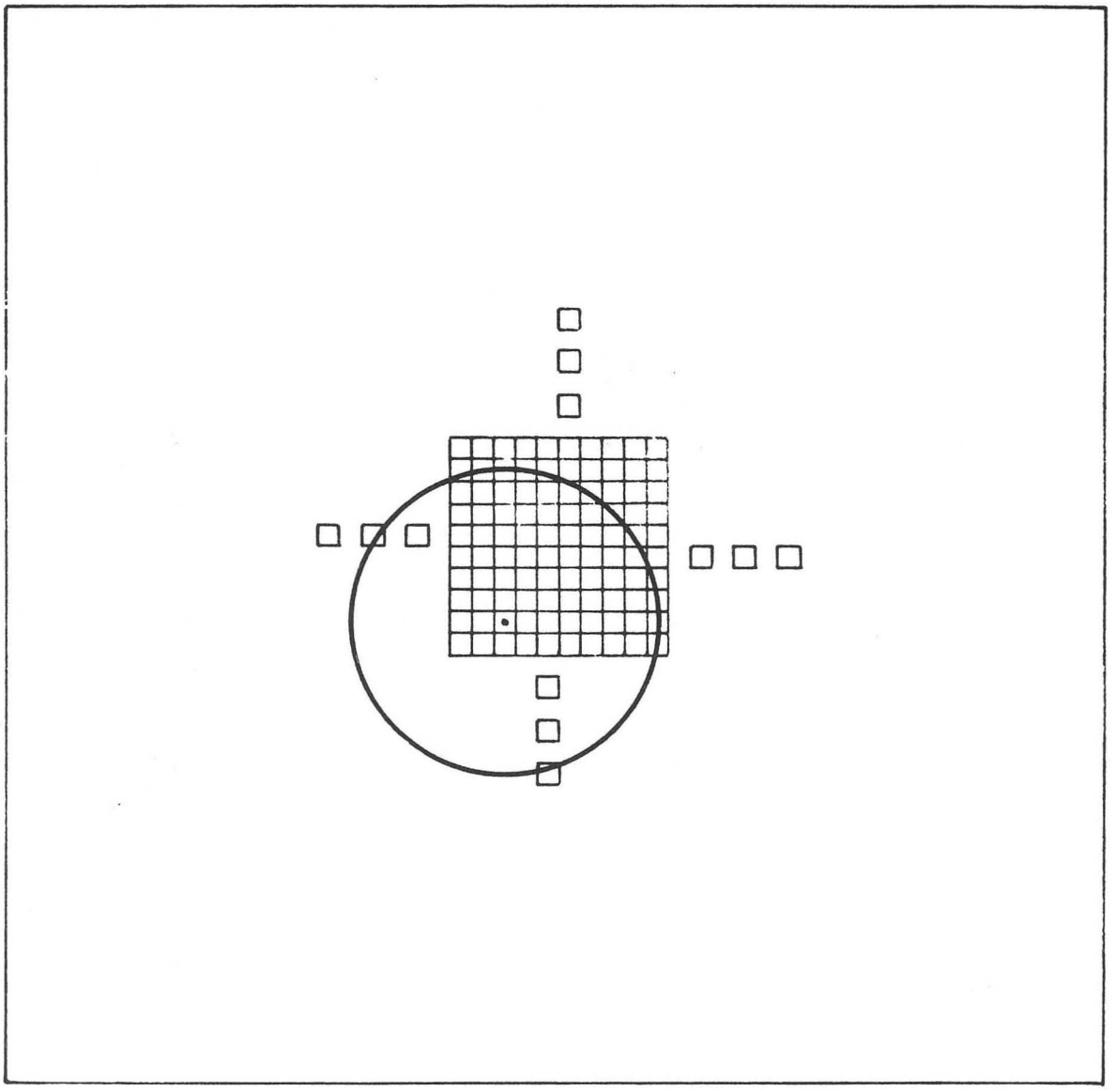

XBL 838-6104

Figure 2.5.5 Schematic of the micro-mosaic electrode showing the perimeter of the bubble at the time of disengagement.

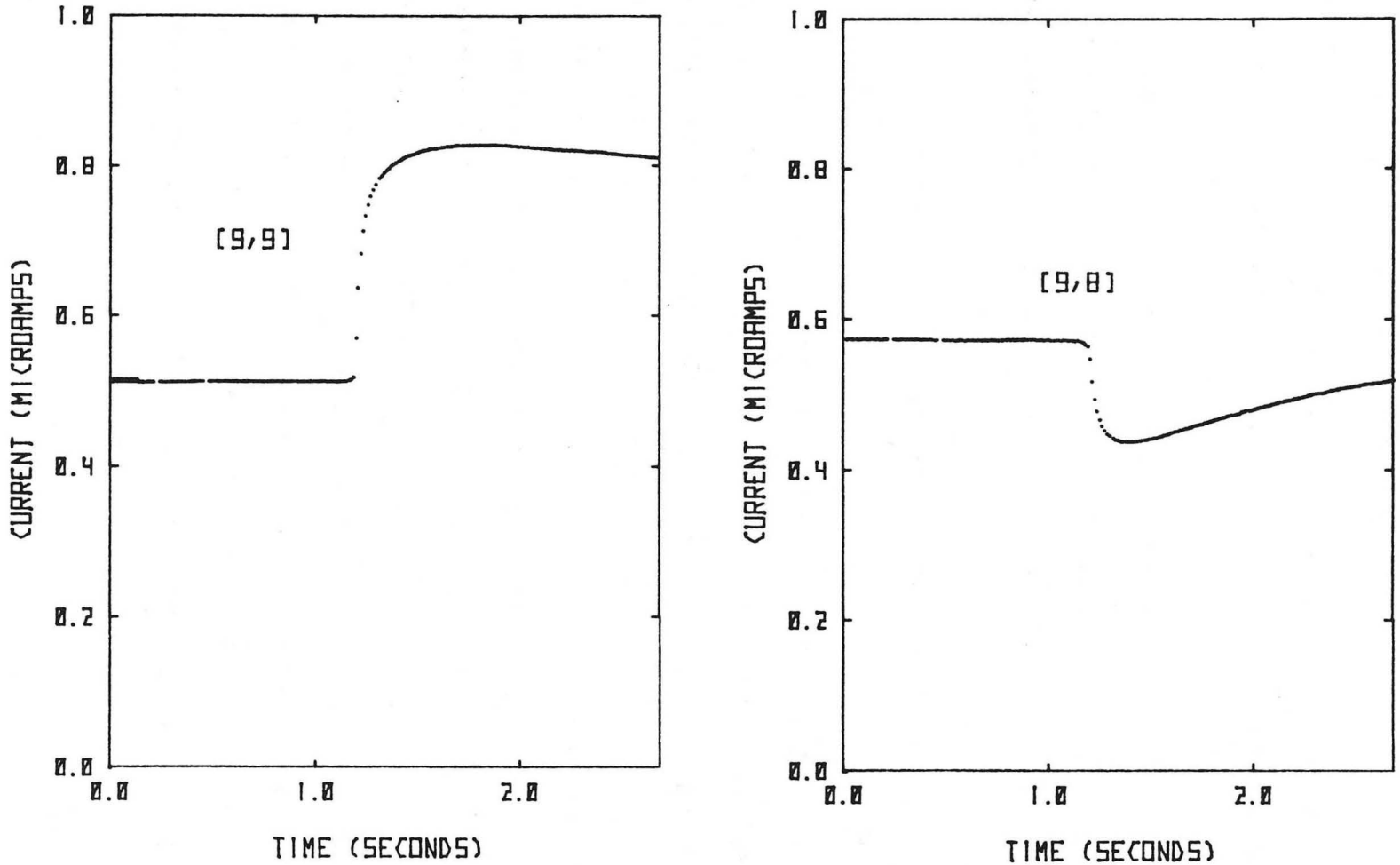

XBL 836-10472

Figure 2.5.6 Limiting current to a segment before and after the disengagement of a 1.4 mm diameter bubble.

electrode elements were defective, including the buffer segment. This is indicated by high value of the free convection limiting current. The inward parallel flow causes a significant increase in the current to a segment, shown in Fig. 2.5.6 (A), while there is a decrease in the current to the neighboring segment, shown in Fig. 2.5.6 (B).

Once the number of defective segments reaches 30 to 40, the assumption that the electrode simulates a continuous surface breaks down completely. Experiments that do not require this assumption can still be conducted.

2.6 Mass-Transfer Studies with a Replica of the Micro-Mosaic Electrode

2.6.1 Description of the Replica of the Micro-Mosaic Electrode

A replica of the micro-mosaic electrode was constructed. It has the same dimensions as the micro-mosaic electrode and is made of platinum, but it is not segmented like the micro-mosaic electrode. The replica does have a small (125 μm diameter) platinum disk at the center of the electrode, which is insulated from the main electrode.

The replica consists of a 0.5 cm x 0.5 cm platinum foil embedded in a 12.4 cm x 12.4 cm lucite base, shown in Fig. 2.6.1.1. The electrode and the lucite lie in the same plane. A 125 μm (0.005 in.) diameter platinum wire embedded in epoxy serves as the disk in the center of the electrode. The relative size of the epoxy area surrounding the wire is shown in Fig. 2.6.1.2. Electrical connections to the main electrode segment and the wire are made from the bottom of the base.

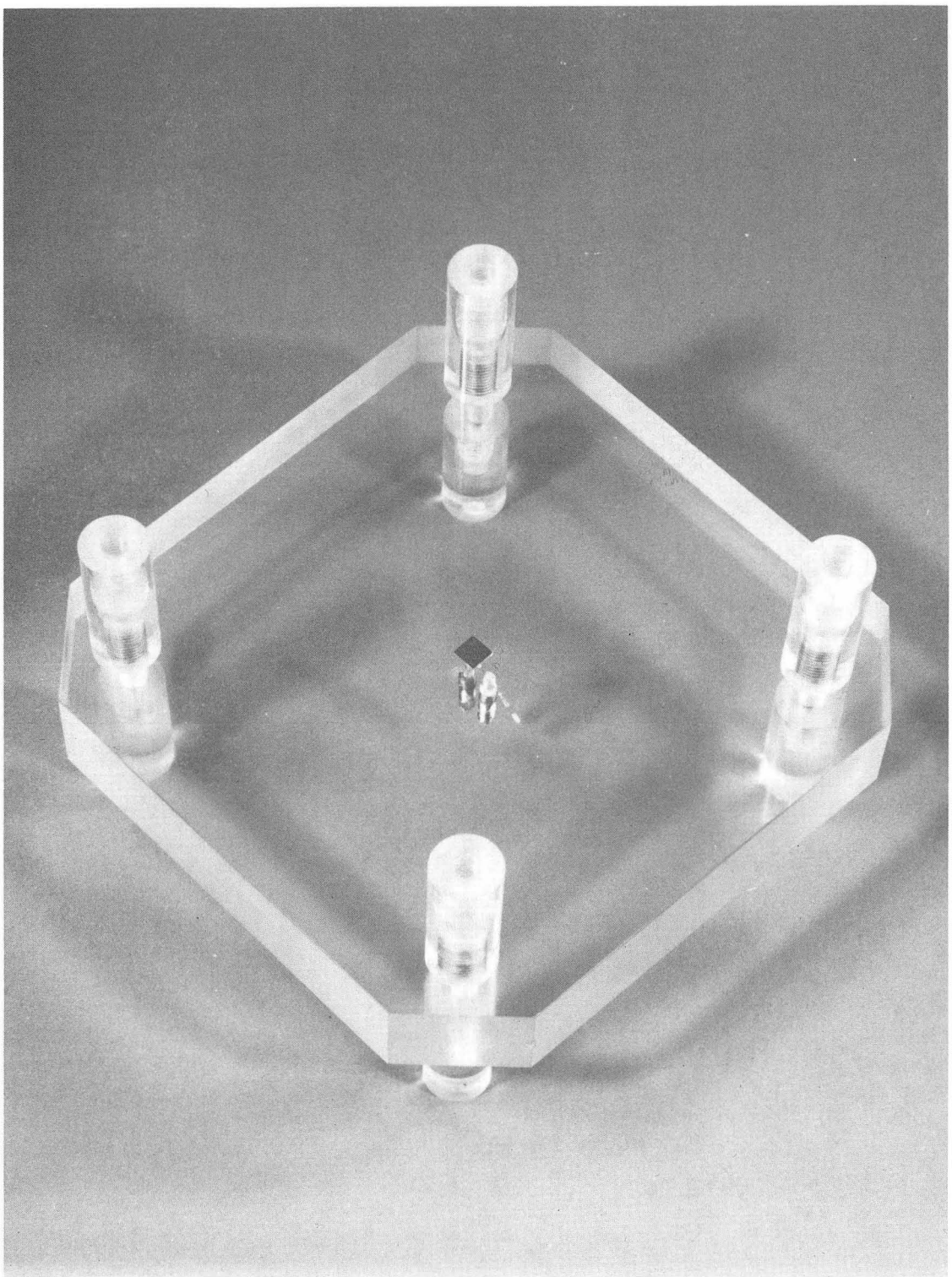

CBB 836-5377

Figure 2.6.1.1 Replica of micro-mosaic electrode.

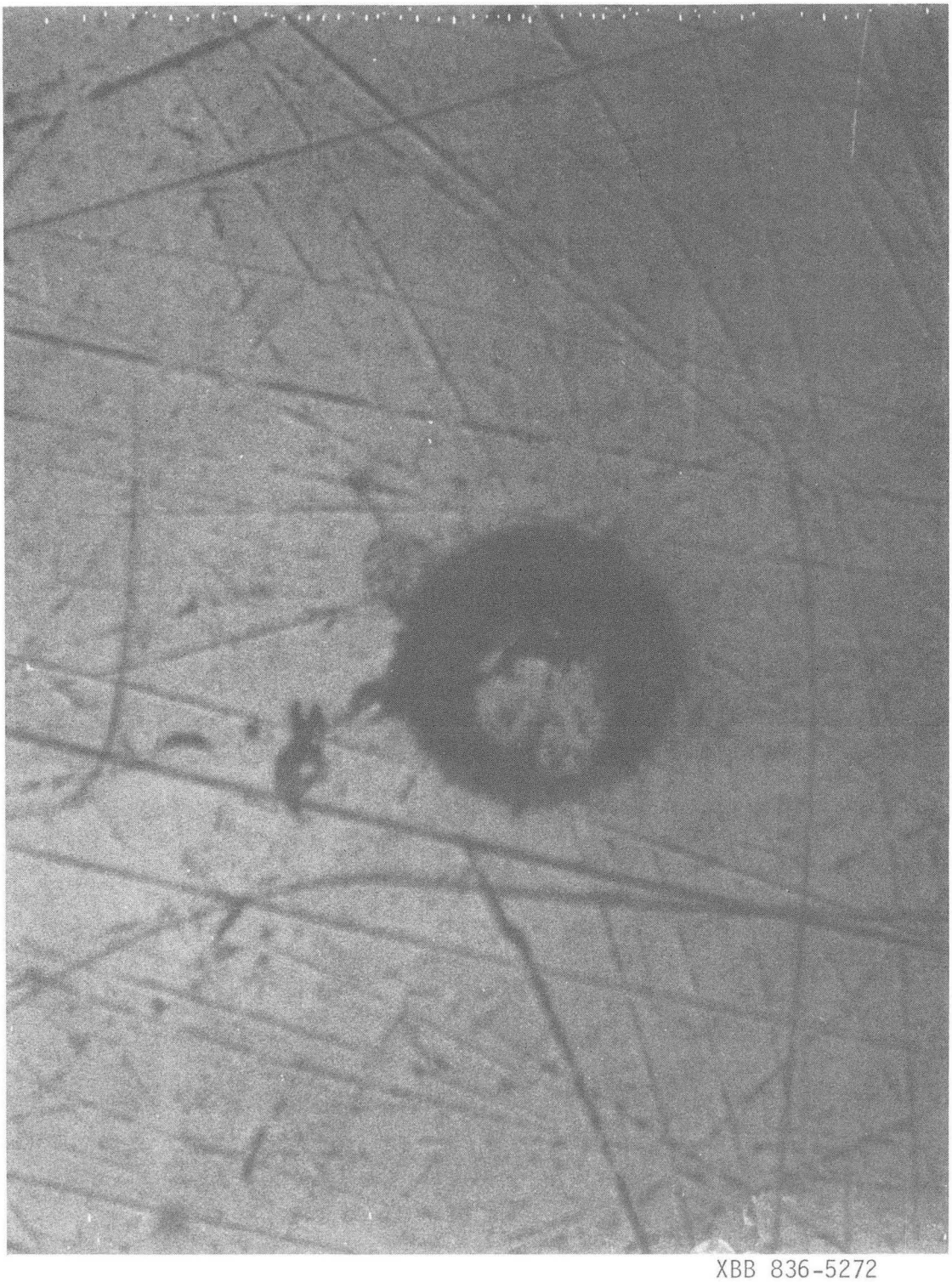

XBB 836-5272

Figure 2.6.1.2 Wire electrode segment at the center of replica.

The base was designed to fit the cell built for the micro-mosaic electrode with the electrode oriented horizontally. The replica with the cell is shown in Fig. 2.6.1.3.

2.6.2 Method and Instrumentation

The replica of the micro-mosaic electrode was used to examine the relationship between the mass-transfer enhancement effect of micro-convection and macro-convection at a gas-evolving surface oriented horizontally. This was accomplished by evolving hydrogen on the main electrode segment and monitoring the current to the wire, which was polarized in the limiting current region for an indicator ion.

The indicator ion reaction, electrolyte composition, and reference electrode used in the studies of individual bubble phenomena were not changed for this study (see Section 2.1). The wire was polarized at -500 mV relative to the reference electrode, which was well into the limiting current potential range for the reduction of ferric ions.

The main electrode segment was polarized from -800 mV to -1000 mV relative to the reference electrode, which was in the hydrogen evolution potential range. The effect of the gas evolution on the current to the wire was measured.

The instrumentation for the replica is basically the same as used in the early mass-transfer studies with the micro-mosaic electrode (see Section 2.3.3). The only real difference is the number of electrode connections to be made. Since the electrode only has two electrical connections, the wire and the main segment, it is a much easier system to use.

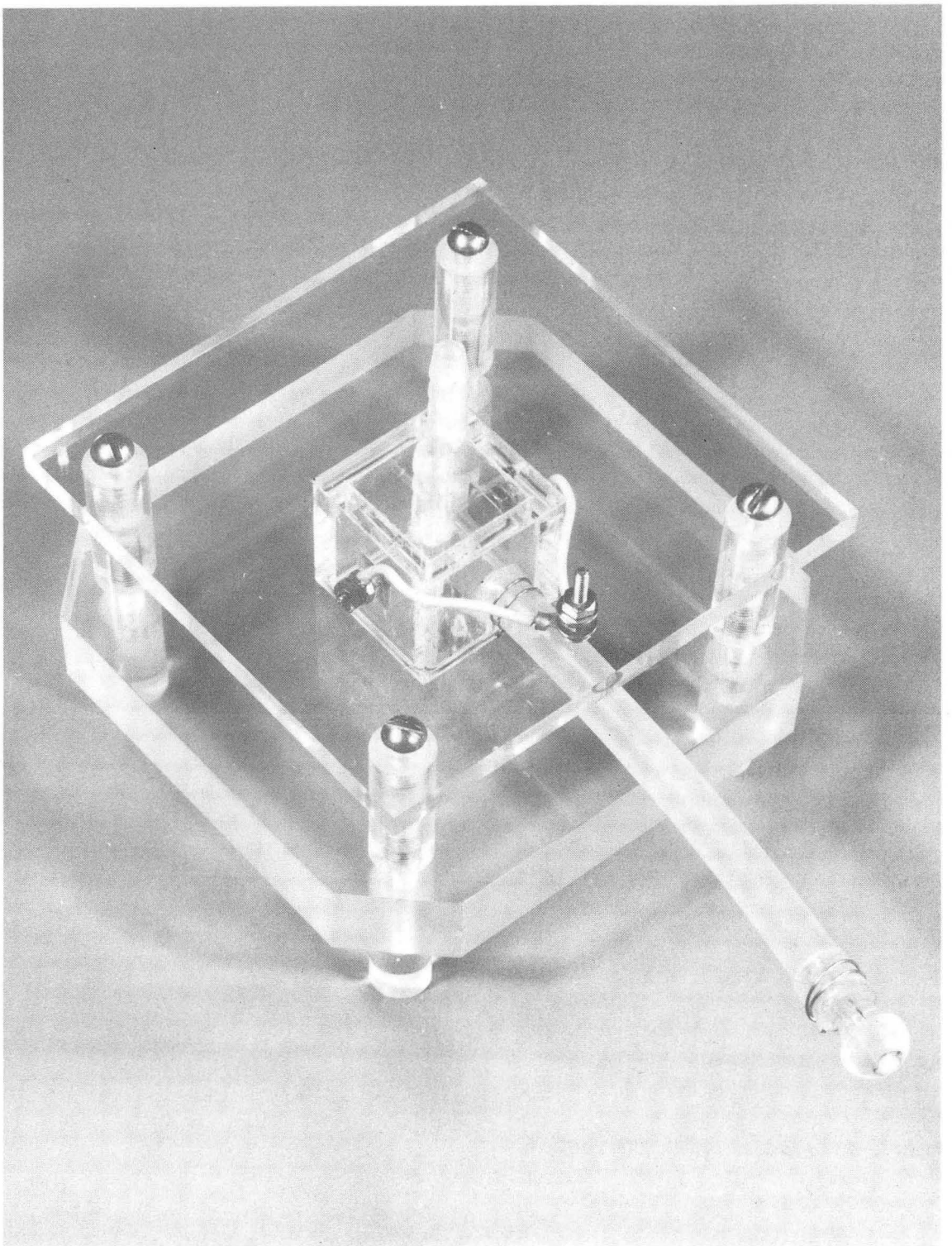

CBB 836-5375

Figure 2.6.1.3 Replica with micro-mosaic electrode cell.

Other mass transfer experiments conducted with the replica included a potential-step experiment and free convection studies.

2.6.3 Results and Discussion

Potential-step experiments similar to those conducted on the micro-mosaic electrode (see Section 2.3.4) were performed on the replica. The current to the entire electrode after a potential-step into the limiting current range for the reduction of ferric ions is given in Fig. 2.6.3.1 (A). This can be compared to Fig. 2.3.4.1 (A), which shows the result of the same experiment with the micro-mosaic electrode. The total electrode current plotted against the inverse square root of time, shown in Fig. 2.6.3.1 (B), exhibits a linear behavior as predicted by Eq. 2.3.4.1. The diffusion coefficient determined for the ferric ions is 4.96×10^{-6} cm^2/sec, which is within 8% of the value obtained using the micro-mosaic electrode.

The free convection limiting current to the entire electrode and to the wire is given in Fig. 2.6.3.2. The amplitude of the fluctuations in the current to the entire electrode are much smaller than was observed for the current to the entire micro-mosaic electrode. In fact the fluctuations are almost obscured by the noise in the signal. The average current to the entire electrode is 0.68 mA which is about 13% smaller than the average current to the micro-mosaic electrode. The fluctuations in the current to the wire are quite apparent. The fluctuations are not as regular as was observed with the micro-mosaic electrode, but the period of 29 seconds is the same as in the previous studies. It was not determined whether the

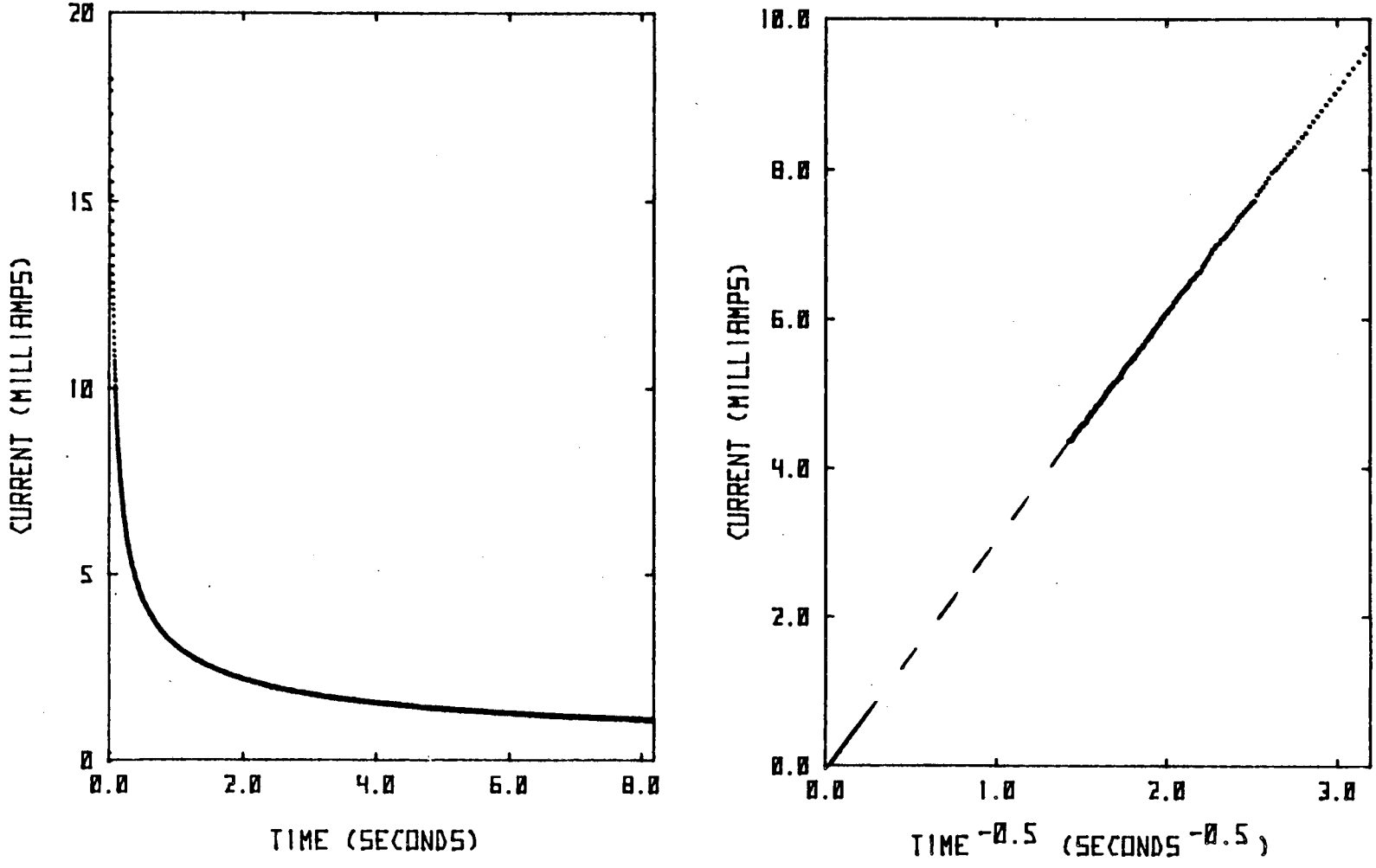

XBL 836-10463

Figure 2.6.3.1 Potential step limiting current to the entire electrode; (A) Time on abscissa; (B) Inverse square root of time on abscissa.

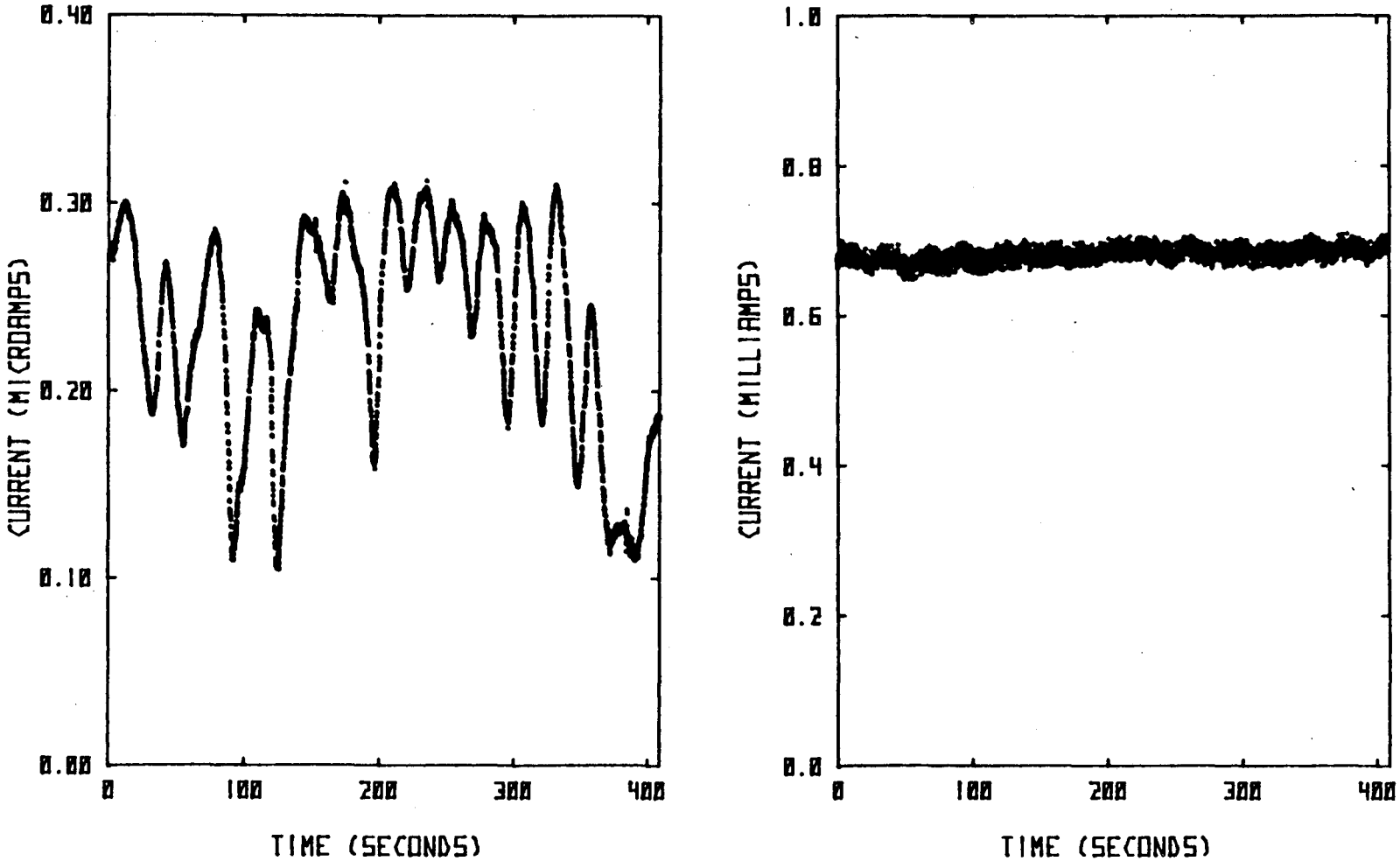

XBL 836-10464

Figure 2.6.3.2 Free convection limiting current; (A) to the wire segment; (B) to the main electrode segment.

irregular fluctuations were a result of the relatively wide epoxy insulating area surrounding the wire or the chaotic behavior observed in the free convection limiting current.

The experimental method developed to examine the role of microconvection and macroconvection on the mass transfer rate to a gas-evolving surface was only partially successful. It was observed in the individual bubble studies with the micro-mosaic electrode (see Section 2.4.2) that a potential difference between two adjacent segments could cause an anodic reaction to occur on one of the segments even though both are polarized cathodically relative to the reference electrode. Oxidation of hydrogen, generated at the main electrode segment, was observed on the wire. This results in a net anodic current to the wire at small gas evolution rates.

The results are given in Figs. 2.6.3.3, 2.6.3.4, and 2.6.3.5. The current to the wire is shown in graph (A) and the current to the main electrode segment in graph (B). In graph (B) of all the figures the cathodic currents are recorded as positive values. A cathodic current is negative on graph (A) in all the figures.

The current to the main electrode segment is the result of two cathodic reactions ($2H^+ + 2e^- \rightarrow H_2$; $Fe^{+++} + e^- \rightarrow Fe^{+++}$). The Nernst boundary layer thickness and thus the average current to the wire, in the absence of the oxidation of hydrogen, can be predicted from the average current to the main electrode segment and the experimental results of Jannssen and Hoogland (12). The predicted average current to the wire; in Fig. 2.6.3.3 (A) is -0.65 μA, in Fig. 2.6.3.4 (A) is -0.94 μA, and in Fig. 2.6.3.5 (A) is -1.62 μA. In each case the

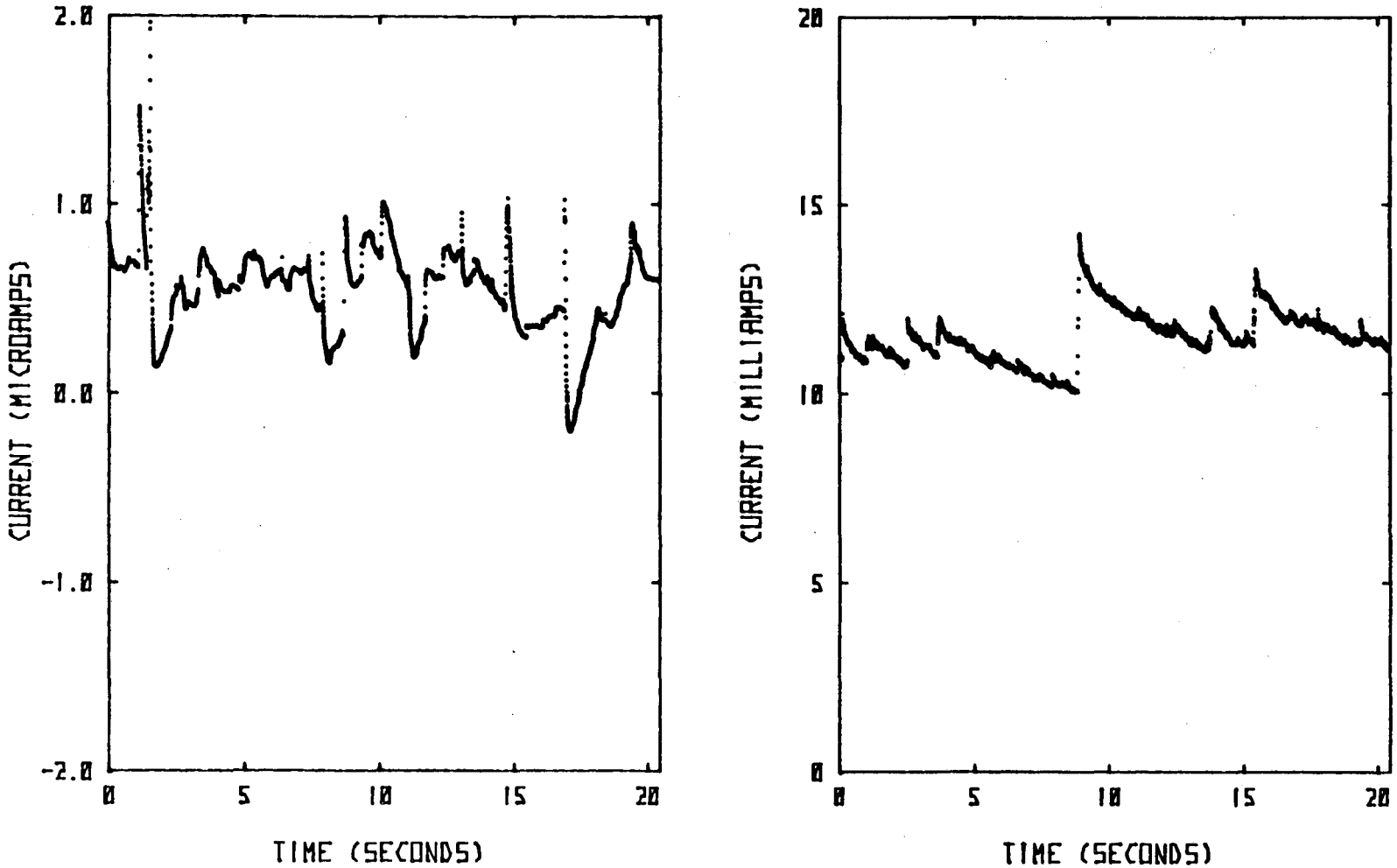

XBL 836-10465

Figure 2.6.3.3 (A) Current to the wire segment; (B) current to the main electrode segment.

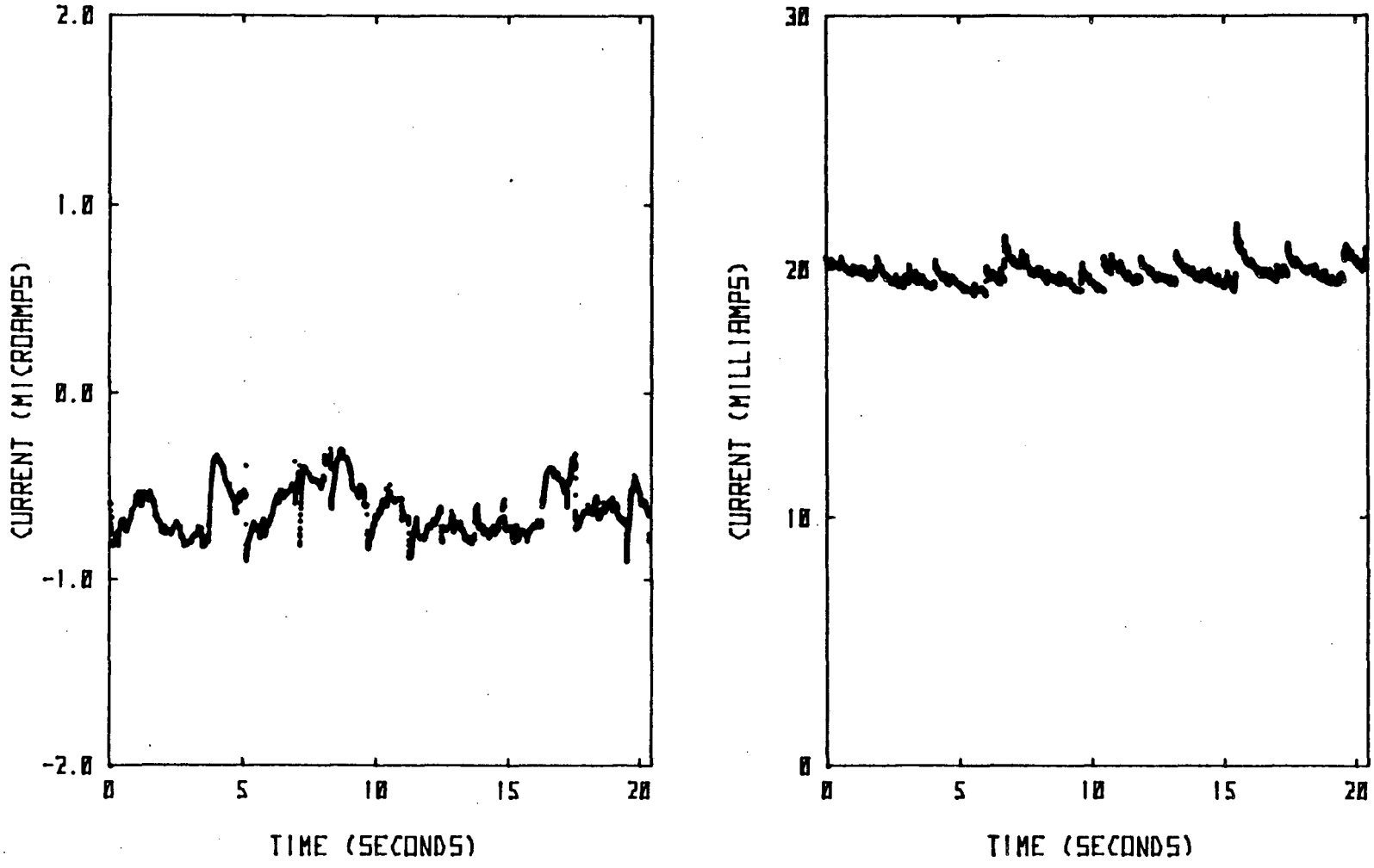

Figure 2.6.3.4 (A) Current to the wire segment; (B) current to the main segment. XBL 836-10466

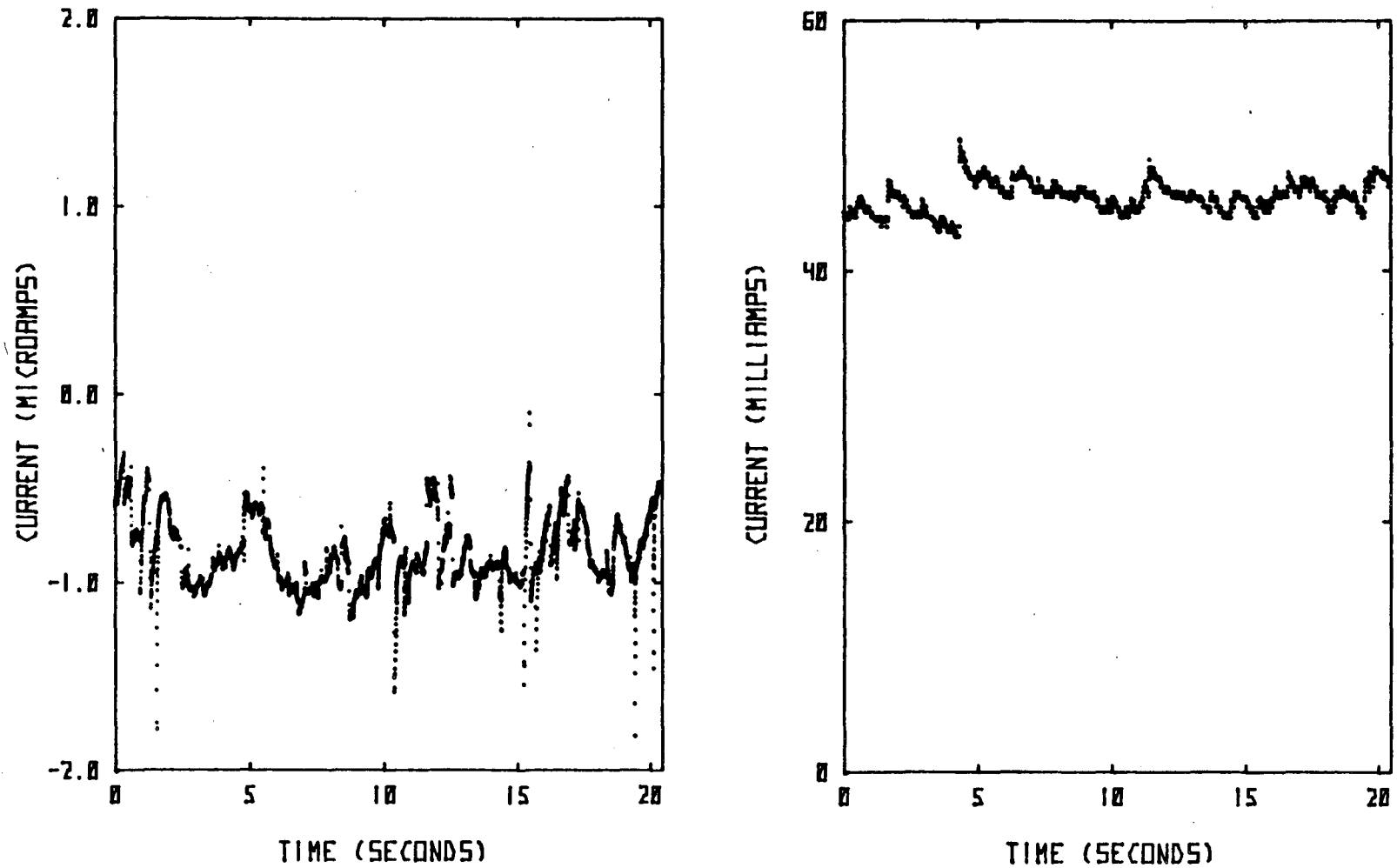

XBL 836-10467

Figure 2.6.3.5 (A) Current to the wire segment; (B) current to the main electrode segment.

predicted value is larger than the actual measured current, indicating that there is indeed an anodic side reaction taking place on the wire.

As a result of the side reaction on the wire it is difficult to make conclusions regarding the relative importance of micro-convection and macro-convection on a gas evolving surface. However some observations can be made about the characteristics of the current versus time curves. If the oxidation of hydrogen on the wire is not mass-transfer limited, then the fluctuations in the current can be attributed to variations in the mass-transfer rate of ferric ions. Furthermore if the macro-convection can be considered in the steady-state the fluctuations can be associated with the micro-convection near the surface. This is indicated by comparing the time constant of the fluctuation, which is of the order of 0.1 seconds, to the ones obtained in the individual bubble studies. Since increasing the gas evolution rate will also increase the rate of bubble phenomena, the frequency of the fluctuations should increase with the gas evolution rate. The amplitude of the fluctuations should not change significantly because the same phenomenon are occurring, only at a faster rate. Both trends are observed.

2.7 Nomenclature

A: Electrode surface area, cm^2.

C: Concentration, moles cm^{-3}.

D: Diffusion coefficient, cm^2 sec^{-1}.

F: Faraday constant, 96,487 C $equiv.^{-1}$.

I: Total current, Amps.

k_c: Proportional control constant, Volt $Amps^{-1}$.

n: Electrons transferred in reaction; equiv $mole^{-1}$.

t: Time, seconds.

V: Potential, Volts.

Greek Letters

τ: Control constant, seconds.

Subscripts

B: Denotes bulk property.

D: Denotes differential control constant.

I: Denotes integral control constant.

S: Denotes initial set point value.

3. THEORETICAL CONSIDERATIONS

To theoretically describe the mass-transfer enhancement to a horizontal surface as a result of a bubble diengagement would require that a set of unsteady non-linear coupled partial differential equations be solved numerically. Modeling of this sophitication is beyond the scope of the present work. However; it is instructive to examine a series of models which describe individual aspects of a bubble disengagement. These include the bubble shape, mass-transfer effects from the ascension of the bubble, and mass-transfer effects from the collapse of the bubble's contact area. The models are quite useful for explaining some of the experimentally observed mass-transfer effects from a bubble disengagement. Since the free-convection mass transfer to a horizontal surface plays an important role in the expeimental studies, the transport equations describing the phenomenon are developed.

3.1 Relevant Transport Equations

Several basic assumptions are made in the theoretical work presented here. First it is assumed that dilute solution transport equations for an isothermal system are applicable to the experimental system. This is a common assumption for aqueous systems of low to moderate electrolyte concentrations. Secondly, the electrolyte is considered to be well-supported. Considering that there is approximately an order of magnitude higher acid concentration than the concentration of the reacting ionic species concentration, this also should be valid. Finally, with the exception of the density in the free-convection work the transport properties are assumed to remain constant.

Initially there are three ionic components in the aqueous electrolyte (H^+, $SO_4^=$, Fe^{+++}). As a result of the ferric ion reaction, a fourth is produced (Fe^{++}). The mass transport equation for each ionic species is given by:

$$\frac{\partial c_i}{\partial t} + v \cdot \nabla c_i = z_i u_i F \nabla \cdot (c_i \nabla \Phi) + D_i \nabla^2 C_i \tag{3.1.1}$$

where the subscript (i) refers to the ionic species (i = 1 for $SO_4^=$; i = 2 for H^+; i = 3 for Fe^{+++}; i = 4 for Fe^{++}). The electroneutrality condition is given by:

$$\sum_{i=1}^{4} z_i c_i = 0 \tag{3.1.2}$$

Following the development of Levich (46), for a well-supported electrolyte the concentrations and potential can be written in terms of a perturbation expansion. If the concentration of the reacting species is zero in the zero approximation and all terms higher than the first order terms are neglected, the dependent variables are given as follows:

$$c_1 = c_1^0 + c_1^1 \tag{3.1.3}$$

$$c_2 = c_2^0 + c_2^1 \tag{3.1.4}$$

$$c_3 = c_3^1 \tag{3.1.5}$$

$$c_4 = c_4^1 \tag{3.1.6}$$

$$\Phi = \Phi^1 \tag{3.1.7}$$

In writing the perturbations in this manner, it is assumed that the supporting electrolyte does not react and therefore the zero approximation terms are constant. This is not strictly true since the protons do react at bubble growth segments. Substituting Equations 3.1.3-7 into the four mass transport equations for the ionic species (Equation 3.1.1) and deleting all second order terms we obtain:

$$\frac{\partial c_1^1}{\partial t} + v \cdot \nabla c_1^1 = z_1 u_1 F \, c_1^0 \, \nabla^2 \Phi^1 + D_1 \nabla^2 c_1^1 \tag{3.1.8}$$

$$\frac{\partial c_2^1}{\partial t} + v \cdot \nabla c_2^1 = z_2 u_2 F \, c_2^0 \nabla^2 \Phi^1 + D_2 \nabla^2 c_2^1 \tag{3.1.9}$$

$$\frac{\partial c_3^1}{\partial t} + v \cdot \nabla c_3^1 = D_3 \nabla^2 c_3^1 \tag{3.1.10}$$

$$\frac{\partial c_4^1}{\partial t} + v \cdot \nabla c_4^1 = D_4 \nabla^2 c_4^1 \tag{3.1.11}$$

It is seen that the reacting species follow the well known convective diffusion equation. The electroneutrality condition and Equations 3.1.8 and 3.1.9 can be combined to eliminate the electric potential and the concentration of one of the supporting electrolyte species, resulting in Equation 3.1.12.

$$\frac{\partial c_1^1}{\partial t} + v \cdot \nabla c_1^1 = D_e \nabla^2 c_1^1 + \frac{z_3 u_1 (D_2 - D_3)}{z_1 u_1 - z_2 u_2} \nabla^2 c_3^1 + \frac{z_4 u_1 (D_2 - D_4)}{z_1 u_1 - z_2 u_2} \nabla^2 c_4^1 \tag{3.1.12}$$

D_e is given by Equation 3.1.13.

$$D_e = \frac{z_1 u_1 D_2 - z_2 u_2 D_1}{z_1 u_1 - z_2 u_2} \tag{3.1.13}$$

The fluid flow is governed by the overall mass balance equation and the momentum balance, or Navier-Stokes, equation, given by Equations 3.1.14 and 3.1.15 respectively.

$$\nabla \cdot \mathbf{v} = 0 \tag{3.1.14}$$

$$\frac{\partial \mathbf{v}}{\partial t} + \mathbf{v} \cdot \nabla \mathbf{v} = -\frac{1}{\rho} \nabla \cdot P + \nu^2 \quad \nabla \mathbf{v} + g \tag{3.1.15}$$

The development of the transport equations which describe the experimental system in this work is not new. The reader should refer to either Newman's (45) or Levich's (61) monograph for a more detailed development.

Nomenclature

c: Concentration, moles cm^{-3}.

D: Diffusion coefficient, cm^2 sec^{-1}.

F: Faraday constant, 96,487 C $equiv.^{-1}$.

g: Acceleration due to gravity, cm sec^{-2}.

P: Pressure, dyne cm^{-2}.

t: Time, sec.

u: Ionic mobility, cm^2 mole J^{-1} sec^{-1}.

v: Velocity, cm sec^{-1}.

z: Charge number of species.

Greek Letters

μ: Viscosity, g cm^{-1} sec^{-1}.

ν: Kinematic viscosity ($\mu\rho^{-1}$), cm^2 sec^{-1}.

ρ: Density, g cm^{-3}.

Φ: Electric potential, volts.

Subscripts

i: Denotes ionic component

1: Denotes $SO_4^{=}$

2: Denotes H^+

3: Denotes Fe^{+++}

4: Denotes Fe^{++}

e: Denotes binary diffusion coefficient for supporting electrolyte.

Superscripts

0: Denotes zero approximation term.

1: Denotes first approximation term.

3.2 Equilibrium Shape of a Bubble Attached to a Horizontal Surface

In the individual bubble phenomena studies, bubbles were observed from above. This allowed the measurement of the maximum bubble diameter, but the overall bubble shape could not be determined. However it is relatively easy to predict the equilibrium shape of a bubble on a horizontal surface. Since the bubbles were grown at a slow rate (~ 30 minutes to release), their shape should be very close to the equilibrium shape before the initiation of the bubble event. The equilibrium shape of bubbles on a horizontal surface indicates the deviations of the bubbles studied with the micro-mosaic electrode from a spherical cap shape. The possibility of having a relatively large bubble with a small base will also be determined.

The development of the equations which govern the shape of the bubble can be found in numerous references (32), (47). Starting with the Laplace equation, which relates the principal radii of curvature of a surface to the pressure difference across the surface, a set of nonlinear coupled ordinary differential equations can be derived. The differential equations, first solved by Bashforth and Adams (48), relate the shape of a bubble to the radius of curvature at the top of the bubble (R_0) and a dimensionless group defined by Equation 3.2.1:

$$\lambda = \frac{(\rho_\alpha - \rho_\beta)\, g\, R_0^2}{\gamma} \tag{3.2.1}$$

The differential equations are given by Equations 3.2.2-4:

$$\frac{\sin \phi}{\tilde{x}} + \frac{1}{\tilde{R}} = 2 + \lambda\, \tilde{z} \tag{3.2.2}$$

$$\tilde{R} = \frac{\left[1 + \left(\frac{d\tilde{z}}{d\tilde{x}}\right)^2\right]^{3/2}}{\frac{d^2\tilde{z}}{d\tilde{x}^2}} \tag{3.2.3}$$

$$\sin \phi = \frac{\frac{d\tilde{z}}{d\tilde{x}}}{\left[1 + \left(\frac{d\tilde{z}}{d\tilde{x}}\right)^2\right]^{1/2}} \tag{3.2.4}$$

with the tilde quantities defined as:

$$\tilde{x} = x/R_0 \tag{3.2.5}$$

$$\tilde{z} = z/R_0 \tag{3.2.6}$$

$$\tilde{R} = R/R_0 \tag{3.2.7}$$

The coordinates of the bubble are shown in Fig. 3.2.1.

The equations are more easily solved by transforming the independent variable to the arc length measured from the top of the bubble. Equations 3.2.3 and 3.2.4 are then given by Equations 3.2.8 and 3.2.9 respectively:

$$\tilde{R} = \frac{\left[1 - \left(\frac{d\tilde{z}}{d\tilde{s}}\right)^2\right]^{1/2}}{\frac{d^2\tilde{z}}{d\tilde{s}^2}} \tag{3.2.8}$$

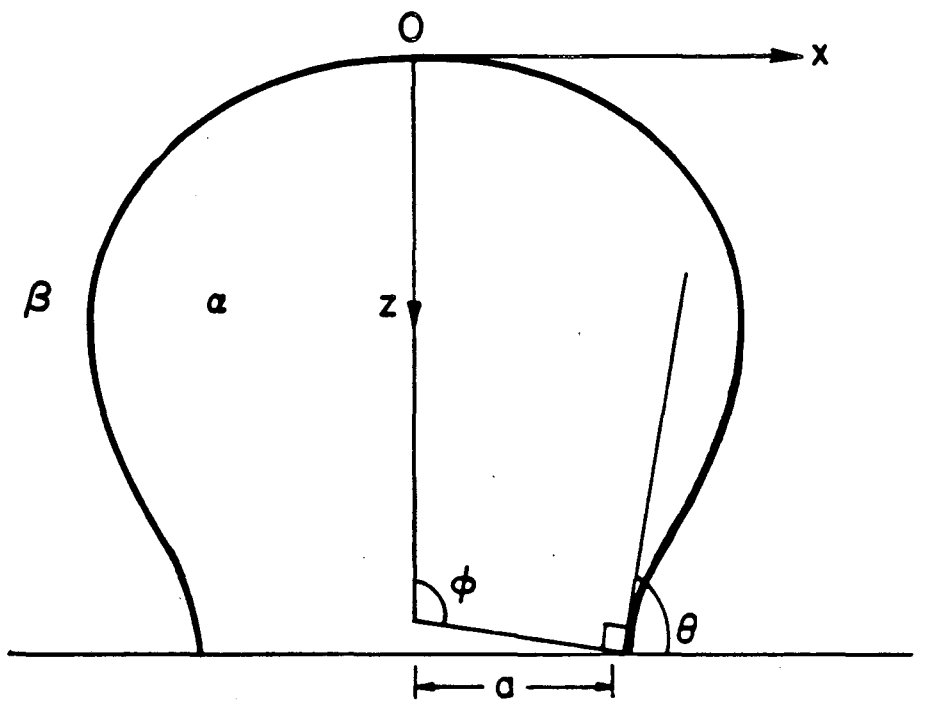

XBL671-359

Figure 3.2.1 Schematic diagram for a bubble attached to a surface.

$$\sin \phi = \frac{d\tilde{z}}{d\tilde{s}} \tag{3.2.9}$$

where the dimensionless arc length is defined as

$$\tilde{s} = \tilde{s}/R_0 \tag{3.2.10}$$

and the equation relating the two bubble coordinates and the arc length is:

$$1 = \left(\frac{d\tilde{x}}{d\tilde{s}}\right)^2 + \left(\frac{d\tilde{z}}{d\tilde{s}}\right)^2 \tag{3.2.11}$$

Equations 3.2.2, 3.2.8, 3.2.9, and 3.2.11 can be solved numerically by the Runge-Kutta method (49) with initial boundary conditions at zero arc length as follows:

$$\tilde{z} = 0 \tag{3.2.12}$$

$$\tilde{x} = 0 \tag{3.2.13}$$

$$\frac{d\tilde{z}}{d\tilde{s}} = 0 \tag{3.2.14}$$

A description and listing of the program which solves the set of differential equations and determines the shape of the bubble are given in Appendix G.

Knowing the physical parameters of the system and the maximum bubble diameter, we can completely describes the shape of the bubble, except for the relative position of the base. That is determined by

setting either the contact angle or the radius of the contact area. The only thing that is known about the contact area was that it was not large enough to cover a complete segment and interrupt the current. Therefore the radius of the contact area is taken to be 50 microns. The values of the surface tension is assumed to be 70 dyne/cm and density difference is approximately 1.0 g/cm^3.

The diameter of the bubbles studied varied from about 0.5 mm to 1.5 mm. The shape of the largest bubble (1.53 mm diameter) is given in Fig. 3.2.2 and the smallest (0.495 mm diameter) in Fig. 3.2.4. An intermediate size bubble (1.1 mm diameter) is shown in Fig. 3.2.3. It can easily be seen that the smaller the bubble the more accurate a spherical approximation becomes. This is to be expected because surface tension effects become more important as bubble size decreases. Even the largest bubble deviates only slightly at its base from a spherical shape.

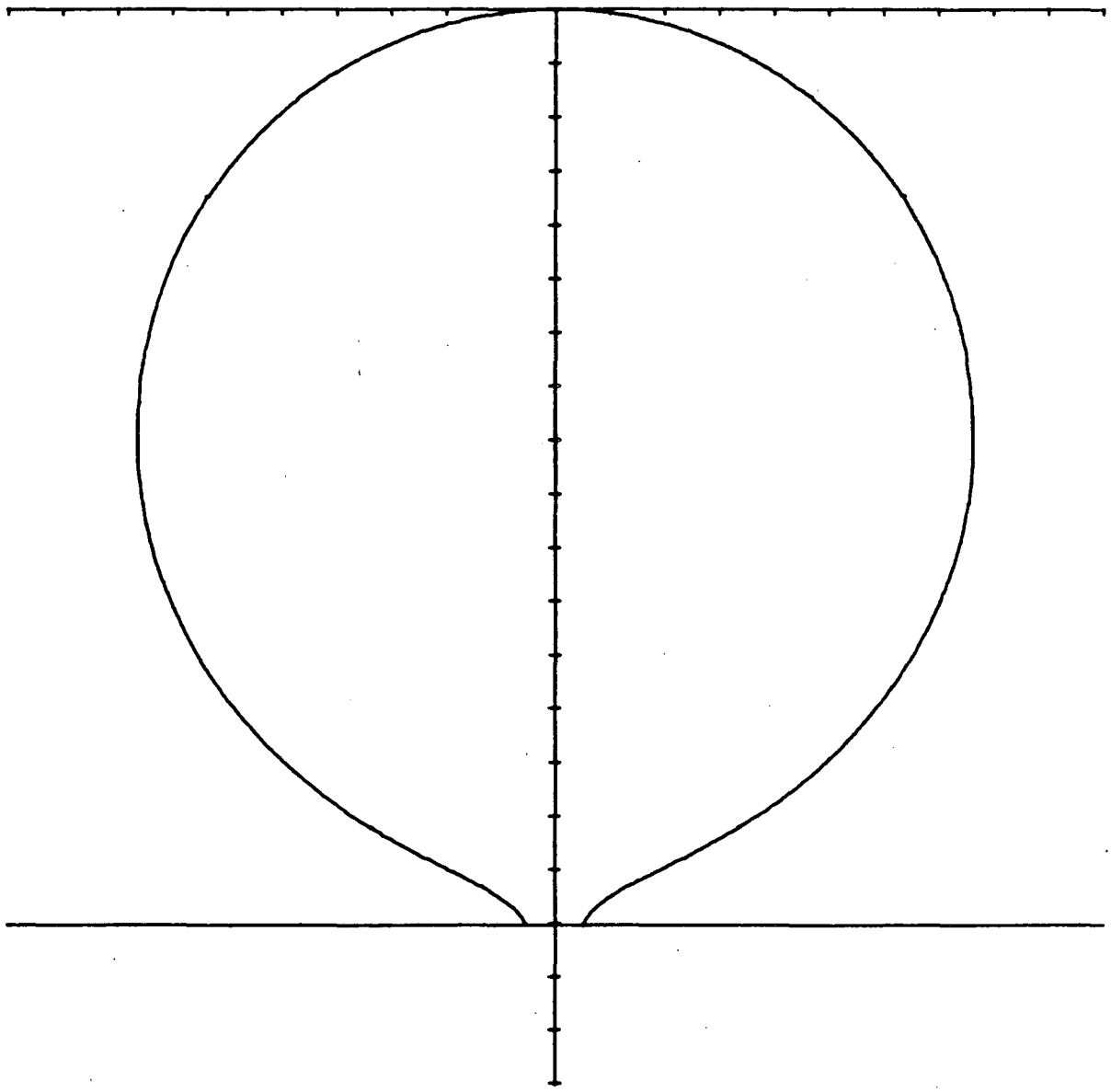

XBL 837-10752

Figure 3.2.2 Shape of a 1.53 mm diameter bubble (γ = 70 dyne/cm, tic marks at 0.1 mm intervals).

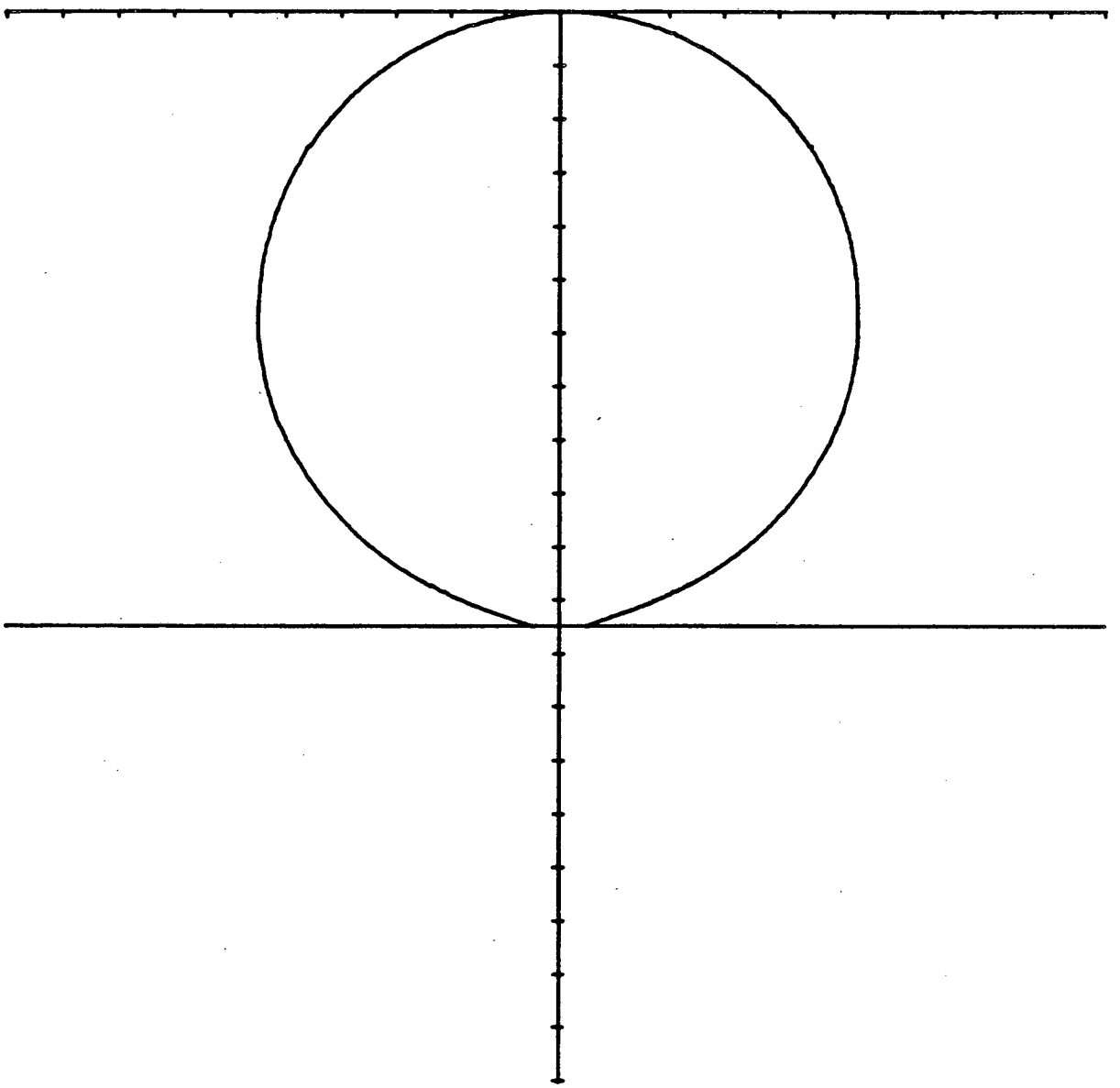

XBL 837-10750

Figure 3.2.3 Shape of a 1.1 mm diameter bubble (γ = 70 dyne/cm, tic marks at 0.1 mm intervals).

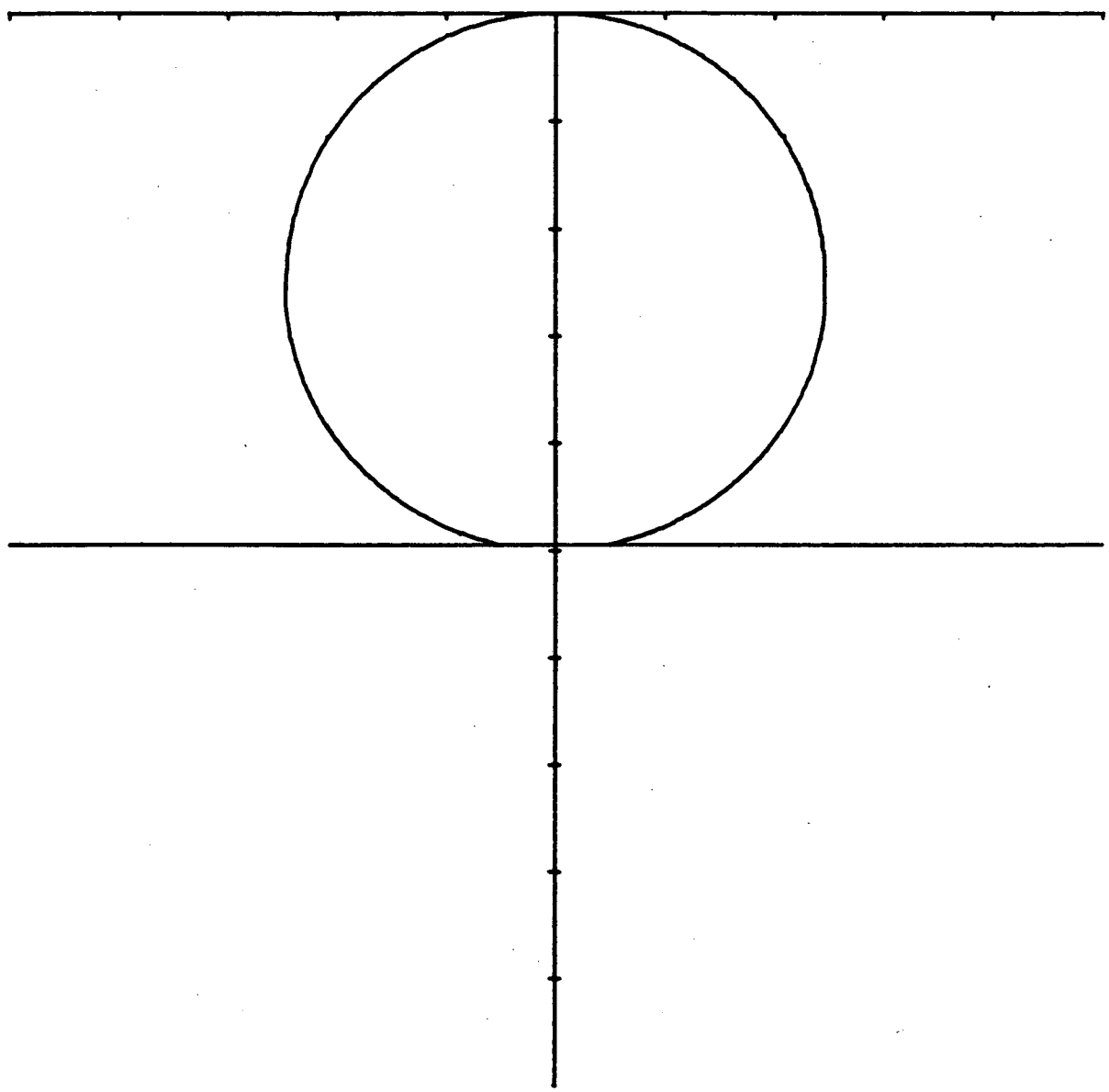

XBL 837-10751

Figure 3.2.4 Shape of a 0.495 mm diameter bubble (γ = 70 dyne/cm, tic marks at 0.1 mm intervals).

Nomenclature

a: Radius of contact area, cm.

g: Acceleration due to gravity, cm sec^{-2}.

R: Radius of curvature, cm.

s: Arc length, cm.

x: Bubble surface coordinate, cm.

z: Bubble surface coordinate, cm.

Greek Letters

α: Gas phase.

β: Liquid phase.

γ: Surface tension, dyne cm^{-1}.

θ: Contact angle.

λ: Dimensionless group.

ρ: Density, g cm^{-3}.

ϕ: Bubble coordinate angle.

Subscripts

α: Denotes α phase.

β: Denotes β phase.

3.3 Mass Transport to a Horizontal Surface Near an Ascending Fluid Sphere

After a bubble disengages from a horizontal surface, it rises away from the electrode. In the following, the effect of the fluid flow generated by the rising bubble on the rate of mass transfer to the surface is determined for a low Reynolds number (Re << 1) flow. This is accomplished by numerically solving the transport equation for the ferric ion (Equation 3.1.10) with the proper boundary conditions. The velocity distribution surrounding the fluid sphere is obtained from an analytical solution developed by Wacholder and Weihs (50).

For a low Reynolds number flow, the Navier-Stokes Equation 3.1.15 reduces to

$$0 = -\nabla P + \mu \nabla^2 \mathbf{v} + \rho \mathbf{g} \tag{3.3.1}$$

The derivation of this equation is presented in standard textbooks and monographs (51), (52). As is often done with rotationally symmetric flows, Equations 3.1.14 and 3.3.1 can be combined by defining a stream function, which depends on the coordinate system chosen. For the ascending fluid sphere a bispherical coordinate system (53) is most convenient. This special coordinate system is shown in Fig. 3.3.1. In this coordinate system the stream function is defined by:

$$v_\eta = -\frac{(\cosh\xi - \cos\eta)^2}{c^2 \sin\eta} \frac{\partial\psi}{\partial\xi} \tag{3.3.2}$$

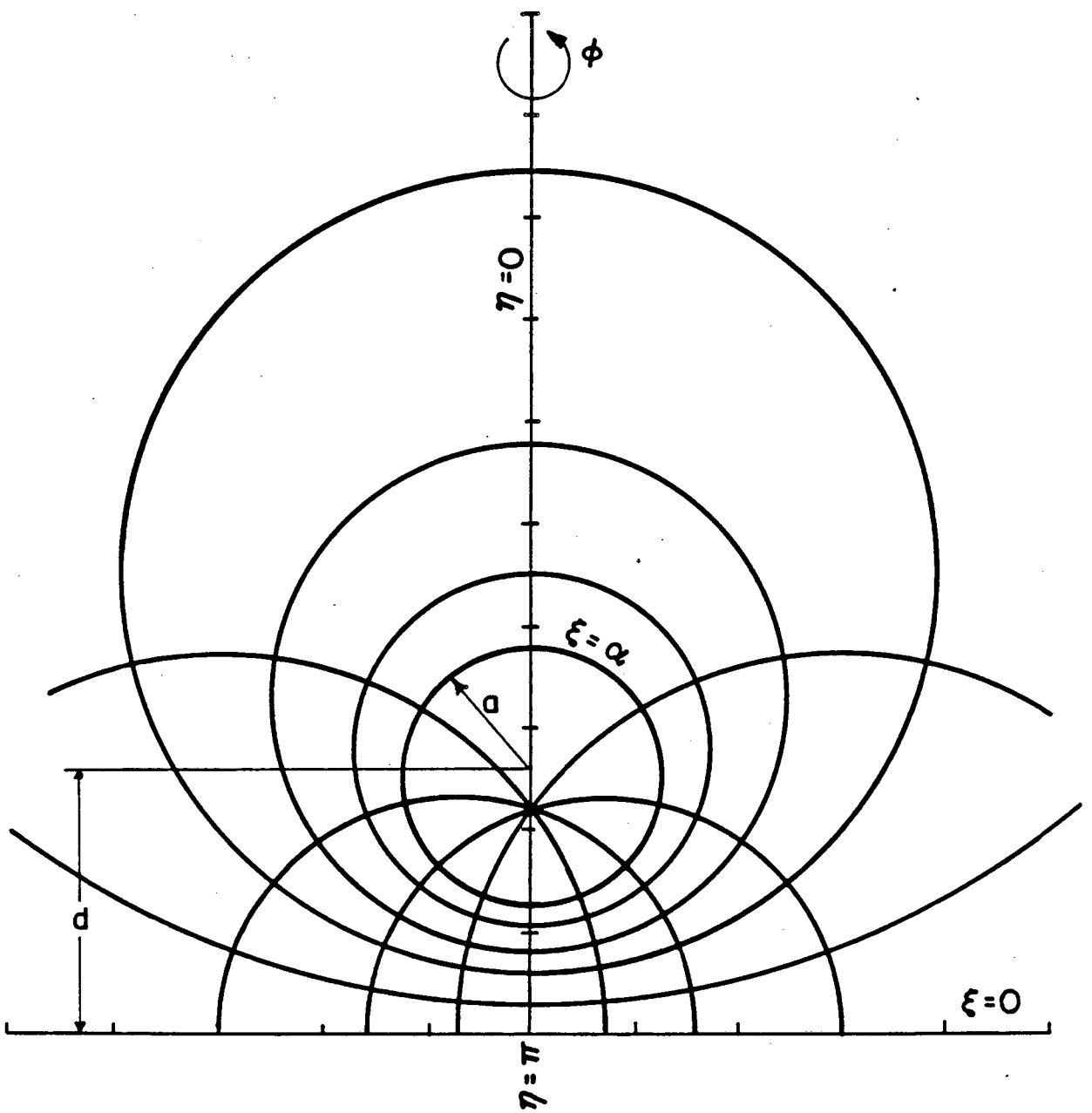

XBL 838-6115

Figure 3.3.1 Bispherical coordinate system.

$$v_\xi = \frac{(\cosh\xi - \cos\eta)^2}{c^2 \sin\eta} \frac{\partial\psi}{\partial\eta} \tag{3.3.3}$$

The resulting fluid flow equation is given by:

$$\nabla^2(\nabla^2 \psi) = 0 \tag{3.3.4}$$

Equation 3.3.4 was solved by Wacholder and Weihs (50) for the fluid inside the sphere (internal flow) and outside the sphere (external flow) with the proper matching conditions on the surface of the sphere. The external velocities can be obtained from their solution using Equations 3.3.2 and 3.3.3:

$$\begin{aligned} v_\eta^e = \sum_{n=0}^{\infty} \Bigg\{ & \frac{-3 \sinh\xi \; W_n(\xi) \; V_n(\cos\eta)}{2 c^2 \sin\eta \, (\cosh\xi - \cos\eta)^{1/2}} \\ & + \frac{(\cosh\xi - \cos\eta)^{1/2}}{c^2 \sin\eta} [A_n (n-1/2) \sinh (n-1/2)\xi \\ & + B_n (n-1/2) \cosh (n-1/2)\xi + C_n(n+3/2) \sinh (n+3/2)\xi \\ & + D_n(n+3/2) \cosh (n+3/2)\xi] \, V_n (\cos\eta) \Bigg\} \end{aligned} \tag{3.3.5}$$

$$\begin{aligned} v_\xi^e = \sum_{n=0}^{\infty} \Bigg\{ & \frac{3 \, W_n(\xi) \, V_n (\cos\eta)}{2 c^2 (\cosh\xi - \cos\eta)^{1/2}} \\ & - \left[\frac{(\cosh\xi - \cos\eta)^{1/2}}{c^2} \right] \frac{W_n(\xi)}{\cos\eta} [n P_{n-1} (\cos\eta) \\ & + (n+1) P_{n+1} (\cos\eta)] \Bigg\} \end{aligned} \tag{3.3.6}$$

Where P_n (cos η) is a Legendre polynomial of degree n and c, $W_n(\xi)$, and V_n (cos η) are defined by Equations 3.3.7-10.

$$c = d \tanh \alpha \tag{3.3.7}$$

$$\alpha = \cosh^{-1} (d/a) \tag{3.3.8}$$

$$W_n(\xi) = A_n \cosh (n-1/2)\xi + B_n \sinh (n-1/2)\xi + C_n \cosh (n+3/2)\xi + D_n \sinh (n+3/2)\xi \tag{3.3.9}$$

$$V_n (\cos \eta) = P_{n-1} (\cos \eta) - P_{n+1} (\cos \eta) \tag{3.3.10}$$

The drag force on the bubble was determined by Wacholder and Weihs and is given by:

$$F = 6\pi \mu^e U a \frac{2+3\sigma}{3(1+\sigma)} \delta\left(\frac{d}{a},\sigma\right) \tag{3.3.11}$$

where

$$\delta\left(\frac{d}{a},\sigma\right) = \frac{4}{3}\left[\frac{3(1+\sigma)}{2+3\sigma}\right] \sinh \alpha \sum_{n=1}^{\infty}$$

$$\frac{n(n+1)}{(2n-1)\ (2n+3)} \{ \sigma [2 \sinh (2n+1)\alpha + (2n+1) \sinh 2\alpha$$

$$- 4 \sinh^2 (n+1/2)\alpha + (2n+1)^2 \sinh^2 \alpha]$$

$$+ 1/2 [(2n+3)\ e^{2\alpha} + 4\ e^{-(2n+1)\alpha} - (2n-1)\ e^{-2\alpha}]\}$$

$$\{\sigma [4 \sinh^2 (n+1/2)\alpha - (2n+1)^2 \sinh^2 \alpha]$$

$$+ [2 \sinh (2n+1)\alpha - (2n+1) \sinh 2\alpha]\}^{-1} \tag{3.3.12}$$

and σ is defined by Equation 3.3.13

$$\sigma = \mu^i/\mu^e \tag{3.3.13}$$

It should be pointed out that the velocity of the sphere (U) is positive when the sphere is approaching the surface.

The mass transport equation for the reacting species (Equation 3.1.10) is solved numerically using the Crank-Nicolson finite difference method (54). The equation is solved over two time periods. In the initial period the bubble is held stationary at a specified point above the surface and the mass transfer to the surface is controlled by diffusion of the species to the electrode. The concentration of the reacting species is initially uniform, then at time equal to zero the surface concentration of the species is set to zero. After a specified time the bubble is released and allowed to rise. During this time period it is much more convenient to step numerically in the distance from the surface to the bubble rather than in time. During the initial time period Equation 3.1.10 transforms to Equation 3.3.14 and in the second time period it converts to Equation 3.3.15.

$$0 = \frac{\partial \tilde{c}}{\partial \tilde{t}_i} - \left[\frac{\lambda \left(\cos \pi \tilde{\eta} \cosh \alpha \tilde{\xi} - 1\right)}{\pi \gamma^2 \sin \pi \tilde{\eta}} \right] \frac{\partial \tilde{c}}{\partial \tilde{\eta}}$$

$$+ \left[\frac{\lambda \sinh \alpha \tilde{\xi}}{\alpha \gamma^2} \right] \frac{\partial \tilde{c}}{\partial \tilde{\xi}} - \frac{\lambda^2}{\pi^2 \gamma^2} \frac{\partial^2 \tilde{c}}{\partial \tilde{\eta}^2} - \frac{\lambda^2}{\alpha^2 \gamma^2} \frac{\partial^2 \tilde{c}}{\partial \tilde{\xi}^2} \qquad (3.3.14)$$

$$0 = \mathrm{Re\ Sc}\,\frac{\partial\tilde{c}}{\partial\tilde{t}_f} + \left[\frac{\mathrm{Re\ Sc}\,(\cosh\alpha\,\tilde{\xi} - \cos\pi\,\tilde{\eta})\tilde{v}_\eta}{\gamma\,\pi}\right.$$

$$\left. - \frac{(\cosh\alpha\,\tilde{\xi} - \cos\pi\,\tilde{\eta})\,(\cos\pi\,\tilde{\eta}\cosh\alpha\,\tilde{\xi} - 1)}{\pi\,\gamma^2\,\sin\pi\,\tilde{\eta}}\right]\frac{\partial\tilde{c}}{\partial\tilde{\eta}}$$

$$+ \left[\frac{\mathrm{Re\ Sc}\,(\cosh\alpha\,\tilde{\xi} - \cos\pi\,\tilde{\eta})\,\tilde{v}_\xi}{\alpha\,\gamma}\right.$$

$$\left. + \frac{\sinh\alpha\,\tilde{\xi}\,(\cosh\alpha\,\tilde{\xi} - \cos\pi\,\tilde{\eta})}{\alpha\,\gamma^2} - \frac{\mathrm{Re\ Sc}\,\tilde{\xi}}{\alpha\sqrt{\tilde{t}_f^{\,2}-1}}\right]\frac{\partial\tilde{c}}{\partial\tilde{\xi}}$$

$$- \left[\frac{(\cosh\alpha\,\tilde{\xi} - \cos\pi\,\tilde{\eta})^2}{\pi^2\,\gamma^2}\right]\frac{\partial^2\tilde{c}}{\partial\tilde{\eta}^2} - \left[\frac{(\cosh\alpha\,\tilde{\xi} - \cos\pi\,\tilde{\eta})^2}{\alpha^2\,\gamma^2}\right]\frac{\partial^2\tilde{c}}{\partial\tilde{\xi}^2} \tag{3.3.15}$$

The dimensionless variables and numbers are defined as follows:

$$\tilde{c} = c_3^1/c_B \tag{3.3.16}$$

$$\tilde{v}_\eta = v_\eta^e/(-U) \tag{3.3.17}$$

$$\tilde{v}_\xi = v_\xi^e/(-U) \tag{3.3.18}$$

$$\tilde{\xi} = \xi/\alpha \tag{3.3.19}$$

$$\tilde{\eta} = \eta/\pi \tag{3.3.20}$$

$$\tilde{t}_i = D_3 t/a^2 \tag{3.3.21}$$

$$\tilde{t}_f = d/a \tag{3.3.22}$$

$$\lambda = \cosh\alpha\,\tilde{\xi} - \cos\pi\,\tilde{\eta} \tag{3.3.23}$$

$$\gamma = c/a \tag{3.3.24}$$

$$Re = \frac{a(-U)}{\nu^e} \tag{3.3.25}$$

$$Sc = \frac{\nu^e}{D_3} \tag{3.3.26}$$

The spatial boundary conditions for both time periods are:

$$\frac{\partial \tilde{c}}{\partial \tilde{\eta}} = 0 \quad \text{at} \quad \tilde{\eta} = 0 \tag{3.3.27}$$

$$\frac{\partial \tilde{c}}{\partial \tilde{\eta}} = 0 \quad \text{at} \quad \tilde{\eta} = 1 \tag{3.3.28}$$

$$\tilde{c} = 0 \quad \text{at} \quad \tilde{\xi} = 0 \tag{3.3.29}$$

$$\frac{\partial \tilde{c}}{\partial \tilde{\xi}} = 0 \quad \text{at} \quad \tilde{\xi} = 1 \tag{3.3.30}$$

The initial condition for the first period is given by Equation 3.3.31 and for the second period the concentration distribution from the end of the first period is used.

$$\tilde{c} = 1 \qquad \text{For all } \tilde{\eta} \text{ and } \tilde{\xi} \tag{3.3.31}$$

The flux of the reacting species and thus the current at any time can be obtained at any time by Equation 3.3.32.

$$N_3\Big|_{\tilde{\xi}=0} = D_3 \left[\frac{(1 - \cos \pi \tilde{\eta})\, c_B}{\alpha\, c} \right] \frac{\partial \tilde{c}}{\partial \tilde{\xi}}\Bigg|_{\tilde{\xi}=0} \tag{3.3.32}$$

The velocity of the bubble at any time and distance from the electrode is determined by setting the drag force (Equation 3.3.11) equal to the

buoyant force on the bubble. The actual time during the second period is determined by integrating along the path of the bubble according to Equation 3.3.33.

$$t = t_0 - \int_{d_0}^{d_f} \frac{1}{U} \, d(d) \qquad (3.3.33)$$

A description and listing of the program used to solve the model is given in Appendix H.

Besides the numerical accuracy the only real limitation to the model is the assumption of a low Reynolds number flow. Since the drag on a rising bubble in an infinite fluid (i.e., in the absence of a surface) increases proportionally with the radius of the bubble and the buoyant force increases with the cube of the radius, the terminal velocity increases with the square of the radius. Thus the Reynolds number increases with the cube of the radius of the bubble. This severely limits the maximum size of the bubble for which the model is applicable. The Reynolds number reaches a value of one for a bubble with a radius of 73 μm. This is much smaller than the bubbles examined in the single bubble disengagement experiments, but the bubbles at a typical gas-evolving electrode in the field are generally smaller than this maximum. It should be noted that this model does not include any effects of the actual disengagement process or of any free or forced convection other than caused by the motion of the bubble itself.

The calculated current distributions are presented as graphs of reduced current density to the electrode versus reduced radial distance from the center line of the bubble along the electrode. The current density is reduced by the current density to the electrode in the absence of the bubble. This current density is given by the Cottrell equation (Equation 2.3.4.1). The Nernst boundary layer thickness from the Cottrell equation is

$$\delta_N = \sqrt{\pi D_3 t} \tag{3.3.34}$$

The radial distance is rendered dimensionless by the radius of the bubble. The physical parameters used in the modeling work are listed in Table 3.3.1.

The numerical accuracy depends on the time step size and the mesh size. Because of the relatively small time step size needed to obtain a stable solution, the limitation on the accuracy is the mesh size. The results of two runs which are equivalent except for different mesh sizes are given in Fig. 3.3.2. Far away from the sphere the reduced current density should approach one and, as expected, the smaller mesh size is more accurate. Values for various mesh sizes are about the same for the first diameter from the center. All other computational work was performed with 40 x 40 mesh points.

The initial distance of the center of the bubble from the surface (d_r) is the one parameter that is difficult to determine for the model. As can be seen in Fig. 3.3.3 varying the distance slightly when the bubble is close to the surface makes very little difference

Table 3.3.1 Input Parameters For Program

Parameter	Value	Units
External Density	1.06	g/cm^3
Internal Density	8.18×10^{-5}	g/cm^3
External Viscosity	1.19	cp
Internal Viscosity	8.75×10^{-3}	cp
Bulk Concentration	0.1	M
Diffusion Coefficient	4.58×10^{-6}	cm^2/sec

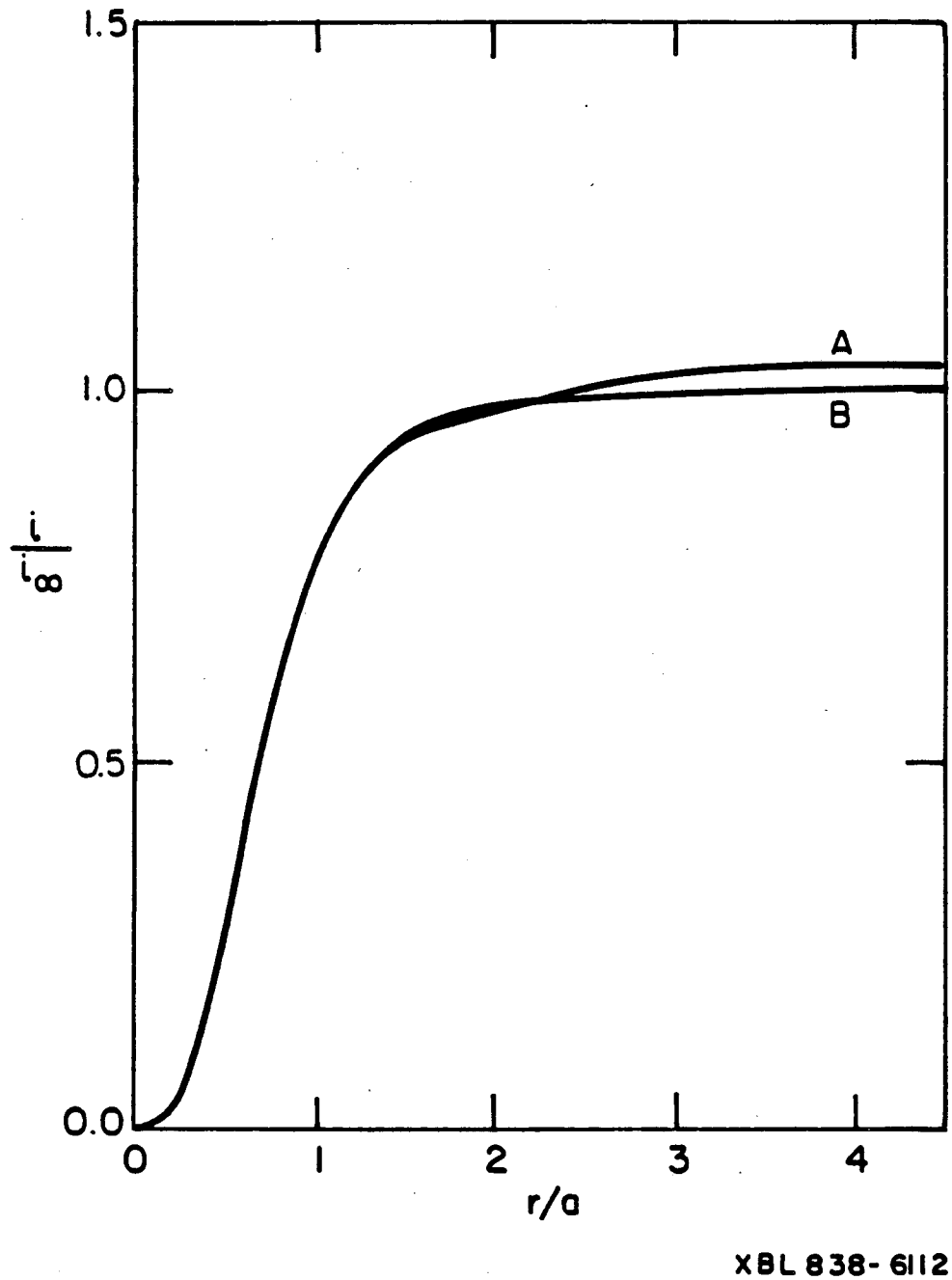

Figure 3.3.2 Limiting current distribution during the first time period (t_i = 1.0 second); (A) 20X20 mesh points; (B) 40X40 mesh points.

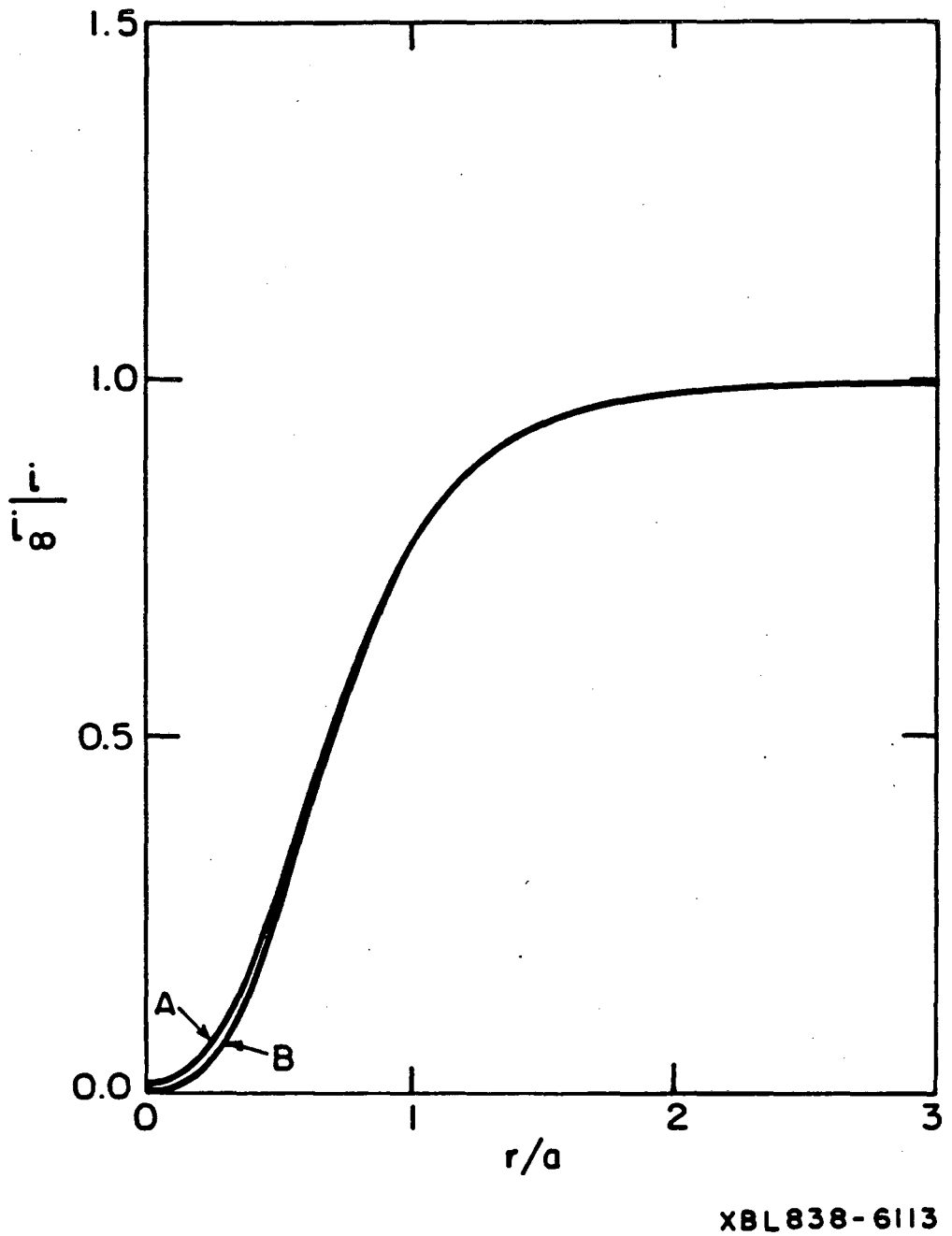

Figure 3.3.3 Limiting current distribution during the first time period (a = 25 microns, t_i = 1.0 second); (A) d_r = 27.5 microns; (B) d_r = 27.0 microns.

in the current during the first time period. However the rate of ascension is affected greatly as a result of the change in the drag on the bubble.

The results of the modeling work is given in Figs. 3.3.4–7. The fact that the rate of mass transfer (i.e., current density) is decreased by the convection generated by the ascension of the bubble is immediately apparent. As can be seen by comparing Fig. 3.3.4 and Fig. 3.3.5, this trend does not depend on the initial distance of the bubble from the surface. It also does not depend on the Nernst boundary layer thickness or the size of the bubble, which is apparent from comparing Fig. 3.3.4 with Fig. 3.3.6 and 3.3.7.

The characteristic decrease in the current density differs significantly from those observed experimentally (see Section 2.4.2). The fact that the time constant for the modeling work is two orders of magnitude smaller than the one observed experimentally, even though the bubbles are more than an order of magnitude larger, indicates that the ascension of the bubble alone does not determine the overall time constant. The collapse of the contact area plays a major role in determining the overall time constant. The decreases in mass-transfer rates are observed much farther from the center line of the bubble in the modeling work. This is a general characteristic of mass transport in low Reynolds number flow.

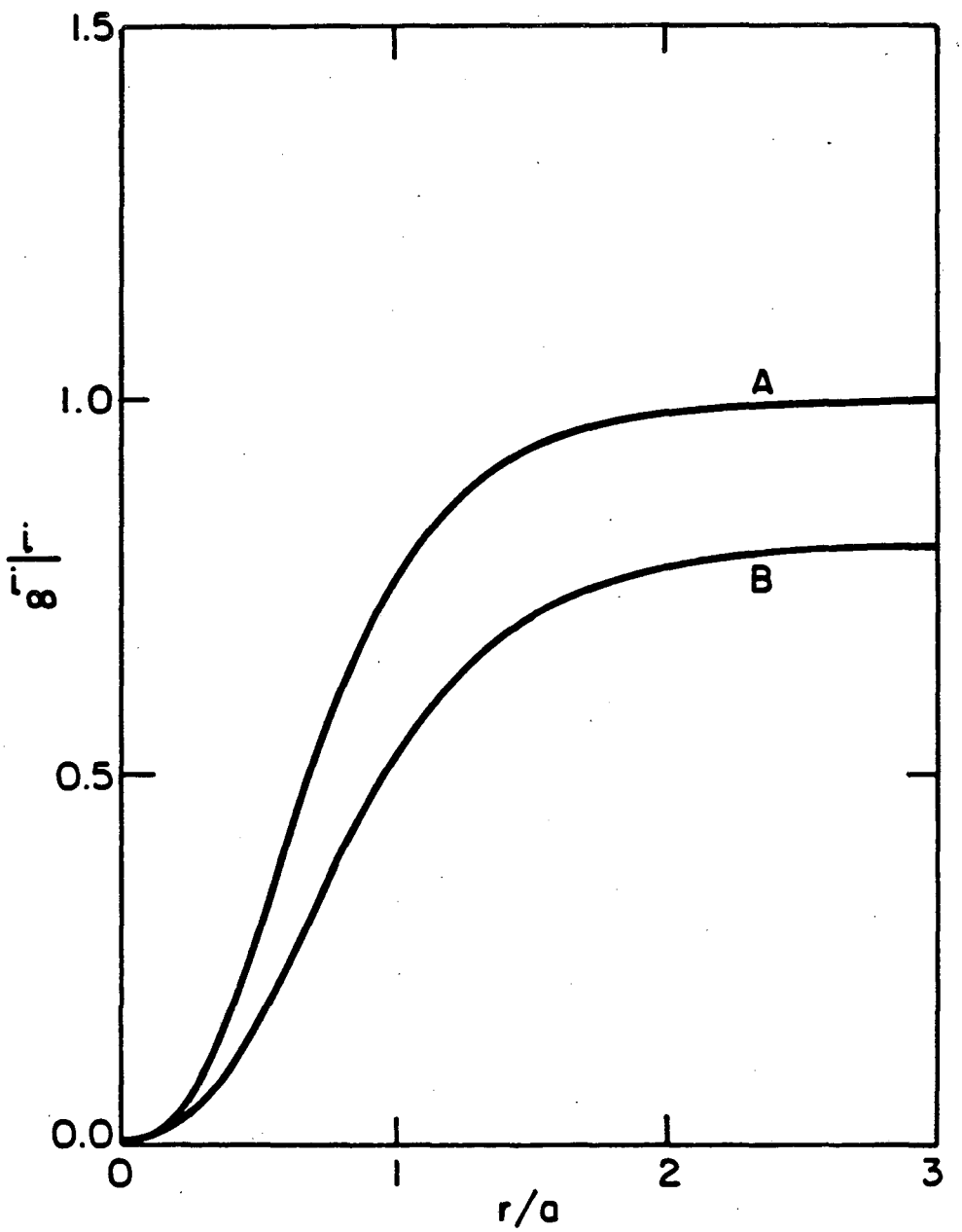

XBL838-6108

Figure 3.3.4 Limiting current distribution before and after the release of the sphere (a = 25 microns, t_r = 1.0 second, d_r = 27.5 microns); (A) t = 1.0 second, d = 27.5 microns; (B) t = 1.003177 seconds, d = 28.7 microns.

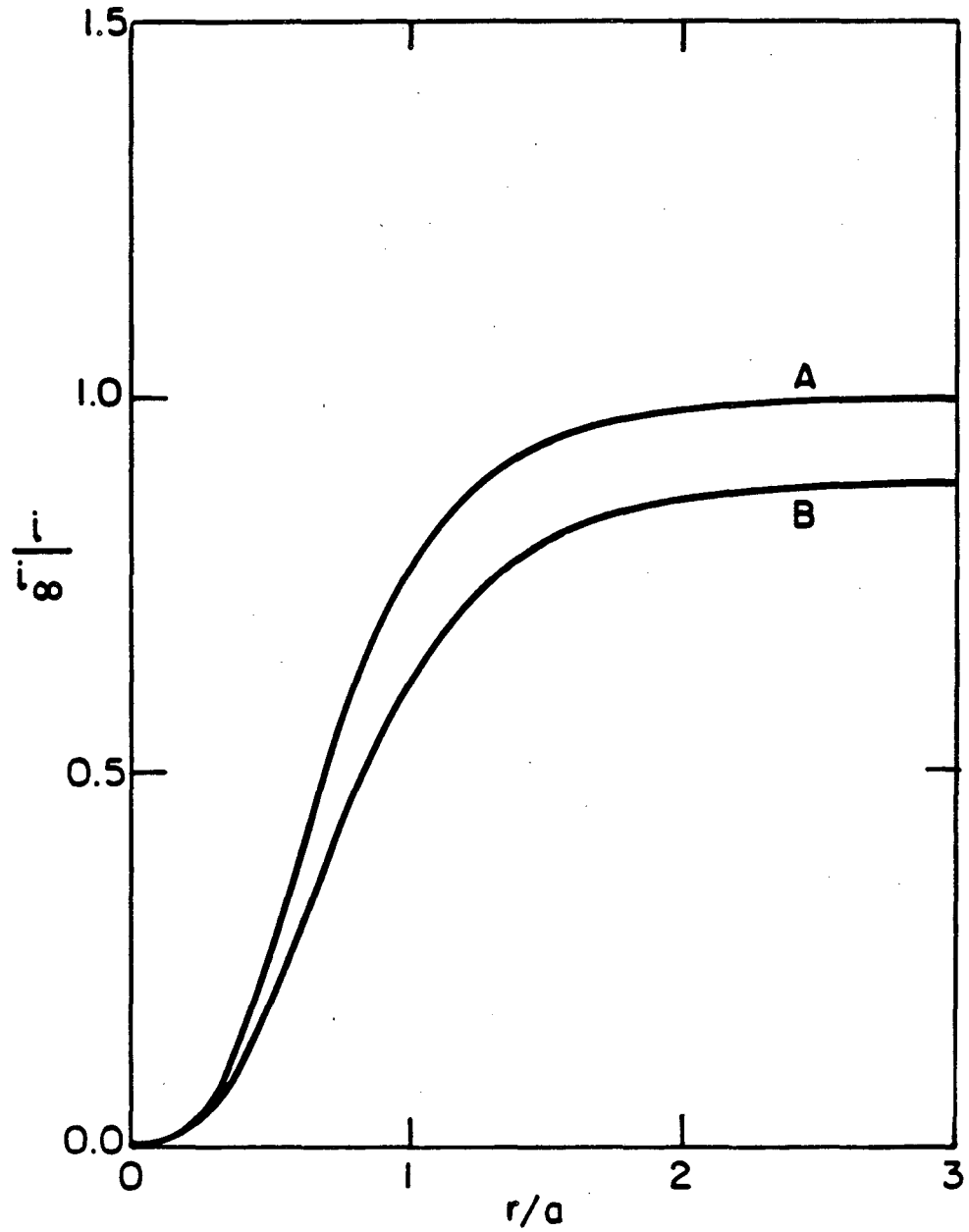

XBL 838-6109

Figure 3.3.5 Limiting current distribution before and after the release of the sphere (a = 25 microns, t_r = 1.0 second, d_r = 27 microns); (A) t = 1.0 second, d = 27 microns; (B) t = 1.001657 seconds, d = 27.5 microns.

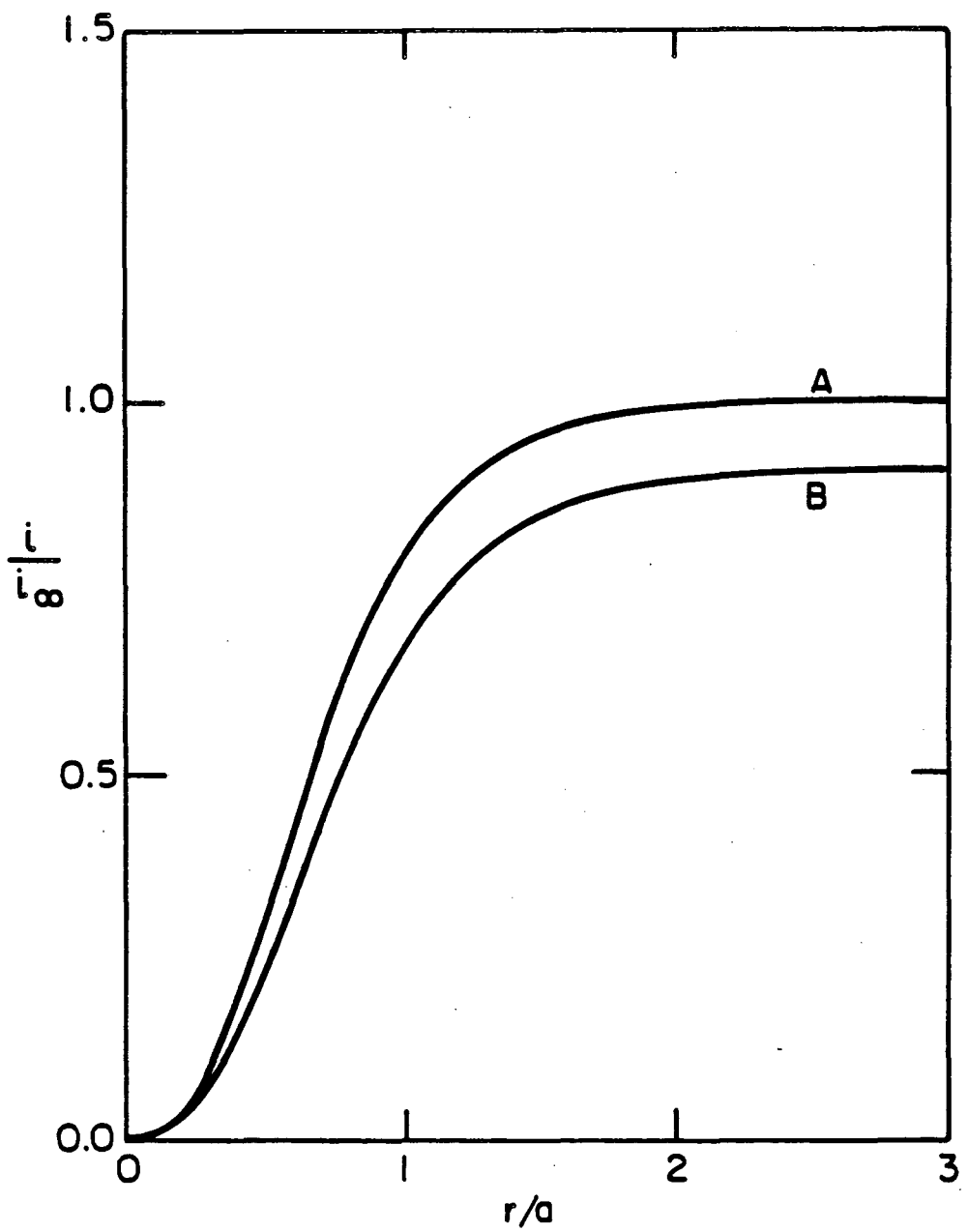

XBL 838-6111

Figure 3.3.6 Limiting current distribution before and after the release of the sphere (a = 25 microns, t_r = 0.5 seconds, d_r = 27.5 microns); (A) t = 0.5 seconds, d = 27.5 microns; (B) t = 0.50143 seconds, d = 28 microns.

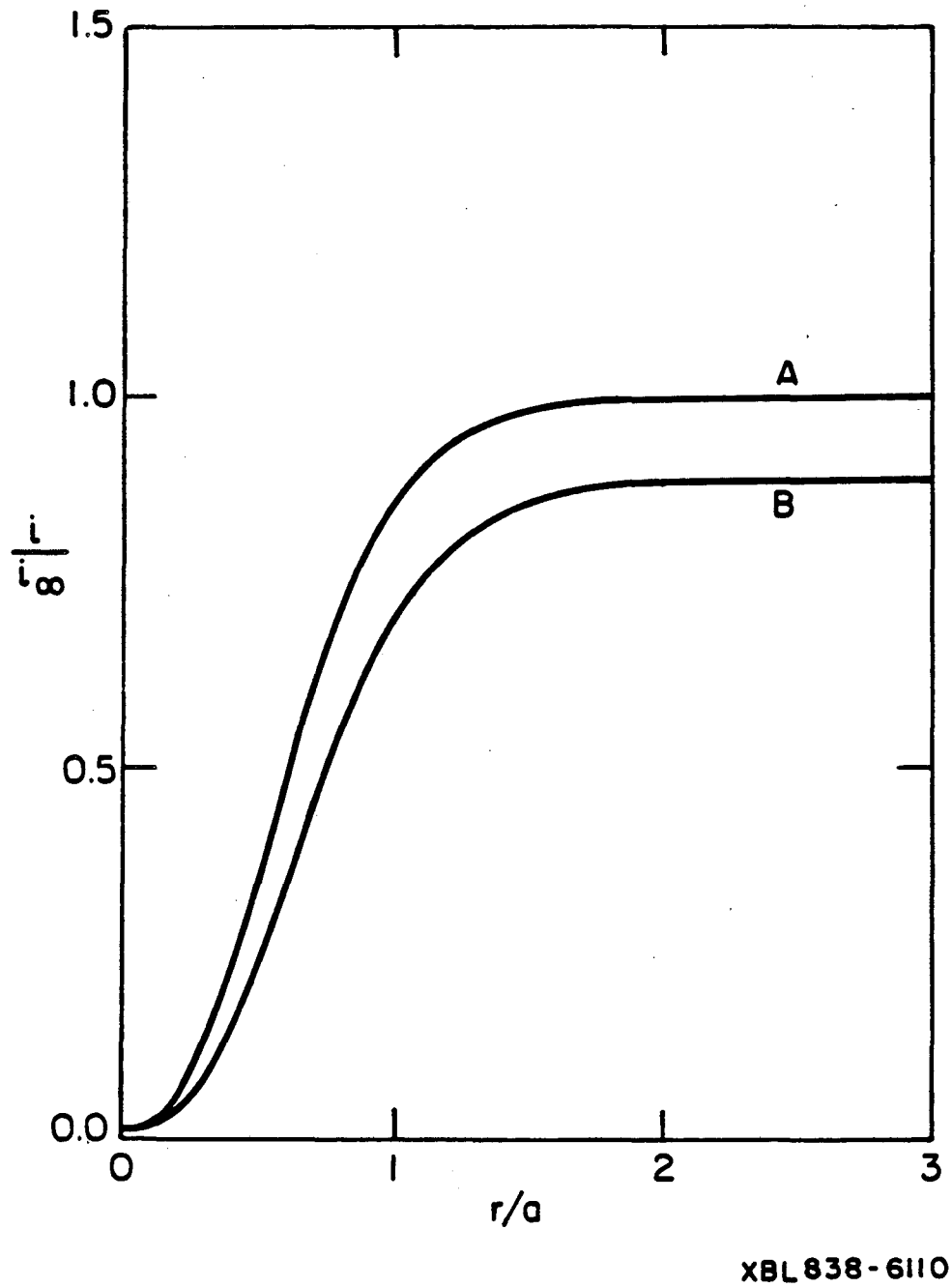

Figure 3.3.7 Limiting current distribution before and after the release of the sphere (a = 50 microns, t_r = 1.0 second, d_r = 55 microns); (A) t = 1.0 second, d = 55 micron; (B) t = 1.0008806 seconds, d = 56.25 microns.

Nomenclature

a: Radius of sphere, cm.

A_n: Velocity coefficient (see reference (50)).

B_n: Velocity coefficient (see reference (50)).

c: Bispherical length parameter, cm.

$\tilde{c}$: Reduced concentration (see Equation 3.3.16).

c_3^1: Ferric ion concentration, moles cm^{-3}.

c_B: Bulk concentration of ferric ions, moles cm^{-3}.

C_n: Velocity coefficient (see reference (50)).

d: Distance between sphere center and surface, cm.

D_3: Diffusion coefficient of ferric ions, cm^2 sec^{-1}.

D_n: Velocity coefficient (see reference (50)).

F: Drag force on sphere, dyne.

g: Acceleration due to gravity, cm sec^{-2}.

i: Current density, Amps cm^{-2}.

n: Summation variable.

N_3: Flux of ferric ions, moles cm^{-2} sec^{-1}.

P: Pressure, dyne cm^{-2}.

P_n: Legendre polynomial of degree n.

r: Radial distance along the surface from the center axis of the sphere, cm.

Re: Reynolds number (see Equation 3.3.25).

Sc: Schmidt number (see Equation 3.3.26).

t: Time, sec.

$\tilde{t}$: Reduced time.

U: Velocity of sphere, cm sec^{-1}.

v: Velocity component, cm sec^{-1}.

v: Velocity, cm sec^{-1}.

$\tilde{v}$: Reduced velocity component.

V_n: Velocity coefficient (see Equation 3.3.10).

W_n: Velocity coefficient (see Equation 3.3.9).

Greek Letters

α: Value of on surface of sphere (see Equation 3.3.8).

γ: See equation 3.3.24.

δ: Correction factor (see Equation 3.3.12).

δ_N: Nearnst boundary layer thickness, cm.

η: Bispherical coordinate.

$\tilde{\eta}$: Reduced bispherical coordinates.

λ: See Equation 3.3.23.

μ: Viscosity, g cm^{-1} sec^{-1}.

ν: Kinematic viscosity, cm^2 sec^{-1}.

ξ: Bispherical coordinate.

$\tilde{\xi}$: Reduced bispherical coordinate.

ρ: Density, g cm^{-3}.

σ: Viscosity ratio (see Equation 3.3.13).

ψ: Stream function, cm^2 sec^{-1}.

Subscripts

f: Denotes final period.

i: Denotes initial period.

r: Denotes quantity at the time of the release of the sphere.

η: Denotes η component.

ξ: Denotes ξ component.

∞: Denotes infinite distance from sphere.

Superscripts

i: Denotes internal phase.

e: Denotes external phase.

3.4 Mass Transport in a Wedge

As a bubble disengages, the contact area collapses which generates a fluid flow near the base. Modeling the movement of the gas-liquid interface along the surface is quite difficult. In order to gain some insight into the mass transfer enhancement effect of the contact area collapse a somewhat idealized situation is examined. Neglecting the effects of the curvature of the gas-liquid interface, the area surrounding the base of a bubble can be approximated by a wedge, pictured in Fig. 3.4.1. The wedge is formed by a solid surface (i.e., the electrode) and a shear free surface (i.e., the gas-liquid interface). The flow is generated by moving the solid surface relative to the free surface, or equivalently, by moving the free surface relative to the solid surface as in the collapse of the contact area. It is assumed that the collapse occurs at a constant velocity and that the Reynolds number for the event is much less than one.

As was done in Section 3.3 the Navier-Stokes equation for a low Reynolds number flow (Equation 3.3.1) can be combined with the overall mass balance equation (Equation 3.1.14) by defining a stream function. For the flow in a wedge a cylindrical coordinate system is the most convenient where the velocity components are given by:

$$v_r = \frac{1}{r} \frac{\partial \psi}{\partial \theta} \tag{3.4.1}$$

$$v_\theta = -\frac{\partial \psi}{\partial r} \tag{3.4.2}$$

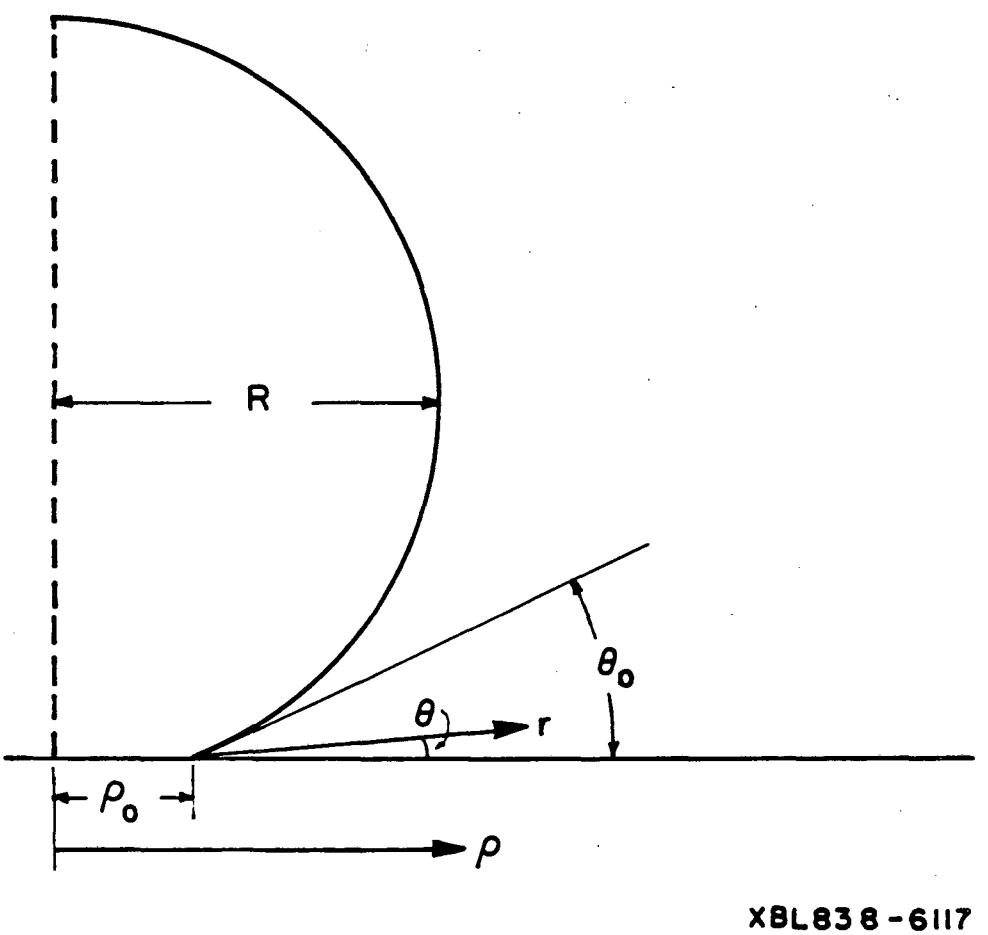

Figure 3.4.1 Schematic of wedge relative to the bubble.

The general solution to Equation 3.3.4 in this geometry can be found in a number of texts (55). The fluid flow boundary conditions are given by Equations 3.4.3-6.

$$v_\theta = 0 \qquad \theta = 0 \tag{3.4.3}$$

$$v_\theta = 0 \qquad \theta = \theta_0 \tag{3.4.4}$$

$$v_r = U \qquad \theta = 0 \tag{3.4.5}$$

$$\frac{1}{r}\frac{\partial v_\theta}{\partial \theta} + \frac{v_r}{r} = 0 \qquad \theta = \theta_0 \tag{3.4.6}$$

Equation 3.4.6 is the no stress condition on the free surface. The particular solution of Equation 3.3.4 is:

$$v_r = \frac{U}{\sin\theta_0 \cos\theta_0 - \theta_0} \left[\sin^2\theta_0 (\sin\theta + \theta\cos\theta) - \theta_0\cos\theta + (\sin\theta_0\cos\theta_0)(\cos\theta - \theta\sin\theta)\right] \tag{3.4.7}$$

$$v_\theta = \frac{-U}{\sin\theta_0 \cos\theta_0 - \theta_0} \left[\theta\sin^2\theta_0 \sin\theta - \theta_0\sin\theta + (\sin\theta_0\cos\theta_0)\,\theta\cos\theta\right] \tag{3.4.8}$$

The stream lines for the wedge flow are shown in Fig. 3.4.2.

The mass transport equation for the ferric ions (Equation 3.1.10) in cylindrical coordinates is given by:

$$\frac{\partial c_3^1}{\partial t} + v_r\frac{\partial c_3^1}{\partial r} + \frac{v_\theta}{r}\frac{c_3^1}{\partial\theta} = D_3\left[\frac{1}{r}\frac{\partial}{\partial r}\left(r\frac{\partial c_3^1}{\partial r}\right) + \frac{1}{r^2}\frac{\partial^2 c_3^1}{\partial\theta^2}\right] \tag{3.4.9}$$

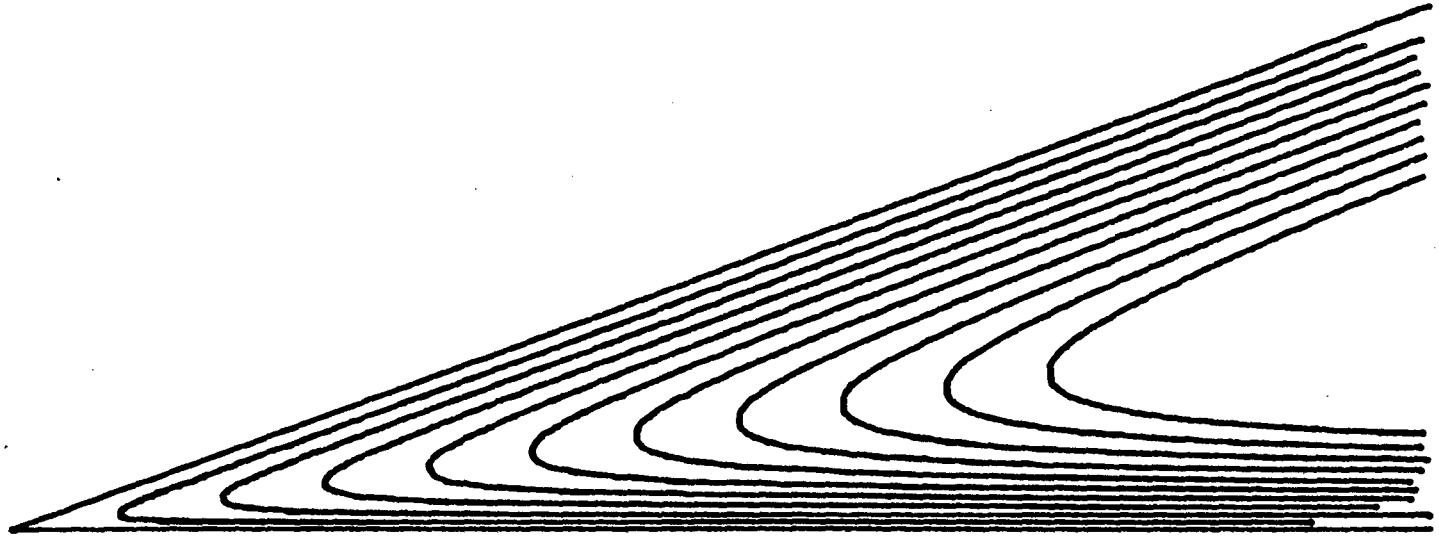

XBL 838-10879

Figure 3.4.2 Schematic of fluid flow stream lines in the wedge.

The boundary conditions on the surface are as follows:

$$\frac{\partial c_3^1}{\partial \theta} = 0 \qquad \theta = \theta_0 \tag{3.4.10}$$

$$c_3^1 = 0 \qquad \theta = 0 \tag{3.4.11}$$

A parabolic concentration profile is chosen as the initial condition. The parameters for the initial profile are determined such that they meet the boundary conditions and that there is a linear increase in the current from the tip of the wedge to the point where the edge of the bubble would be. Past the edge of the bubble the current is set equal to the value at the edge. As in Section 3.3 the mass transport equation is solved numerically using the Crank-Nicolson method. Once the concentration distribution is obtained, the current to the electrode is determined by calculating the flux using Equation 3.4.12.

$$i\Big|_{\theta=0} = \frac{D_3 nF}{r} \frac{\partial c_3^1}{\partial \theta}\Big|_{\theta=0} \tag{3.4.12}$$

The results from the solution of the mass transport equation in a wedge are related to the collapse of the contact area of a bubble by first assuming the bubble to be a spherical cap. From Section 3.2 it is seen that this is a very good assumption for bubbles less than one millimeter in diameter and acceptable for 1.5 mm diameter bubbles. Then, by setting the bubble diameter and the contact angle, the size of the contact area is determined (see reference (5)). It only remains to set either the velocity or the total time of the collapse

and the problem is completely defined. A description and listing of the program are given in Appendix I.

The numerical results for the collapse of the contact area of a bubble are given in Fig. 3.4.3. An increase in the current density surrounding the base of the bubble is observed during the collapse. As expected, the greatest enhancement effect occurs on the section of the electrode originally covered by the base of the bubble. The effect of changing the contact angle can be seen by comparing Fig. 3.4.3 to Fig. 3.4.4. It is seen that the larger the contact angle the greater the enhancement effect. This is due to the fact that the contact area increases with the contact angle, which results in a higher collapse velocity.

The accuracy of the model is questionable since flow effects from the bubble rising during the collapse of the contact area or from free convection are not included. The model should be most accurate near the base of the bubble. In this region the behavior of the current is similar to that observed in the experimental results.

The model allows us to estimate the enhancement effect of a bubble disengagement on the electrode area shielded by the base of the bubble (i.e. the bubbles' contact area). In this respect it will be instructive to examine the solution of the model at large Peclet numbers. As the Peclet number increases, transport by convection becomes increasingly more important than transport by diffusion and three distinct regions of the concentration distribution in the wedge become apparent. One of these is a narrow region next to the electrode surface ($\theta << 1/\sqrt{Pe}$). In this region the transport of

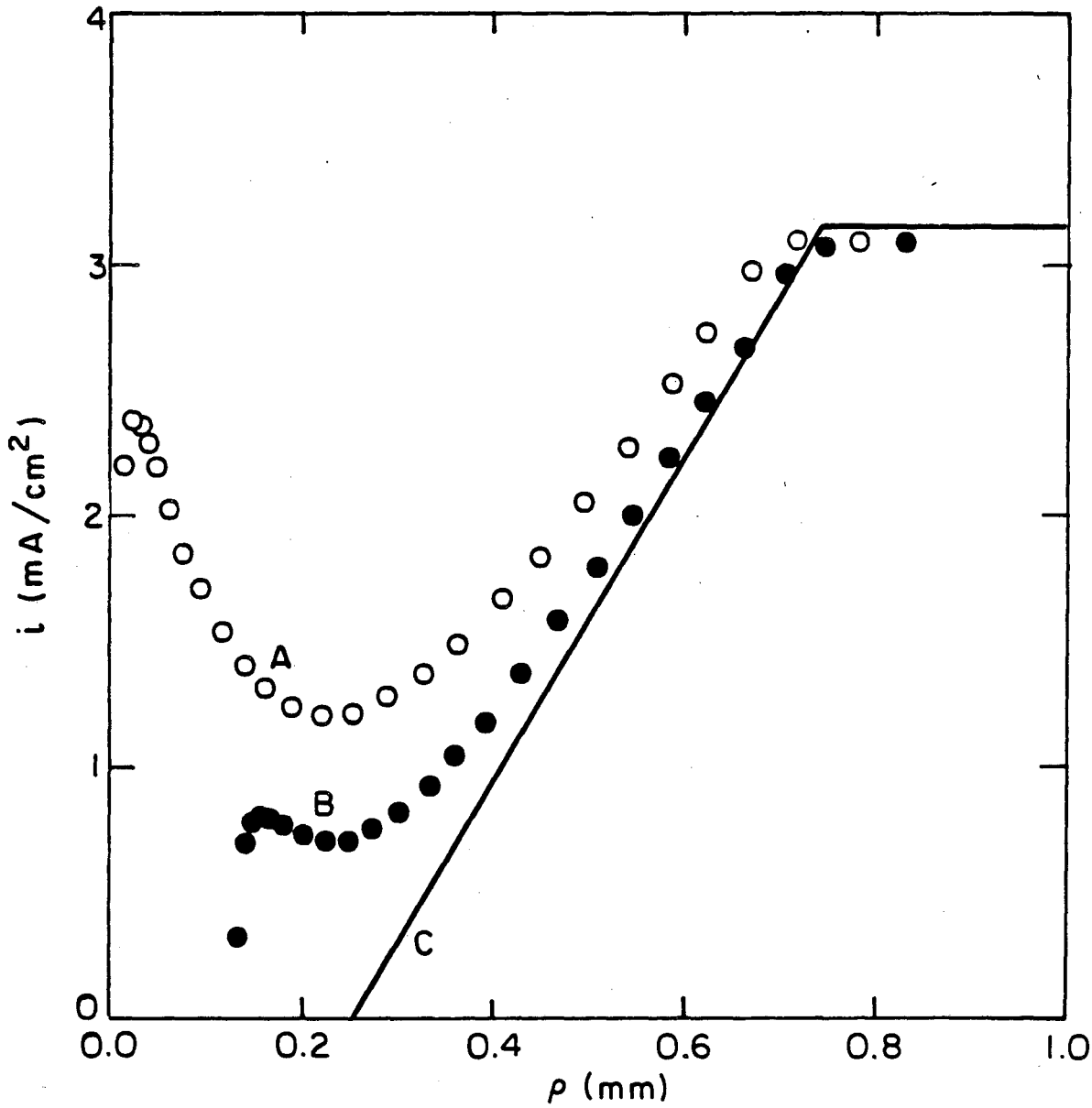

X8L838-6100

Figure 3.4.3 Limiting current distribution during the disengagement of a 1.49 mm diameter bubble (θ_o = 20°, t_r = 0.2 seconds); (A) At the time of release (t = 0.2 seconds); (B) 0.1 seconds before the release time (t = 0.1 seconds); (C) Initial distribution (t = 0.0 seconds).

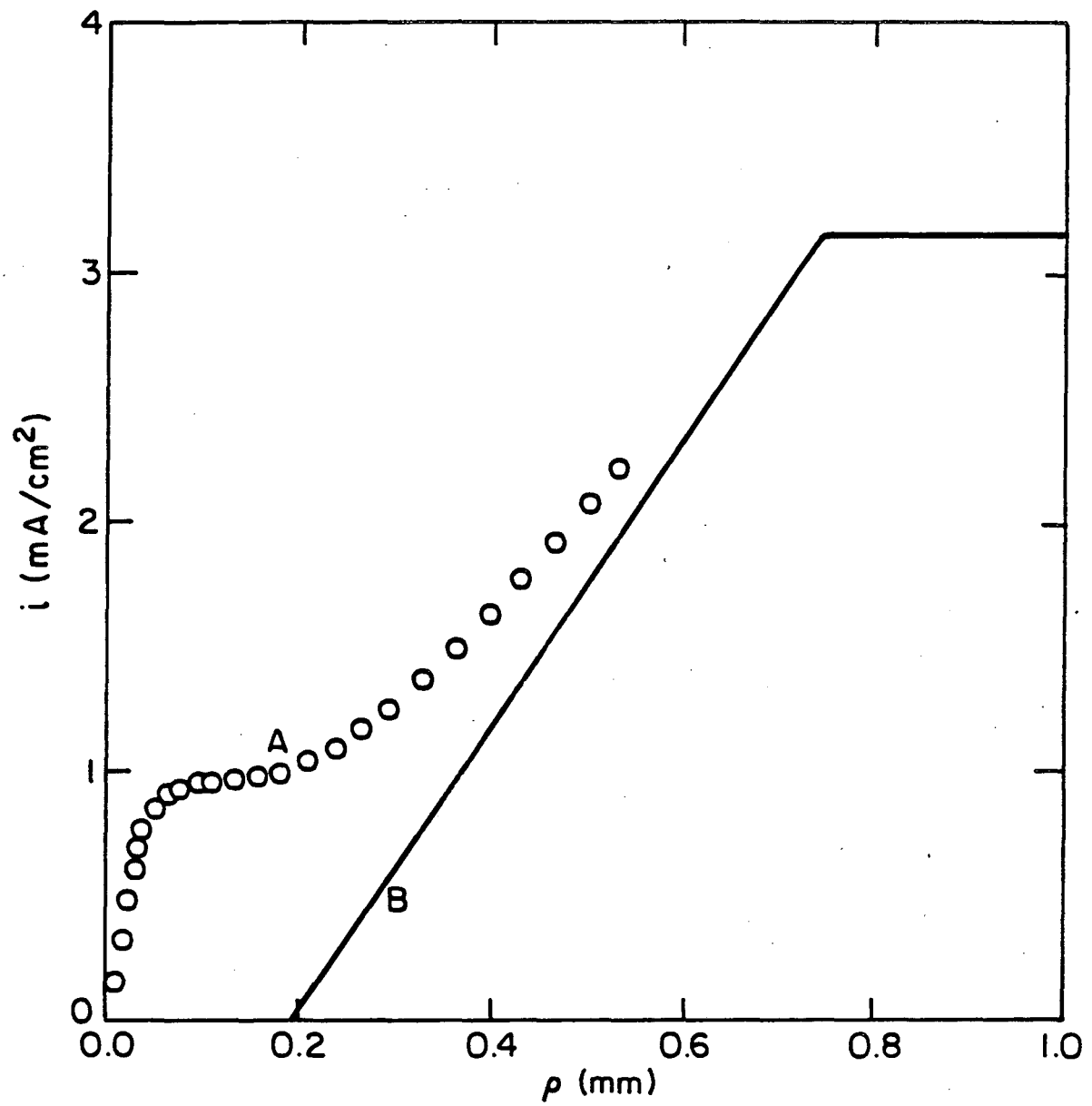

Figure 3.4.4 Limiting current distribution during the disengagement of a 1.49 mm diameter bubble (θ_o = 15°, t_r = 0.2 seconds); (A) At the time of release (t = 0.2 seconds); (B) Initial distribution (t = 0.0 seconds).

ferric ions is dominated by convection and diffusion in the theta direction. Very close to the tip of the wedge diffusion dominates over convection and in the remaining part of the wedge convection dominates. These three regions are a direct analogy to the three regions in the mass transport to a flat plate in laminar flow at high Peclet numbers. This is obviously a singular perturbation problem (56), which is beyond the scope of this work, but it is useful to obtain the infinite Peclet solution.

At an infinite Peclet number the effect of the region next to the tip on the current to the electrode can be neglected. For the narrow region next to the electrode, a set of dimensionless variables of order one can be defined and is given by Equations 3.4.13-19:

$$c = c_3^1/c_B \tag{3.4.13}$$

$$r = r/R \tag{3.4.14}$$

$$\theta = \theta\sqrt{Pe} \tag{3.4.15}$$

$$t = tU/R \tag{3.4.16}$$

$$\tilde{v}_r = v_r/U \tag{3.4.17}$$

$$\tilde{v}_\theta = (v_\theta/U)\sqrt{Pe} \tag{3.4.18}$$

$$Pe = UR/D_3 \tag{3.4.19}$$

Substituting these variables into Equation 3.4.9 we obtain:

$$\frac{\partial\tilde{c}}{\partial\tilde{t}} + \tilde{v}_r\frac{\partial\tilde{c}}{\partial\tilde{r}} + \frac{\tilde{v}_\theta}{\tilde{r}}\frac{\partial\tilde{c}}{\partial\tilde{\theta}} = \frac{1}{Pe}\left[\frac{1}{\tilde{r}}\frac{\partial}{\partial\tilde{r}}\left(\tilde{r}\frac{\partial\tilde{c}}{\partial\tilde{r}}\right)\right] + \frac{1}{\tilde{r}^2}\frac{\partial^2\tilde{c}}{\partial\tilde{\theta}^2} \tag{3.4.20}$$

Equations 3.4.7 and 3.4.8 for the velocity profile can be expanded for small theta, resulting in:

$$v_r = U\left[1 + \left(\frac{2\sin^2\theta_0}{\sin\theta_0\cos\theta_0 - \theta_0}\right)\theta + O(\theta^2) + \ldots\right] \tag{3.4.21}$$

$$v_\theta = -U\left[\theta + \left(\frac{\sin^2\theta_0}{\sin\theta_0\cos\theta_0 - \theta_0}\right)\theta^2 + O(\theta^3) + \ldots\right] \tag{3.4.22}$$

Substituting the velocity profile equations into Equation 3.4.20 and taking the limit as the Peclet number goes to infinity we obtain:

$$\frac{\partial\tilde{c}}{\partial\tilde{t}} + \frac{\partial\tilde{c}}{\partial\tilde{r}} - \left(\frac{\tilde{\theta}}{\tilde{r}}\right)\frac{\partial\tilde{c}}{\partial\tilde{\theta}} = \frac{1}{\tilde{r}^2}\frac{\partial^2\tilde{c}}{\partial\tilde{\theta}^2} \tag{3.4.23}$$

It is now helpful to define two new variables given by Equations 3.4.24 and 3.4.25.

$$\hat{r} = \tilde{r} - \tilde{t} \tag{3.4.24}$$

$$\hat{\theta} = \tilde{r} - \tilde{\theta} \tag{3.4.25}$$

Substituting these variables into Equation 3.4.23 we obtain:

$$\frac{\partial\tilde{c}}{\partial\tilde{t}} = \frac{\partial^2\tilde{c}}{\partial\hat{\theta}^2} \tag{3.4.26}$$

Equation 3.4.26 is the well known unsteady state diffusion equation. It must be solved in two regions along the electrode. In the region not originally covered by the base of the bubble there is no change from the initial current in this case. On the section of the electrode originally covered by the base of the bubble a dramatic increase

is predicted. For this region the boundary conditions and the initial conditions are given by Equations 3.4.27-29.

$$\tilde{c} = 0 \qquad \hat{\theta} = 0 \tag{3.4.27}$$

$$\tilde{c} \rightarrow \alpha + \beta\,\hat{\theta} \qquad \hat{\theta} \rightarrow \infty \tag{3.4.28}$$

$$\tilde{c} = \alpha + \beta\,\hat{\theta} \qquad \tilde{t} = \tilde{t}_0 \tag{3.4.29}$$

here α, β, and $\tilde{t}_0$ are determined by the concentration distribution and flow in the region of the wedge above the narrow region next to the electrode. The solution to Equation 3.4.26 with the above boundary conditions:

$$\tilde{c} = \alpha \operatorname{erf}\left[\frac{\hat{\theta}}{\sqrt{4\,(\tilde{t} - \tilde{t}_0)}}\right] + \beta\,\hat{\theta} \tag{3.4.30}$$

and the current to the electrode in this region is given by:

$$i = \frac{D_3 nF}{c_B R}\,Pe\left[\frac{\alpha}{\sqrt{\pi(\tilde{t} - \tilde{t}_0)}} + \beta\right] \tag{3.4.31}$$

The inverse square root of time dependence on the current is significant because Ibl (10) obtained the same time dependence in the derivation of his displacement model. It is also indicated by this result that the radius of the contact area rather than the radius of the bubble should be used as the characteristic distance over which the periodic disturbance of the boundary layer occurs.

The solution of the mass transport equation in the limiting case of an infinite Peclet number can be compared to the results of the full numerical solution. A computer program listed in Appendix I was written to accomplish this. A comparison of the two results for Peclet numbers of 2000 and 20,000 are given in Figs. 3.4.5 and 3.4.6 respectively. It is seen that extremely high Peclet numbers must be obtained before the limiting case is reasonably accurate. This fact somewhat diminishes the usefulness of the limiting case solution. The fact that there is not any enhancement in the mass-transfer rate to the surface not under the contact area of the bubble for the infinite Peclet number case indicates that the enhancement to this area in the finite Peclet number case is a second order effect. In the finite Peclet number case the enhancement effect is significant only under and near the original contact area of the bubble. A similar behavior of the current near the original contact area of the bubble was observed in the disengagement studies with the micro-mosaic electrode.

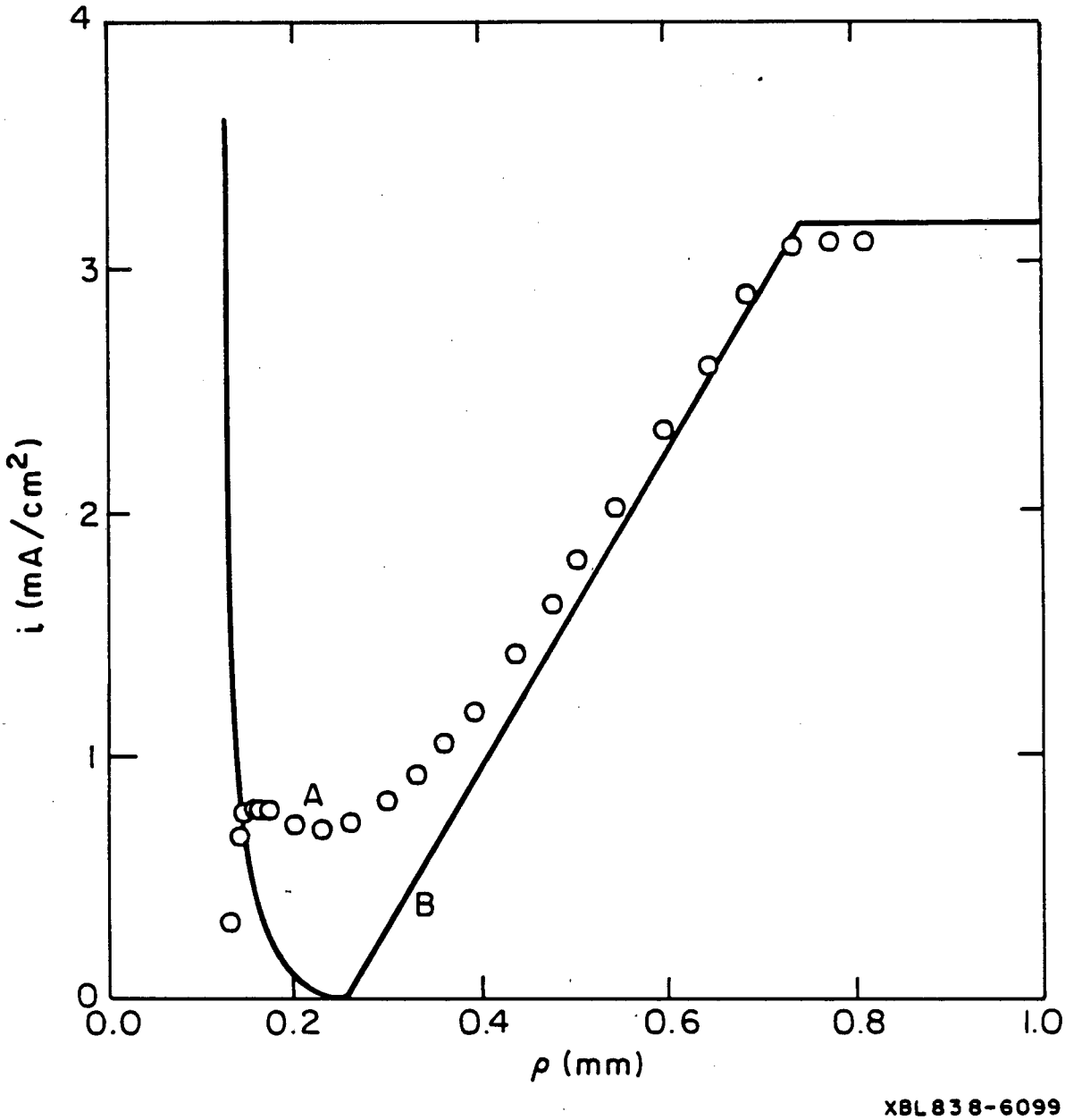

Figure 3.4.5 Limiting current distribution during the disengagement of a 1.49 mm diameter bubble (t_r = 0.2 seconds, t = 0.1 seconds, Pe = 2058); (A) Full numerical solution; (B) Infinite Peclet number solution.

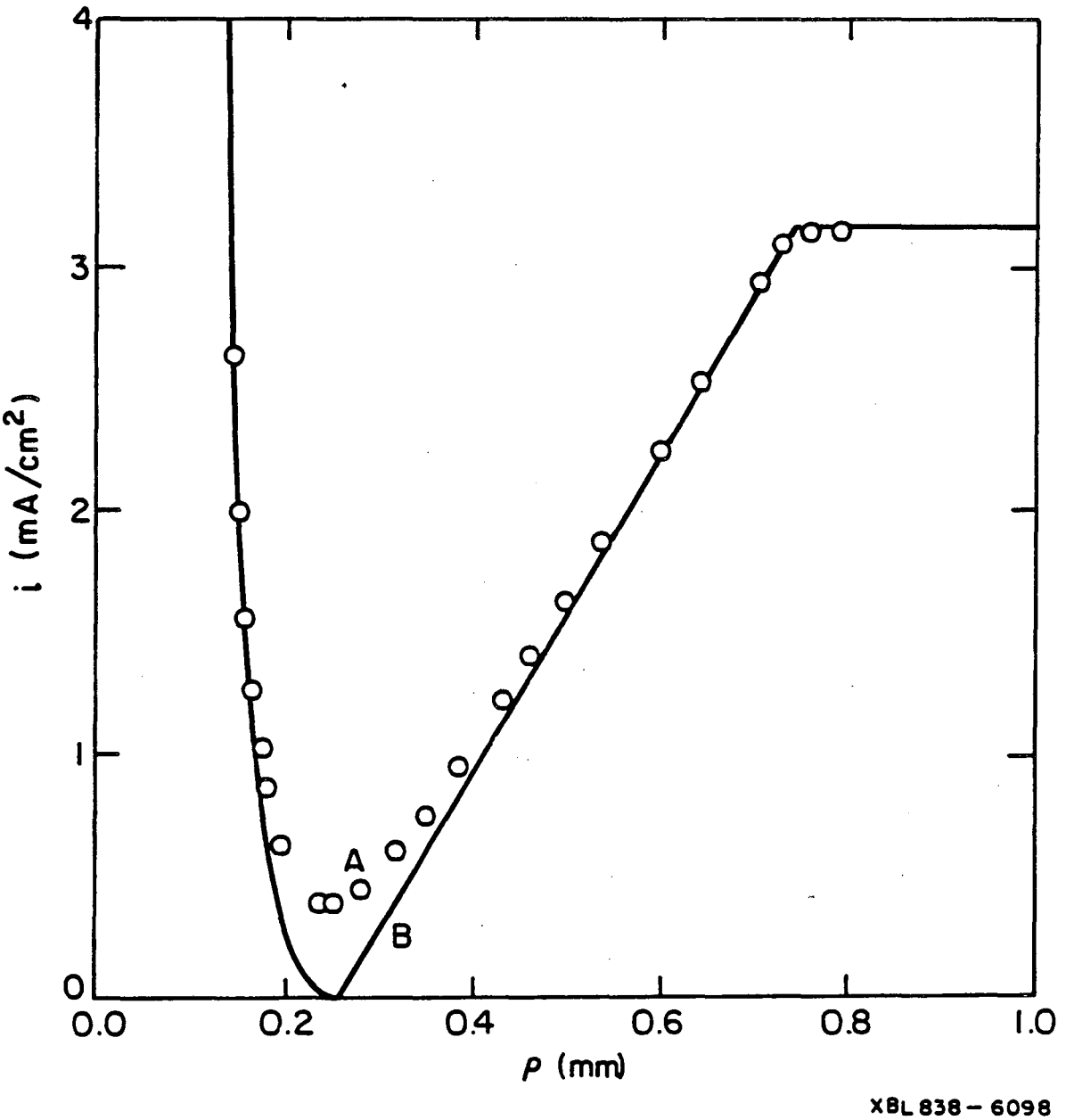

Figure 3.4.6 Limiting current distribution during the disengagement of a 1.49 mm diameter bubble (t_r = 0.02 seconds, t = 0.01 seconds, Pe = 20,581); (A) Full numerical solution; (B) Infinite Peclet number solution.

Nomenclature

$\tilde{c}$: Reduced concentration (see Equation 3.4.13).

c_3^1: Ferric ion concentration, moles cm^{-3}.

c_B: Bulk concentration of ferric ions, moles cm^{-3}.

D_3: Diffusion coefficient of ferric ions, cm^2 sec^{-1}.

F: Faraday constant, 96,487 C $equiv.^{-1}$.

n: Electrons transferred in reaction; equiv. $mole^{-1}$.

Pe: Peclet number (see Equation 3.4.19).

r: Cylindrical coordinate, cm.

$\tilde{r}$: Reduced cylindrical coordinate (see Equation 3.4.14).

$\hat{r}$: See Equation 3.4.24.

R: Radius of bubble, cm.

t: Time, sec.

$\tilde{t}$: Reduced time (see Equation 3.4.16).

$\tilde{t}_o$: Initial reduced time.

U: Contact area collapse velocity, cm sec^{-1}.

v: Velocity component, cm sec^{-1}.

$\tilde{v}$: Reduced velocity component.

<u>Greek Letters</u>

α: Boundary condition parameter.

β: Boundary condition parameter.

θ: Cylindrical coordinate, radians.

θ_o: Contact angle of bubble, radians.

$\hat{\theta}$: See Equation 3.4.25

$\tilde{\theta}$: Reduced cylindrical coordinate (see Equation 3.4.15).

ρ: Radial distance along electrode from center of bubble, cm.

ρ_0: Initial radius of contact area, cm.

ψ: Steam function, $cm^2\ sec^{-1}$.

Subscripts

r: Denotes r component.

θ: Denotes θ component.

3.5 Tranport Equations for Free-Convection Mass Transfer to a Horizontal Surface

The experimental studies of free-convection mass transfer to a horizontal surface (see Section 2.4.2) can be modeled numerically. Only the development of the transport equations is presented here. While the true test of the model will come from solving the equations, it is instructive to examine the model. The source of the density gradients in the electrolyte is not obvious from a superficial investigation of the experimental system. Because of the complexity of the phenomena involved, we will restrict consideration to the flow near the electrode. The development of the equations to describe the mass-transfer process is very similar to the analogous case for heat transfer (57), (58), but the electrochemical aspects of the problem do inject some interesting differences.

The model geometry is shown in Fig. 3.5.1, where a rectangular coordinate system is chosen. The electrode is at the base of the flow cell; the other three sides are fluid surfaces. It was concluded from our experiments that the fluid cells move along the surface. If the coordinate system moves with the cell, the electrode has a characteristic velocity. The plume flow, which is the cause of cell movement, exerts a stress on one side of the cell while the other two fluid sides are stress free.

The mass transport equations for the ionic components of the system are given by 3.1.10, 3.1.11, and 3.1.12. If we assume that the diffusion coefficient of the ferric ion is equal to that of the ferrous ion and that there is no reaction in the bulk, the sum of the

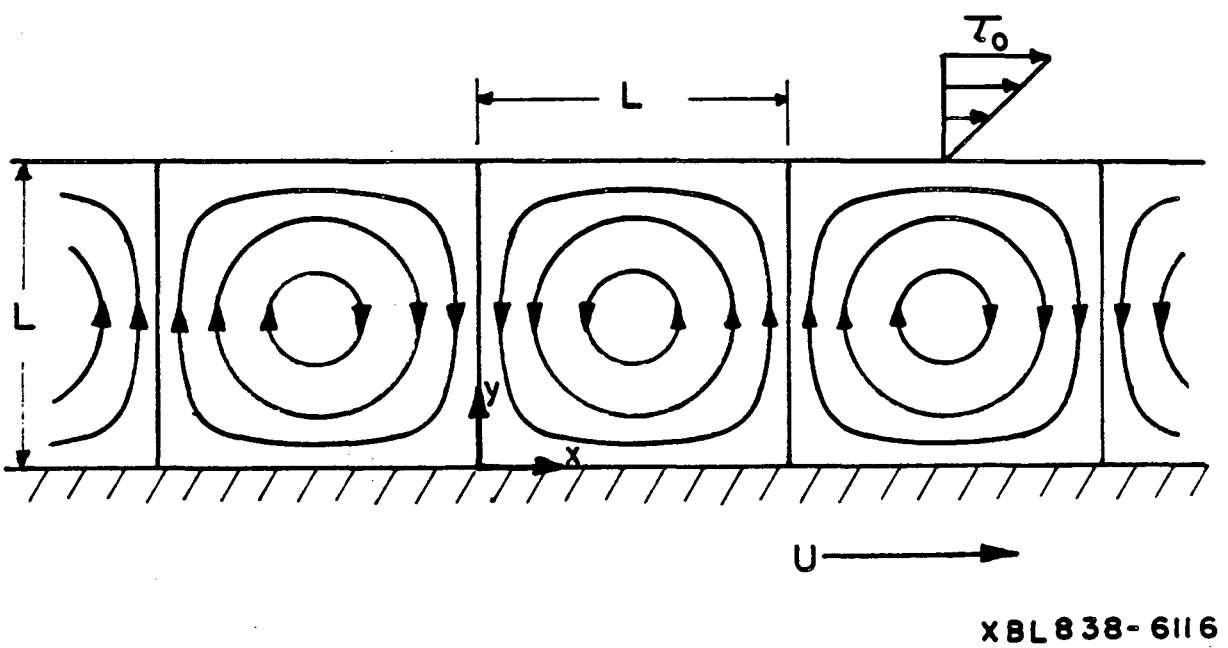

Figure 3.5.1 Schematic of cellular free convection near a horizontal surface.

concentration of these ions is a constant. Since there are initially no ferrous ions in the electrolyte the sum of the concentrations of Fe^{+++} and Fe^{++} must equal the initial bulk concentration of the ferric ions. Mathematically this is given by Equation 3.5.1.

$$c_3^1 + c_4^1 = c_{3B}^1 \tag{3.5.1}$$

This assumption should not introduce any significant error; it eliminates the need for simultaneously solving Equation 3.1.11 with the other transport equations. Equation 3.1.12 then reduces to:

$$\frac{\partial c_1^1}{\partial t} + v \cdot \nabla c_1^1 = D_e \nabla^2 c_1^1 + \frac{u_1(z_3-z_4)(D_2-D_3)}{z_1u_1 - z_2u_2} \nabla^2 c_3^1 \tag{3.5.2}$$

It is now convenient to define dimensionless variables and constants for the mass transport equations:

$$\tilde{c}_1 = c_1^1/c_{1B}^1 \tag{3.5.3}$$

$$\tilde{c}_3 = c_3^1/c_{3B}^1 \tag{3.5.4}$$

$$\tilde{x} = x/L \tag{3.5.5}$$

$$\tilde{y} = y/L \tag{3.5.6}$$

$$\tilde{v}_x = v_x/U \tag{3.5.7}$$

$$\tilde{v}_y = v_y/U \tag{3.5.8}$$

$$\tilde{t} = \frac{tU}{L} \tag{3.5.9}$$

$$Pe = \frac{UL}{D_3} \tag{3.5.10}$$

$$R_1 = \frac{D_3}{D_e} \tag{3.5.11}$$

$$R_2 = \frac{D_3\ (z_1u_1-z_2u_2)}{u_1\ (z_3-z_4)(D_2-D_3)} \tag{3.5.12}$$

$$R_3 = c_3^1/c_{1B}^1 \tag{3.5.13}$$

Substituting these quantities into Equations 3.5.2 and 3.1.10 we obtain:

$$\frac{\partial\tilde{c}_3}{\partial\tilde{t}} + \tilde{v}_x \frac{\partial\tilde{c}_3}{\partial\tilde{x}} + \tilde{v}_y \frac{\partial\tilde{c}_3}{\partial\tilde{y}} = \frac{1}{Pe}\left[\frac{\partial^2\tilde{c}_3}{\partial\tilde{x}^2} + \frac{\partial^2\tilde{c}_3}{\partial\tilde{y}^2}\right] \tag{3.5.14}$$

$$\frac{\partial\tilde{c}_1}{\partial\tilde{t}} + \tilde{v}_x \frac{\partial\tilde{c}_1}{\partial\tilde{x}} + \tilde{v}_y \frac{\partial\tilde{c}_1}{\partial\tilde{y}} = \frac{1}{Pe\ R_1}\left[\frac{\partial^2\tilde{c}_1}{\partial\tilde{x}^2} + \frac{\partial^2\tilde{c}_1}{\partial\tilde{y}^2}\right]$$

$$+ \frac{R_3}{Pe\ R_2}\left[\frac{\partial^2\tilde{c}_3}{\partial\tilde{x}^2} + \frac{\partial^2\tilde{c}_3}{\partial\tilde{y}^2}\right] \tag{3.5.15}$$

with the boundary conditions:

$$\tilde{c}_3 = 1 \qquad \tilde{y} = 1 \tag{3.5.16}$$

$$\tilde{c}_3 = 0 \qquad \tilde{y} = 0 \tag{3.5.17}$$

$$\frac{\partial\tilde{c}_3}{\partial\tilde{x}} = 0 \qquad \tilde{x} = 0 \text{ and } 1 \tag{3.5.18}$$

$$\tilde{c}_1 = 1 \qquad \tilde{y} = 1 \tag{3.5.19}$$

$$\frac{\partial\tilde{c}_3}{\partial\tilde{y}} = R_4 \frac{\partial\tilde{c}_1}{\partial\tilde{y}} \qquad \tilde{y} = 0 \tag{3.5.20}$$

$$\frac{\partial \tilde{c}_1}{\partial \tilde{x}} = 0 \qquad \tilde{x} = 0 \text{ and } 1 \tag{3.5.21}$$

where Equation 3.5.20 was obtained by relating the flux of sulfate ions at the surface to the flux of ferric ions, R_4 is given by:

$$R_4 = \frac{z_2 u_2 D_1 - z_1 u_1 D_2}{(z_3 - z_4)\, u_1 D_2} \tag{3.5.22}$$

If we introduce a stream function and vorticity defined as:

$$v_x = -\frac{\partial \psi}{\partial y} \tag{3.5.23}$$

$$v_y = \frac{\partial \psi}{\partial x} \tag{3.5.24}$$

$$\omega = \frac{\partial^2 \psi}{\partial x^2} + \frac{\partial^2 \psi}{\partial y^2} \tag{3.5.25}$$

into the Navier-Stokes equation we obtain:

$$\rho \left[\frac{\partial \omega}{\partial t} - \frac{\partial \psi}{\partial y}\frac{\partial \omega}{\partial x} + \frac{\partial \psi}{\partial x}\frac{\partial \omega}{\partial y} \right] = \mu \left[\frac{\partial^2 \omega}{\partial x^2} + \frac{\partial^2 \omega}{\partial y^2} \right] - g\,\frac{\partial \rho}{\partial x} \tag{3.5.26}$$

In writing Equation 3.5.26 it is implicitly assumed that the density is considered to be a constant in the overall mass balance. If we make the common assumption that the density varies linearly with species concentration, the density is:

$$\rho = \rho_0 + \alpha_1 c_1^1 + \alpha_2 c_2^1 + \alpha_3 c_3^1 + \alpha_4 c_4^1 \tag{3.5.27}$$

By further assuming that the proportionality constants for the ferric and ferrous ions are equal, Equations 3.5.27 can be reduced to:

$$\rho = \rho_1 + \beta_1 c_1^1 + \beta_3 c_3^1 \tag{3.5.28}$$

where the new constants are defined as:

$$\rho_1 = \rho_o + \frac{\alpha_3 z_2 - \alpha_2 z_4}{z_2} c_{3B}^1 \tag{3.5.29}$$

$$\beta_1 = \frac{\alpha_1 z_2 - \alpha_2 z_1}{z_2} \tag{3.5.30}$$

$$\beta_3 = \frac{\alpha_2 (z_4 - z_3)}{z_2} \tag{3.5.31}$$

Substituting Equation 3.5.28 into Equation 3.5.26, and defining dimensionless variables and constants given by Equations 3.5.32-36, we obtain:

$$\tilde{\psi} = \psi/UL \tag{3.5.32}$$

$$\tilde{\omega} = \frac{\omega L}{U} \tag{3.5.33}$$

$$Gr = \frac{g\ \beta_1\ c_{1B}^1\ L^3}{\nu^2 \rho} \tag{3.5.34}$$

$$Re = \frac{UL}{\nu} \tag{3.5.35}$$

$$R = \frac{\beta_3\ c_{3B}^1}{\beta_1\ c_{1B}^1} \tag{3.5.36}$$

$$\frac{\partial\tilde{\omega}}{\partial\tilde{t}} - \frac{\partial\tilde{\psi}}{\partial\tilde{y}}\frac{\partial\tilde{\omega}}{\partial\tilde{x}} + \frac{\partial\tilde{\psi}}{\partial\tilde{x}}\frac{\partial\tilde{\omega}}{\partial\tilde{y}} = \frac{1}{Re}\left[\frac{\partial^2\tilde{\omega}}{\partial\tilde{x}^2} + \frac{\partial^2\tilde{\omega}}{\partial\tilde{y}^2}\right]$$

$$- \frac{Gr}{Re^2} \frac{\partial \tilde{c}_1}{\partial \tilde{x}} + R_5 \frac{\partial \tilde{c}_3}{\partial \tilde{x}} \tag{3.5.37}$$

$$\tilde{\omega} = \frac{\partial^2 \tilde{\psi}}{\partial \tilde{x}^2} + \frac{\partial^2 \tilde{\psi}}{\partial \tilde{y}^2} \tag{3.5.38}$$

The boundary conditions are:

$$\tilde{\omega} = \tilde{\tau}_o \qquad \tilde{y} = 1 \tag{3.5.39}$$

$$\tilde{\omega} = 0 \qquad \tilde{x} = 0 \text{ and } 1 \tag{3.5.40}$$

$$\tilde{\psi} = 0 \qquad \tilde{x} = 0 \text{ and } 1 \quad \tilde{y} = 0 \text{ and } 1 \tag{3.5.41}$$

$$\frac{\partial \tilde{\psi}}{\partial \tilde{y}} = -1 \qquad \tilde{y} = 0 \tag{3.5.42}$$

where the dimensionless stress is defined as:

$$\tilde{\tau}_o = \frac{\tau_o L}{\mu U} \tag{3.5.43}$$

The problem is now defined except for the initial conditions on the variables. The transport equations to be solved numerically are Equations 3.5.14, 3.5.15, 3.5.37, and 3.5.38. Since the final solution should be a steady-state, one possibility is to solve the steady-state problem. Another possibility is to set the concentration equal to their bulk values and the Grashof number equal to zero, then numerically solve the differential equations and use the resulting solution as the initial condition on the finite Grashof number

case. A set of suggested parameters for the particular experimental system in this work is given in Table 3.5.1.

A close examination of the transport equations reveal the primary source of the density gradients. As a result of electroneutrality, the transport of ferric ions affects the concentration distribution of the sulfate ions. The concentration gradient of the sulfate ion is then responsible for the density gradient. The size of R_5 indicates that the direct contribution of the ferric ions is small compared to that of the sulfate ions.

Table 3.5.1 Suggested Numerical Values Of The Parameters For The Free Convection Model.

Parameter	Value
Grashof Number	143.1
Peclet Number	95.03
Reynolds Number	4.280×10^{-2}
Ratio Number 1	0.1781
Ratio Number 2	-0.5099
Ratio Number 3	0.6667
Ratio Number 4	3.000
Ratio Number 5	-8.130×10^{-3}

Nomenclature

c^1: First approximation concentration, moles cm^{-3}.

c^1_{1B}: Bulk concentration of sulfate ions minus the zero approximation term, moles cm^{-3}.

c^1_{3B}: Bulk concentration of ferric ions, moles cm^{-3}.

$\tilde{c}$: Reduced concentration.

D: Diffusion coefficient, cm^2 sec^{-1}.

g: Acceleration due to gravity, cm sec^{-2}.

Gr: Grashof number (see Equation 3.5.34).

L: Characteristic length, cm.

Pe Peclet number (see Equation 3.5.10).

R_1: See Equation 3.5.11.

R_2: See Equation 3.5.12.

R_3: See Equation 3.5.13.

R_4: See Equation 3.5.22.

R_5: See Equation 3.5.36.

Re: Reynolds number (see Equation 3.5.35).

t: Time, sec.

$\tilde{t}$: Reduced time.

u: Ionic mobility, cm^2 mole J^{-1} sec^{-1}.

U: Characteristic velocity, cm sec^{-1}.

v: Velocity component, cm sec^{-1}.

v: Velocity, cm sec^{-1}.

$\tilde{v}$: Dimensionless velocity component, cm sec^{-1}.

x: Coordinate, cm.

$\tilde{x}$: Dimensionless coordinate.

y: Coordinate, cm.

$\tilde{y}$: Dimensionless coordinate.

z: Charge number.

Greek Letters

α: Proportionality constant for density, g $mole^{-1}$.

β: See Equations 3.5.30 and 3.5.31.

μ: Viscosity, g cm^{-1} sec^{-1}.

ν: Kinematic viscosity, cm^2 sec^{-1}.

ρ: Density, g cm^{-3}.

ρ_0: Density, g cm^{-3}.

ρ_1: See Equation 3.5.29, g cm^{-3}.

τ_0: Stress, dyne cm^{-2}.

$\tilde{\tau}_0$: Dimensionless stress.

ψ: Stream function, cm^2 sec^{-1}.

$\tilde{\psi}$: Dimensionless stream function.

ω: Vorticity, sec^{-1}.

$\tilde{\omega}$: Dimensionless vorticity.

Subscripts

1: Denotes $SO_4^{=}$

2: Denotes H^+

3: Denotes Fe^{+++}

4: Denotes Fe^{++}

e: Denotes binary diffusion coefficient for supporting electrolyte.

x: Denotes x-component.

y: Denotes y-component.

4. CONCLUSIONS

4.1 General Remarks

The need for examining the effect of individual bubble phenomena on the rate of mass transfer to a surface is discussed in Chapter 1. Developing the experimental technique and designing and building the micro-mosaic electrode to perform these studies was an accomplishment that was attained through great effort. The capability of the micromosaic electrode to resolve the time dependent mass transfer distribution in the close vicinity of a bubble phenomena has been demonstrated. The utility of the electrode to examine other mass transport phenomena has also been proven. Results of studies on individual bubble phenomena reported in this work can be used to gain some insight into the mechanism of mass-transfer enhancement at a gas-evolving surface oriented horizontally. These studies should also provide a solid base for future work.

Discussion of the micro-mosaic electrode work will be limited to the studies already completed. Although these fall short of solving the overall problem, individual separation and coalescence phenomena treated here are indeed the key elements of the overall process affecting mass transfer to and from gas-evolving electrodes. When experimental mass-transfer data will have been obtained on all the simultaneous bubble phenomena occuring at a gas-evolving surface, an overall theoretical description of the complete process can be developed with statistical information on the frequency of occurrence of the various phenomena.

Intuition leads one to believe that experimental results from studying individual bubble phenomena on the micro-mosaic electrode is related to large numbers of similar phenomena occurring simultaneously on a gas-evolving electrode. Even though one might not expect the relative change in the current (i.e., mass-transfer rate) to be exactly the same for the bubble events in the two environments, the relative importance of these phenomena on the rate of mass transfer would be expected to show similarity. For example in the studies conducted in this work it was found that the coalescence of two bubbles exhibits a greater enhancement of the mass transfer rate than the disengagement of a bubble. It is believed that this is also true for such phenomena on a gas-evolving, horizontal surface. This belief is further strengthened by the dramatic difference in the relative magnitude of the two effects.

Let us now compare the bubble phenomena produced on the micro-mosaic electrode to the same phenomena on a gas-evolving electrode. If possible, theoretical wodels (see Chapter 3) or, at least, dimensional analysis (59) will be used to predict what effect these differences in the bubble phenomena have relative to the change in the mass transfer rate, in the micro-mosaic electrode studies.

The most obvious difference is the larger size of the bubbles generated on the micro-mosaic electrode when compared to a gas-evolving surface. The bubbles produced on the micro-mosaic electrode are generally one to two orders of magnitude larger than those formed on a gas evolving surface. As previosly pointed out, this is attributed to the macroconvection past the gas evolving surface. The effect of the

larger bubble size on the change in the mass-transfer rate is very complex and each aspect must be examined separately.

4.2 Effect of Macroconvection on Bubble Phenomena

The macroconvection flow field surrounding the bubbles on a gas-evolving surface affects the thickness of the concentration boundary layer and the hydraulic forces on the bubbles. These forces are much greater than those generated by free convection in the micro-mosaic electrode studies. The hydraulic forces from the macroconvection do affect the bubble phenomena and in turn the change in the mass-transfer rate. Presently, not enough experimental or theoretical work yet available to determine the exact effect of the macroconvection on the dynamics of bubble events, but it is believed that all bubble phenomena are affected similarly. In other words the macroconvection would not be expected to change preferentially the enhancement effect of one phenomenon over the other.

The limiting current, before the occurrence of a bubble event, is controlled by free convection on the micro-mosaic electrode. On a gas evolving electrode the background limiting current is controlled by macroconvection. The importance of this is shown in Fig. 4.2.1. The greater the characteristic length of the bubble event (the diameter of the bubble, L) when compared to the thickness of the concentration boundary layer (Nernst boundary layer thickness, δ), the smaller the relative mass-transfer enhancement for the same phenomena. This is a result of the event generating the flow farther from the electrode in a region where little or no concentration gradients exists. The ratio of the characteristic length to thickness of the boundary layer is

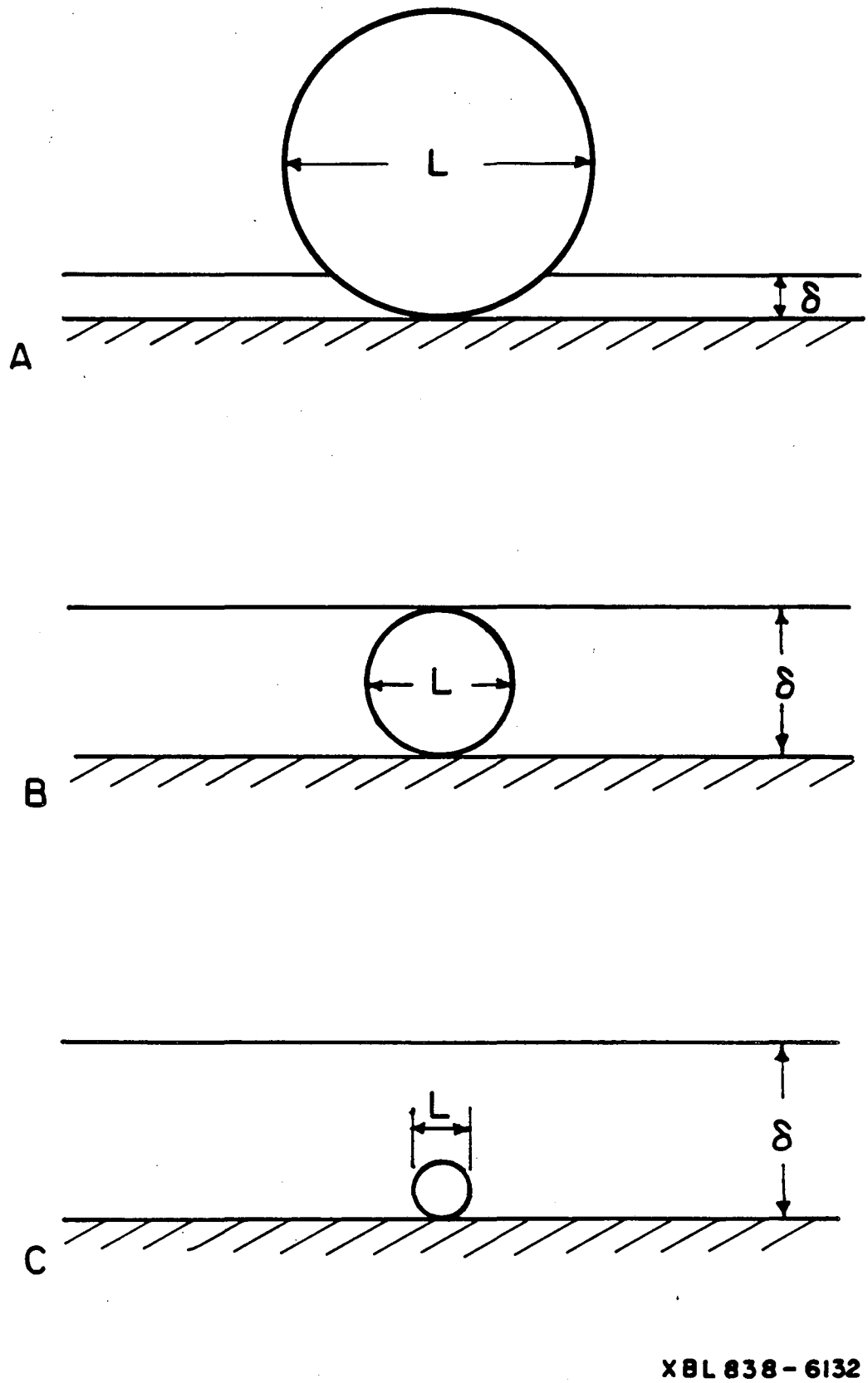

Figure 4.2.1 Schematic of bubble on electrode shoing Nernst boundary layer thickness; (A) $L > \delta$; (B) $L = \delta$; (C) $L < \delta$.

the Sherwood number (L/δ). For the micro-mosaic electrode studies the Sherwood number was between 3.5 and 10.5 depending on the size of the bubble, while on a typical gas-evolving electrode the Sherwood number varies from 5 to 50 (12) depending on the gas evolution rate. Although the bubbles generated on the micro-mosaic electrode are much larger, so is the Nernst boundary layer thickness giving a Sherwood number equal to that of the gas evolving surface within an order of magnitude. The relative change in the mass transport rate as a result of a bubble event would not be expected to be significantly different because of the contrasting modes of mass transfer.

4.3 Effect of Size on the Disengagement of a Bubble

As the bubble size decreases the Reynolds number (UL/ν) for the disengagement phenomenon decreases. Theoretical considerations (see Section 3.3) predict a Reynolds number much smaller than one for an ascending fluid sphere with a bubble diameter in the range of those found on a gas-evolving electrode. This does not include the effect of macroconvection, which would tend to increase the Reynolds number, or the collapse of the contact area, which would tend to reduce it.

Since the Reynolds number for the disengagement is less than unity, the ascending-fluid-sphere model can be used to predict the effect of a bubble disengagement on the mass transfer rate to a gas-evolving surface. Generally the model indicates that there is a decrease in the mass transfer rate to the surface, under the bubble and even past the diameter of the bubble. The imperfections of this model have already been pointed out and do not need to be repeated here. The important fact that can

be deduced from the model is that an ascending bubble generating a low Reynolds number flow does not provide a mechanism suitable for the enhancement of the mass transfer rate to the surface.

One would not expect the mass-transfer enhancement for a bubble disengagement on a gas-evolving surface to be greater than that measured on the micro-mosaic electrode. Indeed on the basis of arguements presented above the enhancement effect should be less. It has been pointed out that the mass-transfer enhancement to the surface under the contact area of the bubble could not be measured in the micro-mosaic electrode studies. Theoretical considerations (see Section 3.4) indicate that the enhancement to the contact area can be significant. This mechanism for mass transfer enhancement also results from the coalescence of bubbles; in fact the effect is doubled because two bubbles are involved.

4.4 Effect of Size on the Coalescence of Two Bubbles

Strictly speaking the coalescence of two bubbles followed by the disengagement of the resulting bubble was studied with the micro-mosaic electrode. Since the enhancement of the mass transfer rate to the surface is largely due to the coalescence (see Section 2.4.2) and because the effect of size on the disengagement has already been discussed, only the coalescence will be examined.

The smaller the bubble the stronger the surface tension forces which cause the collapse of the two bubbles into one. As the surface tension forces increase, fluid is displaced more rapidly during coalescence resulting in a shorter time constant for the phenomenon.

The shorter time constant for coalescence is accompanied by higher fluid velocities, which would tend to increase the mass-transfer enhancement effect. Thus on "real" gas-evolving electrodes, coalescence induced mass transfer enhancement should be even more of a dominant mode compared to the enhancement caused by the coalescence of two relatively large bubbles observed on the micro-mosaic electrode.

4.5 Concluding Remarks

Finding the proper words to end a project on is always difficult. The task is even more difficult because this work does not conclude the project, but only begins it. What started as an ambitious idea has now been developed into a viable research program that should allow interesting and exciting studies to be performed for years to come. Many challenging problems had to be overcome to accomplish this. It was not done without a great deal of effort, but it did provide stimulating work.

In deciding which experiments to conduct with the micro-mosaic electrode a logical progression in the complexity of the experiment was followed. This was the reason for first studying bubble phenomena on a horizontal electrode, although vertical gas-evolving electrodes are more commonly found in industry. The cell has been built to study phenomena on the micro-mosaic electrode oriented vertically. Also a forced convection cell with a rotating disk above the micro-mosaic electrode could be constructed without too much difficulty so that macroconvection effects on bubble phenomena can be measured. There is obviously many directions that the research program can go in from here, all of which should be quite interesting and informative.

Nomenclature

L: Characteristic length, cm.

Sh: Sherwood number.

U: Characteristic velocity, cm sec^{-1}.

Re: Reynolds number.

Greek Letters

δ: Nernst boundary layer thickness, cm.

ν: Kinematic viscosity, cm^2 sec^{-1}.

APPENDIX A

Notes on the Instrumentation for the Multi-Electrode Cell

It was observed that the Pine potentiostat would at times become unstable. This was manifested by large oscillations in the voltage from the voltage followers for the working electrodes (E1 and E2). These oscillations usually occurred when the potentiostat was turned on or when one of the applied potentials of the working electrodes was changed significantly. The oscillations could be damped out by adjustment of the current converter scale control or by placing an additional capacitor in the circuit, as described in the operating manual. Once the potentiostat was steady, it remained stable as long as there was no a large change in the applied potential (e.g. a potential step). A change in the applied potential would not necessarily generate the oscillations.

The wires from the multi-electrode cell's working electrode were attached to a color coded set of wires, through a standard 19 pin Bendix connector. The color code is given in Table A.1 where the assigned electrode number is shown in Fig. 2.2.1.3. The color coded wires were attached to the bus bar by alligator clips.

The current follower, used to convert the segmental current to a voltage, was of a standard design (36). A diagram of the circuit is given in Fig. A.1. Since the operational amplifier was battery powered, the ground was floating. The value of the resistor (R) dictated the current-to-voltage conversion, which was 10 μA/V. The current follower could handle up to 70 μA of current without overloading.

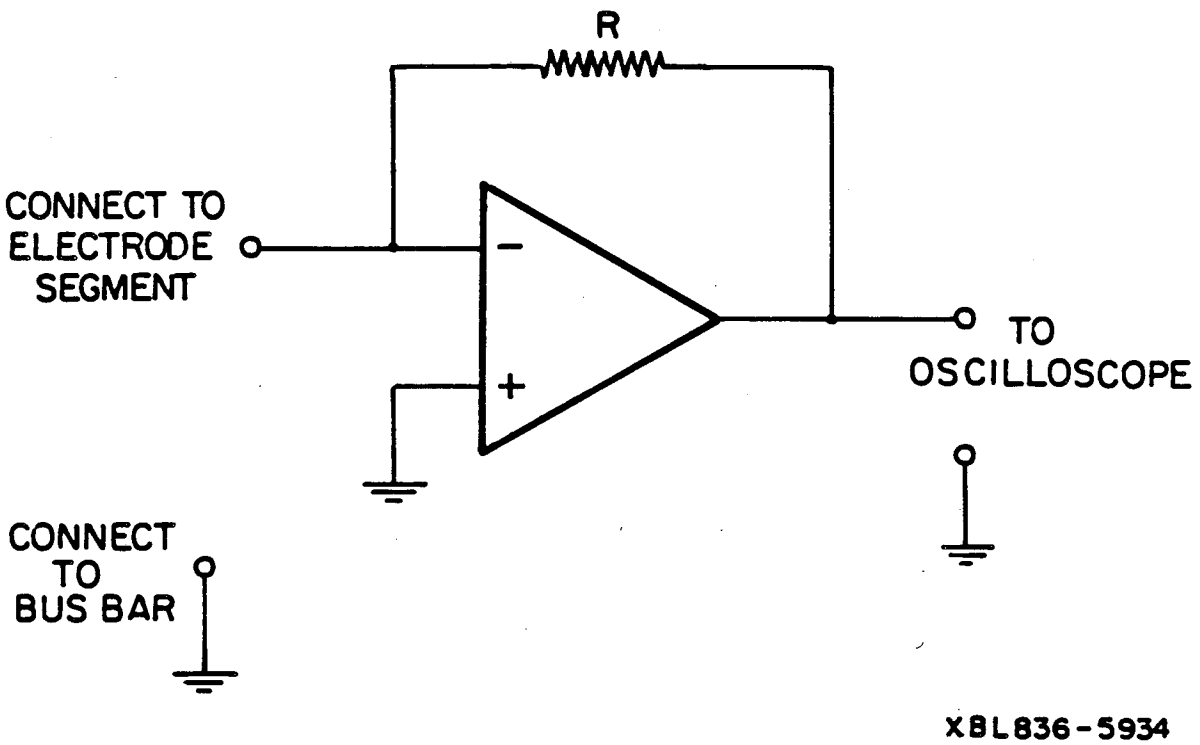

Figure A.1 Schematic of current follower.

Table A.1 Color Code For Multi-Electrode Cell Connector(Stripe Color In Parentheses).

Electrode Number	Wire Color	Electrode Number	Wire Color
1	White(Purple)	11	Blue
2	Orange	12	Yellow
3	Brown	13	White(Orange)
4	Pink	14	White(Green)
5	Green	15	White(Black)
6	White(Gray)	16	White(Brown)
7	Gray	17	White
8	White(Red)	18	Red
9	White(Blue)	19	Purple
10	White(Yellow)		

Noise was a major problem in the system. All external connections were properly shielded. The electronic equipment was connected to a common ground. Using these established methods, the noise was reduced to a sufficiently low level.

APPENDIX B

Design and Fabrication of the Micro-Mosaic Electrode

The micro-mosaic electrode was fabricated with established thin film technology (37). The various layers were deposited or grown on the substrate, then the desired pattern was generated on each layer using a photolithographic process.

Four masks were needed for the pattern generation. Three 10X projection masks were used with a Mann 4800 Step and Repeat Printer and a contact mask was used with a Perkin-Elmer Contact Printer. The design of the masks was digitized with a computer aided design system. A schematic of the pattern on the contact mask is given in Fig. B.1 and the projection masks pattern is presented in Fig. B.2. A close-up view of the projection masks pattern, showing the segmented portion of the micro-mosaic electrode, is given in Fig. B.3. The symmetry in all the patterns should be noted. All the patterns can be broken up into four quadrants with each quadrant having the same design.

One projection mask was needed to generate the pattern in each of the platinum/chromium layer (BERK-3) and in the silicon dioxide (BERK-2). The smallest dimension generated by mask BERK-2 was 20 micron. The critical dimension generated by mask BERK-3 and also for the device was one order of magnitude smaller (2 micron).

The contact mask (BERKIM-3) and a projection mask (BERK-1) were used to define the pattern on the aluminum layer. The center 0.8 cm x 0.8 cm of the wafer was defined with mask BERK-1. Mask

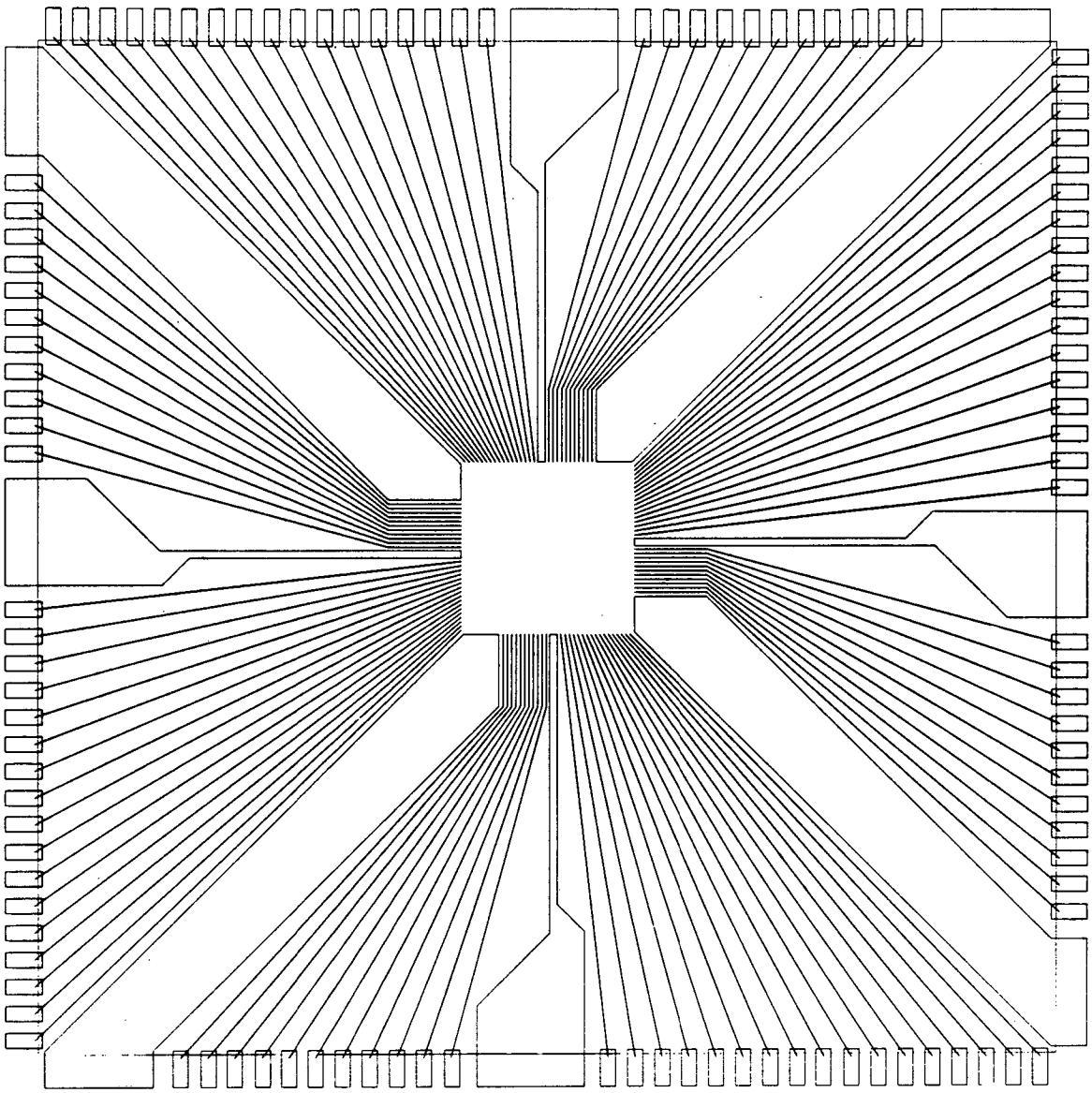

CBB 808-9091

Figure B.1 Contact mask pattern.

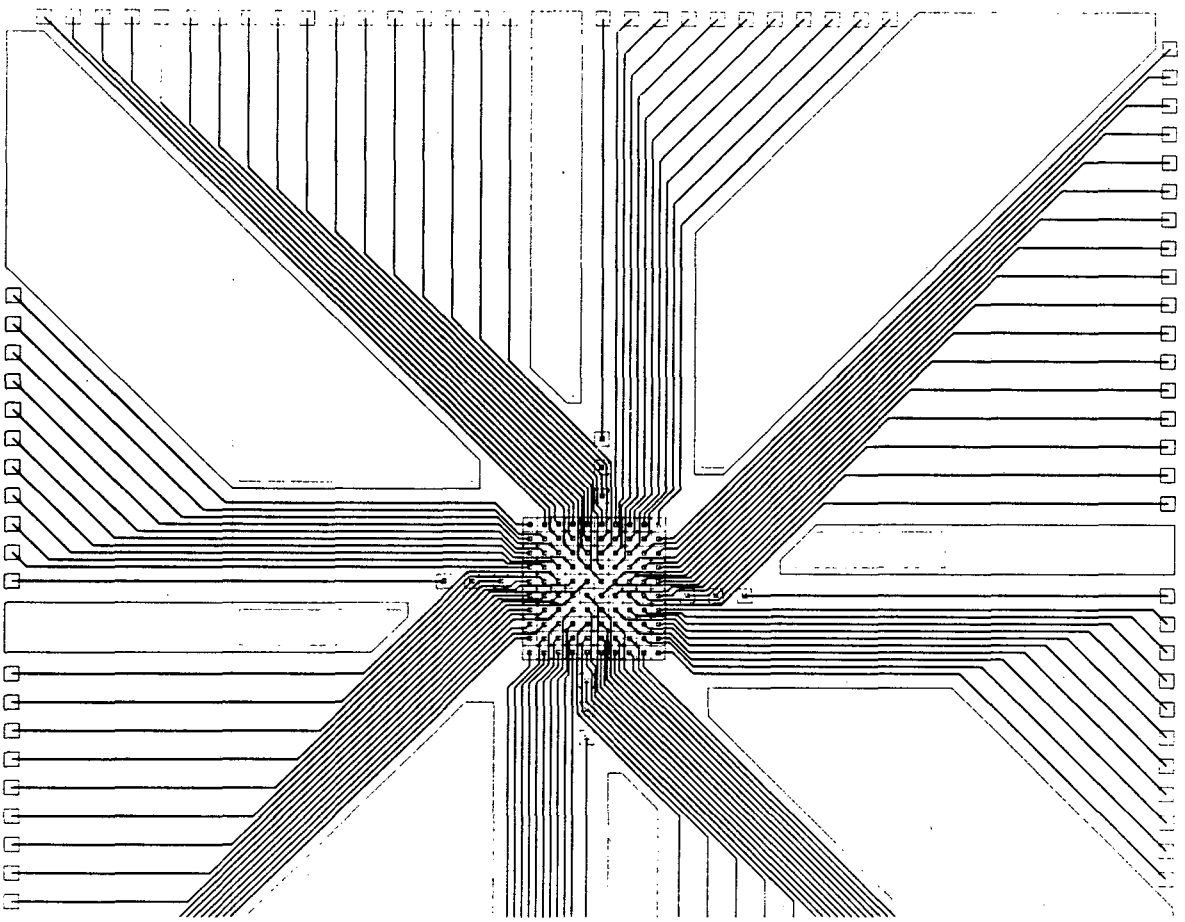

CBB 808-9093

Figure B.2 Projection masks pattern.

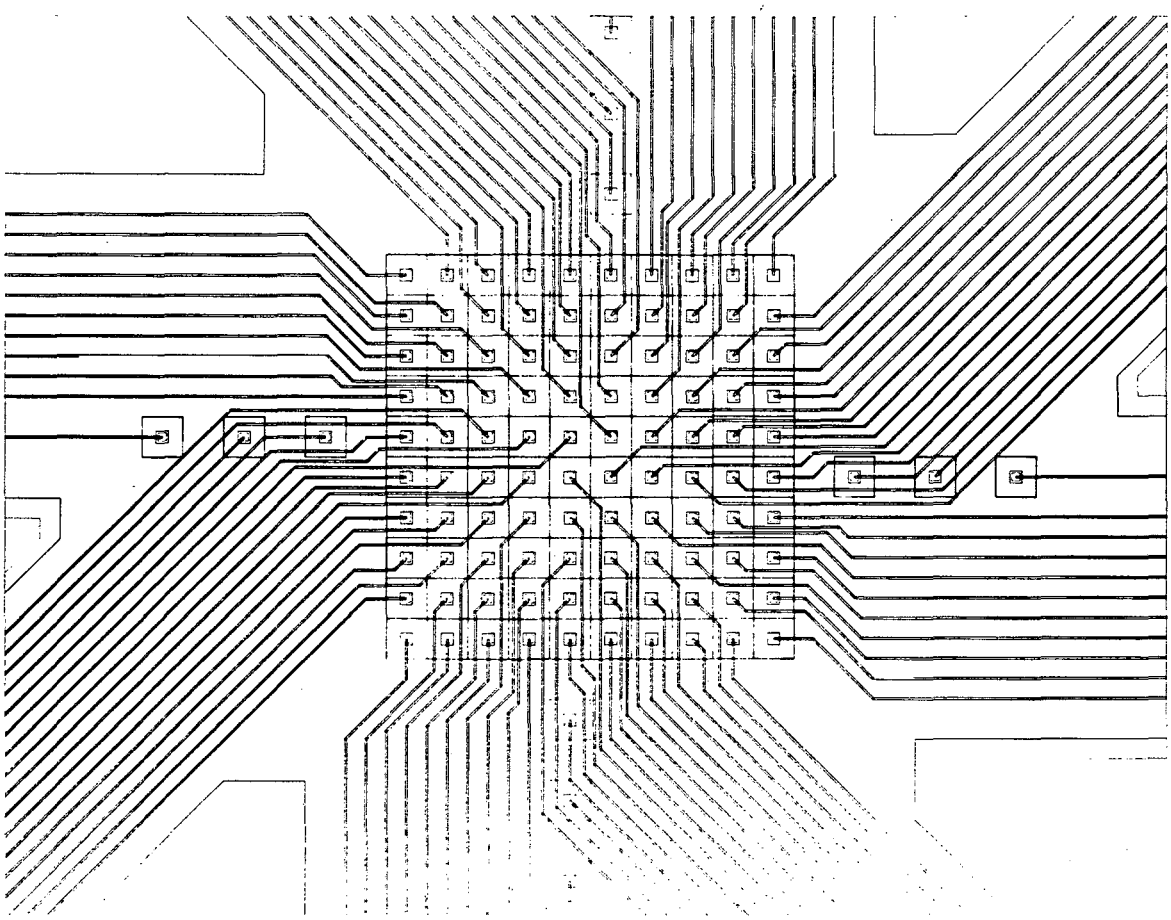

CBB 808-9095

Figure B.3 Close-up of projection masks pattern.

BERKIM-3 was used to define the outer portion of the aluminum layer. The pattern on the inner area overlapped with the pattern on the outer area, so that both masks had to be aligned properly when defining the entire pattern. Special pads were added to the pattern of the projection mask to allow for some alignment error.

The processing steps were as follows:

1) Clean a 3 inch silicon wafer.
2) Thermally grow 1.5 micron field oxide.
3) Deposit 1500 angstroms nitride.
4) Deposit 1200 angstroms aluminum (2% Si).
5) Spin negative resist. Expose pattern (BERK-1). Expose pattern (BERKIM-3). Do not develop between exposures. Etch aluminum and strip resist.
6) Deposit 3000 angstroms low temperature silicon dioxide.
7) Spin negative resist. Expose pattern (BERK-2). Remove mask from Mann 4800 and blanket expose remaining area inside bonding pads. Etch oxide and strip resist.
8) Deposit 300 angstroms chromium.
9) Deposit 1200 angstroms platinum.
10) Spin negative resist. Expose pattern (BERKIM-3), with a paper mask to leave platinum pads around the edge, and develop.
11) Spin positive resist. Expose pattern (BERK-3). Blanket expose remainder of wafer and develop. Ion mill platinum/chromium layer and strip resist.

APPENDIX C

Notes on Instrumentation for Early Mass Transfer Studies with the Micro-Mosaic Electrode

As with the experiments with the multi-electrode cell, noise was also a problem with the micro-mosaic electrode experiments. Because of the lower currents that were to be measured, the signal to noise ratio was much lower. The main improvement in the quality of the signal came from increasing the current-to-voltage conversion on the current follower to 1.0 V/μA. This was done by changing the resistor (R in Fig. A.1) on the current follower. The filter on the digital oscilloscope was also used to eliminate noise. The overall improvement of the signal can be seen by comparing the results from two equivalent experiments, before and after the changes, in Fig. C.1.

Before color coding the electrode connections to the bus bar, the segments first had to be numbered. Since the segmented portion of the electrode forms a two dimensional matrix, a matrix numbering system was used. The columns of the matrix are parallel to the orientation flat on the micro-mosaic electrode wafer and the rows are perpendicular to the flat. By placing the wafer in front of the reader, face-up with the orientation flat on the left, the segment in the first row and column (number [1,1]) is in the upper left hand corner. When the electrode is housed in either of the specialy built cells, the upper left hand corner of the wafer is marked by a small hole drilled in that particular corner of the base, printed circuit

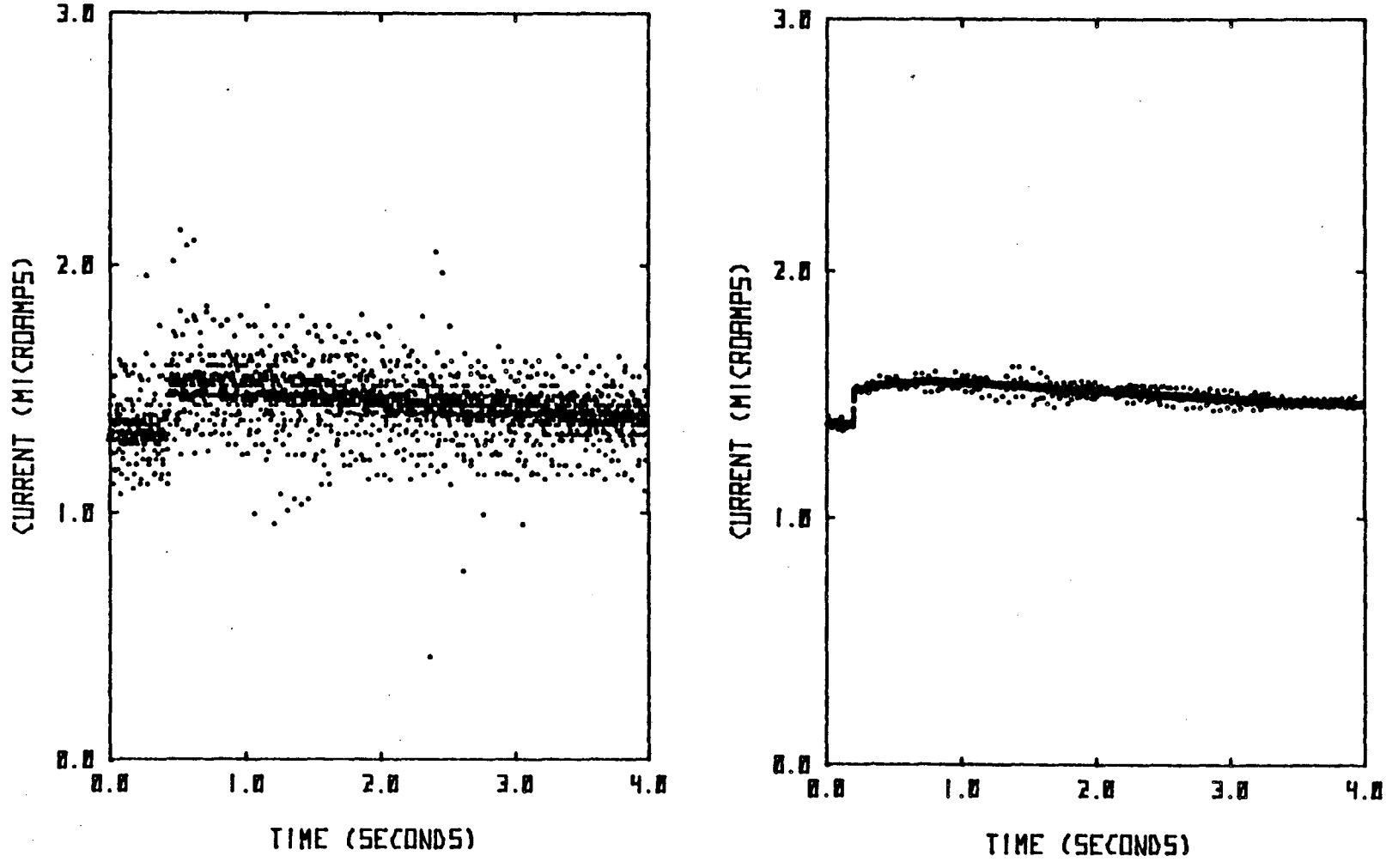

XBL 836-10382

Figure C.1 Experimental results of two equivalent experiments; (A) Before noise reduction improvements; (B) After noise recution improvements.

board, and the actual cell. The other segments in the matrix are numbered accordingly. The specially positioned segments were numbered by taking on the number of the row or the column that they are in. The other number was actually a letter (A, B, or C), where the first letter was given to the segment closest to the electrode matrix. The numbering system for the electrode segments is shown in Fig. C.2.

There are four sets of 35 connections on the printed circuit board. Of the connections 28 are attached to an electrode segment, while six are connected to the buffer segment, and one is a blank (i.e. not connected to anything). The connections were numbered 1 through 35 from left to right when the viewer is facing the board. A printed circuit board connector can be attached to each set. The connectors were numbered, with Roman numerals (I-IV), by placing the small drill hole in the printed circuit board in the upper left hand corner and numbering in a clockwise order.

A shielded multi-conductor cable was attached to each of the four printed circuit board connectors. Each cable has 37 wires with 22 gauge multi-strand wire (BEC. CO.). Each wire in the cable was color coded and insulated. The wires correspond to electrode segments according to Table C.1.

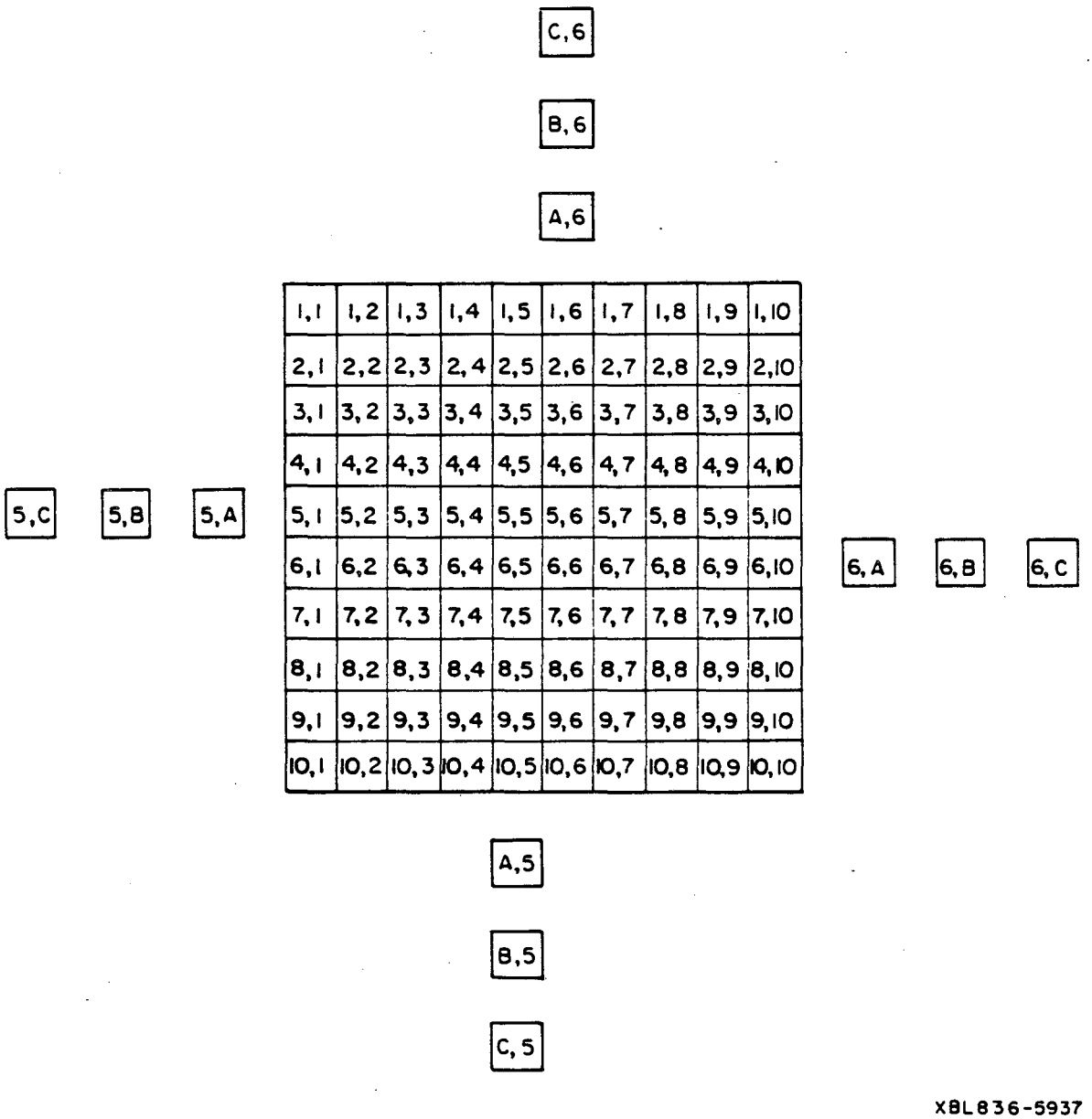

Figure C.2 Micro-mosaic electrode segments numbering system.

Table C.1 Color Code For Micro-Mosaic Electrode Cell Connectors(Stripe Colors In Parentheses).

Connector I Conductor Color Code		
Connector Number	Wire Color	Electrode Number
1	Black(Red,White)	Blank
2	Orange(Green)	Buffer
3	White(Yellow,Red)	Buffer
4	White(Blue,Red)	Buffer
5	Black(White,Brown)	(1,10)
6	Red(White)	(2,9)
7	Red(Green)	(1,9)
8	Orange(Blue,White)	(3,8)
9	Blue(Black)	(2,8)
10	Green(Black)	(1,8)
11	Orange(Green,Black)	(4,7)
12	Orange(Black)	(3,7)
13	Green(White)	(2,7)
14	Green(Brown,Black)	(1,7)
15	Blue(Red)	(C,6)
16	Red(Black)	Buffer
17	Orange	Buffer
18	White(Black)	Buffer
19	Black(White)	(3,6)
20	Green	(2,6)
21	Orange(Red)	(B,6)
22	Black(Red,Green)	(A,6)
23	White(Red)	(1,6)
24	Red(Black,Green)	(4,6)
25	Red	(5,6)
26	White	(1,5)
27	White(Red,Black)	(2,5)
28	Black	(3,5)
29	Blue	(4,5)
30	Black(Red)	(1,4)
31	White(Green,Red)	(2,4)
32	Orange(Black,White)	(3,4)
33	Blue(White,Black)	(1,3)
34	Green(White,Black)	(2,3)
35	Red(White,Black)	(1,2)

(Continued On Next Page)

(Table C.1 Continued)

Connector II Conductor Color Code		
Connector Number	Wire Color	Electrode Number
1	Black(Red,White)	Blank
2	Orange(Green)	Buffer
3	White(Yellow,Red)	Buffer
4	White(Blue,Red)	Buffer
5	Black(White,Brown)	(10,10)
6	Red(White)	(9,9)
7	Red(Green)	(9,10)
8	Blue(Black)	(8,8)
9	Green(Black)	(8,9)
10	Orange(Green,Black)	(8,10)
11	Orange(Black)	(7,7)
12	Green(White)	(7,8)
13	Green(Brown,Black)	(7,9)
14	Orange(Blue,White)	(7,10)
15	Blue(Red)	(6,C)
16	Red(Black)	Buffer
17	Orange	Buffer
18	White(Black)	Buffer
19	Black(White)	(6,8)
20	Green	(6,9)
21	Orange(Red)	(6,B)
22	Black(Red,Green)	(6,A)
23	White(Red)	(6,10)
24	Red(Black,Green)	(6,7)
25	Red	(6,6)
26	White	(5,10)
27	White(Red,Black)	(5,9)
28	Black	(5,8)
29	Blue(Gray)	(5,7)
30	Black(Red)	(4,10)
31	White(Green,Red)	(4,9)
32	Orange(Black,White)	(4,8)
33	Blue(White,Black)	(3,10)
34	Green(White,Black)	(3,9)
35	Red(White,Black)	(2,10)

(Continued On Next Page)

(Table C.1 Continued)

Connector III Conductor Color Code		
Connector Number	Wire Color	Electrode Number
1	Black(Red,White)	Blank
2	Orange(Green)	Buffer
3	White(Yellow,Red)	Buffer
4	White(Blue,Red)	Buffer
5	Black(White,Brown)	(10,1)
6	Red(White)	(9,2)
7	Red(Green)	(10,2)
8	Orange(White,Blue)	(8,3)
9	Blue(Black)	(9,3)
10	Green(Black)	(10,3)
11	Orange(Green,Black)	(7,4)
12	Orange(Black)	(8,4)
13	Green(White)	(9,4)
14	Green(Brown,Black)	(10,4)
15	Blue(Red)	(C,5)
16	Red(Black)	Buffer
17	Orange	Buffer
18	White(Black)	Buffer
19	Black(White)	(8,5)
20	Green	(9,5)
21	Orange(Red)	(B,5)
22	Black(Red,Green)	(A,5)
23	White(Red)	(10,5)
24	Red(Black,Green)	(7,5)
25	Red	(6,5)
26	White	(10,6)
27	White(Red,Black)	(9,6)
28	Black	(8,6)
29	Blue	(7,6)
30	Black(Red)	(10,7)
31	White(Green,Red)	(9,7)
32	Orange(Black,White)	(8,7)
33	Blue(White,Black)	(10,8)
34	Green(White,Black)	(9,8)
35	Red(White,Black)	(10,9)

(Continued On Next Page)

(Table C.1 Continued)

Connector IV Conductor Color Code		
Connector Number	Wire Color	Electrode Number
1	Black(Red,White)	Blank
2	Orange(Green)	Buffer
3	White(Yellow,Red)	Buffer
4	White(Blue,Red)	Buffer
5	Black(White,Brown)	(1,1)
6	Red(White)	(2,2)
7	Red(Green)	(2,1)
8	Orange(Blue,White)	(3,3)
9	Blue(Black)	(3,2)
10	Green(Black)	(3,1)
11	Orange(Green,Black)	(4,4)
12	Orange(Black)	(4,3)
13	Green(White)	(4,2)
14	Green(Brown,Black)	(4,1)
15	Blue(Red)	(5,C)
16	Red(Black)	Buffer
17	Orange	Buffer
18	White(Black)	Buffer
19	Black(White)	(5,3)
20	Green	(5,2)
21	Orange(Red)	(5,B)
22	Black(Red,Green)	(5,A)
23	White(Red)	(5,1)
24	Red(Black,Green)	(5,4)
25	Red	(5,5)
26	White	(6,1)
27	White(Red,Black)	(6,2)
28	Black	(6,3)
29	Blue(Gray)	(6,4)
30	Black(Red)	(7,1)
31	White(Green,Red)	(7,2)
32	Orange(Black,White)	(7,3)
33	Blue(White,Black)	(8,1)
34	Green(White,Black)	(8,2)
35	Red(White,Black)	(9,1)

APPENDIX D

Oscilloscope Data Transfer and Plotting Programs

A set of programs was developed to transfer data from the Nicolet 1090A and 4094 digital oscilloscopes to a Hewlett Packard desktop computer (9825T). The programs will also store and/or plot the data on a Hewlett Packard digital plotter (9826A). They are written in a Hewlett Packard Language (HPL). The programs are stored on track ϕ of a magnetic tape cartridge titled, "Program Tape". A description and listing of each program file follows:

File 0 (Program D.1): This program was written for gas evolution data on a Nicolet 1090A digital oscilloscope. It is designed to record a single waveform with all the memory on the oscilloscope, after a step in the potential to the micro-mosaic electrode. Besides the oscilloscope data, the plug-in parameters along with the current-to-voltage conversion, the run number, system temperature, ferric ion concentration, and position of the segment being monitored are also stored. Various bubble parameters are stored; such as size, position on electrode, and the time and length of the release potential pulse under the bubble. All data is stored on a magnetic tape. The program will also retrieve data from the tape and plot it. The plotting routine does not label the axes, which are optional, but it does print out all the relevant information for the experiment.

File 1 (Program D.2): This program was written to retrieve data stored by Program D.1 and plot the current versus the inverse square root of

time, either with or without the axes. As with Program D.1, all relevant parameters are printed out with the plot.

File 2 (Program D.3): This program is almost the same as Program D.1. Like D.1 it was written for the early gas evolution experiments. It was used for experiments with a constant electrode potential and without a pulse in the potential to the segment under the bubble. Therefore the input/output pulse information has been deleted from the program.

File 3 (Program D.4): The program is similar to Program D.1, except that it is for general experimental results on the oscilloscope. All specific information for the gas evolution experiments has been deleted. Space is provided to store an 80 letter statement with the results.

File 4 (Program D.5): This program was written for general experimental data on the Nicolet 4094 digital oscilloscope. It will transfer any number of waveforms from the oscilloscope and record them on an 8 inch flexible (floppy) disk, with a Hewlett Packard flexible disk drive (9885M) interfaced to the computer. This program has a plotting routine plotting routine that is similar to the one in Program D.1.

File 5 (Program D.6): This program is a general plotting routine. It will set-up and label the axes according to input commands from the user. The program will put a title and a three line caption on the graph also. It is written to draw the graph with lettering in a rectangular area with a height-to-length ratio of 9.5/7. The program was

designed to be used in conjunction with Programs D.1-5, where a high quality plot is needed. This is accomplished by first running Program D.6, then use one of the other routines to retrieve the data from storage and plot the results.

File 6 (Program D.7): This program draws a schematic of the micromosaic electrode. It also marks the segment where the current was monitored and draws an outline of the bubble. Marking the perimeter of the electrode is an option. The program is written to draw the figure on a square area. It is designed to be used as an option in conjunction with the plotting routines.

```
0: dsp "THIS
 PROGRAM RECORDS
  AND PLOTS"
1: wait 5000
2: dim E$[15,8]
3: dim D,I,W,
 B$[10],C$[10],
 G,C,T,L,V,B,F,
 Y$[8208]
4: dim A$[5]
5: buf "data",
 Y$,2
6: ent "IS DATA
 TO BE TRANSFERR
 ED ?",A$
7: if cap(A$)="Y
 ES";gto 16
8: ent "WHAT
 TRACK ?",U
9: ent "WHAT
 FILE ?",E
10: trk U
11: ldf 0,E$
12: ldf E,D,I,W,
 B$,C$,G,C,T,L,
 V,B,F,Y$
13: spc
14: prt "RUN
 NUMBER ",E$[E]
15: gto 53
16: ent "BUBBLE
 DIAMETER IN
 MICRONS",D
17: ent "TIME
 OF RELEASE PULS
 E IN MSEC",I
18: ent "LENGTH
 OF PULSE IN
 MSEC",W
19: ent "COORDIN
 ATS OF BUBBLE
 SEGMENT",B$
20: ent "COORDIN
 ATES OF CURRENT
  SEGMENT",C$
21: ent "SEGMENT
  DIFFERENCE IN
 MICRONS",G
22: ent "Fe CONC
 ENTRATION IN
 MOLES/LITER",C
23: ent "TEMPERA
 TURE IN DEG C",
 T
24: ent "TIME/
 PONT IN MSEC",L
25: ent "MAX
 SCALE VOLTAGE
 IN VOLTS",V
26: ent "BASE
 LINE VOLTAGE
 IN VOLTS",B
27: dsp "VOLTAGE
 -TO-CURRENT
 CONVERSION"
28: wait 5000
29: ent "IN MICR
 OAMPS/VOLT",F
30: dsp "IN ORDE
 R TO ECHANGE
 DATA"
31: wait 5000
32: dsp "PRESS
 CONTINUE"
33: stp
34: wtc 2,3;wtc
 2,0;wait 75
35: tfr 2,"data"
 ,4096
36: wtc 2,3
37: dsp "DATA
 HAS BEEN TRANSF
 ERRED"
38: wait 5000
39: ent "IS DATA
  TO BE STORRED
 ?",A$
40: if cap(A$)#"
 YES";gto 51
41: ent "ON WHIC
 H TRACK ?",U
42: ent "ON WHIC
 H FILE ?",E
43: trk U
44: if E#1;ldf
 0,E$
45: ent "RUN
 NUMBER",E$[E]
46: rcf 0,E$
47: rcf E,D,I,W,
 B$,C$,G,C,T,L,
 V,B,F,Y$
48: dsp "DATA
 IS RECORDED"
49: wait 5000
50: prt "RUN
 NUMBER ",E$[E],
 " IS STORRED
 ON TRACK ",U,"
 AND FILE ",E
51: ent "IS THE
 DATA TO BE PLOT
 TED ?",A$
52: if cap(A$)#"
 YES";gto 103
53: flt 6
54: spc
55: prt "BUBBLE
 DIAMETER =",D,
 " MICRONS"
56: spc
57: prt "INITIAL
  TIME OF RELEAS
 E PULSE =",I,"
 MSEC"
58: spc
59: prt "LENGTH
 OF PULSE =",W,
 " MSEC"
60: spc
61: prt "THE
 BUBLE WAS GENER
 ATED AT ",B$
62: spc
63: prt "THE
 CURRENT WAS
 MONITORED AT ",
 C$
64: spc
65: prt "THE
 CENTER-TO-CENTE
 R DIFFERENCE
 =",G," MICRONS"
66: spc
67: prt "THE
 FERRIC ION CONC
 ENTRATION =",C,
 " MOLES/LITER"
68: spc
69: prt "THE
 SOLUTION TEMPER
 ATURE =",T,"
 DEG C"
70: ent "IS THE
 AXIS TO BE PLOT
 TED ?",A$
71: if cap(A$)#"
 YES";gto 88
72: (Y-B)*F+P
73: 4.095*L+Q
74: spc
75: prt "YMAX =
 ",P," MICROAMPS
 "
76: spc
77: prt "XMAX =
 ",Q," SEC"
78: spc
79: scl 0,Q,0,P
80: ent "WHAT
 IS XTIC ?",R
81: ent "WHAT
 IS YTIC ?",S
82: spc
83: prt "XTIC =
 ",R," SEC"
84: prt "YTIC =
 ",S," MICROAMPS
 "
85: axe 0,0,R,S
86: axe 0,P,R,P
87: axe Q,0,Q,S
88: pen
89: ent "DO YOU
 WANT A POINT
 PLOT ?",A$
90: if cap(A$)#"
 YES";sfg 1
91: for J=1 to
 4096
92: J-1→K
93: L*K/1000→X
94: itf(Y$[2*J-
 1,2*J])*V*.0005
 →Z
95: (Z-B)*F+Y
96: if flg1=0;
 gto 100
97: if J=4096;
 plt X,Y,-1
98: if J#4096;
 plt X,Y
99: gto 102
100: plt X,Y,-2
101: pen
102: next J
103: end
*17761
```

Program D.1 Listing

```
0: dim E$[15,8]
1: dim D,I,W,
 B$[10],C$[10],
 G,C,T,L,V,B,F,
 Y$[8208]
2: dim A$[5]
3: buf "data",
 Y$,2
4: ent "WHAT
 TRACK ?",U
5: ent "WHAT
 FILE ?",E
6: trk U
7: ldf 0,E$
8: ldf E,D,I,W,
 B$,C$,G,C,T,L,
 V,B,F,Y$
9: spc
10: prt "RUN
 NUMBER ",E$[E]
11: flt 6
12: spc
13: prt "BUBBLE
 DIAMETER =",D,
 " MICRONS"
14: spc
15: prt "INITIAL
  TIME OF RELEAS
 E PULSE =",I,"
 MSEC"
16: spc
17: prt "LENGTH
 OF PULSE =",W,
 " MSEC"
18: spc
19: prt "THE
 BUBLE WAS GENER
 ATED AT ",B$
20: spc
21: prt "THE
 CURRENT WAS
 MONITORED AT ",
 C$
22: spc
23: prt "THE
 CENTER-TO-CENTE
 R DIFFERENCE
 =",G," MICRONS"
24: spc
25: prt "THE
 FERRIC ION CONC
 ENTRATION =",C,
 " MOLES/LITER"
26: spc
27: prt "THE
 SOLUTION TEMPER
 ATURE =",T,"
 DEG C"
28: ent "IS THE
 AXIS TO BE PLOT
 TED ?",A$
29: if cap(A$)#"
 YES";gto 47
30: itf(Y$[99,
 100])*V*.0005→Z
31: (Z-B)*F+P
32: 1/(L*49/1000
 )↑.5→Q
33: spc
34: prt "YMAX =
 ",P," MICROAMPS
 "
35: spc
36: prt "XMAX =
 ",Q," 1/rSEC"
37: spc
38: scl 0,Q,0,P
39: ent "WHAT
 IS XTIC ?",R
```

Program D.2 Listing

```
0: dsp "THIS
 PROGRAM RECORDS
  AND PLOTS"
1: wait 5000
2: dim E$[15,8]
3: dim D,B$[10],
 C$[10],G,C,T,L,
 V,B,F,Y$[8208]
4: dim A$[5]
5: buf "data",
 Y$,2
6: ent "IS DATA
 TO BE TRANSFERR
 ED ?",A$
7: if cap(A$)="Y
 ES";gto 16
8: ent "WHAT
 TRACK ?",U
9: ent "WHAT
 FILE ?",E
10: trk U
11: ldf 0,E$
12: ldf E,D,B$,
 C$,G,C,T,L,V,B,
 F,Y$
13: spc
14: prt "RUN
 NUMBER ",E$[E]
15: gto 51
16: ent "BUBBLE
 DIAMETER IN
 MICRONS",D
17: ent "COORDIN
 ATS OF BUBBLE
 SEGMENT",B$
18: ent "COORDIN
 ATES OF CURRENT
  SEGMENT",C$
19: ent "SEGMENT
  DIFFERENCE IN
 MICRONS",G
20: ent "Fe CONC
 ENTRATION IN
 MOLES/LITER",C
21: ent "TEMPERA
 TURE IN DEG C",
 T
22: ent "TIME/
 PONT IN MSEC",L
23: ent "MAX
 SCALE VOLTAGE
 IN VOLTS",V
24: ent "BASE
 LINE VOLTAGE
 IN VOLTS",B
25: dsp "VOLTAGE
 -TO-CURRENT
 CONVERSION"
26: wait 5000
27: ent "IN MICR
 OAMPS/VOLT",F
28: dsp "IN ORDE
 R TO ECHANGE
 DATA"
29: wait 5000
30: dsp "PRESS
 CONTINUE"
31: stp
32: wtc 2,3;wtc
 2,0;wait 75
33: tfr 2,"data"
 ,4096
34: wtc 2,3
35: dsp "DATA
 HAS BEEN TRANSF
 ERRED"
36: wait 5000
37: ent "IS DATA
  TO BE STORRED
 ?",A$
38: if cap(A$)#"
 YES";gto 49
39: ent "ON WHIC
 H TRACK ?",U
40: ent "ON WHIC
 H FILE ?",E
41: trk U
42: if E#1;ldf
 0,E$
43: ent "RUN
 NUMBER",E$[E]
44: rcf 0,E$
45: rcf E,D,B$,
 C$,G,C,T,L,V,B,
 F,Y$
46: dsp "DATA
 IS RECORDED"
47: wait 5000
48: prt "RUN
 NUMBER ",E$[E],
 " IS STORRED
 ON TRACK ",U,"
 AND FILE ",E
49: ent "IS THE
 DATA TO BE PLOT
 TED ?",A$
50: if cap(A$)#"
 YES";gto 112
51: flt 6
52: spc
53: prt "BUBBLE
 DIAMETER =",D,
 " MICRONS"
54: spc
55: prt "THE
 BUBLE WAS GENER
 ATED AT ",B$
56: spc
57: prt "THE
 CURRENT WAS
 MONITORED AT ",
 C$
58: spc
59: prt "THE
 CENTER-TO-CENTE
 R DIFFERENCE
 =",G," MICRONS"
60: spc
61: prt "THE
 FERRIC ION CONC
 ENTRATION =",C,
 "*MOLES/LITER"
62: spc
63: prt "THE
 SOLUTION TEMPER
 ATURE =",T,"
 DEG C"
64: 0→H
65: for J=1 to
 4096
66: itf(Y$[2*J-
 1,2*J])*V*.0005
 →Z
67: (Z-B)*F→rJ
68: if J=1;rJ→I;
 rJ→W
69: if J<=10;H+
 rJ→H
70: if rJ>I;rJ→I
71: if rJ<W;rJ→W
72: next J
73: H*.1→H
74: ent "IS THE
 AXIS TO BE PLOT
 TED ?",A$
75: if cap(A$)#"
 YES";gto 98
76: dsp "INITIAL
  VALUE = ",H,
 "MICROAMPS"
77: wait 5000
78: dsp "YMAX =
 ",I,"MICROAMPS"
79: wait 5000
80: enp "YMAX
 IN MICROAMPS",P
81: dsp "YMIN =
 ",W,"MICROAMPS"
82: wait 5000
83: enp "YMIN
 IN MICROAMPS",O
84: 4.095*L→Q
85: spc
86: prt "XMAX =
 ",Q," SEC"
87: spc
88: scl 0,Q,O,P
89: ent "WHAT
 IS XTIC ?",R
90: ent "WHAT
 IS YTIC ?",S
91: spc
92: prt "XTIC =
 ",R," SEC"
93: prt "YTIC =
 ",S," MICROAMPS
 "
94: O→P→Z
95: axe 0,O,R,S
96: axe 0,P,R,Z
97: axe Q,O,Q,S
98: pen
99: ent "DO YOU
 WANT A POINT
 PLOT ?",A$
100: if cap(A$)#
 "YES";gto 1
101: for J=1 to
 4096
102: J-1→K
103: L*K/1000→X
104: rJ→Y
105: if flg1=0;
 gto 109
106: if J=4096;
 plt X,Y,-1
107: if J#4096;
 plt X,Y
108: gto 111
109: plt X,Y,-2
110: pen
111: next J
112: end
*9503
```

```
40: ent "WHAT
 IS YTIC ?",S
41: spc
42: prt "XTIC =
 ",R," 1/rSEC"
43: prt "YTIC =
 ",S," MICROAMPS
 "
44: axe 0,0,R,S
45: axe 0,P,R,P
46: axe Q,0,Q,S
47: pen
48: ent "DO YOU
 WANT A POINT
 PLOT ?",A$
49: if cap(A$)#"
 YES";gto 1
50: for J=50 to
 250
51: J-1→K
52: 1/(L*K/1000)
 ↑.5→X
53: itf(Y$[2*J-
 1,2*J])*V*.0005
 →Z
54: (Z-B)*F→Y
55: if flg1=0;
 gto 59
56: if J=250;
 plt X,Y,-1
57: if J#250;
 plt X,Y
58: gto 61
59: plt X,Y,-2
60: pen
61: next J
62: end
*7928
```

Program D.3 Listing

```
0: dsp "THIS
 PROGRAM RECORDS
  AND PLOTS"
1: wait 5000
2: dim E$[15,8]
3: dim C$[160],
 L,V,B,F,Y$[8208
 ]
4: dim A$[5]
5: buf "data",
 Y$,2
6: ent "IS DATA
 TO BE TRANSFERR
 ED ?",A$
7: if cap(A$)="Y
 ES";gto 16
8: ent "WHAT
 TRACK ?",U
9: ent "WHAT
 FILE ?",E
10: trk U
11: ldf 0,E$
12: ldf E,C$,L,
 V,B,F,Y$
13: spc
14: prt "RUN
 NUMBER ",E$[E]
15: gto 46
16: ent "COMMENT
 S :",C$
17: ent "TIME/
 POINT IN MSEC",
 L
18: ent "MAX
 SCALE VOLTAGE
 IN VOLTS",V
19: ent "BASE
 LINE VOLTAGE
 IN VOLTS",B
20: dsp "VOLTAGE
 -TO-CURRENT
 CONVERSION"
21: wait 5000
22: ent "IN MILL
 IAMPS/VOLT",F
23: dsp "IN ORDE
 R TO ECHANGE
 DATA"
24: wait 5000
25: dsp "PRESS
 CONTINUE"
26: stp
27: wtc 2,3;wtc
 2,0;wait 75
28: tfr 2,"data"
 ,4096
29: wtc 2,3
30: dsp "DATA
 HAS BEEN TRANSF
 ERRED"
31: wait 5000
32: ent "IS DATA
 TO BE STORRED
 ?",A$
33: if cap(A$)#"
 YES";gto 44
34: ent "ON WHIC
 H TRACK ?",U
35: ent "ON WHIC
 H FILE ?",E
36: if E#1;ldf
 0,E$
37: trk U
38: ent "RUN
 NUMBER",E$[E]
39: rcf 0,E$
40: rcf E,C$,L,
 V,B,F,Y$
41: dsp "DATA
 IS RECORDED"
42: wait 5000
43: prt "RUN
 NUMBER ",E$[E],
 " IS STORRED
 ON TRACK ",U,"
 AND FILE ",E
44: ent "IS THE
 DATA TO BE PLOT
 TED ?",A$
45: if cap(A$)#"
 YES";gto 99
46: flt 6
47: spc
48: prt "COMMENT
 S:"
49: spc
50: prt C$
51: 0→H
52: for J=1 to
 4096
53: if(Y$[2*J-
 1,2*J])*V*.0005
 →Z
54: (Z-B)*F→rJ
55: if J=1;rJ→I;
 rJ→W
56: if J<=10;H+
 rJ→H
57: if rJ>I;rJ→I
58: if rJ<W;rJ→W
59: next J
60: H*.1→H
61: ent "IS THE
 AXIS TO BE PLOT
 TED ?",A$
62: if cap(A$)#"
 YES";gto 85
63: dsp "INITIAL
  VALUE = ",H,
 "MILLIAMPS"
64: wait 5000
65: dsp "YMAX =
 ",I,"MILLIAMPS"
66: wait 5000
67: enp "YMAX
 IN MILLIAMPS",P
68: dsp "YMIN =
 ",W,"MILLIAMPS"
69: wait 5000
70: enp "YMIN
 IN MILLIAMPS",O
71: 4.095*L→Q
72: spc
73: prt "XMAX =
 ",Q," SEC"
74: spc
75: scl 0,Q,O,P
76: ent "WHAT
 IS XTIC ?",R
77: ent "WHAT
 IS YTIC ?",S
78: spc
79: prt "XTIC =
 ",R," SEC"
80: prt "YTIC =
 ",S," MILLIAMPS
 "
81: O+P→Z
82: axe 0,O,R,S
83: axe 0,P,R,Z
84: axe Q,O,Q,S
85: pen
86: ent "DO YOU
 WANT A POINT
 PLOT ?",A$
87: if cap(A$)#"
 YES";sfg 1
88: for J=1 to
 4096
89: J-1→K
90: L*K/1000→X
91: rJ→Y
92: if flg1=0;
 gto 96
93: if J=4096;
 plt X,Y,-1
94: if J#4096;
 plt X,Y
95: gto 98
96: plt X,Y,-2
97: pen
98: next J
99: end
*13374
```

Program D.4 Listing

```
0: dsp "4094
 OSCILLOSCOPE
 PROGRAM"
1: wait 2000
2: dsp "RECORDS
 AND PLOTS DATA"
3: wait 2000
4: cfg 1,2
5: dim B$[485],
 V[32],H$[32,
 55],C$[80],D$[3
 1760]
6: dim R$[6]
7: dim Q$[5]
8: buf "data",
 D$,3
9: ent "IS DATA
 TO BE TRANSFERR
 ED ?",Q$
10: if cap(Q$)="
 YES";gto 16
11: ent "WHAT
 IS THE FILE
 NAME?",R$
12: asgn R$,1
13: sread 1;B$,
 V[*],H$,C$,D$
14: prt "RUN
 NUMBER ",R$
15: gto 70
16: dsp "IN ORDE
 R TO ECHANGE
 DATA"
17: wait 2000
18: dsp "PRESS
 CONTINUE"
19: stp
20: fxd 0
21: wrt 727,"W"
22: red 727,E
23: if E#0;dsp
 "ERROR # ",E,"
 IN W";stp
24: red 727,B$
25: val(B$[1,
 2])→A
26: val(B$[3+A*
 15,4+A*15])→E
27: if E#0;dsp
 "ERROR # ",E,"
 IN W OUTPUT";
 stp
28: wrt 727,"D,
 4,0,0,15872,1"
29: red 727,E
30: if E#0;dsp
 "ERROR # ",E,"
 IN D";stp
31: tfr 727,"dat
 a",31744
32: red 727,E
33: if E#0;dsp
 " ERROR # ",E,
 " IN D OUTPUT";
 stp
34: for I=1 to A
35: wrt 727,"N,
 ",B$[(I-1)*15+
 11,(I-1)*15+12]
36: red 727,E
37: if E#0;dsp
 "ERROR # ",E,"
 IN N";stp
38: red 727,H$[I
 ]
39: val(H$[I,53,
 54])→E
40: if E#0;dsp
 "ERROR # ",E,"
 IN N OUTPUT";
 stp
```

Program D.5 Listing

```
41: next I
42: dsp "DATA
 HAS BEEN TRANSF
 ERRED"
43: wait 2000
44: ent "IS DATA
 TO BE STORRED
 ?",Q$
45: if cap(Q$)#"
 YES";sfg 2;gto
 51
46: ent "WHAT
 IS 6 CHARACTER
 FILE NAME?",R$
47: if len(R$)=6
 ;jmp 4
48: dsp "FILE
 NAME IMPROPER
 LENGTH";wait
 2000
49: dsp "PRESS
 CONTINUE TO
 RESET";stp
50: jmp -4
51: for I=1 to A
52: dsp "WAVEFOR
 M # ",I
53: wait 2000
54: dsp "CURRENT
 -TO-VOLTAGE
 CONVERSION"
55: wait 2000
56: ent "IN mA/
 VOLT FOR WAVEFO
 RM",V[I]
57: next I
58: if fl#2=1;
 gto 75
59: ent "COMMENT
 S :",C$
60: ent "DO YOU
 WANT TO CHECK
 DISK SPACE",Q$
61: if cap(Q$)="
 YES";cat 0
62: dsp "PRESS
 CONTINUE TO
 STORE";stp
63: open R$,150
64: asgn R$,1
65: sprt 1,B$,
 V[*],H$,C$,D$,
 "end"
66: dsp "DATA
 IS RECORDED"
67: wait 2000
68: ent "IS THE
 DATA TO BE PLOT
 TED ?",Q$
69: if cap(Q$)#"
 YES";gto 132
70: spc
71: val(B$[1,
 2])→A
72: prt "COMMENT
 S:"
73: spc
74: prt C$
75: dsp "THERE
 IS(ARE) ",A,"
 WAVEFORMS"
76: wait 2000
77: flt 5
78: if A=1;1→M;
 jmp 3
79: ent "WHICH
 ONE IS TO BE
 PLOTTED",M
80: if M>A;dsp
 "NOT A VALID
 #";wait 2000;
 jmp -1
81: val(H$[M,5,
 9])*10↑val(H$[M
 ,11,13])→r1
82: val(H$[M,14,
 18])*10↑val(H$[
 M,20,22])→r2
83: val(H$[M,23,
 28])→r3
84: val(H$[M,29,
 34])→r4
85: val(H$[M,35,
 40])→r5
86: val(B$[5+15*
 (M-1),10+15*(M-
 1)])→r6
87: val(B$[13+
 15*(M-1),14+15*
 (M-1)])→r7
88: ent "DO YOU
 WANT T=0 AT
 TRIGGER TIME",
 Q$
89: if cap(Q$)="
 YES";r4*65536+
 r5→T;jmp 2
90: 0→T
91: ent "IS THE
 AXIS TO BE PLOT
 TED ?",Q$
92: if cap(Q$)#"
 YES";gto 116
93: dsp "YMAX=",
 (32000-r3)*r1*
 V[M],"VOLTS(OR
 mA)"
94: wait 5000
95: enp "YMAX
 IN VOLTS(OR
 MILLIAMPS)",P
96: dsp "YMIN=",
 (-32000-r3)*r1*
 V[M],"VOLTS(OR
 mA)"
97: wait 5000
98: enp "YMIN
 IN VOLTS(OR
 MILLIAMPS)",O
99: (r6-1-T)*
 r2→Q
100: -T*r2→U
101: spc
102: prt "XMAX
 = ",Q," SEC"
103: spc
104: prt "XMIN
 = ",U," SEC"
105: spc
106: scl U,Q,O,P
107: ent "WHAT
 IS XTIC ?",R
108: ent "WHAT
 IS YTIC ?",S
109: spc
110: prt "XTIC
 = ",R," SEC"
111: prt "YTIC
 = ",S," VOLTS(O
 R MILLIAMPS)"
112: O+P→Z
113: axe U,O,R,S
114: axe U,P,R,Z
115: axe Q,O,Q,S
116: pen
117: ent "DO
 YOU WANT A POIN
 T PLOT ?",Q$
118: if cap(Q$)#
 "YES";sfg 1
119: for J=M to
 15872-A+M by r7
120: (J-M)/r7→K
121: (K-T)*r2→X
122: (itf(D$[2*
 J-1,2*J])-r3)*
 r1*V[M]→Y
123: if fl#1=0;
 gto 127
124: if J=15872-
 A+M;plt X,Y,-1
125: if J#15872-
 A+M;plt X,Y
126: gto 129
127: plt X,Y,-2
128: pen
129: next J
130: ent "DO
 YOU WANT TO
 PLOT ANOTHER
 CURVE",Q$
131: if cap(Q$)=
 "YES";gto 79
132: end
*23502
```

```
0: dsp "PLOT
 LABLE PROGRAM";
 wait 1000
1: dim S[6],H[2]
 ,A$[30],B$[35],
 C$[45],D$[3,
 55],G[2]
2: ent "x-min?",
 S[1];stp
3: ent "x-max?",
 S[2];stp
4: ent "y-min?",
 S[3];stp
5: ent "y-max?",
 S[4];stp
6: ent "x-tic?",
 S[5];stp
7: ent "y-tic?",
 S[6];stp
8: ent "# of
 digits dsp afte
 r x-decimal?",
 G[1];stp
9: ent "# of
 digits dsp afte
 r y-decimal?",
 G[2];stp
10: ent "title?"
 ,A$;stp
11: ent "x-capti
 on?",B$;stp
12: ent "y-capti
 on?",C$;stp
13: ent "line 1
 caption?",D$[1]
 ;stp
14: ent "line 2
 caption?",D$[2]
 ;stp
15: ent "line 3
 caption?",D$[3]
 ;stp
16: fxd G[1]
17: S[2]-(7/5)(S
 [2]-S[1])+.2(S[
 2]-S[1])→A
18: S[2]+.2(S[2]
 -S[1])→B
19: S[4]-(8.5/
 7)(S[4]-S[3])-
 .05(S[4]-S[3])→
 C
20: S[4]+(1/7)(S
 [4]-S[3])-.05(S
 [4]-S[3])→D
21: scl A,B,C,D
22: pen
23: plt S[1],
 S[3],-2
24: (1/16/4.5)(S
 [2]-S[1])→H[1]
25: (1/16/7)(S[4
 ]-S[3])→H[2]
26: int((S[2]-
 S[1])/S[5])→M
27: int((S[4]-
 S[3])/S[6])→N
28: for I=1 to M
29: iplt S[5],0,
 0
30: iplt 0,H[2],
 0
31: iplt 0,-H[2]
 ,0
32: next I
33: plt S[2],
 S[3],0
34: for I=1 to N
```

Program D.6

Listing

```
35: iplt 0,S[6],
 0
36: iplt -H[1],
 0,0
37: iplt H[1],0,
 0
38: next I
39: plt S[2],
 S[4],-1
40: plt S[1],
 S[3],-2
41: for I=1 to N
42: iplt 0,S[6],
 0
43: iplt H[1],0,
 0
44: iplt -H[1],
 0,0
45: next I
46: plt S[1],
 S[4],0
47: for I=1 to M
48: iplt S[5],0,
 0
49: iplt 0,-H[2]
 ,0
50: iplt 0,H[2],
 0
51: next I
52: plt S[2],
 S[4],-1
53: csiz 1.5,2,
 1.357,0
54: for I=0 to M
55: S[1]+I*S[5]+
 U
56: -(len(str(U)
 )/2+.3)+V
57: plt U,S[3],0
58: cplt V,-1.25
59: lbl U
60: next I
61: fxd G[2]
62: for I=0 to N
63: S[3]+I*S[6]+
 U
64: -(len(str(U)
 )+1)+V
65: plt S[1],U,0
66: cplt V,-.3
67: lbl U
68: next I
69: csiz 1.5,2,
 1.357,0
70: for I=1 to 3
71: 3-I→J
72: plt A,C,0
73: cplt 0,J
74: lbl D$[I]
75: next I
76: csiz 1.75,2,
 1.357,0
77: -(len(B$)/2+
 .3)+V
78: (S[2]-S[1])/
 2+S[1]→U
79: plt U,S[3],0
80: cplt V,-3
81: lbl B$
82: dev
83: csiz 1.75,2,
 1.357,90
84: -(len(C$)/2+
 .3)+V
85: (S[4]-S[3])/
 2+S[3]→U
86: plt A,U,0
87: cplt V,-1
88: lbl C$
89: csiz 2,2,
 1.357,0
90: -(len(A$)/2+
 .3)+V
91: (S[2]-S[1])/
 2+S[1]→U
92: plt U,D,0
93: cplt V,-1
94: lbl A$
95: stp fend
*23036
```

```
0: dim O$[5]
1: ent "DO YOU
 WANT TO SET
 PERIMETER",O$
2: if cpr(O$)#"Y
 ES";stp 1
3: scl -25,25,-
 25,25
4: pen
5: for I=-5 to 5
6: plt I,-5,-2
7: plt I,5,-1
8: next I
9: for I=-5 to 5
10: plt -5,I,-2
11: plt 5,I,-1
12: next I
13: for J=1 to 4
14: for I=0 to
 4 by 2
15: if J=1;0+Y;-
 11+I→X
16: if J=2;-1+Y;
 6+I→X
17: if J=3;0+X;
 6+I→Y
18: if J=4;-1+X;
 -11+I→Y
19: plt X,Y,-2
20: plt X+1,Y,0
21: plt X+1,Y+1,
 0
22: plt X,Y+1,0
23: plt X,Y,-1
24: next I
25: next J
26: if flg1=1;
 jmp 6
27: plt -25,-25,
 -2
28: plt -25,25,0
29: plt 25,25,0
30: plt 25,-25,0
31: plt -25,-25,
 -1
32: ent "X-COORD
 INATE OF BUBBLE
 ",U
33: ent "Y-COORD
 INATE OF BUBBLE
 ",V
34: ent "RADIUS
 OF BUBBLE",R
35: plt U,V,-2
36: pen
37: U+R→A
38: U-R→B
39: 2+R/100→D
40: plt A,V,-2
41: for J=1 to 2
42: for I=0 to
 100
43: if J=1;A-I*
 D→X
44: if J=2;B+I*
 D→X
45: V+(-1)↑J*
 √(R↑2-(X-U)↑2)→
 Y
46: plt X,Y,0
47: next I
48: next J
49: pen
50: ent "X COORD
 INATE OF MONITO
 R SEGMENT",X
51: ent "Y COORD
 INATE OF MONITO
 R SEGMENT",Y
52: plt X,Y,0
53: csiz 2,1,1,0
54: cplt -.3,-.3
55: lbl "*"
56: end
*9055
```

Program D.7 Listing

APPENDIX E

Notes on the Data Acquisition and Control System for the Micro-Mosaic Electrode Cell

The system developed was designed specifically for the experiments described in the main body of this dissertation. However, it was meant to be reasonably flexible for other experiments planned for the future. As in the early experiments a numbering and coding scheme had to be developed for the system. The numbering system used for the micro-mosaic electrode segments and the printed circuit board connections were adapted from the early experiments, described in Appendix C. The numbering scheme for the color-coded multi-conductor cables, which connect the micro-mosaic electrode cell to the junction box, is given in Table E.1.

The set of ten terminal strips with twelve screw connectors on each in the junction box, form a 12 x 10 matrix of connections. A matrix numbering system was adopted for the system with connection [1,1] in the upper left hand corner of the box. The upper left hand corner is established by placing the box in front of you with the input and output cables coming out of the side facing you. The screw connections allow for relatively easy changes in the scheme for attaching the wires from the cell. Because of the large number of connections to be made, a standard scheme was set and is given in Table E.1.

The 120 channels of the current follower are numbered consecutively. The current input connections are made with a 120 pin Elco (8016 series) connector, which uses a lettering system to designate

Table E.1 Color Code And Numbering Scheme For Data Acquisition And Control System(Stripe Colors In Parentheses).

Current Follower Channel Number & Letter	Multiplexer Channel Number	Junction Box Output Cable Number and Wire Color	Junction Box Connector Number	Junction Box Input Cable Number and Wire Color	Electrode Number and Connector Number
1-A	5	I-Green(White,Black)	(12,2)	Blank	
2-B	6	I-Orange(Black,Green)	(12,3)	Blank	
3-C	7	II-Black(White)	(12,4)	Blank	
4-D	8	II-Orange	(12,5)	Blank	
5-E	9	I-Black	(1,1)	III-White(Red,Green)	(10,9)-35
6-F	10	I-Red	(2,1)	III-Green(Black,Brown)	(9,8)-34
7-H	11	I-Green	(3,1)	III-Red(Black,Green)	(10,8)-33
8-J	12	I-White	(4,1)	III-Red(Black)	(8,7)-32
9-K	13	I-White(Black)	(5,1)	III-Blue(Brown,White)	(9,7)-31
10-L	14	I-Orange	(6,1)	III-Green(Black,White)	(10,7)-30
11-M	15	I-Red(White)	(7,1)	III-Red(Black,White)	(7,6)-29
12-N	16	I-Orange(Black)	(8,1)	III-Orange(Red)	(8,6)-28
13-P	17	I-Green(Black)	(9,1)	III-Blue(Red)	(9,6)-27
14-R	18	I-Red(Black)	(10,1)	III-Orange(Black)	(10,6)-26
15-S	19	I-Black(White)	(11,1)	III-Black(Red,Green)	(6,5)-25
16-T	20	I-Green(White)	(12,1)	III-Blue(White,Black)	(7,5)-24
17-U	21	I-Black(Red,White)	(1,2)	III-Green(Black)	(10,5)-23
18-V	22	I-White(Red,Yellow)	(2,2)	III-Blue(Black)	(A,5)-22
19-W	23	I-Black(Brown,White)	(3,2)	III-White	(B,5)-21
20-X	24	I-Orange(Blue,White)	(4,2)	III-Blue	(9,5)-20
21-Y	25	I-White(Red,Blue)	(5,2)	III-White(Red)	(8,5)-19
22-Z	26	I-Orange(Green)	(6,2)	III-Black(Red)	(C,5)-15
23-AA	27	I-White(Red)	(7,2)	III-Red	(10,4)-14
24-AB	28	I-Orange(Red)	(8,2)	III-Green	(9,4)-13
25-AC	29	I-Red(Green)	(9,2)	III-Red(White)	(8,4)-12
26-AD	30	I-White(Black,Red)	(10,2)	III-Black	(7,4)-11
27-AE	31	I-Red(Black,White)	(11,2)	III-Orange	(10,3)-10
28-AF	32	II-Black(Red,Green)	(1,3)	III-White(Black,Red)	(9,3)-9
29-AH	33	II-White(Red,Green)	(2,3)	III-Black(White,Red)	(8,3)-8
30-AJ	34	II-Orange(Black,Green)	(3,3)	III-Orange(Black,White)	(10,2)-7

(continued on next page)

(Table E.1 Continued)

Current Follower Channel Number & Letter	Multiplexer Channel Number	Junction Box Output Cable Number and Wire Color	Junction Box Connector Number	Junction Box Input Cable Number and Wire Color	Electrode Number and Connector Number
31-AK	35	II-Green(Brown,Black)	(4,3)	III-Green(White)	(9,2)-6
32-AL	36	II-Red(Green,Black)	(5,3)	III-White(Blue,Red)	(10,1)-5
33-AM	37	II-Black(White,Brown)	(6,3)	II-Green(Browwn,Black)	(2,10)-35
34-AN	38	I-Black(Red,Green)	(7,3)	II-Red(Black,Green)	(3,9)-34
35-AP	39	I-Orange(Black,White)	(8,3)	II-White(Red,Green)	(3,10)-33
36-AR	40	I-Red(Green,Black)	(9,3)	II-White(Red,Yellow)	(4,8)-32
37-AS	41	I-White(Red,Green)	(10,3)	II-Orange(Blue,White)	(4,9)-31
38-AT	42	I-Green(Brown,Black)	(11,3)	II-Red(White)	(4,10)-30
39-AU	43	II-White(Red,Black)	(1,4)	II-Orange(Black)	(5,7)-29
40-AV	44	II-Black(Red,White)	(2,4)	II-Blue(Black)	(5,8)-28
41-AW	45	II-Orange(Black,White)	(3,4)	II-Black(White,Brown)	(5,9)-27
42-AX	46	II-White(Red,Yellow)	(4,4)	II-Black(White)	(5,10)-26
43-AY	47	II-Green(White,Black)	(5,4)	II-Green	(6,6)-25
44-AZ	48	II-Red(White,Black)	(6,4)	II-Black(Red)	(6,7)-24
45-BA	49	II-Red(White)	(7,4)	II-Black(Red,Green)	(6,10)-23
46-BB	50	II-Red(Green)	(8,4)	II-Blue(White,Black)	(6,A)-22
47-BC	51	II-Orange(Blue,White)	(9,4)	II-Black	(6,B)-21
48-BD	52	II-White(Red,Blue)	(10,4)	II-Red	(6,9)-20
49-BE	53	II-Orange(Green)	(11,4)	II-White	(6,8)-19
50-BF	54	II-White(Red)	(1,5)	II-Blue	(6,C)-15
51-BH	55	II-Orange(Black)	(2,5)	II-Orange(Black,White)	(7,10)-14
52-BJ	56	II-Red(Black)	(3,5)	II-Blue(Red)	(7,9)-13
53-BK	57	II-Green(Black)	(4,5)	II-Red(Black)	(7,8)-12
54-BL	58	II-Black(Red)	(5,5)	II-Orange(Black,Green)	(7,7)-11
55-BM	59	II-Orange(Red)	(6,5)	II-Red(Green)	(8,10)-10
56-BN	60	II-Green(White)	(7,5)	II-White(Red)	(8,9)-9
57-BP	61	II-White	(8,5)	II-Orange(Green)	(8,8)-8
58-BR	62	II-Green	(9,5)	II-White(Black,Red)	(9,10)-7
59-BS	63	II-Red	(10,5)	II-Orange(Red)	(9,9)-6
60-BT	64	II-White(Black)	(11,5)	II-Green(Black)	(10,10)-5

(continued on next page)

(Table E.1 Continued)

Current Follower Channel Number & Letter	Multiplexer Channel Number	Junction Box Output Cable Number and Wire Color	Junction Box Connector Number	Junction Box Input Cable Number and Wire Color	Electrode Number and Connector Number
61-BU	69	III-Orange	(12,6)	Blank	
62-BV	70	III-Black(White,Brown)	(12,7)	Blank	
63-BW	71	III-White(Blue,Red)	(12,8)	Blank	
64-BX	72	IV-Orange	(12,9)	Blank	
65-BY	73	III-Green(Black)	(1,6)	IV-Red(Green)	(9,1)-35
66-BZ	74	III-Orange(Black)	(2,6)	IV-White(Blue,Red)	(8,2)-34
67-CA	75	III-Red(Black)	(3,6)	IV-Orange(Blue,White)	(8,1)-33
68-CB	76	III-Green(White)	(4,6)	IV-Orange(Green)	(7,3)-32
69-CC	77	III-White(Red)	(5,6)	IV-White(Red,Yellow)	(7,2)-31
70-CD	78	III-Orange(Red)	(6,6)	IV-Black(White,Brown)	(7,1)-30
71-CE	79	III-White(Black)	(7,6)	IV-Red(Black)	(6,4)-29
72-CF	80	III-White	(8,6)	IV-Black(Red,White)	(6,3)-28
73-CH	81	III-Black	(9,6)	IV-Blue(Red)	(6,2)-27
74-CJ	82	III-Green	(10,6)	IV-Orange	(6,1)-26
75-CK	83	III-Red	(11,6)	IV-Orange(Red)	(5,5)-25
76-CL	84	III-Orange(White,Black)	(1,7)	IV-Black(Red)	(5,4)-24
77-CM	85	III-Black(Red,Green)	(2,7)	IV-Green(White)	(5,1)-23
78-CN	86	III-White(Red,Yellow)	(3,7)	IV-Green(Black)	(5,A)-22
79-CP	87	III-Green(White,Black)	(4,7)	IV-Orange(Black)	(5,B)-21
80-CR	88	III-Red(Black,White)	(5,7)	IV-White(Red)	(5,2)-20
81-CS	89	III-Orange(Black,Green)	(6,7)	IV-Green	(5,3)-19
82-CT	90	III-Green(Brown,Black)	(7,7)	IV-White(Black)	(5,C)-15
83-CU	91	III-Red(Black,Green)	(8,7)	IV-Blue	(4,1)-14
84-CV	92	III-Red(White)	(9,7)	IV-Red(White)	(4,2)-13
85-CW	93	III-White(Red,Green)	(10,7)	IV-Blue(Black)	(4,3)-12
86-CX	94	III-Black(White)	(11,7)	IV-Red(White,Black)	(4,4)-11
87-CY	95	IV-Green(Black,White)	(1,8)	IV-White(Black,Red)	(3,1)-10
88-CZ	96	IV-Black(Red,White)	(2,8)	IV-Green(Black,White)	(3,2)-9
89-DA	97	IV-Red(Black,White)	(3,8)	IV-Black(White)	(3,3)-8
90-DB	98	IV-Black(Red,Green)	(4,8)	IV-Orange(Black,Green)	(2,1)-7

(continued on next page)

(Table E.1 Continued)

Current Follower Channel Number & Letter	Multiplexer Channel Number	Junction Box Output Cable Number and Wire Color	Junction Box Connector Number	Junction Box Input Cable Number and Wire Color	Electrode Number and Connector Number
91-DC	99	IV-Orange(Black,White)	(5,8)	IV-Blue(White,Black)	(2,2)-6
92-DD	100	IV-White(Red,Black)	(6,8)	IV-Green(Black,Brown)	(1,1)-5
93-DE	101	III-Red(Green)	(7,8)	I-Green(Black,Brown)	(1,2)-35
94-DF	102	III-Orange(Blue,White)	(8,8)	I-Red(Black,Green)	(2,3)-34
95-DH	103	III-Orange(Green)	(9,8)	I-White(Red,Green)	(1,3)-33
96-DJ	104	III-White(Black,Red)	(10,8)	I-White(Red,Yellow)	(3,4)-32
97-DK	105	III-Black(Red,White)	(11,8)	I-Orange(Blue,White)	(2,4)-31
98-DL	106	IV-Red(Black)	(1,9)	I-Red(White)	(1,4)-30
99-DM	107	IV-Green(White)	(2,9)	I-Orange(Black)	(4,5)-29
100-DN	108	IV-White(Red)	(3,9)	I-Blue(Black)	(3,5)-28
101-DP	109	IV-Black(Red)	(4,9)	I-Black(White,Brown)	(2,5)-27
102-DR	110	IV-Orange(Red)	(5,9)	I-Black(White)	(1,5)-26
103-DS	111	IV-Red(White)	(6,9)	I-Green	(5,6)-25
104-DT	112	IV-Red	(7,9)	I-Black(Red)	(4,6)-24
105-DU	113	IV-White(Black)	(8,9)	I-Black(Red,Green)	(1,6)-23
106-DV	114	IV-White	(9,9)	I-Blue(White,Black)	(A,6)-22
107-DW	115	IV-Black	(10,9)	I-Black	(B,6)-21
108-DX	116	IV-Green	(11,9)	I-Red	(2,6)-20
109-DY	117	IV-Orange(Green)	(1,10)	I-White	(3,6)-19
110-DZ	118	IV-Orange(Blue,White)	(2,10)	I-Blue	(C,6)-15
111-EA	119	IV-Red(Green)	(3,10)	I-Orange(Black,White)	(1,7)-14
112-EB	120	IV-Orange(Black,Green)	(4,10)	I-Blue(Red)	(2,7)-13
113-EC	121	IV-White(Red,Yellow)	(5,10)	I-Red(Black)	(3,7)-12
114-ED	122	IV-White(Blue,Red)	(6,10)	I-Orange(Black,Green)	(4,7)-11
115-EE	123	IV-White(Red,Green)	(7,10)	I-Red(Green)	(1,8)-10
116-EF	124	IV-Green(Brown,Black)	(8,10)	I-White(Red)	(2,8)-9
117-EH	125	IV-Black(White,Brown)	(9,10)	I-Orange(Green)	(3,8)-8
118-EJ	126	IV-Green(Black)	(10,10)	I-White(Black,Red)	(1,9)-7
119-EK	127	IV-Red(Black,Green)	(11,10)	I-Orange(Red)	(2,9)-6
120-EL	128	IV-Orange(Black)	(12,10)	I-Green(Black)	(1,10)-5

each individual connection. The color coding from the wires connecting the junction box to the current follower is given in Table E.1. The corresponding connections of the voltage outputs to the multiplexer channels are also listed in the same.

The multiplexer system is set to monitor all the segments sequentially. At its fastest rate, the system takes a reading from each segment at about 75 times per second. Because of the 10 Hz filters on the inputs to the multiplexer, the maximum number of readings that can be taken without introducing errors is 100 times per second. If data is needed to be obtained at a faster rate for more than four segments during each experiment, the 16 channel input card without the filters can be used. This would also require a change in the arrangement of the wires from the current follower to the multiplexer. This change would not be simple, but could be done in a few hours. Slower data acquisition rates present no problem and are only limited by the storage space on the flexible disk.

The junction box and all cables are completely shielded, to reduce the noise in the system. The digital oscilloscope results can be used to examine the quality of the signal from the current follower. This data can be compared to the same results from the multiplexer, as in Fig. E.1. Generally the signal-to-noise ratio from the current follower is as good or better than in the early experiments. Also, the 10 Hz filters on the multiplexer inputs vertually eliminates all 60 Hz and higher frequency noise.

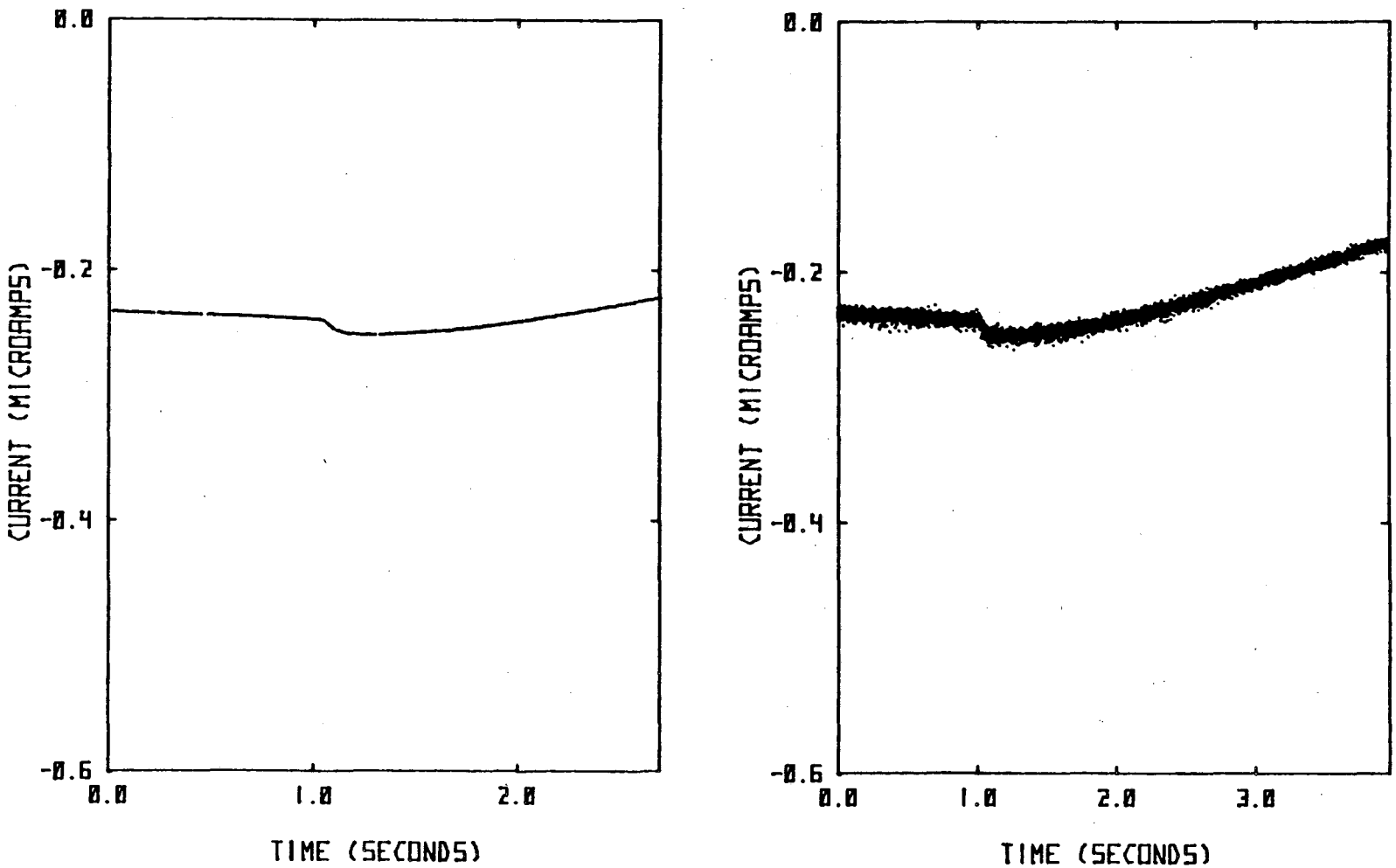

XBL 836-10363

Figure E.1 Experimental result monitored by two devices; (A) Multiplerer; (B) Digital oscilloscope.

APPENDIX F

Data Acquisition and Control System Operating Program

The program for the system is written in a Hewlett Packard Language (HPL). It is stored in a magnetic tape cartridge titled, "Data Acquisition and Control Tape." More specifically the program is stored in 18 separate files on track zero of the tape. A data file and three function key files are stored on track one of the tape. The tape cartridge must be left in the computer at all times while running the program. This is necessary since it is not possible to store all the program in the computer at once. A description and listing of each program file follows:

File Ø (Program F.1): This portion of the program serves as a starting point for the entire program. The computer will automatically run this program file after a power outage. The program will initialize a flexible disk if needed. This is not the bootstrap routine for a new disk, but it sets up a file for transferring information between program files. This should only be done once for each disk. At the end of the program file, a branch is set up. If data is to be output, Program F.7 is loaded and run. Otherwise, it is assumed that an experiment is to be conducted and Program F.2 is loaded and run. In this program and all other program files, "Yes or No" questions can be answered from the keyboard by pressing a special function key for yes (f6) or no (f7).

File 1 (Program F.2): This portion of the program prompts the user for parameters and decisions needed for conducting an experiment. Default values for the parameters can be used, or can be input from the keyboard. A list of the parameters and their default values is given in Table F.1. The program automatically allots storage space on the flexible disk for the parameters used and data to be obtained. Which program files are to be loaded and run depend on the user's answers to three questions.

1) Is the data acquisition to be ended when the computer memory buffer is loaded?
2) Is the bubble growth to be computer controlled?
3) Is data to be taken with the digital oscilloscope?

Exactly how the answers to these questions affect the flow of the program is depicted in the chart in Fig. F.1.

Fig. 2 (Program F.3): This is the portion of the program that actually controls and retrieves data from the multiplexer. It also controls the growth of bubbles. The total memory of the computer is split up into four buffers. Two of the buffers are the same size. The size of these buffers is set such that it will require a quarter of a second for the multiplexer to fill. One buffer size is set at the maximum and the other is set to take up the remaining space in the memory. Once computer control of bubble growth has begun, the multiplexer can be started by pressing a special function key (fØ). After starting of the multiplexer, data is stored consequentially in each of the two equal size buffers. While data is being stored in the

Table F.1 Input Parameters For Program F.2

Parameter Requested	Parameter Units	Default Value
Multiplexer Throughput Rate	kHz	None
Multiplexer Maximum Voltage	volts	0.64
Number Of Multiplexer Channels	None	128
Total Data Acquisition Time	Seconds	None
Initial Digital Function Generator Voltage Difference	mV	-300
Maximum Digital Function Generator Voltage Difference	mV	-500
Potentiostat Bubble Current Setting	microamps	-15
Potentiostat Current-To-Voltage Conversion	microamps/volt	50

(Continued on next page)

(Table F.1 Continued)

Parameter Requested	Parameter Units	Default Value
Proportional Control Number	None	-20
Derivative Control Number	seconds	0.01
Integral Control Number	1/seconds	3
Timing Channel Triangular Wave Frequency	Hz	0.5
Timing Channel Peak-To-Peak Voltage	volts	1.0
Current-To-Voltage Conversion For Each Multiplexer Channel	microamps/volt	Dependent On Channel Assignment
Number Of Bubbles Generated	None	None
Segment Numbers At Which Bubbles Were Generated	None	None
Ferric Ion Concentration	moles/liter	None
Comments(Maximum 80 Characters)	None	None
Run Number (6 Characters)	None	None

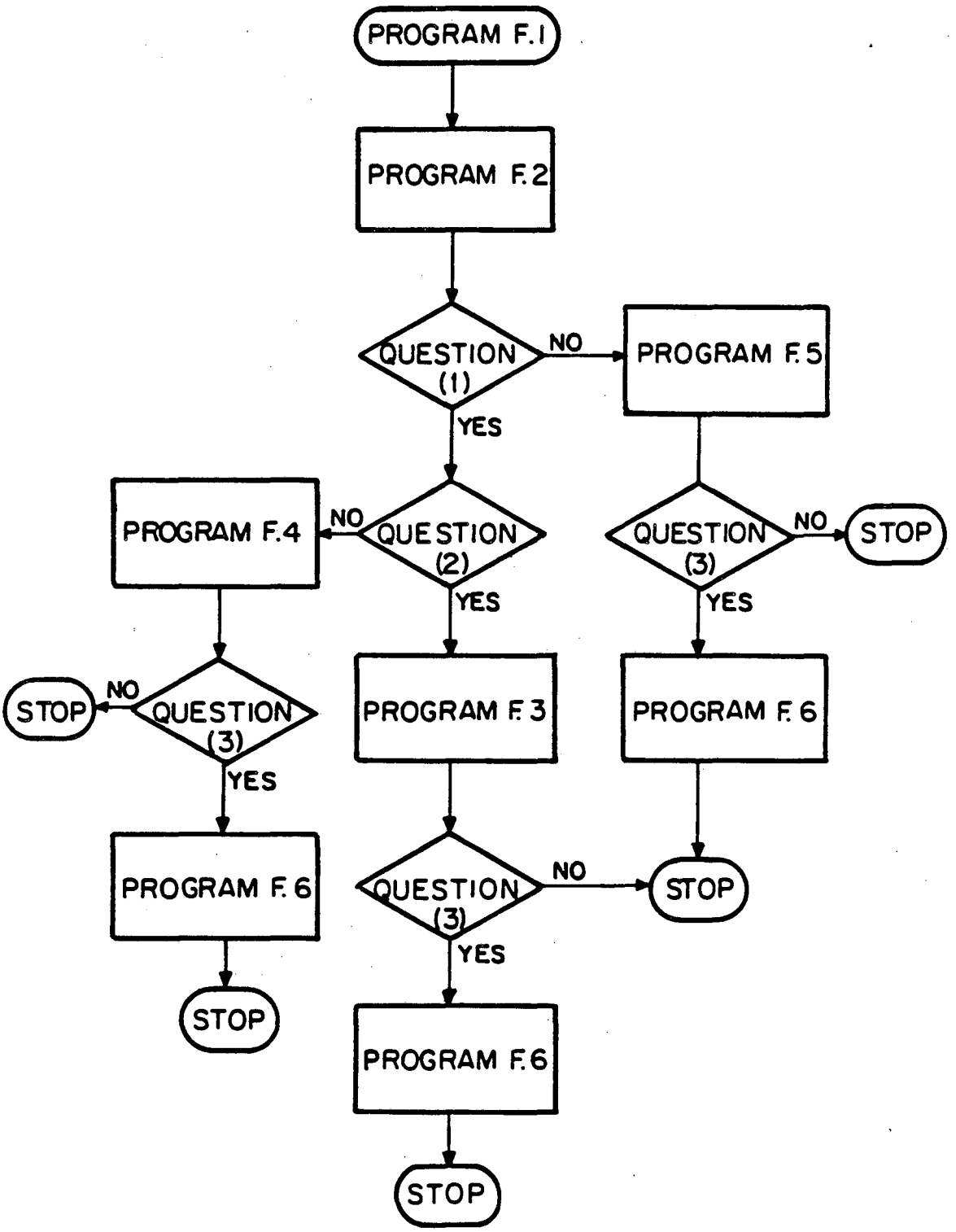

XBL 836-5935

Figure F.1 Input program flow chart.

first buffer, a reading is taken by the computer from the digital voltmeter. If the voltage reading is more than 5 away from the set value and the data acquisition is to be internally triggered, then a flag is set. During the storage of data in the second buffer, the voltmeter reading is used to estimate the proper applied voltage for the digital function generator. The function generator is then instructed to be set at the estimated voltage. Between filling the memory buffers a flag is checked to determine if the buffers should be saved. The flag can be set internally, as described, or from the keyboard by pressing a special function key (f1). If the flag is set the computer is directed to set the function generator voltage to zero and to fill the other two larger buffers. Otherwise, the two smaller buffers are cleared and the cycle begins again. After all the buffers are filled, they are stored on a flexible disk.

File 3 (Program F.4): This portion of the program is similar to Program F.3, except that it does not control bubble growth. Therefore the data acquisition system must be triggered from the keyboard by pressing a special function key (fØ). All other aspects of the program file are basically the same.

File 4 (Program F.5): This portion of the program controls and retrieves data from the multiplexer. It is used when the computer memory is to be loaded more than once. Control of the growth of bubbles is an option on this program file. It is similar to Program F.3, but there are some significant differences. The computer memory is split up into two equal size buffers. One buffer is loaded continuously

until the system is triggered. If the bubble growth is to be controlled, the control takes place on one half second cycles during the loading of the buffer. Once triggered the buffers are loaded and stored on a flexible disk consecutively for a specified amount of time.

File 5 (Program F.6): This part of the program simply loads the data on the digital oscilloscope into the computer and stores it on a flexible disk. This program file is loaded and run automatically when the user indicates that data is to be taken with the oscilloscope.

File 6 (Program F.7): This portion of the program prompts the user to find out which information and in what form the data is to be output. The user can choose between a plot of the results from a single multiplexer channel or a plot of all the electrode segments at a given time. A plot of any channel of the digital oscilloscope data can also be obtained. Which program files are loaded and run depend on the type of plot requested. A flow chart of what files are loaded and run for the various options is given in Fig. F.2.

File 7 (Program F.8): This portion of the program retrieves the information needed to make a plot of one of the multiplexer channel against time or number. The information needed for the plot consists of the digital data from the multiplexer and the conversion parameters. The conversion parameters are needed to change the digital data into the desired form.

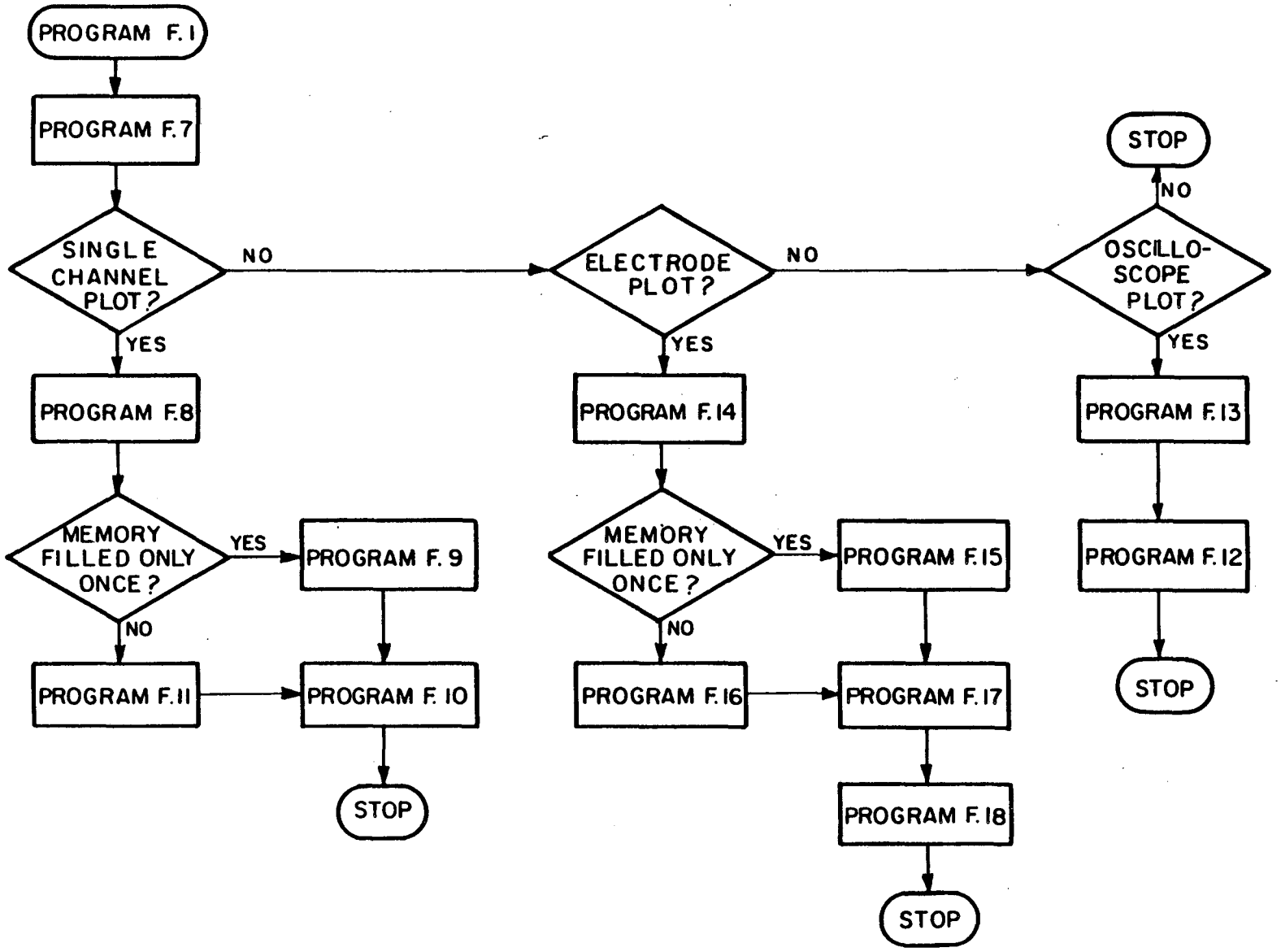

Figure F.2 Output program flow chart.

File 8 (Program F.9): This portion of the program reduces the data into a form suitable for plotting. If the multiplexer measurements are to be plotted against the number of the data point, it is just a matter of changing the digital multiplexer data into its decimal equivalent. However, if a relative time plot is requested, the timing channel data from the multiplexer must be converted to a relative time for the plot. This is done by two different methods in order to check the accuracy of the system.

File 9 (Program F.10): This portion of the program generates and labels the axes for a plot of a single multiplexer channel. It also plots the data points obtained during the experiment from the multiplexer channel.

File 10 (Program F.11): This portion of the program is similar to Program F.9. It performs the same task, except that it is used to reduce data obtained by loading the memory buffers more than once.

File 11 (Program F.12): This portion of the program retrieves the oscilloscope data from the flexible disk and plots the results of one channel. It generates and labels the axes as well as plotting the data.

File 12 (Program F.13): This portion of the program sets the file pointer on the flexible disk data file right before the oscilloscope data. This allows Program F.12 to retrieve the oscilloscope data from the file.

File 13 (Program F.14): This portion of the program retrieves the timing channel information from the flexible disk. The program is similar to Program F.8.

File 14 (Program F.15): This portion of the program reduces the timing channel data to determine the relative time at which the data points were taken with the multiplexer. This is done by the same method that was used in Program F.9.

File 15 (Program F.16): This portion of the program performs the same task as Program F.15, except that it is used in cases in which the memory buffers were loaded more than once. It is similar to Program F.11.

File 16 (Program F.17): This portion of the program retrieves the information needed to make a plot of the current to each segment in the electrode matrix at a given time. The data is also reduced and interpolated to determine the current for each segment at the set time.

File 17 (Program F.18): This portion of the program generates and labels the axes for a three dimensional plot of the current to a segment verses the spatial coordinates of the segment. It also plots the data. This plotting routine is relatively simple and does not give a perspective view of the data.

```
0: dim Q$[5]
1: trk 1;ldk 2;
 trk 0
2: ent "DID THE
 SYSTEM GO DOWN"
 ,Q$
3: if cap(Q$)="Y
 ES";ldp 1
4: ent "IS THE
 DISK TO BE INIT
 IALIZED?",Q$
5: if cap(Q$)#"Y
 ES";gto 10
6: dsp "LOAD
 DISK"
7: wait 5000
8: dsp "PRESS
 CONTINUE TO
 INITIALIZE";
 stp
9: open "trfil",
 50
10: ent "DO YOU
 WANT TO CHECK
 DISK SPACE",Q$
11: if cap(Q$)="
 YES";cat 0
12: ent "DO YOU
 WANT TO OUTPUT
 DATA?",Q$
13: if cap(Q$)="
 YES";ldp 6
14: ldp 1
15: end
*5247
```

Program F.1 Listing

```
0: dsp "DATA
 ACQUISITION &
 CONTROL"
1: wait 2000
2: dsp "OF MICRO
 -MOSAIC ELECTRO
 DE"
3: wait 2000
4: dim E$[128,
 5],Z[128]
5: dim A[10],
 B[5],B$[4,5],
 C[10],F[9],F$[1
 0,5],G$[80],
 R$[6]
6: dim Q$[5]
7: trk 1;ldk 2;
 trk 0
8: dsp "IS DATA
 ACQUISITION TO
 BE ENDED"
9: wait 2000
10: ent "WHEN
 THE BUFFER IS
 LOADED?",Q$
11: if cap(Q$)="
 YES";0→F[6];
 sfg 3
12: dsp "WHAT
 THROUGHPUT RATE
  IS SET ON"
13: wait 2000
14: ent "THE
 MULTIPLEXER(IN
 kHz)?",C[9]
15: if C[9]=10
 and flg3=0;gto
 29
16: if C[9]=10
 and flg3=1;gto
 33
17: if C[9]=5
 and flg3=0;gto
 29
18: if C[9]=5
 and flg3=1;gto
 33
19: if C[9]=2.5
 and flg3=0;gto
 29
20: if C[9]=2.5
 and flg3=1;gto
 33
21: if C[9]=1.25
  and flg3=0;
 gto 29
22: if C[9]=1.25
  and flg3=1;
 gto 33
23: dsp "AN ACCE
 PTABLE THROUGHP
 UT RATE"
24: wait 2000
25: dsp "WAS
 NOT ENTERED"
26: wait 2000
27: dsp "PRESS
 CONTINUE TO
 RESET";stp
28: gto 12
29: dsp "WHAT
 IS DATA ACQUISI
 TION TIME"
30: wait 2000
31: ent "IN SEC.
 ",C[10]
32: int(C[9]*
 C[10]*1000)+
 1→F[8]
33: 1→C[8]
34: 1→B[1]
35: 1→A[10]
36: 40000→H
37: dsp "IS THE
 BUBBLE GROWTH"
38: wait 2000
39: ent "TO BE
 COMPUTER CONTRO
 LED?",Q$
40: if cap(Q$)#"
 YES";0→A[10];
 gto 79
41: dsp "ARE
 DEFAULT VALUES"
42: wait 2000
43: ent "TO BE
 USED?",Q$
44: if cap(Q$)="
 YES";gto 70
45: ent "INITIAL
  VOLTAGE DIFFER
 ENCE(mV)?",A[1]
46: -abs(A[1])→A
 [1]
47: ent "MAXIMUM
  VOLTAGE DIFFER
 ENCE(mV)?",A[2]
48: -abs(A[2])→A
 [2]
49: if A[2]<=A[1
 ];gto 54
50: dsp "ERROR
 IN VOLTAGES"
51: wait 2000
52: dsp "PRESS
 CONTINUE TO
 RESET";stp
53: gto 45
54: if A[2]<-
 500;gto 50
55: if A[1]<-
 500;gto 50
56: ent "WHAT
 IS THE CURRENT
 SETTING(uA)?",
 A[3]
57: -abs(A[3])→A
 [3]
58: dsp "WHAT
 IS THE"
59: wait 2000
60: dsp "CURRENT
 -TO-VOLTAGE"
61: wait 2000
62: ent "CONVERS
 ION(uA/Volt)?",
 A[5]
63: dsp "SET
 CONTROL PARAMET
 ERS"
64: wait 2000
65: ent "PROPORT
 IONAL CONTROL
 #",A[4]
66: -abs(A[4])→A
 [4]
67: ent "DERRIVA
 TIVE CONTROL #
 (sec.)",A[7]
68: ent "INTEGRA
 L CONTROL # (1/
 sec.)",A[8]
69: gto 77
70: -300→A[1]
71: -500→A[2]
72: -15→A[3]
73: -20→A[4]
74: 50→A[5]
75: .01→A[7]
76: 3→A[8]
77: A[3]/A[5]→A[
 6]
78: .5→A[9]
79: dsp "IS DATA
  TO BE TAKEN"
80: wait 2000
81: ent "WITH
 THE OSCILLOSCOP
 E?",Q$
82: if cap(Q$)#"
 YES";0→B[1];
 3000→H;gto 95
83: dsp "WHAT
 IS THE CURRENT-
 TO-VOLTAGE"
84: wait 2000
85: dsp "CONVERS
 ION IN uA/V
 FOR CHANNEL"
86: wait 2000
87: ent "# 1A(IN
 PUT 1.0 FOR
 VOLTAGE)",B[2]
88: ent "# 1B(IN
 PUT 1.0 FOR
 VOLTAGE)",B[3]
89: ent "# 2A(IN
 PUT 1.0 FOR
 VOLTAGE)",B[4]
90: ent "# 2B(IN
 PUT 1.0 FOR
 VOLTAGE)",B[5]
91: ent "CHANNEL
  ASSIGNMENT
 FOR 1A",B$[1]
92: ent "CHANNEL
  ASSIGNMENT
 FOR 1B",B$[2]
93: ent "CHANNEL
  ASSIGNMENT
 FOR 2A",B$[3]
94: ent "CHANNEL
  ASSIGNMENT
 FOR 2B",B$[4]
95: dsp "ARE
 DEFAULT VALUES"
96: wait 2000
97: dsp "FOR
 DATA ACQUISITIO
 N"
98: wait 2000
99: ent "TO BE
 USED?",Q$
100: if cap(Q$)=
 "YES";gto 135
101: dsp "TRIANG
 ULAR WAVE PARAM
 ETERS"
102: wait 2000
103: ent "WHAT
 IS THE FREQUENC
 Y(Hz)?",C[1]
104: dsp "WHAT
 IS THE"
105: wait 2000
106: ent "PEAK-
 TO-PEAK VOLTAGE
 (Volts)?",C[2]
107: dsp "DATA
 ACQUISTION PARA
 METERS"
108: wait 2000
109: ent "WHAT
 IS THE MAX VOLT
 AGE(Volts)?",
 C[3]
110: if C[2]>C[3
 ]*2;gto 123
111: if C[3]=10.
 24;1→C[4];gto
 129
```

Program F.2 Listing

```
112: if C[3]=5.1
 2;2→C[4];gto
 129
113: if C[3]=2.5
 6;4→C[4];gto
 129
114: if C[3]=1.2
 8;8→C[4];gto
 129
115: if C[3]=.64
 ;16→C[4];gto
 129
116: if C[3]=.32
 ;32→C[4];gto
 129
117: if C[3]=.16
 ;64→C[4];gto
 129
118: if C[3]=.08
 ;128→C[4];gto
 129
119: if C[3]=.04
 ;256→C[4];gto
 129
120: if C[3]=.02
 ;512→C[4];gto
 129
121: if C[3]=.01
 ;1024→C[4];gto
 129
122: if C[3]=.00
 5;2048→C[4];
 gto 129
123: dsp "AN
 ACCEPTABLE MAXI
 MUM"
124: wait 2000
125: dsp "VOLTAG
 E WAS NOT ENTER
 ED"
126: wait 2000
127: dsp "PRESS
 CONTINUE TO
 RESET";stp
128: gto 109
129: ent "TOTAL
 # OF CHANNELS",
 C[5]
130: if C[5]<=12
 8;gto 140
131: dsp "ERROR
 IN CHANNEL NUMB
 ER"
132: wait 2006
133: dsp "PRESS
 CONTINUE TO
 RESET";stp
134: gto 129
135: .5→C[1]
136: 1→C[2]
137: .64→C[3]
138: 16→C[4]
139: 128→C[5]
140: ln(10.24/
 C[3])/ln(2)*
 2048→C[6]
141: cmp(C[6]-
 32768)→C[7]
142: cmpC[6]→C[6
 ]
143: dsp "ARE
 DEFAULT VALUES"
144: wait 2000
145: dsp "FOR
 CHANNEL ASSIGNM
 ENTS"
146: wait 2000
147: ent "TO BE
 USED?",Q$
148: if cap(Q$)=
 "YES";trk 1;
 ldf 0,E$,E[*];
 trk 0;gto 159
149: for I=1 to
 C[5]
150: dsp "CHANNE
 L",I,"ASSIGNMEN
 T"
151: wait 2000
152: ent "WHAT
 IS THE INPUT
 #?",E$[I]
153: dsp "WHAT
 IS THE CURRENT-
 TO-VOLTAGE"
154: wait 2000
155: dsp "CONVER
 SION (uA/Volt)?
 "
156: wait 2000
157: ent "ENTER
 1.0 FOR VOLTAGE
  INPUT",E[I]
158: next I
159: ent "ARE
 THERE CHANGES
 TO BE MADE?",Q$
160: if cap(Q$)#
 "YES";gto 171
161: ent "WHICH
 CHANNEL?",r1
162: ent "WHAT
 IS THE INPUT
 #?",E$[r1]
163: dsp "WHAT
 IS THE CURRENT-
 TO-VOLTAGE"
164: wait 2000
165: dsp "CONVER
 SION (uA/Volt)?
 "
166: wait 2000
167: ent "ENTER
 1.0 FOR VOLTAGE
  INPUT",E[r1]
168: ent "ARE
 THERE FURTHER
 CHANGES?",Q$
169: if cap(Q$)#
 "YES";gto 171
170: gto 161
171: if A[10]=0;
 0→C[8];jmp 5
172: dsp "IS
 THE DATA ACQUIS
 ITION"
173: wait 2000
174: ent "TO BE
 TRIGGERED MANUA
 LLY?",Q$
175: if cap(Q$)=
 "YES";0→C[8]
176: ent "# OF
 BUBBLE GENERATI
 ON SITES",F[1]
177: for I=1 to
 F[1]
178: ent "SEGMEN
 T # FOR BUBBLE
 GENERATION",
 F$[I]
179: next I
180: ent "FE
 CONCENTRATION(m
 oles/liter)",
 F[2]
181: ent "COMMEN
 TS:",G$
182: ent "6 CHAR
 ACTER RUN #",R$
183: if flg3=0;
 gto 189
184: int(500*
 C[9]/(2*C[5]))*
 2*C[5]+16→F[3]
185: int((28000-
 1000*C[9])/(2*
 C[5]))*2*C[5]+
 16→F[4]
186: int(30000/
 (2*C[5]))*2*
 C[5]+16→F[5]
187: int((H+2*
 F[3]+F[4]+F[5])
 /252)+1→F[9]
188: gto 192
189: int(28000/
 (2*C[5]))*2*
 C[5]+16→F[6]
190: 2*int(F[8]/
 F[6])+F[7]
191: int((H+(F[7
 ]+1)*(F[6]+4))/
 252)+1→F[9]
192: prt "THE
 DATA REQUIRES"
193: prt F[9],"
  RECORDS"
194: open R$,
 F[9]
195: asgn R$,1
196: asgn "trfil
 ",2
197: sprt 1,E$,
 E[*],A[*],B[*],
 B$,C[*],F[*],
 F$,G$,R$,"end"
198: sprt 2,A[*
 ],B[1],C[*],F[*
 ],"end"
199: if flg3=0;
 gto 202
200: if A[10]=1;
 ldp 2
201: ldp 3
202: ldp 4
203: end
*10761
```

```
0: dim A[10],
 C[10],F[9],V[2]
 ,Q[3]
1: asgn "trfil",
 2
2: sread 2,A[*],
 B,C[*],F[*]
3: F[3]→J
4: F[4]→K
5: F[5]→L
6: dim A$[J],
 B$[J],C$[K],
 D$[L]
7: (F[3]-16)/2→J
8: (F[4]-16)/2→K
9: (F[5]-16)/2→L
10: buf "data1",
 A$,4
11: buf "data2",
 B$,4
12: buf "data3",
 C$,4
13: buf "data4",
 D$,4
14: wti 0,10
15: trk 1;ldk 1;
 trk 0
16: cfg
17: 0→S
18: A[1]→R
19: dev "dvm",
 722,"fgn",717
20: wrt "dvm",
 "F1R7T3M3A1H0D1
 "
21: fxd 0
22: dsp "TO BEGI
 N COMPUTER CONT
 ROL"
23: wait 2000
24: dsp "PRESS
 CONTINUE";stp
25: wrt "fgn",
 "FU00F",str(A[1
 ]),"MV"
26: for I=1 to 3
27: trg "dvm"
28: jmp bit(6,
 rds("dvm"))
29: red "dvm",
 V[1]
30: V[1]-A[6]→Q[
 I]
31: if I=1;jmp 2
32: S+(Q[I-1]+
 Q[I])/2*A[9]→S
33: wait 400
34: next I
35: A[4]*(Q[3]+
 A[7]*(.5*Q[1]-
 2*Q[2]+1.5*Q[3]
 )/A[9]+A[8]*S)+
 A[1]→V[2]
36: Q[2]→Q[1]
37: Q[3]→Q[2]
38: if V[2]>0;
 0→V[2]
39: if V[2]<A[2]
 ;A[2]→V[2]
40: wait 200
41: wrt "fgn",
 str(V[2]),"MV"
42: wait 200
43: trg "dvm"
44: jmp bit(6,
 rds("dvm"))
45: red "dvm",
 V[1]
46: V[1]-A[6]→Q[
 3]
```

Program F.3 Listing

```
47: S+(Q[3]+Q[2]
 )/2*A[9]→S
48: V[2]→R
49: if flg1=1;
 gto 51
50: gto 35
51: dsp "BEGIN
 DATA ACQUISITIO
 N"
52: wti 6,C[7];
 wti 6,C[6];wti
 6,C[7]
53: tfr 10,"data
 1",J
54: A[4]*(Q[3]+
 A[7]*(.5*Q[1]-
 2*Q[2]+1.5*Q[3]
 )/A[9]+A[8]*S)+
 A[1]→V[2]
55: Q[2]→Q[1]
56: Q[3]→Q[2]
57: if V[2]>0;
 0→V[2]
58: if V[2]<A[2]
 ;A[2]→V[2]
59: wrt "fgn",
 str(V[2]),"MV"
60: jmp rds("dat
 a1")>0
61: wti 6,C[7];
 wti 6,C[6];wti
 6,C[7]
62: tfr 10,"data
 2",J
63: trg "dvm"
64: jmp bit(6,
 rds("dvm"))
65: red "dvm",
 V[1]
66: V[1]-A[6]→Q[
 3]
67: if abs(Q[3])
 >.05*abs(A[6])
 and C[8]=1;sfg
 2
68: S+(Q[3]+Q[2]
 )/2*A[9]→S
69: V[2]→R
70: jmp rds("dat
 a2")>0
71: if flg2=1;
 wrt "fgn","0MV"
 ;gto 74
72: buf "data1";
 buf "data2"
73: gto 52
74: wti 6,C[7];
 wti 6,C[6];wti
 6,C[7];beep
75: tfr 10,"data
 3",K
76: jmp rds("dat
 a3")>0
77: wti 6,C[7];
 wti 6,C[6];wti
 6,C[7]
78: tfr 10,"data
 4",L
79: jmp rds("dat
 a4")>0
80: dsp "TO STOR
 E DATA PRESS
 CONTINUE";stp
81: sprt 1,A$,
 B$,C$,D$,"end"
82: buf "data1";
 buf "data2";
 buf "data3";
 buf "data4"
83: dsp "END OF
 DATA ACQUISITIO
 N"
84: wait 2000
85: if B=1;ldp 5
86: end
*13402
```

Program F.4 Listing

```
0: dim A[10],
 C[10],F[9],V[2]
 ,Q[3]
1: asgn "trfil",
 2
2: sread 2,A[*],
 B,C[*],F[*]
3: F[3]→J
4: F[4]→K
5: F[5]→L
6: dim A$[J],
 B$[J],C$[K],
 D$[L]
7: (F[3]-16)/2→J
8: (F[4]-16)/2→K
9: (F[5]-16)/2→L
10: buf "data1",
 A$,4
11: buf "data2",
 B$,4
12: buf "data3",
 C$,4
13: buf "data4",
 D$,4
14: wti 0,10
15: trk 1;ldk 3;
 trk 0
16: cfg
17: dsp "TO BEGI
 N DATA ACQUISIT
 ION"
18: wait 2000
19: dsp "PRESS
 CONTINUE";stp
20: wti 6,C[7];
 wti 6,C[6];wti
 6,C[7]
21: tfr 10,"data
 1",J
22: jmp rds("dat
 a1")>0
23: if flg1=1;
 gto 29
24: buf "data1";
 buf "data2"
25: wti 6,C[7];
 wti 6,C[6];wti
 6,C[7]
26: tfr 10,"data
 2",J
27: jmp rds("dat
 a2")>0
28: gto 20
29: wti 6,C[7];
 wti 6,C[6];wti
 6,C[7];beep
30: tfr 10,"data
 3",K
31: jmp rds("dat
 a3")>0
32: wti 6,C[7];
 wti 6,C[6];wti
 6,C[7]
33: tfr 10,"data
 4",L
34: jmp rds("dat
 a4")>0
35: sprt 1,B$,
 A$,C$,D$,"end"
36: buf "data1";
 buf "data2";
 buf "data3";
 buf "data4"
37: dsp "END OF
 DATA ACQUISITIO
 N"
38: wait 2000
39: if B=1;ldp 5
40: end
*31113
```

Program F.5 Listing

```
0: dim A[10],
 C[10],F[9],V[2]
 ,Q[3]
1: asgn "trfil",
 2
2: sread 2,A[*],
 B,C[*],F[*]
3: F[6]→J
4: dim A$[J],
 B$[J]
5: (F[6]-16)/2→J
6: J/(C[9]*1000)
 →K
7: int(K/.5)→L
8: buf "data1",
 A$,4
9: buf "data2",
 B$,4
10: wti 0,10
11: trk 1;ldk 1;
 trk 0
12: cfg
13: if A[10]=0;
 gto 48
14: 0→S
15: A[1]→R
16: dev "dvm",
 722,"fgn",717
17: wrt "dvm",
 "F1R7T3M3A1H0D1
 "
18: fxd 0
19: dsp "TO BEGI
 N COMPUTER CONT
 ROL"
20: wait 2000
21: dsp "PRESS
 CONTINUE";stp
22: wrt "fgn",
 "FU0OF",str(A[1
 ]),"MV"
23: for I=1 to 3
24: trg "dvm"
25: jmp bit(6,
 rds("dvm"))
26: red "dvm",
 V[1]
27: V[1]-A[6]→Q[
 I]
28: if I=1;jmp 2
29: S+(Q[I-1]+
 Q[I])/2*A[9]→S
30: wait 400
31: next I
32: A[4]*(Q[3]+
 A[7]*(.5*Q[1]-
 2*Q[2]+1.5*Q[3]
 )/A[9]+A[8]*S)+
 A[1]→V[2]
33: Q[2]→Q[1]
34: Q[3]→Q[2]
35: if V[2]>0;
 0→V[2]
36: if V[2]<A[2]
 ;A[2]→V[2]
37: wait 200
38: wrt "fgn",
 str(V[2]),"MV"
39: wait 200
40: trg "dvm"
41: jmp bit(6,
 rds("dvm"))
42: red "dvm",
 V[1]
43: V[1]-A[6]→Q[
 3]
44: S+(Q[3]+Q[2]
 )/2*A[9]→S
45: V[2]→R
```

```
46: if flg1=1;
 gto 52
47: gto 32
48: dsp "TO BEGI
 N DATA ACQUISIT
 ION"
49: wait 2000
50: dsp "PRESS
 CONTINUE";stp
51: gto 53
52: dsp "BEGIN
 DATA ACQUISITIO
 N"
53: wti 6,C[7];
 wti 6,C[6];wti
 6,C[7]
54: tfr 10,"data
 1",J
55: if A[10]=0;
 gto 73
56: for I=1 to L
57: A[4]*(Q[3]+
 A[7]*(.5*Q[1]-
 2*Q[2]+1.5*Q[3]
 )/A[9]+A[8]*S)+
 A[1]→V[2]
58: Q[2]→Q[1]
59: Q[3]→Q[2]
60: if V[2]>0;
 0→V[2]
61: if V[2]<A[2]
 ;A[2]→V[2]
62: wait 200
63: wrt "fgn",
 str(V[2]),"MV"
64: wait 200
65: trg "dvm"
66: jmp bit(6,
 rds("dvm"))
67: red "dvm",
 V[1]
68: V[1]-A[6]→Q[
 3]
69: if abs(Q[3])
 >.1*abs(A[6])
 and C[8]=1;sfg
 2
70: S+(Q[3]+Q[2]
 )/2*A[9]→S
71: V[2]→R
72: next I
73: jmp rds("dat
 a1")>0
74: if A[10]=0
 and flg1=1;beep
 ;gto 78
75: if flg2=1;
 wrt "fgn","0MV"
 ;beep;gto 78
76: buf "data1"
77: gto 53
78: for I=2 to
 F[7] by 2
79: buf "data2"
80: wti 6,C[7];
 wti 6,C[6];wti
 6,C[7]
81: tfr 10,"data
 2",J
82: jmp rds("dat
 a2")>0
83: sprt 1,A$,
 "end"
84: buf "data1"
85: wti 6,C[7];
 wti 6,C[6];wti
 6,C[7]
86: tfr 10,"data
 1",J
87: jmp rds("dat
 a1")>0
88: sprt 1,B$,
 "end"
89: next I
90: sprt 1,A$
91: buf "data1";
 buf "data2"
92: dsp "END OF
 DATA ACQUISITIO
 N"
93: wait 2000
94: if B=1;ldp 5
95: end
*9687
```

```
0: dim E$[65],
 H$[4,55],D$[317
 60]
1: buf "data",
 D$,3
2: dsp "PRESS
 CONTINUE TO
 TRF. OSC. DATE"
 ;stp
3: fxd 0
4: wrt 727,"W"
5: red 727,E
6: if E#0;dsp
 "ERROR # ",E,"
 IN W";stp
7: red 727,B$
8: val(B$[1,2])→
 A
9: val(B$[3+A*
 15,4+A*15])→E
10: if E#0;dsp
 "ERROR # ",E,"
 IN W OUTPUT";
 stp
11: if A>4;dsp
 "TO MANY WAVEFO
 RMS";stp
12: wrt 727,"D,
 4,0,0,15872,1"
13: red 727,E
14: if E#0;dsp
 "ERROR # ",E,"
 IN D";stp
15: tfr 727,"dat
 a",31744
16: red 727,E
17: if E#0;dsp
 " ERROR # ",E,
 " IN D OUTPUT";
 stp
18: for I=1 to A
19: wrt 727,"N,
 ",B$[(I-1)*15+
 11,(I-1)*15+12]
20: red 727,E
21: if E#0;dsp
 "ERROR # ",E,"
 IN N";stp
22: red 727,H$[I
 ]
23: val(H$[I,53,
 54])→E
24: if E#0;dsp
 "ERROR # ",E,"
 IN N OUTPUT";
 stp
25: next I
26: sprt 1,B$,
 H$,D$,"end"
27: dsp "DATA
 HAS BEEN TRF.
 AND STORRED"
28: end
*18535
```

Program F.6
Listing

```
0: dsp "DATA
 OUTPUT PROGRAM"
1: wait 2000
2: dim E$[128,
 5],E[128],A[10]
 ,B[5],B$[4,5],
 C[10],F[9],F$[1
 0,5],G$[80],
 R$[6]
3: dim P[8],P$[5
 ],Q$[5]
4: trk 1;ldk 2;
 trk 0
5: ent "6 CHARAC
 TER RUN #",R$
6: asgn R$,1
7: asgn "trfil",
 2
8: sread 1,E$,
 E[*],A[*],B[*],
 B$,C[*],F[*],
 F$,G$,R$
9: prt " RUN #
 ",R$
10: spc 2
11: fxd 0
12: prt F[1],"
 BUBBLES GENERAT
 ED"
13: prt "AT SEGM
 ENT(S)"
14: for I=1 to
 F[1]
15: prt F$[I]
16: next I
17: spc 2
18: flt 3
19: prt "FE CONC
 .= ",F[2],"
 MOLES/LITER"
20: spc 2
21: prt "COMMENT
 S: ",G$
22: spc 2
23: ent "PRINT
 CHANNEL ASSIGNM
 ENTS?",Q$
24: if cap(Q$)#"
 YES";gto 31
25: for I=1 to
 C[5]
26: fxd 0
27: prt "CHANNEL
 # ",I
28: prt "SEGMENT
 ",E$[I]
29: spc
30: next I
31: ent "CHANNEL
 PLOT?",Q$
32: if cap(Q$)#"
 YES";gto 48
33: ent "WHICH
 CHANNEL?",P[1]
34: ent "PLOT
 AGAINST TIME",
 Q$
35: 0→P[2]
36: if cap(Q$)#"
 YES";1→P[2];
 gto 43
37: ent "1st
 TIMING RAMP
 CHANNEL?",P[4]
38: ent "2nd
 TIMING RAMP
 CHANNEL?",P[5]
39: P[4]→J
40: E[J]→P[6]
41: P[5]→J
42: E[J]→P[7]
43: P[1]→J
44: E[J]→P[3]
45: E$[J]→P$
46: sprt 2,P[*],
 P$,C[*],F[*],
 "end"
47: ldp 7
48: ent "ELECTRO
 DE PLOT?",Q$
49: if cap(Q$)#"
 YES";gto 59
50: ent "1st
 TIMMING RAMP
 CHANNEL?",P[1]
51: ent "2nd
 TIMMING RAMP
 CHANNEL?",P[2]
52: ent "TIME
 OF PLOT(SECONDS
 )?",P[5]
53: P[1]→J
54: E[J]→P[3]
55: P[2]→J
56: E[J]→P[4]
57: sprt 2,P[*],
 C[*],F[*],R$,
 "end"
58: ldp 13
59: if B[1]=0;
 gto 74
60: ent "OSCILLO
 SCOPE PLOT?",Q$
61: if cap(Q$)#"
 YES";gto 73
62: ent "PLOT
 CHANNEL 1A?",Q$
63: if cap(Q$)="
 YES";1→P[1];
 B[2]→P[2];B$[1]
 →P$;gto 71
64: ent "PLOT
 CHANNEL 1B?",Q$
65: if cap(Q$)="
 YES";2→P[1];
 B[3]→P[3];B$[2]
 →P$;gto 71
66: ent "PLOT
 CHANNEL 2A?",Q$
67: if cap(Q$)="
 YES";3→P[1];
 B[4]→P[4];B$[3]
 →P$;gto 71
68: ent "PLOT
 CHANNEL 2B?",Q$
69: if cap(Q$)="
 YES";4→P[1];
 B[5]→P[5];B$[4]
 →P$;gto 71
70: gto 73
71: sprt 2,P[*],
 P$,C[*],F[*],
 "end"
72: ldp 12
73: dsp "NO MORE
 OPTIONS"
74: end
*17048
```

Program F.7 Listing

```
0: asgn "trfil",
 2
1: dim P[8],P$[5
 ],C[10],F[9]
2: sread 2,P[*],
 F$,C[*],F[*]
3: P[1]→O
4: C[5]→N
5: P[4]→R;P[5]→S
6: if F[6]>0;
 gto 53
7: F[3]→J
8: F[4]→K
9: F[5]→L
10: dim R$[L]
11: buf "data1",
 R$,4
12: (F[3]-16)/
 (2*N)→J
13: (F[4]-16)/
 (2*N)→K
14: (F[5]-16)/
 (2*N)→L
15: 2*J+K+L→M
16: dim X$[2*M],
 Y$[2*M],Z$[2*M]
17: F[3]-16→I
18: sread 1,R$[1
 ,I]
19: for I=0 to
 J-1
20: if P[2]=1;
 gto 23
21: R$[(N*I+R)*
 2-1,(N*I+R)*
 2]→X$[2*I+1,2*
 I+2]
22: R$[(N*I+S)*
 2-1,(N*I+S)*
 2]→Z$[2*I+1,2*
 I+2]
23: R$[(N*I+O)*
 2-1,(N*I+O)*
 2]→Y$[2*I+1,2*
 I+2]
24: next I
25: buf "data1"
26: F[3]-16→I
27: sread 1,R$[1
 ,I]
28: for I=0 to
 J-1
29: if P[2]=1;
 gto 32
30: R$[(N*I+R)*
 2-1,(N*I+R)*
 2]→X$[2*(J+I)+
 1,2*(J+I)+2]
31: R$[(N*I+S)*
 2-1,(N*I+S)*
 2]→Z$[2*(J+I)+
 1,2*(J+I)+2]
32: R$[(N*I+O)*
 2-1,(N*I+O)*
 2]→Y$[2*(J+I)+
 1,2*(J+I)+2]
33: next I
34: buf "data1"
35: F[4]-16→I
36: sread 1,R$[1
 ,I]
37: for I=0 to
 K-1
38: if P[2]=1;
 gto 41
39: R$[(N*I+R)*
 2-1,(N*I+R)*
 2]→X$[2*(2*J+
 I)+1,2*(2*J+I)+
 2]
40: R$[(N*I+S)*
 2-1,(N*I+S)*
 2]→Z$[2*(2*J+
 I)+1,2*(2*J+I)+
 2]
41: R$[(N*I+O)*
 2-1,(N*I+O)*
 2]→Y$[2*(2*J+
 I)+1,2*(2*J+I)+
 2]
42: next I
43: buf "data1"
44: sread 1,R$
45: for I=0 to
 L-1
46: if P[2]=1;
 gto 49
47: R$[(N*I+R)*
 2-1,(N*I+R)*
 2]→X$[2*(2*J+K+
 I)+1,2*(2*J+K+
 I)+2]
48: R$[(N*I+S)*
 2-1,(N*I+S)*
 2]→Z$[2*(2*J+K+
 I)+1,2*(2*J+K+
 I)+2]
49: R$[(N*I+O)*
 2-1,(N*I+O)*
 2]→Y$[2*(2*J+K+
 I)+1,2*(2*J+K+
 I)+2]
50: next I
51: buf "data1"
52: gto 69
53: F[6]→J
54: dim R$[J]
55: buf "data1",
 R$,4
56: (F[6]-16)/
 (2*N)→J
57: (F[7]+1)*J→M
58: dim X$[2*M],
 Y$[2*M],Z$[2*M]
59: for K=0 to
 F[7]
60: sread 1,R$
61: for I=0 to
 J-1
62: if P[2]=1;
 gto 65
63: R$[(N*I+R)*
 2-1,(N*I+R)*
 2]→X$[2*(I+J*
 K)+1,2*(I+J*K)+
 2]
64: R$[(N*I+S)*
 2-1,(N*I+S)*
 2]→Z$[2*(I+J*
 K)+1,2*(I+J*K)+
 2]
65: R$[(N*I+O)*
 2-1,(N*I+O)*
 2]→Y$[2*(I+J*
 K)+1,2*(I+J*K)+
 2]
66: next I
67: buf "data1"
68: next K
69: asgn "trfil"
 ,2
70: sprt 2,P[*],
 P$,C[*],F[*],
 Y$,"end"
71: if P[2]=0;
 sprt 2,X$,Z$,
 "end"
72: if F[6]>0;
 ldp 10
73: ldp 8
74: end
*14630
```

Program F.8 Listing

```
0: asgn "trfil",
 2
1: dim P[8],C[10
 ],F[9],R$[6]
2: sread 2,P[*],
 C[*],F[*],R$
3: C[5]→N
4: 0→G;0→H
5: P[1]→R;P[2]→S
6: (F[3]-16)/(2*
 N)→J
7: (F[4]-16)/(2*
 N)→K
8: (F[5]-16)/(2*
 N)→L
9: 2*J+K+L→M
10: dim X[M],
 Z[M],T[M],D[M],
 A[5],B[5],X$[2*
 M],Z$[2*M]
11: sread 2,X$,
 Z$
12: for I=0 to
 J-1
13: cmpitf(X$[I*
 2+1,I*2+2])*
 (.005/C[4])*
 P[3]→X[I+1]
14: cmpitf(Z$[I*
 2+1,I*2+2])*
 (.005/C[4])*
 P[4]→Z[I+1]
15: if I<=3;gto
 20
16: (-X[I+1]+8*
 X[I]-8*X[I-2]+
 X[I-3])/12→D[I-
 1]
17: if I<=4;gto
 20
18: if D[I-1]>0
 and D[I-2]<0;I-
 2→A[G+1];G+1→G
19: if D[I-1]<0
 and D[I-2]>0;I-
 2→B[H+1];H+1→H
20: next I
21: 0→D[1];0→D[2
 ];0→D[J-1];0→D[
 J]
22: for I=0 to
 J-1
23: cmpitf(X$[(I
 +J)*2+1,(I+J)*
 2+2])*(.005/
 C[4])*P[3]→X[J+
 I+1]
24: cmpitf(Z$[(I
 +J)*2+1,(I+J)*
 2+2])*(.005/
 C[4])*P[4]→Z[J+
 I+1]
25: if I<=3;gto
 30
26: (-X[J+I+1]+
 8*X[J+I]-8*X[J+
 I-2]+X[J+I-3])/
 12→D[J+I-1]
27: if I<=4;gto
 30
28: if D[J+I-
 1]>0 and D[I+J-
 2]<0;J+I-2→A[G+
 1];G+1→G
29: if D[J+I-
 1]<0 and D[I+J-
 2]>0;J+I-2→B[H+
 1];H+1→H
30: next I
31: 0→D[J+1];
 0→D[J+2];0→D[2*
 J-1];0→D[2*J]
32: for I=0 to
 K-1
33: cmpitf(X$[(2
 *J+I)*2+1,(2*J+
 I)*2+2])*(.005/
 C[4])*P[3]→X[2*
 J+I+1]
34: cmpitf(Z$[(2
 *J+I)*2+1,(2*J+
 I)*2+2])*(.005/
 C[4])*P[4]→Z[2*
 J+I+1]
35: if I<=3;gto
 40
36: (-X[2*J+I+
 1]+8*X[2*J+I]-
 8*X[2*J+I-2]+
 X[2*J+I-3])/
 12→D[2*J+I-1]
37: if I<=4;gto
 40
38: if D[2*J+I-
 1]>0 and D[2*J+
 I-2]<0;2*J+I-
 2→A[G+1];G+1→G
39: if D[2*J+I-
 1]<0 and D[2*J+
 I-2]>0;2*J+I-
 2→B[H+1];H+1→H
40: next I
41: 0→D[2*J+1];
 0→D[2*J+2];0→D[
 2*J+K-1];0→D[2*
 J+K]
42: for I=0 to
 L-1
43: cmpitf(X$[(2
 *J+K+I)*2+1,(2*
 J+K+I)*2+2])*
 (.005/C[4])*
 P[3]→X[2*J+K+I+
 1]
44: cmpitf(Z$[(2
 *J+K+I)*2+1,(2*
 J+K+I)*2+2])*
 (.005/C[4])*
 P[4]→Z[2*J+K+I+
 1]
45: if I<=3;gto
 50
46: (-X[2*J+K+I+
 1]+8*X[2*J+K+
 I]-8*X[2*J+K+I-
 2]+X[2*J+K+I-
 3])/12→D[2*J+K+
 I-1]
47: if I<=4;gto
 50
48: if D[2*J+K+
 I-1]>0 and D[2*
 J+K+I-2]<0;2*J+
 K+I-2→A[G+1];G+
 1→G
49: if D[2*J+K+
 I-1]<0 and D[2*
 J+K+I-2]>0;2*J+
 K+I-2→B[H+1];H+
 1→H
50: next I
51: 0→D[2*J+K+
 1];0→D[2*J+K+
 2];0→D[2*J+K+L-
 1];0→D[2*J+K+L]
52: 0→U
53: cfg 1
54: if G=0;gto
 64
55: for I=1 to G
56: A[I]→E
57: if flg1=1;
 gto 60
58: if E>2*J+15
 and E<2*J+K-15;
 sfg 1;E→U
59: if E>2*J+K+
 15 and E<2*J+K+
 L-15;sfg 1;E→U
60: for F=E-2
 to E+3
61: 0→D[F]
62: next F
63: next I
64: cfg 2
65: 0→V
66: if flg1=1;
 sfg 2
67: if H=0;gto
 77
68: for I=1 to H
69: B[I]→E
70: if flg2=1;
 gto 73
71: if E>2*J+15
 and E<2*J+K-15;
 sfg 2;E→V
72: if E>2*J+K+
 15 and E<2*J+K+
 L-15;sfg 2;E→V
73: for F=E-2
 to E+3
74: 0→D[F]
75: next F
76: next I
77: 0→Q;0→r14;
 M→r18
78: for I=1 to M
79: Q+abs(D[I])→
 Q
80: if D[I]=0;
 r18-1→r18;0→T[I
 ];gto 83
81: abs(X[I]-
 Z[I])→T[I]
82: r14+T[I]→r14
83: next I
84: Q/r18→Q
85: r14/r18→r14
86: if V≠0;V→U
87: if U=0;dsp
 "NO MAX OR MIN
 RECORDED";wait
 2000;C[2]/2→r9;
 gto 109
88: 0→r1;0→r2;
 0→r3;0→r4
89: for I=U-12
 to U-3
90: r1+I*X[I]→r1
91: r2+I→r2
92: r3+X[I]→r3
93: r4+I*I→r4
94: next I
95: (10*r1-r2*
 r3)/(10*r4-r2*
 r2)→r5
96: r3/10-r5*r2/
 10→r6
97: 0→r1;0→r2;
 0→r3;0→r4
98: for I=U+4
 to U+13
99: r1+I*X[I]→r1
100: r2+I→r2
101: r3+X[I]→r3
102: r4+I*I→r4
103: next I
104: (10*r1-r2*
 r3)/(10*r4-r2*
 r2)→r7
105: r3/10-r7*
 r2/10→r8
106: abs((r6*r7-
 r5*r8)/(r7-r5))
 →r9
107: abs((C[2]/
 2-r9)/C[2])→r10
108: if r10>.01;
 dsp "Vmax DID
 NOT CORRELATE";
 stp
109: r9*C[1]*
 4→r11
110: Q/r11→r12
111: r12/C[5]→r1
 3
112: Q/C[5]*(P[2
 ]-P[1])→r15
113: abs((r15-
 r14)/r14)→r16
114: if r16>.1;
 dsp "TIMMING
 CHANNELS DO
 NOT CHECK";stp
115: (P[1]-1)*
 r13→T[1]
116: for I=2 to
 J
117: T[I-1]+r12→
 T[I]
118: next I
119: if J>4;gto
 128
120: J→r19;J+
 2→r20;2*J→r21;
 cfg 3
121: T[r19]+abs(
 X[r19+1]-X[r19]
 )/r11→T[r19+1]
122: for I=r20
 to r21
123: T[I-1]+r12→
 T[I]
124: next I
125: if flg3=0;
 sfg 3;2*J→r19;
 2*J+2→r20;2*J+
 K→r21;gto 121
126: sfg 4;J→r17
127: 2*J+K→J;
 gto 129
128: cfg 3;cfg
 4;J→r17
129: if D[J-2]>0
  and D[J+3]>0;
 T[J]+(X[J+1]-
 X[J])/r11→T[J+
 1];gto 137
130: if D[J-2]<0
  and D[J+3]<0;
 T[J]+(X[J]-X[J+
 1])/r11→T[J+1];
 gto 137
131: if D[J-2]=0
  or D[J+3]=0;
 gto 135
132: if D[J-2]>0
 ;T[J-2]+(r9-
 X[J-2]+(r9-X[J+
 3]))/r11-2*r12→
 T[J+1];gto 137
133: T[J-2]+(r9+
 X[J-2]+(r9+X[J+
 3]))/r11-2*r12→
 T[J+1]
134: gto 137
```

Program F.9 Listing

```
0: dim S[6],H[2]
 ,A$[30],B$[35],
 C$[45],D$[3,
 55],G[2],Q$[5]
1: asgn "trfil",
 2
2: sread 2,Z
3: dim X[Z],Y[Z]
4: sread 2,X[*],
 Y[*],C$,B$,A$
5: ent "PLOT
 ABSOLUTE VALUES
 ?",Q$
6: if cap(Q$)#"Y
 ES";gto 10
7: for I=1 to Z
8: abs(Y[I])→Y[I
 ]
9: next I
10: ent "IS THE
 AXIS TO BE PLOT
 TED?",Q$
11: if cap(Q$)#"
 YES";gto 114
12: flt 3
13: 0→S[1]
14: X[Z]→S[2]
15: Y[1]→M
16: Y[1]→N
17: for I=2 to Z
18: if Y[I]>M;
 Y[I]→M
19: if Y[I]<N;
 Y[I]→N
20: next I
21: dsp "MIN Y-
 VALUE IS ",N
22: wait 2000
23: ent "GRAPH
 MIN Y-VALUE?",
 S[3]
24: dsp "MAX Y-
 VALUE IS ",M
25: wait 2000
26: ent "GRAPH
 MAX Y-VALUE?",
 S[4]
27: dsp "MAX
 GRAPH X-VALUE
 IS ",X[Z];wait
 2000
28: ent "X-TIC?"
 ,S[5]
29: ent "Y-TIC?"
 ,S[6]
30: ent "# OF
 DIGETS DSP AFTE
 R X-DECIMAL?",
 G[1]
31: ent "# OF
 DIGETS DSP AFTE
 R Y-DECIMAL?",
 G[2]
32: ent "LINE 1
 CAPTION?",D$[1]
33: ent "LINE 2
 CAPTION?",D$[2]
34: ent "LINE 3
 CAPTION?",D$[3]
35: fxd G[1]
36: S[2]-(7/5)(S
 [2]-S[1])+.2(S[
 2]-S[1])→A
37: S[2]+.2(S[2]
 -S[1])→B
38: S[4]-(8.5/
 7)(S[4]-S[3])-
 .05(S[4]-S[3])→
 C
39: S[4]+(1/7)(S
 [4]-S[3])-.05(S
 [4]-S[3])→D
40: scl A,B,C,D
41: pen
42: plt S[1],
 S[3],-2
43: (1/16/4.5)(S
 [2]-S[1])→H[1]
44: (1/16/7)(S[4
 ]-S[3])→H[2]
45: int((S[2]-
 S[1])/S[5])→M
46: int((S[4]-
 S[3])/S[6])→N
47: for I=1 to M
48: iplt S[5],0,
 0
49: iplt 0,H[2],
 0
50: iplt 0,-H[2]
 ,0
51: next I
52: plt S[2],
 S[3],0
53: for I=1 to N
54: iplt 0,S[6],
 0
55: iplt -H[1],
 0,0
56: iplt H[1],0,
 0
57: next I
58: plt S[2],
 S[4],-1
59: plt S[1],
 S[3],-2
60: for I=1 to N
61: iplt 0,S[6],
 0
62: iplt H[1],0,
 0
63: iplt -H[1],
 0,0
64: next I
65: plt S[1],
 S[4],0
66: for I=1 to M
67: iplt S[5],0,
 0
68: iplt 0,-H[2]
 ,0
69: iplt 0,H[2],
 0
70: next I
71: plt S[2],
 S[4],-1
72: csiz 1.5,2,
 1.357,0
73: for I=0 to M
74: S[1]+I*S[5]→
 U
75: -(len(str(U)
 )/2+.3)→V
76: plt U,S[3],0
77: cplt V,-1.25
78: lbl U
79: next I
80: fxd G[2]
81: for I=0 to N
82: S[3]+I*S[6]→
 U
83: -(len(str(U)
 )+1)→V
84: plt S[1],U,0
85: cplt V,-.3
86: lbl U
87: next I
88: csiz 1.5,2,
 1.357,0
```

```
135: for I=2 to
 J
136: T[I-1]+r12→
 T[I]
137: next I
138: if J>4;gto
 147
139: J→r19;J+
 2→r20;2*J→r21;
 cfg 3
140: T[r19]+abs(
 X[r19+1]-X[r19]
 )/r11→T[r19+1]
141: for I=r20
 to r21
142: T[I-1]+r12→
 T[I]
143: next I
144: if flg3=0;
 sfg 3;2*J→r19;
 2*J+2→r20;2*J+
 K→r21;gto 140
145: sfg 4;J→r17
146: 2*J+K→J;
 gto 148
147: cfg 3;cfg
 4;J→r17
148: if D[J-2]>0
  and D[J+3]>0;
 T[J]+(X[J+1]-
 X[J])/r11→T[J+
 1];gto 156
149: if D[J-2]<0
  and D[J+3]<0;
 T[J]+(X[J]-X[J+
 1])/r11→T[J+1];
 gto 156
150: if D[J-2]=0
  or D[J+3]=0;
 gto 154
151: if D[J-2]>0
 ;T[J-2]+(r9-
 X[J-2]+(r9-X[J+
 3]))/r11-2*r12→
 T[J+1];gto 156
152: T[J-2]+(r9+
 X[J-2]+(r9+X[J+
 3]))/r11-2*r12→
 T[J+1]
153: gto 156
154: if D[J-8]>0
 ;T[J-8]+(r9-
 X[J-8]+(r9-X[J+
 9]))/r11-8*r12→
 T[J+1];gto 156
155: T[J-8]+(r9+
 X[J-8]+(r9+X[J+
 9]))/r11-8*r12→
 T[J+1]
156: if flg4=1;
 r17→J;gto 166
157: if flg3=1;
 J/2→J;gto 162
158: for I=J+2
 to 2*J
159: T[I-1]+r12→
 T[I]
160: next I
161: sfg 3;2*
 J→J;gto 148
162: for I=2*J+
 2 to 2*J+K
163: T[I-1]+r12→
 T[I]
164: next I
165: sfg 4;2*J+
 K→J;gto 148
166: for I=2*J+
 K+2 to 2*J+K+L
167: T[I-1]+r12→
 T[I]
168: next I
169: asgn "trfil
 ",2
170: if P[2]=0;
 sprt 2,M,T[*],
 Y[*],N$,O$,R$;
 gto 172
171: sprt 2,M,
 X[*],Y[*],N$,
 O$,R$
172: ldp 9
173: end
*8521
```

Figure F.10 Listing

```
89: for I=1 to 3
90: 3-I→J
91: plt A,C,0
92: cplt 0,J
93: lbl D$[I]
94: next I
95: csiz 1.75,2,
 1.357,0
96: -(len(B$)/2+
 .3)→V
97: (S[2]-S[1])/
 2+S[1]→U
98: plt U,S[3],0
99: cplt V,-3
100: lbl B$
101: deg
102: csiz 1.75,
 2,1.357,90
103: -(len(C$)/
 2+.3)→V
104: (S[4]-S[3])
 /2+S[3]→U
105: plt A,U,0
106: cplt V,-1
107: lbl C$
108: csiz 2,2,
 1.357,0
109: -(len(A$)/
 2+.3)→V
110: (S[2]-S[1])
 /2+S[1]→U
111: plt U,D,0
112: cplt V,-1
113: lbl A$
114: ent "DO
 YOU WANT A POIN
 T PLOT?",Q$
115: cfg 1
116: if cap(Q$)#
 "YES";sfg 1
117: pen
118: for I=1 to
 Z
119: if flg1=1;
 gto 122
120: plt X[I],
 Y[I],-2
121: pen;gto 124
122: if I=1;plt
 X[I],Y[I],-2;
 gto 124
123: plt X[I],
 Y[I],2
124: next I
125: pen
126: stp ;end
*28238
```

```
0: asgn "trfil",
 2
1: dim P[8],P$[5
 ],C[10],F[9],
 N$[35],O$[45],
 R$[30]
2: sread 2,P[*],
 P$,C[*],F[*]
3: if P[3]=1
 and P$[1,1]#"["
 ;"POTENTIAL
 DIFFERENCE (VOL
 TS)"→N$;gto 5
4: "CURRENT (MIC
 ROAMPS)"→N$
5: if P[2]=0;
 "TIME (SECONDS)
 "→O$;gto 7
6: "POINT #"→O$
7: fxd 0
8: "CHANNEL #
 "→R$
9: str(P[1])→R$[
 11,14]
10: "- SYSTEM #
 "→R$[15,25]
11: P$→R$[26,30]
12: C[5]→N
13: 0→G;0→H
14: P[4]→R;P[5]→
 S
15: (F[6]-16)/
 (2*N)→J
16: (F[7]+1)*J→M
17: dim X[M],
 Y[M],Z[M],T[M],
 D[M],A[5],B[5],
 X$[2*M],Y$[2*
 M],Z$[2*M]
18: sread 2,Y$
19: if P[2]=0;
 sread 2,X$,Z$
20: for K=0 to
 F[7]
21: for I=0 to
 J-1
22: if P[2]=1;K*
 J+I+1→X[K*J+I+
 1];gto 30
23: cmpitf(X$[(1
 +J*K)*2+1,(I+J*
 K)*2+2])*(.005/
 C[4])*P[6]→X[I+
 J*K+1]
24: cmpitf(Z$[(I
 +J*K)*2+1,(I+J*
 K)*2+2])*(.005/
 C[4])*P[7]→Z[I+
 J*K+1]
25: if I<=3;gto
 30
26: (-X[I+J*K+
 1]+8*X[I+J*K]-
 8*X[I+J*K-2]+
 X[I+J*K-3])/
 12→D[I+J*K-1]
27: if I<=4;gto
 30
28: if D[I+J*K-
 1]>0 and D[I+J*
 K-2]<0;I+J*K-
 2→A[G+1];G+1→G
29: if D[I+J*K-
 1]<0 and D[I+J*
 K-2]>0;I+J*K-
 2→B[H+1];H+1→H
30: cmpitf(Y$[(I
 +J*K)*2+1,(I+J*
 K)*2+2])*(.005/
 C[4])*P[3]→Y[I+
 J*K+1]
```

```
31: next I
32: 0→D[J*K+1];
 0→D[J*K+2];0→D[
 (K+1)*J-1];0→D[
 (K+1)*J]
33: next K
34: if P[2]=1;
 gto 116
35: 0→U
36: cfg 1
37: if G=0;gto
 48
38: for I=1 to G
39: A[I]→E
40: if flg1=1;
 gto 44
41: for K=0 to
 F[7]
42: if E>K*J+15
 and E<J*(K+1)-
 15;sfg 1;E→U
43: next K
44: for F=E-2
 to E+3
45: 0→D[F]
46: next F
47: next I
48: cfg 2
49: 0→V
50: if flg1=1;
 sfg 2
51: if H=0;gto
 62
52: for I=1 to H
53: B[I]→E
54: if flg2=1;
 gto 58
55: for K=0 to
 F[7]
56: if E>K*J+15
 and E<(K+1)*J-
 15;sfg 2;E→V
57: next K
58: for F=E-2
 to E+3
59: 0→D[F]
60: next F
61: next I
62: 0→Q;0→r14
63: for I=1 to M
64: Q+abs(D[I])→
 Q
65: if D[I]=0;
 0→T[I];gto 68
66: abs(X[I]-
 Z[I])→T[I]
67: r14+T[I]→r14
68: next I
69: Q/(M-6*(G+
 H)-4*F[7])→Q
70: r14/(M-6*(G+
 H)-4*F[7])→r14
71: if V#0;V→U
72: if U=0;dsp
 "NO MAX OR MIN
 RECORDED";wait
 2000;C[2]/2+r9;
 gto 94
73: 0→r1;0→r2;
 0→r3;0→r4
74: for I=U-13
 to U-3
75: r1+I*X[I]→r1
76: r2+I→r2
77: r3+X[I]→r3
78: r4+I*I→r4
79: next I
80: (10*r1-r2*
 r3)/(10*r4-r2*
 r2)→r5
```

```
81: r3/10-r5*r2/
 10→r6
82: 0→r1;0→r2;
 0→r3;0→r4
83: for I=U+4
 to U+13
84: r1+I*X[I]→r1
85: r2+I→r2
86: r3+X[I]→r3
87: r4+I*I→r4
88: next I
89: (10*r1-r2*
 r3)/(10*r4-r2*
 r2)→r7
90: r3/10-r7*r2/
 10→r8
91: abs((r6*r7-
 r5*r8)/(r7-r5))
 →r9
92: abs((C[2]/2-
 r9)/C[2])→r10
93: if r10>.01;
 dsp "Vmax DID
 NOT CORRELATE";
 stp
94: r9*C[1]*4→r1
 1
95: Q/r11→r12
96: r12/C[5]→r13
97: Q/C[5]*(P[5]
 -P[4])→r15
98: abs((r15-
 r14)/r14)→r16
99: if r16>.1;
 dsp "TIMMING
 CHANNELS DO
 NOT CHECK";stp
100: (P[1]-1)*
 r13→T[1]
101: for K=0 to
 F[7]
102: for I=2 to
 J
103: T[I+J*K-1]+
 r12→T[I+J*K]
104: next I
105: if K=F[7];
 gto 115
106: J*(K+1)→L
107: if D[L-2]>0
  and D[L+3]>0;
 T[L]+(X[L+1]-
 X[L])/r11→T[L+
 1];gto 115
108: if D[L-2]<0
  and D[L+3]<0;
 T[L]+(X[L]-X[L+
 1])/r11→T[L+1];
 gto 115
109: if D[L-2]=0
  or D[L+3]=0;
 gto 113
110: if D[L-2]>0
 ;T[L-2]+(r9-
 X[L-2]+(r9-X[L+
 3]))/r11-2*r12→
 T[L+1];gto 115
111: T[L-2]+(r9+
 X[L-2]+(r9+X[L+
 3]))/r11-2*r12→
 T[L+1]
112: gto 115
113: if D[L-8]>0
 ;T[L-8]+(r9-
 X[L-8]+(r9-X[L+
 9]))/r11-8*r12→
 T[L+1];gto 115
```

Program F.11 Listing

```
0: dim S[6],H[2]
 ,A$[30],B$[35],
 C$[45],D$[3,
 55],G[2],Q$[5]
1: dim X$[65],
 Y$[31760],H$[4,
 55],P[8],P$[5]
2: asgn "trfil",
 2
3: buf "data",
 Y$,3
4: sread 2,P[*],
 P$
5: sread 1,X$,
 H$,Y$
6: fxd 0
7: val(X$[1,2])→
 r8
8: for I=0 to
 r8-1
9: P[1]+1→K
10: 15+I*15→J
11: if val(X$[J,
 J])=P[1]-1;val(
 X$[J-12,J-11])→
 r9;P[K]→r10
12: next I
13: P[1]→I
14: if P[I+1]=1
 and P$[1,1]#"["
 ;"POTENTIAL
 DIFFERENCE (VOL
 TS)"→C$;gto 16
15: "CURRENT
 (MICROAMPS)"→C$
16: "TIME (SECON
 DS)"→B$
17: if P[1]=1;
 "CHANNEL 1A"→A$
18: if P[1]=2;
 "CHANNEL 1B"→A$
19: if P[1]=3;
 "CHANNEL 2A"→A$
20: if P[1]=4;
 "CHANNEL 2B"→A$
21: " - SYSTEM
 # "→A$[11,22]
22: P$→A$[23,28]
23: val(H$[r9,5,
 9])*10↑val(H$[r
 9,11,13])→r1
24: val(H$[r9,
 14,18])*10↑val(
 H$[r9,20,22])→r
 2
25: val(H$[r9,
 23,28])→r3
26: val(H$[r9,
 29,34])→r4
27: val(H$[r9,
 35,40])→r5
28: val(X$[5+15*
 (r9-1),10+15*
 (r9-1)])→r6
29: val(X$[13+
 15*(r9-1),14+
 15*(r9-1)])→r7
30: ent "DO YOU
 WANT T=0 AT
 TRIGGER TIME",
 Q$
31: if cap(Q$)="
 YES";r4*65536+
 r5→T;jmp 2
32: 0→T
33: ent "IS THE
 AXIS TO BE PLOT
 TED?",Q$
34: if cap(Q$)#"
 YES";gto 134
35: flt 3
36: -T*r2→U
37: dsp "MIN X-
 VALUE IS ",U
38: wait 2000
39: ent "GRAPH
 MIN X-VALUE?",
 S[1]
40: (r6-1-T)*
 r2→S[2]
41: dsp "MIN Y-
 VALUE IS ",(-
 32000-r3)*r1*
 r10
42: wait 2000
43: ent "GRAPH
 MIN Y-VALUE?",
 S[3]
44: dsp "MAX Y-
 VALUE IS ",(320
 00-r3)*r1*r10
45: wait 2000
46: ent "GRAPH
 MAX Y-VALUE?",
 S[4]
47: dsp "MAX
 GRAPH X-VALUE
 IS ",S[2];wait
 2000
48: ent "X-TIC?"
 ,S[5]
49: ent "Y-TIC?"
 ,S[6]
50: ent "# OF
 DIGETS DSP AFTE
 R X-DECIMAL?",
 G[1]
51: ent "# OF
 DIGETS DSP AFTE
 R Y-DECIMAL?",
 G[2]
52: ent "LINE 1
 CAPTION?",D$[1]
53: ent "LINE 2
 CAPTION?",D$[2]
54: ent "LINE 3
 CAPTION?",D$[3]
55: fxd G[1]
56: S[2]-(7/5)(S
 [2]-S[1])+.2(S[
 2]-S[1])→A
57: S[2]+.2(S[2]
 -S[1])→B
58: S[4]-(8.5/
 7)(S[4]-S[3])-
 .05(S[4]-S[3])→
 C
59: S[4]+(1/7)(S
 [4]-S[3])-.05(S
 [4]-S[3])→D
60: scl A,B,C,D
61: pen
62: plt S[1],
 S[3],-2
63: (1/16/4.5)(S
 [2]-S[1])→H[1]
64: (1/16/7)(S[4
 ]-S[3])→H[2]
65: int((S[2]-
 S[1])/S[5])→M
66: int((S[4]-
 S[3])/S[6])→N
67: for I=1 to M
68: iplt S[5],0,
 0
69: iplt 0,H[2],
 0
70: iplt 0,-H[2]
 ,0
71: next I
72: plt S[2],
 S[3],0
73: for I=1 to N
74: iplt 0,S[6],
 0
75: iplt -H[1],
 0,0
76: iplt H[1],0,
 0
77: next I
78: plt S[2],
 S[4],-1
79: plt S[1],
 S[3],-2
80: for I=1 to N
81: iplt 0,S[6],
 0
82: iplt H[1],0,
 0
83: iplt -H[1],
 0,0
84: next I
85: plt S[1],
 S[4],0
86: for I=1 to M
87: iplt S[5],0,
 0
88: iplt 0,-H[2]
 ,0
89: iplt 0,H[2],
 0
90: next I
91: plt S[2],
 S[4],-1
92: csiz 1.5,2,
 1.357,0
93: for I=0 to M
94: S[1]+I*S[5]→
 U
95: -(len(str(U)
 )/2+.3)→V
96: plt U,S[3],0
97: cplt V,-1.25
98: lbl U
99: next I
100: fxd G[2]
101: for I=0 to
 N
102: S[3]+I*S[6]
 →U
103: -(len(str(U
 ))+1)→V
104: plt S[1],U,
 0
105: cplt V,-.3
106: lbl U
107: next I
108: csiz 1.5,2,
 1.357,0
109: for I=1 to
 3
110: 3-I→J
111: plt A,C,0
112: cplt 0,J
113: lbl D$[I]
114: next I
115: csiz 1.75,
 2,1.357,0
116: -(len(B$)/
 2+.3)→V
117: (S[2]-S[1])
 /2+S[1]→U
118: plt U,S[3],
 0
119: cplt V,-3
120: lbl B$
121: deg
122: csiz 1.75,
 2,1.357,90
123: -(len(C$)/
 2+.3)→V
124: (S[4]-S[3])
 /2+S[3]→U
125: plt A,U,0
126: cplt V,-1
114: T[L-8]+(r9+
 X[L-8]+(r9+X[L+
 9]))/r11-8*r12→
 T[L+1]
115: next K
116: asgn "trfil
 ",2
117: if P[2]=0;
 sprt 2,M,T[*],
 Y[*],N$,O$,R$;
 gto 119
118: sprt 2,M,
 X[*],Y[*],N$,
 O$,R$
119: ldp 9
120: end
*30769
```

Program F.12 Listing

```
127: lbl C$
128: csiz 2,2,
 1.357,0
129: -(len(A$)/
 2+.3)→V
130: (S[2]-S[1])
 /2+S[1]→U
131: plt U,D,0
132: cplt V,-1
133: lbl A$
134: ent "DO
 YOU WANT A POIN
 T PLOT?",Q$
135: cfg 1
136: if cap(Q$)#
 "YES";sfg 1
137: for J=r9
 to 15872-r8+r9
 by r7
138: (J-r9)/r7→K
139: (K-T)*r2→X
140: (itf(Y$[2*
 J-1,2*J])-r3)*
 r1*r10→Y
141: if flg1=0;
 gto 145
142: if J=15872-
 r8+r9;plt X,Y,-
 1
143: if J#15872-
 r8+r9;plt X,Y
144: gto 147
145: plt X,Y,-2
146: pen
147: next J
148: pen
149: stp ;end
*9954
```

```
0: asgn "trfil",
 2
1: dim P[8],P$[5
 ],C[10],F[9]
2: sread 2,P[*],
 P$,C[*],F[*]
3: C[5]→N
4: if F[6]>0;
 gto 24
5: F[3]→J
6: F[4]→K
7: F[5]→L
8: dim R$[J],
 S$[K],T$[L]
9: buf "data1",
 R$,4
10: buf "data2",
 S$,4
11: buf "data3",
 T$,4
12: (F[3]-16)/
 (2*N)→J
13: (F[4]-16)/
 (2*N)→K
14: (F[5]-16)/
 (2*N)→L
15: sread 1,R$
16: buf "data1"
17: sread 1,R$
18: buf "data1"
19: sread 1,S$
20: buf "data2"
21: sread 1,T$
22: buf "data3"
23: gto 32
24: F[6]→J
25: dim R$[J]
26: buf "data1",
 R$,4
27: (F[6]-16)/
 (2*N)→J
28: for K=0 to
 F[7]
29: sread 1,R$
30: buf "data1"
31: next K
32: asgn "trfil"
 ,2
33: sprt 2,P[*],
 P$
34: ldp 11
35: end
*17615
```

Program F.13 Listing

```
0: asgn "trfil",
 2
1: dim P[8],C[10
 ],F[9],R$[6]
2: sread 2,P[*],
 C[*],F[*],R$
3: C[5]→N
4: P[1]→R;P[2]→S
5: if F[6]>0;
 gto 43
6: F[3]→J
7: F[4]→K
8: F[5]→L
9: dim S$[J],
 T$[K],U$[L]
10: buf "data1",
 S$,4
11: buf "data2",
 T$,4
12: buf "data3",
 U$,4
13: (F[3]-16)/
 (2*N)→J
14: (F[4]-16)/
 (2*N)→K
15: (F[5]-16)/
 (2*N)→L
16: 2*J+K+L→M
17: dim X$[2*M],
 Z$[2*M]
18: sread 1,S$
19: for I=0 to
 J-1
20: S$[(N*I+R)*
 2-1,(N*I+R)*
 2]→X$[2*I+1,2*
 I+2]
21: S$[(N*I+S)*
 2-1,(N*I+S)*
 2]→Z$[2*I+1,2*
 I+2]
22: next I
23: buf "data1"
24: sread 1,S$
25: for I=0 to
 J-1
26: S$[(N*I+R)*
 2-1,(N*I+R)*
 2]→X$[2*(J+I)+
 1,2*(J+I)+2]
27: S$[(N*I+S)*
 2-1,(N*I+S)*
 2]→Z$[2*(J+I)+
 1,2*(J+I)+2]
28: next I
29: buf "data1"
30: sread 1,T$
31: for I=0 to
 K-1
32: T$[(N*I+R)*
 2-1,(N*I+R)*
 2]→X$[2*(2*J+
 I)+1,2*(2*J+I)+
 2]
33: T$[(N*I+S)*
 2-1,(N*I+S)*
 2]→Z$[2*(2*J+
 I)+1,2*(2*J+I)+
 2]
34: next I
35: buf "data2"
36: sread 1,U$
37: for I=0 to
 L-1
38: U$[(N*I+R)*
 2-1,(N*I+R)*
 2]→X$[2*(2*J+K+
 I)+1,2*(2*J+K+
 I)+2]
39: U$[(N*I+S)*
 2-1,(N*I+S)*
 2]→Z$[2*(2*J+K+
 I)+1,2*(2*J+K+
 I)+2]
40: next I
41: buf "data3"
42: gto 57
43: F[6]→J
44: dim S$[J]
45: buf "data1",
 S$,4
46: (F[6]-16)/
 (2*N)→J
47: (F[7]+1)*J→M
48: dim X$[2*M],
 Z$[2*M]
49: for K=0 to
 F[7]
50: sread 1,S$
51: for I=0 to
 J-1
52: S$[(N*I+R)*
 2-1,(N*I+R)*
 2]→X$[2*(I+J*
 K)+1,2*(I+J*K)+
 2]
53: S$[(N*I+S)*
 2-1,(N*I+S)*
 2]→Z$[2*(I+J*
 K)+1,2*(I+J*K)+
 2]
54: next I
55: buf "data1"
56: next K
57: asgn "trfil"
 ,2
58: sprt 2,P[*],
 C[*],F[*],R$,
 X$,Z$,"end"
59: if F[6]>0;
 ldp 15
60: ldp 14
61: end
*10561
```

Program F.14 Listing

```
0: asgn "trfil";
 2
1: dim P[8],P$[5
 ],C[10],F[9];
 N$[35],G$[45],
 R$[30]
2: sread 2,P[*];
 P$,C[*],F[*]
3: if P[3]=1
 and P$[1,1]#"["
 ;"POTENTIAL
 DIFFERENCE (VOL
 TS)"→N$;gto 5
4: "CURRENT (MIC
 ROAMPS)"→N$
5: if P[2]=0;
 "TIME (SECONDS)
 "→O$;gto 7
6: "POINT #"→O$
7: fxd 0
8: "CHANNEL #
 "→R$
9: str(P[1])→R$[
 11,14]
10: "- SYSTEM #
 "→R$[15,25]
11: P$→R$[26,30]
12: C[5]→N
13: 0→G;0→H
14: P[4]→R;P[5]→
 S
15: (F[3]-16)/
 (2*N)→J
16: (F[4]-16)/
 (2*N)→K
17: (F[5]-16)/
 (2*N)→L
18: 2*J+K+L→M
19: dim X[M],
 Y[M],Z[M],T[M],
 D[M],A[5],B[5],
 X$[2*M],Y$[2*
 M],Z$[2*M]
20: sread 2,Y$
21: if P[2]=0;
 sread 2,X$,Z$
22: for I=0 to
 J-1
23: if P[2]=1;I+
 1→X[I+1];gto 31
24: cmpitf(X$[I*
 2+1,I*2+2])*
 (.005/C[4])*
 P[6]→X[I+1]
25: cmpitf(Z$[I*
 2+1,I*2+2])*
 (.005/C[4])*
 P[7]→Z[I+1]
26: if I<=3;gto
 31
27: (-X[I+1]+8*
 X[I]-8*X[I-2]+
 X[I-3])/12→D[I-
 1]
28: if I<=4;gto
 31
29: if D[I-1]>0
 and D[I-2]<0;I-
 2→A[G+1];G+1→G
30: if D[I-1]<0
 and D[I-2]>0;I-
 2→B[H+1];H+1→H
31: cmpitf(Y$[I*
 2+1,I*2+2])*
 (.005/C[4])*
 P[3]→Y[I+1]
32: next I
33: 0→D[1];0→D[2
 ];0→D[J-1];0→D[
 J]
34: for I=0 to
 J-1
35: if P[2]=1;J+
 I+1→X[J+I+1];
 gto 43
36: cmpitf(X$[(I
 +J)*2+1,(I+J)*
 2+2])*(.005/
 C[4])*P[6]→X[J+
 I+1]
37: cmpitf(Z$[(I
 +J)*2+1,(I+J)*
 2+2])*(.005/
 C[4])*P[7]→Z[J+
 I+1]
38: if I<=3;gto
 43
39: (-X[J+I+1]+
 8*X[J+I]-8*X[J+
 I-2]+X[J+I-3])/
 12→D[J+I-1]
40: if I<=4;gto
 43
41: if D[J+I-
 1]>0 and D[I+J-
 2]<0;J+I-2→A[G+
 1];G+1→G
42: if D[J+I-
 1]<0 and D[I+J-
 2]>0;J+I-2→B[H+
 1];H+1→H
43: cmpitf(Y$[(I
 +J)*2+1,(I+J)*
 2+2])*(.005/
 C[4])*P[3]→Y[J+
 I+1]
44: next I
45: 0→D[J+1];
 0→D[J+2];0→D[2*
 J-1];0→D[2*J]
46: for I=0 to
 K-1
47: if P[2]=1;2*
 J+I+1→X[2*J+I+
 1];gto 55
48: cmpitf(X$[(2
 *J+I)*2+1,(2*J+
 I)*2+2])*(.005/
 C[4])*P[6]→X[2*
 J+I+1]
49: cmpitf(Z$[(2
 *J+I)*2+1,(2*J+
 I)*2+2])*(.005/
 C[4])*P[7]→Z[2*
 J+I+1]
50: if I<=3;gto
 55
51: (-X[2*J+I+
 1]+8*X[2*J+I]-
 8*X[2*J+I-2]+
 X[2*J+I-3])/
 12→D[2*J+I-1]
52: if I<=4;gto
 55
53: if D[2*J+I-
 1]>0 and D[2*J+
 I-2]<0;2*J+I-
 2→A[G+1];G+1→G
54: if D[2*J+I-
 1]<0 and D[2*J+
 I-2]>0;2*J+I-
 2→B[H+1];H+1→H
55: cmpitf(Y$[(2
 *J+I)*2+1,(2*J+
 I)*2+2])*(.005/
 C[4])*P[3]→Y[2*
 J+I+1]
56: next I
57: 0→D[2*J+1];
 0→D[2*J+2];0→D[
 2*J+K-1];0→D[2*
 J+K]
58: for I=0 to
 L-1
59: if P[2]=1;2*
 J+K+I+1→X[2*J+
 K+I+1];gto 67
60: cmpitf(X$[(2
 *J+K+I)*2+1,(2*
 J+K+I)*2+2])*
 (.005/C[4])*
 P[6]→X[2*J+K+I+
 1]
61: cmpitf(Z$[(2
 *J+K+I)*2+1,(2*
 J+K+I)*2+2])*
 (.005/C[4])*
 P[7]→Z[2*J+K+I+
 1]
62: if I<=3;gto
 67
63: (-X[2*J+K+I+
 1]+8*X[2*J+K+
 I]-8*X[2*J+K+I-
 2]+X[2*J+K+I-
 3])/12→D[2*J+K+
 I-1]
64: if I<=4;gto
 67
65: if D[2*J+K+
 I-1]>0 and D[2*
 J+K+I-2]<0;2*J+
 K+I-2→A[G+1];G+
 1→G
66: if D[2*J+K+
 I-1]<0 and D[2*
 J+K+I-2]>0;2*J+
 K+I-2→B[H+1];H+
 1→H
67: cmpitf(Y$[(2
 *J+K+I)*2+1,(2*
 J+K+I)*2+2])*
 (.005/C[4])*
 P[3]→Y[2*J+K+I+
 1]
68: next I
69: 0→D[2*J+K+
 1];0→D[2*J+K+
 2];0→D[2*J+K+L-
 1];0→D[2*J+K+L]
70: if P[2]=1;
 gto 169
71: 0→U
72: cfg 1
73: if G=0;gto
 83
74: for I=1 to G
75: A[I]→E
76: if flg1=1;
 gto 79
77: if E>2*J+15
 and E<2*J+K-15;
 sfg 1;E→U
78: if E>2*J+K+
 15 and E<2*J+K+
 L-15;sfg 1;E→U
79: for F=E-2
 to E+3
80: 0→D[F]
81: next F
82: next I
83: cfg 2
84: 0→V
85: if flg1=1;
 sfg 2
86: if H=0;gto
 96
87: for I=1 to H
88: B[I]→E
89: if flg2=1;
 gto 92
90: if E>2*J+15
 and E<2*J+K-15;
 sfg 2;E→V
91: if E>2*J+K+
 15 and E<2*J+K+
 L-15;sfg 2;E→V
92: for F=E-2
 to E+3
93: 0→D[F]
94: next F
95: next I
96: 0→Q;0→r14;
 M→r18
97: for I=1 to M
98: Q+abs(D[I])→
 Q
99: if D[I]=0;
 r18-1→r18;0→T[I
 ];gto 102
100: abs(X[I]-
 Z[I])→T[I]
101: r14+T[I]→r1
 4
102: next I
103: Q/r18→Q
104: r14/r18→r14
105: if V#0;V→U
106: if U=0;dsp
 "NO MAX OR MIN
 RECORDED";wait
 2000;C[2]/2+r9;
 gto 128
107: 0→r1;0→r2;
 0→r3;0→r4
108: for I=U-12
 to U-3
109: r1+I*X[I]→r
 1
110: r2+I→r2
111: r3+X[I]→r3
112: r4+I*I→r4
113: next I
114: (10*r1-r2*
 r3)/(10*r4-r2*
 r2)→r5
115: r3/10-r5*
 r2/10→r6
116: 0→r1;0→r2;
 0→r3;0→r4
117: for I=U+4
 to U+13
118: r1+I*X[I]→r
 1
119: r2+I→r2
120: r3+X[I]→r3
121: r4+I*I→r4
122: next I
123: (10*r1-r2*
 r3)/(10*r4-r2*
 r2)→r7
124: r3/10-r7*
 r2/10→r8
125: abs((r6*r7-
 r5*r8)/(r7-r5))
 →r9
126: abs((C[2]/
 2-r9)/C[2])→r10
127: if r10>.01;
 dsp "Vmax DID
 NOT CORRELATE";
 stp
128: r9*C[1]*
 4→r11
129: Q/r11→r12
130: r12/C[5]→r1
 3
131: Q/C[5]*(P[5
 ]-P[4])→r15
132: abs((r15-
 r14)/r14)→r16
133: if r16>.1;
 dsp "TIMMING
 CHANNELS DO
 NOT CHECK";stp
134: (P[1]-1)*
 r13→T[1]
```

Program F.15 Listing

```
0: asgn "trfil",
 2
1: dim P[8],C[10
 ],F[9],R$[6]
2: sread 2,P[*],
 C[*],F[*],R$
3: C[5]→N
4: 0→G;0→H
5: P[1]→R;P[2]→S
6: (F[6]-16)/(2*
 N)→J
7: (F[7]+1)*J→M
8: dim X[M],Z[M]
 ,T[M],D[M],A[5]
 ,B[5],X$[2*M],
 Z$[2*M]
9: sread 2,X$,Z$
10: for K=0 to
 F[7]
11: for I=0 to
 J-1
12: cmpitf(X$[(I
 +J*K)*2+1,(I+J*
 K)*2+2])*(.005/
 C[4])*P[3]+X[I+
 J*K+1]
13: cmpitf(Z$[(I
 +J*K)*2+1,(I+J*
 K)*2+2])*(.005/
 C[4])*P[4]→Z[I+
 J*K+1]
14: if I<=3;gto
 19
15: (-X[I+J*K+
 1]+8*X[I+J*K]-
 8*X[I+J*K-2]+
 X[I+J*K-3])/
 12→D[I+J*K-1]
16: if I<=4;gto
 19
17: if D[I+J*K-
 1]>0 and D[I+J*
 K-2]<0;I+J*K-
 2→A[G+1];G+1→G
18: if D[I+J*K-
 1]<0 and D[I+J*
 K-2]>0;I+J*K-
 2→B[H+1];H+1→H
19: next I
20: 0→D[J*K+1];
 0→D[J*K+2];0→D[
 (K+1)*J-1];0→D[
 (K+1)*J]
21: next K
22: 0→U
23: cfg 1
24: if G=0;gto
 35
25: for I=1 to G
26: A[I]→E
27: if flg1=1;
 gto 31
28: for K=0 to
 F[7]
29: if E>K*J+15
 and E<J*(K+1)-
 15;sfg 1;E→U
30: next K
31: for F=E-2
 to E+3
32: 0→D[F]
33: next F
34: next I
35: cfg 2
36: 0→V
37: if flg1=1;
 sfg 2
38: if H=0;gto
 49
39: for I=1 to H
40: B[I]→E
41: if flg2=1;
 gto 45
42: for K=0 to
 F[7]
43: if E>K*J+15
 and E<(K+1)*J-
 15;sfg 2;E→V
44: next K
45: for F=E-2
 to E+3
46: 0→D[F]
47: next F
48: next I
49: 0→Q;0→r14
50: for I=1 to M
51: Q+abs(D[I])→
 Q
52: if D[I]=0;
 0→T[I];gto 55
53: abs(X[I]-
 Z[I])→T[I]
54: r14+T[I]→r14
55: next I
56: Q/(M-6*(G+
 H)-4*F[7])→Q
57: r14/(M-6*(G+
 H)-4*F[7])→r14
58: if V≠0;V→U
59: if U=0;dsp
 "NO MAX OR MIN
 RECORDED";wait
 2000;C[2]/2→r9;
 gto 81
60: 0→r1;0→r2;
 0→r3;0→r4
61: for I=U-12
 to U-3
62: r1+I*X[I]→r1
63: r2+I→r2
64: r3+X[I]→r3
65: r4+I*I→r4
66: next I
67: (10*r1-r2*
 r3)/(10*r4-r2*
 r2)→r5
68: r3/10-r5*r2/
 10→r6
69: 0→r1;0→r2;
 0→r3;0→r4
70: for I=U+4
 to U+13
71: r1+I*X[I]→r1
72: r2+I→r2
73: r3+X[I]→r3
74: r4+I*I→r4
75: next I
76: (10*r1-r2*
 r3)/(10*r4-r2*
 r2)→r7
77: r3/10-r7*r2/
 10→r8
78: abs((r6*r7-
 r5*r8)/(r7-r5))
 →r9
79: abs((C[2]/2-
 r9)/C[2])→r10
80: if r10>.01;
 dsp "Vmax DID
 NOT CORRELATE";
 stp
81: r9*C[1]*4→r1
 1
82: Q/r11→r12
83: r12/C[5]→r13
84: Q/C[5]*(P[2]
 -P[1])→r15
85: abs((r15-
 r14)/r14)→r16
86: if r16>.1;
 dsp "TIMMING
 CHANNELS DO
 NOT CHECK";stp
87: (P[1]-1)*
 r13→T[1]
88: for K=0 to
 F[7]
89: for I=2 to J
90: T[I+J*K-1]+
 r12→T[I+J*K]
91: next I
92: if K=F[7];
 gto 102
93: J*(K+1)→L
94: if D[L-2]>0
 and D[L+3]>0;
 T[L]+(X[L+1]-
 X[L])/r11→T[L+
 1];gto 102
95: if D[L-2]<0
 and D[L+3]<0;
 T[L]+(X[L]-X[L+
 1])/r11→T[L+1];
 gto 102
96: if D[L-2]=0
 or D[L+3]=0;
 gto 100
97: if D[L-2]>0;
 T[L-2]+(r9-X[L-
 2]+(r9-X[L+3]))
 /r11-2*r12→T[L+
 1];gto 102
98: T[L-2]+(r9+
 X[L-2]+(r9+X[L+
 3]))/r11-2*r12→
 T[L+1]
99: gto 102
100: if D[L-5]>0
 ;T[L-5]+(r9-
 X[L-5]+(r9-X[L+
 6]))/r11-5*r12→
 T[L+1];gto 102
101: T[L-5]+(r9+
 X[L-5]+(r9+X[L+
 6]))/r11-5*r12→
 T[L+1]
102: next K
103: if P[5]<T[2
 ];dsp "TIME
 TOO SHORT";stp
104: for I=3 to
 M
105: if T[I]>=P[
 5];gto 108
106: next I
107: dsp "TIME
 TOO LONG";stp
108: T[I-2]→P[6]
109: T[I-1]→P[7]
110: T[I]→P[8]
111: asgn "trfil
 ",2
112: sprt 2,I,
 r13,P[*],R$,
 "end"
113: ldp 16
114: end
*11460
```

Program F.16 Listing

```
0: asgn "trfil",
 2
1: dim P[8],R$[6
 ]
2: sread 2,I,D,
 P[*],R$
3: asgn R$,1
4: dim E$[128,
 5],E[128],A[10]
 ,B[5],B$[4,5],
 C[10],F[9],F$[1
 0,5],G$[80]
5: sread 1,E$,
 E[*],A[*],B[*],
 B$,C[*],F[*],
 F$,G$,R$
6: C[5]→N
7: if F[6]>0;
 gto 78
8: F[3]→J
9: F[4]→K
10: F[5]→L
11: dim U$[L]
12: buf "data1",
 U$,4
13: (F[3]-16)/
 (2*N)→J
14: (F[4]-16)/
 (2*N)→K
15: (F[5]-16)/
 (2*N)→L
16: 2*J+K+L→M
17: dim Y$[3,2*
 N]
18: cfg 1;cfg 2
19: F[3]-16→O
20: sread 1,U$[1
 ,0]
21: if I-2>J;
 gto 32
22: if I-1>J;
 sfg 1;I-2→Q;
 gto 25
23: if I>J;sfg
 2;I-1→Q;gto 25
24: I→Q
25: for O=I-2
 to Q
26: for R=1 to N
27: U$[(N*O+R)*
 2-1,(N*O+R)*
 2]→Y$[O-(I-3),
 2*R-1,2*R]
28: next R
29: next O
30: if flg1=1
 or flg2=1;gto
 32
31: gto 103
32: buf "data1"
33: F[3]-16→O
34: sread 1,U$[1
 ,0]
35: if flg1=1;I-
 1→S;gto 41
36: if flg2=1;
 I→S;gto 41
37: I-2→S
38: if I-2>2*J;
 gto 49
39: if I-1>2*J;
 sfg 1;I-2→Q;
 gto 42
40: if I>2*J;
 sfg 2;I-1→Q;
 gto 42
41: I→Q
42: for O=S to Q
43: for R=1 to N
44: U$[(N*(O-J)+
 R)*2-1,(N*(O-
 J)+R)*2]→Y$[O-
 (I-3),2*R-1,2*
 R]
45: next R
46: next O
47: if flg1=1
 or flg2=1;gto
 49
48: gto 103
49: buf "data1"
50: F[4]-16→O
51: sread 1,U$[1
 ,0]
52: if flg1=1;I-
 1→S;gto 58
53: if flg1=2;
 I→S;gto 58
54: I-2→S
55: if I-2>2*J+
 K;gto 66
56: if I-1>2*J+
 K;sfg 1;I-2→Q;
 gto 59
57: if I>2*J+K;
 sfg 2;I-1→Q;
 gto 59
58: I→Q
59: for O=S to Q
60: for R=1 to N
61: U$[(N*(O-2*
 J)+R)*2-1,(N*
 (O-2*J)+R)*2]→Y
 $[O-(I-3),2*R-
 1,2*R]
62: next R
63: next O
64: if flg1=1
 or flg2=1;gto
 66
65: gto 103
66: buf "data1"
67: sread 1,U$
68: if flg1=1;I-
 1→S;gto 71
69: if flg2=1;
 I→S;gto 71
70: I-2→S
71: for O=S to I
72: for R=1 to N
73: U$[(N*(O-2*
 J-K)+R)*2-1,(N*
 (O-2*J-K)+R)*
 2]→Y$[O-(I-3),
 2*R-1,2*R]
74: next R
75: next O
76: buf "data1"
77: gto 103
78: F[6]→J
79: dim S$[J]
80: buf "data1",
 S$,4
81: (F[6]-16)/
 (2*N)→J
82: (F[7]+1)*J→M
83: dim Y$[3,2*
 N]
84: cfg 1;cfg 2;
 cfg 3
85: for K=1 to
 F[7]+1
86: sread 1,S$
87: if flg1=1;I-
 1→S;gto 93
88: if flg2=1;
 I→S;gto 93
89: I-2→S
90: if I-2>J*K;
 gto 100
91: if I-1>J*K;
 sfg 1;I-2→Q;
 gto 94
92: if I>J*K;
 sfg 2;I-1→Q;
 gto 94
93: I→Q
94: for O=S to Q
95: for R=1 to N
96: O-(K-1)*J→V
97: S$[(N*V+R)*
 2-1,(N*V+R)*
 2]→Y$[O-(I-3),
 2*R-1,2*R]
98: next R
99: next O
100: buf "data1"
101: if Q=I;gto
 103
102: next K
103: asgn "trfil
 ",2
104: sprt 2,P[*
 ],C[*],D,E[*],
 E$,Y$,"end"
105: ldp 17
106: end
*13304
```

Program F.17 Listing

```
0: asgn "trfil",
 2
1: dim H[3],H$[3
 ,60],P[8],C[10]
 ,E[128],E$[128,
 5]
2: sread 2,P[*],
 C[*],D,E[*],E$
3: C[5]→N
4: dim Q$[5],
 J$[4],K$[4],
 T[3],Y[3],Y$[3,
 2*N],X[4],L$[4,
 55]
5: sread 2,Y$
6: cfg 1;cfg 2;
 cfg 3;cfg 4;
 cfg 5;cfg 6
7: ent "MAXIMUM
 CURRENT (MICROA
 MPS)?",H[1]
8: ent "CURRENT
 INCREMENT (MICR
 OAMPS)?",H[2]
9: ent "DECIMAL
 PLACES?",H[3]
10: fxd 2
11: "TIME OF
 CURRENT DISTRIB
 UTION IS "→L$[1
 ,1,32]
12: len(str(P[5]
 ))→I
13: str(P[5])→L$
 [1,33,33+I]
14: "SECONDS"→L$
 [1,34+I,43+I]
15: ent "LINE
 #2 OF CAPTION",
 L$[2]
16: ent "LINE
 #3 OF CAPTION",
 L$[3]
17: ent "LINE
 #4 OF CAPTION",
 L$[4]
18: 1000+r6
19: r6*(cos(10)+
 cos(45))/5+r5
20: -(.25*r5+r6*
 cos(45))→r1
21: r5*7+r1→r2
22: -8.5*r5+r6→r
 3
23: r6+r5→r4
24: scl r1,r2,
 r3,r4
25: pen
26: plt 0,0,-2
27: plt 'tranx'(
 0,1000,0),'tran
 y'(0,1000,0)
28: iplt 'tranx'
 (0,20,0),'trany
 '(0,20,0)
29: iplt 'tranx'
 (0,-20,0),'tran
 y'(0,-20,0)
30: for J=1 to
 10
31: iplt 'tranx'
 (0,0,100),'tran
 y'(0,0,100)
32: iplt 'tranx'
 (0,20,0),'trany
 '(0,20,0)
33: iplt 'tranx'
 (0,-20,0),'tran
 y'(0,-20,0)
34: next J
35: for J=1 to
 10
```

Program F.18 Listing

```
36: iplt 'tranx'
 (0,0,20),'tran
 y'(0,0,20)
37: iplt 'tranx'
 (0,0,-20),'tran
 y'(0,0,-20)
38: iplt 'tranx'
 (0,-100,0),'tra
 ny'(0,-100,0)
39: next J
40: H[2]/H[1]*
 1000→r7
41: for J=r7 to
 1000 by r7
42: iplt 'tranx'
 (r7,0,0),'tranx
 '(r7,0,0)
43: iplt 20,0
44: iplt -20,0
45: next J
46: plt 'tranx'(
 1000,0,1000),
 'trany'(1000,0,
 1000)
47: plt 'tranx'(
 1000,0,0),'tran
 y'(1000,0,0)
48: plt 0,0
49: plt 'tranx'(
 0,0,1000),'tran
 y'(0,0,1000)
50: pen
51: fxd 0
52: csiz 1.25,2,
 1.357,-10
53: for J=0 to
 10
54: -(len(str(J)
 )/2+.3)→r8
55: plt 'tranx'(
 0,1020,J*100),
 'trany'(0,1020,
 J*100),0
56: cplt r8,-1
57: lbl J
58: next J
59: csiz 1.25,2,
 1.357,0
60: for J=0 to 9
61: 10-J→K
62: plt 'tranx'(
 0,K*100,1020),
 'trany'(0,K*
 100,1020),0
63: cplt .2,-.3
64: lbl K
65: next J
66: csiz 1.25,2,
 1.357,0
67: fxd H[3]
68: for J=r7 to
 1000 by r7
69: plt 'tranx'(
 J,0,1020),'tran
 y'(J,0,1020),0
70: cplt .2,-.3
71: J/r7*H[2]→r8
72: lbl r8
73: next J
74: csiz 1.5,2,
 1.357,-10
75: plt 'tranx'(
 0,1200,250),
 'trany'(0,1200,
 250),0
76: lbl "ELECTRO
 DE POSITION"
77: plt 'tranx'(
 0,1200,250),
 'trany'(0,1200,
 250),0
78: cplt 3,-1
79: lbl "X100
 MICRONS"
80: csiz 1.5,2,
 1.357,45
81: plt 'tranx'(
 0,900,1200),
 'trany'(0,900,
 1200),0
82: lbl "ELECTRO
 DE POSITION"
83: plt 'tranx'(
 0,900,1200),
 'trany'(0,900,
 1200),0
84: cplt 3,-1
85: lbl "X100
 MICRONS"
86: csiz 1.5,2,
 1.357,90
87: plt 'tranx'(
 200,0,r2),'tran
 y'(200,0,r2),0
88: cplt 0,3
89: lbl "CURRENT
  TO A SEGMENT"
90: plt 'tranx'(
 200,0,r2),'tran
 y'(200,0,r2),0
91: cplt 5.5,2
92: lbl "MICROAM
 PS"
93: csiz 2,2,
 1.357,0
94: plt r1,r4,0
95: cplt 3,-1
96: lbl "CURRENT
  DISTRIBUTION
 ON MOSAIC ELECT
 RODE"
97: csiz 1.75,2,
 1.357,0
98: for I=1 to 4
99: 5-I→K
100: plt r1,r3,0
101: cplt 0,K
102: lbl L$[I]
103: next I
104: ent "PLOT
 ABSOLUTE VALUES
 ?",Q$
105: if cap(Q$)=
 "YES":sf 3;
 gto 108
106: ent "PLOT
 THE NEGATIVE
 OF THE VALUES?"
 ,Q$
107: if cap(Q$)=
 "YES":sf 4
108: ent "LEAVE
 OUT MAX & MIN
 VALUES?",Q$
109: if cap(Q$)=
 "YES":sf 5
110: fxd 0
111: for J=1 to
 10
112: for I=1 to
 10
113: if I=10;
 0→K;" 0"→K$[1,
 2];jmp 2
114: str(I)→K$[1
 ,2];I→K
115: if J=10;
 0→L;" 0"→K$[3,
 4];jmp 2
116: str(J)→K$[3
 ,4];J→L
117: if fl2=0;
 gto 121
118: K$→J$
119: J$[1,2]→K$[
 3,4]
120: J$[3,4]→K$[
 1,2]
121: for M=1 to
 N
122: if E$[M,2,
 2]=K$[2,2] and
 E$[M,4,4]=K$[4,
 4];gto 125
123: next M
124: if M=N+1;
 pen;gto 147
125: for O=1 to
 3
126: P[5+O]+(M-
 1)*D→T[O]
127: cmpitf(Y$[O
 ,2*M-1,2*M])*
 (.005/C[4])*
 E[M]→Y[O]
128: if fl3=1;
 abs(Y[O])→Y[O]
129: if fl4=1;-
 Y[O]→Y[O]
130: next O
131: 3→O
132: if P[5]<T[2
 ];2→O
133: Y[O-1]+(T[O
 ]-P[5])/(T[O]-
 T[O-1])*(Y[O]-
 Y[O-1])→V
134: V/H[1]*1000
 →r9
135: cf 6
136: if r9>1000
 or r9<10;sf 6
137: if fl5=1
 and fl6=1;pen;
 gto 147
138: if fl2=1;
 gto 143
139: if K$[2,
 2]="1" and K$[4
 ,4]="1";r9→X[1]
140: if K$[2,
 2]="0" and K$[4
 ,4]="1";r9→X[2]
141: if K$[2,
 2]="0" and K$[4
 ,4]="0";r9→X[3]
142: if K$[2,
 2]="1" and K$[4
 ,4]="0";r9→X[4]
143: if fl2=0;
 gto 146
144: plt 'tranx'
 (r9,100*J-50,
 100*I-50),'tran
 y'(r9,100*J-50,
 100*I-50),-2
145: gto 147
146: plt 'tranx'
 (r9,100*I-50,
 100*J-50),'tran
 y'(r9,100*I-50,
 100*J-50),-2
147: next I
148: pen
149: next J
150: if fl2=0;
 sf 2;gto 110
151: plt 'tranx'
 (0,50,50),'tran
 y'(0,50,50),-2
152: plt 'tranx'
 (X[1],50,50),
 'trany'(X[1],
 50,50),-2
153: plt 'tranx'
 (0,50,50),'tran
 y'(0,50,50),-2
154: plt 'tranx'
 (0,950,50),'tra
 ny'(0,950,50),-
 2
155: plt 'tranx'
 (X[2],950,50),
 'trany'(X[2],
 950,50),-2
156: plt 'tranx'
 (0,950,50),'tra
 ny'(0,950,50),-
 2
157: plt 'tranx'
 (0,950,950),
 'trany'(0,950,
 950),-2
158: plt 'tranx'
 (X[3],950,950),
 'trany'(X[3],
 950,950),-2
159: plt 'tranx'
 (0,950,950),
 'trany'(0,950,
 950),-2
160: plt 'tranx'
 (0,50,950),'tra
 ny'(0,50,950),-
 2
161: plt 'tranx'
 (X[4],50,950),
 'trany'(X[4],
 50,950),-2
162: plt 'tranx'
 (0,50,950),'tra
 ny'(0,50,950),-
 2
163: plt 'tranx'
 (0,50,50),'tran
 y'(0,50,50),-2
164: pen
165: end
166: "tranx":ret
  p3*cos(10)-p2*
 sin(45)
167: "trany":ret
  p1-p3*sin(10)-
 p2*cos(45)
*5733
```

BLANK PAGE

Appendix G

Equilibrium Bubble Shape Program

The program is written in a Hewlett Packard Language (HPL) for a desktop computer and digital plotter previously described (Section 2.3.3). The program is listed in listing G.1.

The Runge-Kutta numerical method basically integrates a system of first order nonlinear coupled differential equations. The equations can be transformed into such a system by substituting Equations 3.2.8 and 3.2.9 into Equation 3.2.2 and redefining the dependent variables, given by Equations G.1-3.

$$\tilde{z} = f(\tilde{s}) \tag{G.1}$$

$$\tilde{x} = h(\tilde{s}) \tag{G.2}$$

$$\frac{d\tilde{z}}{d\tilde{s}} = g(\tilde{s}) \tag{G.3}$$

The set of equations to be solved are then given by Equations G.4-6.

$$\frac{dg}{d\tilde{s}} = [2 + \lambda f - g/h](1 - g^2)^{1/2} \tag{G.4}$$

$$\frac{df}{d\tilde{s}} = g \tag{G.5}$$

$$\frac{dh}{d\tilde{s}} = (1 - g^2)^{1/2} \tag{G.6}$$

The initial boundary conditions are now given by Equations G.7-9.

$$g = 0 \tag{G.7}$$

$$f = 0 \tag{G.8}$$

$$h = 0 \tag{G.9}$$

All the parameters needed for a specific solution of the equations are entered in response to prompts from the computer. The shape of the bubble will then be plotted on the digital plotter. Along with the bubble shape, the user obtains a printed output of various calculated bubble quantities such as the maximum bubble radius, the bubble height, the bubble volume, and either the contact angle or the contact area radius.

```
0: dsp "BUBBLE
 PLOT PROGRAM"
1: wait 3000
2: flt 4
3: dim Z[2],X[2]
 ,F[5],G[5],H[5]
 ,K[3,4]
4: dim P[101],
 Q[101],L[101],
 Q$[5]
5: 0→V;0→Z[1];
 0→X[1];1→J;0→F[
 1];0→G[1];0→H[1
 ];0→O
6: 1→T;1→K;0→P[1
 ];0→Q[1];180→L[
 1]
7: 0→r6
8: (r2-1)/2→A
9: (2-r2)/2→B
10: -r2/2→C
11: 1+r2/2→D
12: spc 3
13: prt "INPUT
 DATA"
14: spc 2
15: enp "WHAT
 IS BETA?",L
16: spc
17: enp "WHAT
 IS R?",R
18: spc
19: enp "DIMENSI
 ONLESS STEP
 SIZE(0.01)?",W
20: W→S
21: spc
22: ent "SET
 CONTACT ANGLE-
 1 OR RADIUS-
 2?",Q
23: if Q≠1 and
 Q≠2;jmp -1
24: if Q=2;gto
 28
25: enp "CONTACT
  ANGLE IN DEGRE
 ES?",U
26: sin(180-U)→U
27: gto 29
28: enp "CONTACT
  AREA RADIUS?",
 U
29: ent "PLOT
 CONTACT ANGLE?"
 ,Q$
30: if cap(Q$)="
 YES";isf 5
31: spc
32: enp "MAXIMUM
  X ON PLOT?",r1
33: spc
34: enp "MAXIMUM
  Z ON PLOT?",r2
35: scl -r1,r1,-
 r2,0
36: spc
37: enp "XTIC?",
 r3
38: spc
39: enp "ZTIC?",
 r4
40: spc 3
41: prt "OUTPUT
 RESULTS";spc 2
42: axe 0,0,r3,
 r4
43: pen
44: plt 0,0,-2
45: 0→Y
46: plt X[1],Y,2
47: if J<101;
 gto 70
48: pen
49: plt P[1],
 Q[1],-2
50: for I=2 to J
51: plt P[I],
 Q[I],2
52: next I
53: if fl5=0;
 gto 59
54: pen
55: plt L[1],
 Q[1],-2
56: for I=1 to J
57: plt L[I],
 Q[I],2
58: next I
59: P[J]→P[1];
 Q[J]→Q[1];L[J]→
 L[1];1→J
60: pen
61: plt X[1],Y,-
 2
62: if fl9=1;
 gto 115
63: gto 70
64: if K<3;S*
 .1→S;K+1→K;gto
 70
65: -T→T;1-abs(1
 -G[1])→G[1];
 prt "BUBBLE
 RADIUS = ",X[1]
 ,"UNITS"
66: W→S;1→K
67: gto 70
68: if K<3;S*
 .1→S;K+1→K;gto
 70
69: W→S;1→K;gto
 115
70: for I=1 to 4
71: if G[I]>1;
 gto 64
72: if Q=2;gto
 76
73: if T=-1 and
 U=1;gto 115
74: if T=-1 and
 G[I]<U;gto 68
75: gto 77
76: if T=-1 and
 H[I]*R<U;gto 68
77: if fl2=0;
 sfg 2;S→K[1,I];
 gto 79
78: S*T*((2+L*
 F[I]-G[I]/H[I])
 *r(1-G[I]*G[I])
 )→K[1,I]
79: S*G[I]→K[2,
 I]
80: T*S*r(1-G[I]
 *G[I])→K[3,I]
81: if I>1;gto
 86
82: G[1]+K[1,1]/
 2→G[2]
83: F[1]+K[2,1]/
 2→F[2]
84: H[1]+K[3,1]/
 2→H[2]
85: gto 95
86: if I>2;gto
 91
87: G[1]+A*K[1,
 1]+B*K[1,2]→G[3
 ]
88: F[1]+A*K[2,
 1]+B*K[2,2]→F[3
 ]
89: H[1]+A*K[3,
 1]+B*K[3,2]→H[3
 ]
90: gto 95
91: if I>3;gto
 95
92: G[1]+C*K[1,
 2]+D*K[1,3]→G[4
 ]
93: F[1]+C*K[2,
 2]+D*K[2,3]→F[4
 ]
94: H[1]+C*K[3,
 2]+D*K[3,3]→H[4
 ]
95: next I
96: G[1]+(K[1,
 1]+K[1,2])/6+
 (K[1,3]+K[1,
 4])/3→G[5]
97: F[1]+(K[2,
 1]+K[2,2])/6+
 (K[2,3]+K[2,
 4])/3→F[5]
98: H[1]+(K[3,
 1]+K[3,2])/6+
 (K[3,3]+K[3,
 4])/3→H[5]
99: J+1→J
100: H[5]*R→X[2]
101: F[5]*R→Z[2]
102: π/2*(Z[2]-
 Z[1])*(X[1]↑2+
 X[2]↑2)→r7
103: V+r7→V
104: r6+π/2*(Z[2
 ]-Z[1])*(Z[1]*
 X[1]↑2+Z[2]*
 X[2]↑2)→r6
105: X[2]→X[1];
 Z[2]→Z[1];F[5]→
 F[1];G[5]→G[1];
 H[5]→H[1]
106: -Z[1]→Y
107: if T=-1;
 0→r5;jmp 2
108: 180→r5
109: -X[1]→P[J];
 Y→Q[J];(r5-T*
 asn(G[1]))*(r1/
 180)→L[J]
110: O+S*R→O
111: if Q=2;gto
 114
112: if T=1 or
 U<G[1];gto 46
113: gto 115
114: if T=1 or
 U<X[1];gto 46
115: if fl9=0;
 sfg 1;gto 48
116: pen
117: if fl5=1;
 axe 0,Y,r1/18;
 jmp 2
118: axe 0,Y
119: spc
120: prt "BUBBLE
  HEIGHT = ",-Y,
 " UNITS"
121: spc
122: if Q=1;gto
 126
123: L[J]*(180/
 r1)→P
124: prt "CONTAC
 T ANGLE = ",P,
 " DEGREES"
125: gto 128
126: if X[1]<0;
 0→X[1]
127: prt "RADIUS
  OF CONTACT
 AREA = ",X[1],
 " UNITS"
128: spc
129: prt "ARC
 LENGTH = ",O,"
 UNITS"
130: spc
131: prt "VOLUME
  = ",V,"UNITS↑3
 "
132: spc
133: r6/V→r6
134: prt "Z VALU
 E OF THE CENTER
  OF MASS = ",
 r6," UNITS"
135: spc
136: (3*V/π/4)↑(
 1/3)→r8
137: prt "RADIUS
  OF BUBBLE AFTE
 R RELEASE = ",
 r8," UNITS"
138: spc 3
139: stp ;end
*30542
```

Program G.1 Listing.

Appendix H

Bubble Release Program

The program is written in FORTRAN and was executed on a CDC7600 computer. The program is listed in listing H.1.

Besides the physical parameters of the system such as viscosity, density, the diffusion coefficient and the bulk concentration there is a relatively small number of adjustable parameters for a bubble of a fixed diameter. The length of time before the release of the bubble and the initial and final distance from the bubble to the electrode must be set.

Equations 3.3.14 and 3.3.15 are written in the Crank-Nicolson symmetric finite difference form at each mesh point. The resulting system of algebraic equations is solved at each time step using successive overrelaxation (49).

All relevant quantities are printed in the output. The Reynolds number is printed every time step. The current distribution is printed every ten time steps, while the concentration and velocity distribution is printed every 100 steps.

Program H.1 Listing.

```
      PROGRAM BUBREL (INPUT,OUTPUT)
      DIMENSION Y(3)
      COMMON/SET1/IMAX,JMAX,ISOR,MAXSOR,GC(40,40),EC(40,40),HC(40,40),
     1FC(40,40),RC(40,40,3),K,WSOR/SET2/ALPHA,DELTA,U,SIG,VISE,DENE,DEN
     2I,G,ARAD/SET3/DINT,RT,DELT,D(3),T,CORD,DELN,RRN,RN,DELE,
     3VN(40,40,3),VE(40,40,3),E,RE,PI,KMAXAR,KMAXBR,TREL
      READ 1,DIFF,DENE,DENI,VISE,VISI,ARAD,CINT,NEL
    1 FORMAT(4E20.13,/,3E20.13,I5)
      READ 2,DINT,DFIN,TREL
    2 FORMAT(3E20.13)
      READ 3,IMAX,JMAX,KMAXBR,KMAXAR
    3 FORMAT(4I3)
      READ 4,WSOR,MAXSOR,JSKIP,KFST
    4 FORMAT(F5.2,3I3)
      PRINT 1,DIFF,DENE,DENI,VISE,VISI,ARAD,CINT,NEL
      PRINT 2,DINT,DFIN,TREL
      PRINT 4,WSOR,MAXSOR,JSKIP,KFST
      IF(JSKIP.EQ.1) GO TO 80
      READ 120,((RC(I,J,KMAXBR),J=1,JMAX),I=1,IMAX)
  120 FORMAT(4E20.13)
   80 CONTINUE
      PI=3.14159265
      RIMAX=IMAX
      RJMAX=JMAX
      DELN=1.0/(RIMAX-1.0)
      DELE=1.0/(RJMAX-1.0)
      SIG=VISI/VISE
      NRCT=0
      NRCTCK=0
      NRCTCC=0
      G=980.665
      FAR=96487.0
      SEL=NEL
      IF(JSKIP.NE.1) GO TO 5
      IF(TREL.LE.1.0E-20) GO TO 5
      X=DINT/ARAD
      CALL AHCOS(ALPHA,X)
      CORD=DINT*TANH(ALPHA)
      GAMA=CORD/ARAD
      RKMAXB=KMAXBR
      TSTP=1.0E-10
      RT=0.0
      T=0.0
      NSTP=2
      KSTP=1
   41 IF(T.LT.1.0E-20) GO TO 42
      TSTP=(SQRT(T/DIFF))*0.00003
   42 CONTINUE
      IF(TSTP.LT.(TREL-T)) GO TO 20
      NSTP=1
      DELT=(((TREL-T)*DIFF)/(ARAD**2.0))/(RKMAXB-1.0)
      GO TO 21
   20 DELT=((TSTP*DIFF)/(ARAD**2.0))/(RKMAXB-1.0)
```

```
 21 CONTINUE
    DO 6 I=1,IMAX
    RI=I-1
    RRN=RI*DELN
    RN=PI*RRN
    DO 7 J=1,JMAX
    RJ=J-1
    RE=RJ*DELE
    E=ALPHA*RE
    RLAM=COSH(E)-COS(RN)
    IF(I.EQ.1.OR.I.EQ.IMAX) GO TO 8
    EC(I,J)=-(RLAM*(COS(RN)*COSH(E)-1.0)*DELT)/(4.0*DELN*PI*(GAMA
   1**2.0)*SIN(RN))
  8 FC(I,J)=(RLAM*SINH(E)*DELT)/(4.0*DELE*ALPHA*(GAMA**2.0))
    GC(I,J)=-((RLAM/(PI*GAMA))**2.0)*DELT/(2.0*(DELN**2.0))
    HC(I,J)=-((RLAM/(ALPHA*GAMA))**2.0)*DELT/(2.0*(DELE**2.0))
  7 CONTINUE
  6 CONTINUE
    DO 23 I=1,IMAX
    DO 24 J=1,JMAX
    IF(KSTP.EQ.1)  GO TO 25
    RC(I,J,1)=RC(I,J,KMAXBR)
    GO TO 24
 25 RC(I,J,1)=1.0
 24 CONTINUE
 23 CONTINUE
    KSTP=2
    DO 10 K=2,KMAXBR
    RT=DELT+RT
    T=RT/DIFF*(ARAD**2.0)
    CALL LDINMA
    NRCT=NRCT+1
    IF(NRCT.EQ.1.OR.NRCT.EQ.NRCTCK) GO TO 51
    IF((1.0001*T).GT.TREL) GO TO 51
    GO TO 55
 51 CONTINUE
    PRINT 107,T,RT
    PRINT 109
    NRCTCK=NRCTCK+100
    DO 52 I=1,IMAX
    RI=I-1
    RRN=RI*DELN
    RN=PI*RRN
    DO 53 J=1,JMAX
    RJ=J-1
    RE=RJ*DELE
    E=ALPHA*RE
    PRINT 108,RRN,RN,RE,E,RC(I,J,K)
 53 CONTINUE
 52 CONTINUE
107 FORMAT(#TIME(SEC) = #,E15.8,5X,#REDUCED TIME = #,E15.8)
109 FORMAT(5X,#REDUCED N      #,5X,#N#,19X,#REDUCED E      #,5X,
   1#E#,19X,#REDUCED CONC.  N VEL.(CM/SEC)E VEL.(CM/SEC)#)
```

```
108 FORMAT(5X,E15.8,5X,E15.8,5X,E15.8,5X,E15.8,5X,E15.8)
 55 CONTINUE
 10 CONTINUE
    IF(NRCT.EQ.1.OR.NRCT.EQ.NRCTCC) GO TO 85
    IF((T*1.0001).GT.TREL) GO TO 85
    GO TO 86
 85 PRINT 105
    NRCTCC=NRCTCC+10
105 FORMAT(5X,#   TIME(SEC)  #,6X,# REDUCED TIME  #,5X,#  N(BIPOLAR)#
   1,8X,#     R(CM)     #,# FLUX(MOLES/SEC/CM**2)  #,#  I(MA/CM**2) #)
    DO 26 I=1,IMAX
    RI=I-1
    RRN=RI*DELN
    RN=PI*RRN
    FLN=((DIFF*(1.0-COS(RN))*CINT)/(ALPHA*CORD))*((2.0*RC(I,4,KMAXBR)
   1-9.0*RC(I,3,KMAXBR)+18.0*RC(I,2,KMAXBR)-11.0*RC(I,1,KMAXBR))/
   2(6.0*DELE))
    CURI=FLN*SEL*FAR*1000.0
    IF(I.EQ.1)  RCORD=0.0
    IF(I.GT.1) RCORD=CORD*SIN(RN)/(1.0-COS(RN))
    PRINT 104,T ,RT ,RN,RCORD,FLN,CURI
104 FORMAT(5X,E15.8,5X,E15.8,5X,E15.8,5X,E15.8,5X,E15.8,5X,E15.8)
 26 CONTINUE
 86 CONTINUE
    IF(NSTP.EQ.2) GO TO 41
    IF(KFST.EQ.1) GO TO 29
    NRCT=0
    NRCTCK=0
    NRCTCC=10
    GO TO 31
  5 CONTINUE
    T=0.0
    IF(JSKIP.NE.1) T=TREL
 31 CONTINUE
    RKMAXA=KMAXAR
    D(1)=DINT
 30 KSTOP=1
    IF(NRCT.LT.10) DELTMX=0.00001
    IF(NRCT.GE.10) DELTMX=1.1*DELTMX
    DELT=(DFIN-D(1))/ARAD/(RKMAXA-1.0)
    IF(DELT.LT.DELTMX) GO TO 27
    KSTOP=2
    DELT=DELTMX
 27 CONTINUE
    CALL VELGEN
    DO 11 I=1,IMAX
    DO 12 J=1,JMAX
    IF(TREL.GT.1.0E-20) GO TO 17
    RC(I,J,1)=1.0
    GO TO 12
 17 RC(I,J,1)=RC(I,J,KMAXBR)
 12 CONTINUE
 11 CONTINUE
```

```
      RC(1,1,1)=1.0
      DO 13 K=2,KMAXAR
      RT=D(K)/ARAD
      CALL AHCOS(ALPHA,RT)
      CALL UDELTA
      CORD=D(K)*TANH(ALPHA)
      GAMA=CORD/ARAD
      REY=-ARAD*U*DENE/VISE
      SCH=VISE/(DENE*DIFF)
      DO 14 I=1,IMAX
      RI=I-1
      RRN=RI*DELN
      RN=PI*RRN
      DO 15 J=1,JMAX
      RJ=J-1
      RE=RJ*DELE
      E=ALPHA*RE
      RLAM=COSH(E)-COS(RN)
      IF(I.EQ.1.OR.I.EQ.IMAX) GO TO 16
      EC(I,J)=((RLAM*(VN(I,J,K)/(-U)))/(PI*GAMA)-(RLAM*(COS(RN)*COSH(E)
     1-1.0))/(REY*SCH*PI*(GAMA**2.0)*SIN(RN)))*DELT/(4.0*DELN)
   16 FC(I,J)=((RLAM*(VE(I,J,K)/(-U)))/(GAMA*ALPHA)+(SINH(E)*RLAM)/
     1(REY*SCH*ALPHA*(GAMA**2.0))-RE/(ALPHA*SQRT((RT**2.0)-1.0)))*DELT
     2/(4.0*DELE)
      GC(I,J)=(-((RLAM/(PI*GAMA))**2.0))*DELT/(2.0*(DELN**2.0))
     1/(REY*SCH)
      HC(I,J)=(-((RLAM/(ALPHA*GAMA))**2.0))*DELT/(2.0*(DELE**2.0))
     1/(REY*SCH)
   15 CONTINUE
   14 CONTINUE
      CALL LDINMA
      NRCT=NRCT+1
      IF(NRCT.EQ.1.OR.NRCT.EQ.NRCTCK) GO TO 56
      IF((D(KMAXAR)*1.0001).GT.DFIN) GO TO 56
      GO TO 57
   56 CONTINUE
      PRINT 107,T,RT
      PRINT 109
      NRCTCK=NRCTCK+100
      DO 58 I=1,IMAX
      RI=I-1
      RRN=RI*DELN
      RN=PI*RRN
      DO 59 J=1,JMAX
      RJ=J-1
      RE=RJ*DELN
      E=ALPHA*RE
      PRINT 110,RRN,RN,RE,E,RC(I,J,K),VN(I,J,K),VE(I,J,K)
   59 CONTINUE
   58 CONTINUE
  110 FORMAT(5X,E15.8,5X,E15.8,5X,E15.8,5X,E15.8,5X,3E15.8)
   57 CONTINUE
   13 CONTINUE
```

```
      IF(TREL.LT.1.0E-20) TREL=1.0
      KMAXBR=KMAXAR
      Y(1)=1.0/U
      RT=DELT/4.0+RT
      CALL AHCOS(ALPHA,RT)
      CALL UDELTA
      Y(2)=1.0/U
      RT=DELT/4.0+RT
      CALL AHCOS(ALPHA,RT)
      CALL UDELTA
      Y(3)=1.0/U
      T=T-(DELT/12.0)*(Y(1)+4.0*Y(2)+Y(3))*ARAD
      D(1)=RT*ARAD
      CORD=RT*ARAD*TANH(ALPHA)
      REY=-ARAD*U*DENE/VISE
      PRINT 106,REY
  106 FORMAT(#     REY =  #,E15.8)
      IF(NRCT.EQ.1.OR.NRCT.EQ.NRCTCC) GO TO 87
      GO TO 88
   87 PRINT 105
      NRCTCC=NRCTCC+10
      DO 28 I=1,IMAX
      RI=I-1
      RRN=RI*DELN
      RN=PI*RRN
      FLN=((DIFF*(1.0-COS(RN))*CINT)/(ALPHA*CORD))*((2.0*RC(I,4,KMAXAR)
     1-9.0*RC(I,3,KMAXAR)+18.0*RC(I,2,KMAXAR)-11.0*RC(I,1,KMAXAR))/
     2(6.0*DELE))
      CURI=FLN*SEL*FAR*1000.0
      IF(I.GT.1) RCORD=CORD*SIN(RN)/(1.0-COS(RN))
      IF(I.EQ.1)  RCORD=0.0
      PRINT 104,T,RT,RN,RCORD,FLN,CURI
   28 CONTINUE
   88 CONTINUE
      IF(KSTOP.EQ.1) GO TO 29
      IF(D(1)*1.00001.GE.DFIN)  GO TO 29
      GO TO 30
   29 CONTINUE
      STOP
      END
      SUBROUTINE AHCOS(Y,X)
      Y=0.0
      IF((X-1.0).LE.1.0E-10) RETURN
      Y=0.4
      DO 1N=1,100
      YG=Y
      DELY=(X-COSH(YG))/(SINH(YG))
      Y=YG+DELY
      IF(Y.LE.0.0) Y=ABS(Y)
      IF(ABS(DELY/Y).LE.1.0E-10) RETURN
    1 CONTINUE
      PRINT 2,DELY,Y,X
    2 FORMAT(#AHCOS DID NOT CONVERGE#,/,# DELY = #,E20.13,/,# Y = #,
```

```
     1E20.13,/,# X = #,E20.13)
      END
      SUBROUTINE LEPO(X,Y,N)
      DIMENSION Y(205)
      Y(1)=1.0
      IF(N.EQ.1) RETURN
      Y(2)=X
      IF(N.EQ.2) RETURN
      DO 1 I=3,N
      RI=I-2
      Y(I)=((2.0*RI+1.0)/(RI+1.0))*X*Y(I-1)-(RI/(RI+1.0))*Y(I-2)
    1 CONTINUE
      RETURN
      END
      SUBROUTINE UDELTA
      COMMON /SET2/ALPHA,DELTA,U,SIG,VISE,DENE,DENI,G,ARAD
      SUM=0.0
      DO 1 M=1,100
      RM=M
      A=SIG*(4.0*(SINH((RM+0.5)*ALPHA))**2.0-((2.0*RM+1.0)*SINH(ALPHA)
     1)**2.0)+(2.0*SINH((2.0*RM+1.0)*ALPHA)-(2.0*RM+1.0)*SINH(2.0*
     2ALPHA))
      B=2.0*SINH((2.0*RM+1.0)*ALPHA)+(2.0*RM+1.0)*SINH(2.0*ALPHA)
     1-4.0*(SINH((RM+0.5)*ALPHA))**2.0+((2.0*RM+1.0)*SINH(ALPHA))**2.0
      C=(2.0*RM+3.0)*EXP(2.0*ALPHA)+4.0*EXP(-(2.0*RM+1.0)*ALPHA)-
     1(2.0*RM-1.0)*EXP(-2.0*ALPHA)
      D=RM*(RM+1.0)/((2.0*RM-1.0)*(2.0*RM+3.0))
      DSUM=D*(SIG*B+0.5*C)/A
      SUM=SUM+DSUM
      IF(ABS(DSUM/SUM).LE.0.000001) GO TO 2
    1 CONTINUE
      PRINT 102
  102 FORMAT(# UDELTA DID NOT CONVERGE #)
      GO TO 1000
    2 DELTA=(4.0/3.0)*(3.0*(1.0+SIG)/(2.0+3.0*SIG))*SINH(ALPHA)*SUM
      U=-(2.0*(ARAD**2.0)*(DENE-DENI)*G)/(3.0*VISE*((2.0+3.0*SIG)/(
     11.0+SIG))*DELTA)
      RETURN
 1000 CONTINUE
      END
      SUBROUTINE VELGEN
      COMMON/SET1/IMAX,JMAX,ISOR,MAXSOR,GC(40,40),EC(40,40),HC(40,40),
     1FC(40,40),RC(40,40,3),K,WSOR/SET2/ALPHA,DELTA,U,SIG,VISE,DENE,DEN
     2I,G,ARAD/SET3/DINT,RT,DELT,D(3),T,CORD,DELN,RRN,RN,DELE,
     3VN(40,40,3),VE(40,40,3),E,RE,PI,KMAXAR,KMAXBR,TREL
      DIMENSION Y(3),RL(3),RG(3),S(3),P(205)
      RT=D(1)/ARAD
      CALL AHCOS(ALPHA,RT)
      CALL UDELTA
      Y(1)=1.0/U
      RT=DELT/4.0+RT
      CALL AHCOS(ALPHA,RT)
      CALL UDELTA
```

```
      Y(2)=1.0/U
      RT=DELT/4.0+RT
      CALL AHCOS(ALPHA,RT)
      CALL UDELTA
      Y(3)=1.0/U
      T=T   -(DELT/12.0)*(Y(1)+4.0*Y(2)+Y(3))*ARAD
      D(2)=RT*ARAD
      DO 1 K=2,KMAXAR
      CORD=D(K)*TANH(ALPHA)
      DO 2 I=1,IMAX
      RI=I-1
      RRN=RI*DELN
      RN=PI*RRN
      SUMIN=0.0
      DO 3 J=1,JMAX
      RJ=J-1
      RE=RJ*DELE
      E=ALPHA*RE
      IF(J.GT.1) GO TO 4
      VN(I,J,K)=0.0
      VE(I,J,K)=0.0
      GO TO 3
    4 CONTINUE
      SUMEN=0.0
      SUMEE=0.0
      RM=1.0
   15 CONTINUE
      MCHECK=0
      RL(1)=(RM*(RM+1.0)/(2.0*RM+1.0))*(SQRT(2.0))*(((EXP(-(RM-0.5)
     1*ALPHA))/(2.0*RM-1.0))-((EXP(-(RM+1.5)*ALPHA))/(2.0*RM+3.0)))
      RL(2)=(RM*(RM+1.0)/(2.0*RM+1.0))*((EXP(-(RM-0.5)*ALPHA))-(EXP(-(
     1RM+1.5)*ALPHA)))/(-SQRT(2.0))
      RL(3)=(1.0/(2.0*SQRT(2.0)))*(RM*(RM+1.0)/(2.0*RM+1.0))*((2.0*RM-
     11.0)*(EXP(-(RM-0.5)*ALPHA))-(2.0*RM+3.0)*(EXP((-RM+1.5)*ALPHA)))
      RG(1)=COSH((RM-0.5)*ALPHA)
      RG(3)=COSH((RM+1.5)*ALPHA)
      S(1)=SINH((RM-0.5)*ALPHA)
      S(3)=SINH((RM+1.5)*ALPHA)
      A=(2.0*RM+3.0)*S(3)-(2.0*RM-1.0)*S(1)
      B=S(3)/(2.0*RM+3.0)-S(1)/(2.0*RM-1.0)
      C=RG(3)-RG(1)
      F=((2.0*RM+3.0)**2.0)*RG(3)-((2.0*RM-1.0)**2.0)*RG(1)
      RDEL=4.0*(2.0*RM+3.0)*(2.0*(2.0*RM+1.0)*SIG*(A*B-C**2.0)+F*B-
     1A*C)
      CM=-2.0*(2.0*RM+3.0)*U*(CORD**2.0)*(2.0*(2.0*RM+1.0)*SIG*(2.0*
     1RL(2)*B-RL(1)*C)+RL(1)*(-A)+4.0*RL(3)*B)/RDEL
      AM=-CM
      DM=2.0*U*(CORD**2.0)*(2.0*(2.0*RM+1.0)*SIG*(2.0*RL(2)*C-RL(1)*
     1A)-RL(1)*F+4.0*RL(3)*C)/RDEL
      BM=-((2.0*RM+3.0)/(2.0*RM-1.0))*DM
      IF(I.EQ.1.OR.I.EQ.IMAX) GO TO 5
      IF(J.LT.JMAX) GO TO 5
      SAM=(-U*(CORD**2.0)*RL(2)-AM*(2.0*RM-1.0)*S(1)-BM*(2.0*RM-1.0)*
```

```
     1RG(1)-CM*(2.0*RM+3.0)*S(3)-DM*(2.0*RM+3.0)*RG(3))/(-4.0*EXP(-(
     2RM-0.5)*ALPHA))
      SBM=-SAM*(EXP(-(RM-0.5)*ALPHA))/(EXP(-(RM+1.5)*ALPHA))
    5 CONTINUE
      WM=AM*(COSH((RM-0.5)*E))+BM*(SINH((RM-0.5)*E))+CM*(COSH((RM+1.5)*
     1E))+DM*SINH((RM+1.5)*E)
      X=COS(RN)
      M=RM+2.1
      CALL LEPO(X,P,M)
      VM=P(M-2)-P(M)
      IF(I.GT.1.AND.I.LT.IMAX) GO TO 6
      DSUMEN=0.0
      GO TO 9
    6 CONTINUE
      DSUMEN=(3.0*SINH(E)*WM*VM)/(2.0*(CORD**2.0)*SIN(RN)*SQRT(COSH(E)-
     1COS(RN)))-((SQRT(COSH(E)-COS(RN)))*(AM*(RM-0.5)*(SINH((RM-0.5)*
     2E))+BM*(RM-0.5)*(COSH((RM-0.5)*E))+CM*(RM+1.5)*(SINH((RM+1.5)*E))
     3+DM*(RM+1.5)*(COSH((RM+1.5)*E)))*VM)/((CORD**2.0)*SIN(RN))
      DSUMEN=-DSUMEN
    9 CONTINUE
      DSUMEE=((-3.0*WM*VM)/(2.0*(CORD**2.0)*(SQRT(COSH(E)-COS(RN)))))
     1+((WM*(SQRT(COSH(E)-COS(RN)))*(RM*P(M-2)+(RM+1.)*P(M)))
     2/(COS(RN)*(CORD**2.0)))
      DSUMEE=-DSUMEE
      IF(I.EQ.1.OR.I.EQ.IMAX) GO TO 13
      IF(J.LT.JMAX) GO TO 13
      DSUMIN=((3.0*SINH(ALPHA)*(SAM*EXP(-(RM-0.5)*ALPHA)+SBM*EXP(-(RM+
     11.5)*ALPHA))*VM)/((SQRT(COSH(ALPHA)-COS(RN)))*2.0*(CORD**2.0)*
     2SIN(RN)))+(((SQRT(COSH(ALPHA)-COS(RN)))*(SAM*(RM-0.5)*EXP(-(RM-0.5
     3)*ALPHA)+SBM*(RM+1.5)*EXP(-(RM+1.5)*ALPHA))*VM)/((CORD**2.0)*
     4SIN(RN)) )
      DSUMIN=-DSUMIN
      SUMIN=SUMIN+DSUMIN
      IF(ABS(DSUMIN/SUMIN).GE.0.00001) MCHECK=1
   13 CONTINUE
      SUMEN=SUMEN+DSUMEN
      SUMEE=SUMEE+DSUMEE
      IF(I.EQ.1.OR.I.EQ.IMAX) GO TO 18
      IF(ABS(DSUMEN/SUMEN).GE.0.00001.OR.ABS(DSUMEE/SUMEE).GE.0.00001)
     1  MCHECK=1
      GO TO 19
   18 IF(ABS(DSUMEE/SUMEE).GE.0.00001) MCHECK=1
   19 CONTINUE
      IF(MCHECK.EQ.0) GO TO 14
      RM=RM+1.0
      IF(RM.LT.200.0) GO TO 15
      PRINT 103
  103 FORMAT(# THE VELOCITY DID NOT CONVERGE #)
      STOP
   14 CONTINUE
      VN(I,J,K)=SUMEN
      VE(I,J,K)=SUMEE
      IF(I.EQ.1.OR.I.EQ.IMAX)   GO TO 16
```

```
      IF(J.LT.JMAX) GO TO 16
      VELCK=ABS(SUMEN-SUMIN-U*(SINH(E)*SIN(RN))/(COSH(E)-COS(RN)))
      VELCK=VELCK/ABS(SUMIN)
      IF(VELCK.LE.0.005) GO TO 16
      PRINT 102,VELCK
  102 FORMAT(# SPHERE SURFACE VELOCITY DID NOT MATCH #,/,# VELCK = #,
     1E15.8)
   16 CONTINUE
    3 CONTINUE
    2 CONTINUE
      IF(K.EQ.KMAXAR)  GO TO 1
      Y(1)=1.0/U
      DO 17 I=2,3
      RT=RT+DELT/2.0
      CALL AHCOS(ALPHA,RT)
      CALL UDELTA
      Y(I)=1.0/U
   17 CONTINUE
      D(K+1)=RT*ARAD
      T=T-(DELT/6.0)*(Y(1)+4.0*Y(2)+Y(3))*ARAD
    1 CONTINUE
      RETURN
 1000 CONTINUE
      END
      SUBROUTINE LDINMA
      COMMON/SET1/IMAX,JMAX,ISOR,MAXSOR,GC(40,40),EC(40,40),HC(40,40),
     1FC(40,40),RC(40,40,3),K,WSOR
      DIMENSION RA(40,40),RB(40,40),RE(40,40),RF(40,40),RG(40,40),
     1R(40,40),RD(40,40)
      IFN=IMAX-1
      JFN=JMAX-1
      DO 1 I=2,IFN
      DO 2 J=2,JFN
      RA(I,J)=GC(I,J)-EC(I,J)
      RB(I,J)=HC(I,J)-FC(I,J)
        RE(I,J)=1.0-2.0*GC(I,J)- 2.0*HC(I,J)
      RF(I,J)=FC(I,J)+HC(I,J)
      RG(I,J)=EC(I,J)+GC(I,J)
      RD(I,J)=(1.0+2.0*GC(I,J)+2.0*HC(I,J))*RC(I,J,K-1)-RG(I,J)*
     1RC(I+1,J,K-1)-RA(I,J)*RC(I-1,J,K-1)-RF(I,J)*RC(I,J+1,K-1)-RB(I,J)
     2*RC(I,J-1,K-1)
    2 CONTINUE
    1 CONTINUE
      DO 3 I=1,IMAX
      DO 4 J=1,JMAX
      RC(I,J,K)=RC(I,J,K-1)
      IF(J.EQ.1) RC(I,J,K)=0.0
    4 CONTINUE
    3 CONTINUE
      RC(1,1,K)=1.0
      DO 5 ISOR=1,MAXSOR
      KCHK=0
      DO 6 I=1,IMAX
```

```
      DO 7 J=1,JMAX
      IF(J.EQ.1) GO TO 8
      IF(I.EQ.1.AND.J.EQ.JMAX)  GO TO 9
      IF(I.EQ.IMAX.AND.J.EQ.JMAX) GO TO 10
      IF(I.EQ.1) GO TO 11
      IF(I.EQ.IMAX) GO TO 12
      IF(J.EQ.JMAX) GO TO 13
      R(I,J)=((RD(I,J)-RA(I,J)*RC(I-1,J,K)-RB(I,J)*RC(I,J-1,K)-RF(I,J)
     1*RC(I,J+1,K)-RG(I,J)*RC(I+1,J,K))/RE(I,J))-RC(I,J,K)
      GO TO 14
    8 R(I,J)=0.0
      GO TO 18
    9 R(I,J)=((1.0+2.0*GC(I,J)+2.0*HC(I,J))*RC(I,J,K-1)-(2.0*GC(I,J))
     1*RC(I+1,J,K-1)-(2.0*HC(I,J))*RC(I,J-1,K-1)-(2.0*HC(I,J))*
     2RC(I,J-1,K)-(2.0*GC(I,J))*RC(I+1,J,K))/(1.0-2.0*GC(I,J)-2.0*
     3HC(I,J))-RC(I,J,K)
      GO TO 14
   10 R(I,J)=((1.0+2.0*GC(I,J)+2.0*HC(I,J))*RC(I,J,K-1)-(2.0*GC(I,J))
     1*RC(I-1,J,K-1)-(2.0*HC(I,J))*RC(I,J-1,K-1)-(2.0*GC(I,J))*RC(I-1,
     2J,K)-(2.0*HC(I,J))*RC(I,J-1,K))/(1.0-2.0*GC(I,J)-2.0*HC(I,J))-
     3RC(I,J,K)
      GO TO 14
   11 R(I,J)=((1.0+2.0*GC(I,J)+2.0*HC(I,J))*RC(I,J,K-1)-(2.0*GC(I,J))*
     1RC(I+1,J,K-1)-(FC(I,J)+HC(I,J))*RC(I,J+1,K-1)+(FC(I,J)-HC(I,J))*
     2RC(I,J-1,K-1)-(HC(I,J)-FC(I,J))*RC(I,J-1,K)-(FC(I,J)+HC(I,J))*
     3RC(I,J+1,K)-(2.0*GC(I,J))*RC(I+1,J,K))/(1.0-2.0*GC(I,J)-2.0*
     4HC(I,J))-RC(I,J,K)
      GO TO 14
   12 R(I,J)=((1.0+2.0*GC(I,J)+2.0*HC(I,J))*RC(I,J,K-1)-(2.0*GC(I,J))*
     1RC(I-1,J,K-1)-(FC(I,J)+HC(I,J))*RC(I,J+1,K-1)+(FC(I,J)-HC(I,J))*
     2RC(I,J-1,K-1)-(2.0*GC(I,J))*RC(I-1,J,K)-(HC(I,J)-FC(I,J))*
     3RC(I,J-1,K)-(FC(I,J)+HC(I,J))*RC(I,J+1,K))/(1.0-2.0*GC(I,J)-2.0*
     4HC(I,J))-RC(I,J,K)
      GO TO 14
   13 R(I,J)=((1.0+2.0*GC(I,J)+2.0*HC(I,J))*RC(I,J,K-1)-(EC(I,J)+
     1GC(I,J))*RC(I+1,J,K-1)+(EC(I,J)-GC(I,J))*RC(I-1,J,K-1)-2.0
     2*HC(I,J)*RC(I,J-1,K-1)-(GC(I,J)-EC(I,J))*RC(I-1,J,K)-(2.0*
     3HC(I,J))*RC(I,J-1,K)-(EC(I,J)+GC(I,J))*RC(I+1,J,K))/(1.0-2.0*
     4GC(I,J)-2.0*HC(I,J))-RC(I,J,K)
   14 IF(ABS(R(I,J)/RC(I,J,K)).GE.0.0001) KCHK=1
   18 CONTINUE
      RC(I,J,K)=RC(I,J,K)+(R(I,J)*WSOR)
      IF(RC(I,J,K).LT.-0.00001) RC(I,J,K)= 0.00001
      IF(RC(I,J,K).GT. 1.00001) RC(I,J,K)= 1.0
    7 CONTINUE
    6 CONTINUE
      IF(KCHK.EQ.1) GO TO 5
      GO TO 15
    5 CONTINUE
      PRINT 100
  100 FORMAT(# LDINMA DID NOT CONVERGE #)
      DO 20 I=1,IMAX
      RI=I
```

```
      DO 21 J=1,JMAX
      RJ=J
      PRINT 120,RI,RJ,RC(I,J,K-1),RC(I,J,K),R(I,J)
      PRINT 121,RA(I,J),RB(I,J),RE(I,J),RF(I,J),RG(I,J),RD(I,J)
  120 FORMAT(5E15.8)
  121 FORMAT(6E15.8)
   21 CONTINUE
   20 CONTINUE
      STOP
   15 CONTINUE
      RETURN
      END
```

Appendix I

Collapse of Bubble Contact Area Programs

The program used to solve the mass transport equation is written in FORTRAN and was executed on a CDC7600 computer. The numerical method used to solve the differential equation is the same that is used in the bubble release program (see Appendix H). The program is listed in listing I.1.

The program used to calculate the results for the infinite Peclet number solution is written in a Hewlett Packard Language (HPL) for a desktop computer and digital plotter previously described (Section 2.3.3). Besides generating a graph of the limiting case solution the program includes a plotting routine for plotting results from the numerical solution. The program is listed in listing I.2.

Program I.1 Listing.

```
      PROGRAM BUBCOL (INPUT,OUTPUT)
      DIMENSION RC(101,51,2),A(101,51),B(101,51),E(101,51),F(101,51),
     1RESID(101,51)
      READ 1,D,ARAD,BASEI,SEL,CBULK
    1 FORMAT(3E20.13,F2.0,E18.11)
      READ 2,THETAO,NSET,VALSET
    2 FORMAT(E20.13,I5,E20.13)
      READ 3,IMAX,JMAX,KMAX
    3 FORMAT(3I5)
      PI=3.141592654
      RHOO=ARAD*SIN(THETAO)
      AREA=PI*(RHOO**2)
      IF(NSET.NE.1) GO TO 10
      U=VALSET
      TMAX=RHOO/U
      GO TO 11
   10 TMAX=VALSET
      U=RHOO/TMAX
   11 FAR=96487.0
      PRINT 8,D,ARAD,BASEI,SEL,CBULK
    8 FORMAT(#DIFFUSION COEFICIENT = #,E20.13,# CM**2/SEC#/
     1#BUBBLE RADIUS = #,E20.13,# CM#/#BASE CURRENT = #,E20.13,
     2# AMPS/CM**2#/#THERE IS #,F2.0,# EQUIV./MOLE#/
     3# BULK CONCENTRATION = #,E20.13,# MOLE/CM**3#)
      PRINT 9,THETAO,RHOO,U,TMAX,AREA
    9 FORMAT(#CONTACT ANGLE = #,E20.13,# RADIANS#/
     1#RADIUS OF BASE = #,E20.13,# CM#/#COLLAPSE VELOCITY = #,
     2E20.13,# CM/SEC #/
     3#RELEASE TIME = #,E20.13,# SECONDS#/# BASE AREA = #,
     4E20.13,# CM**2#)
      RMAX=ARAD
      RIMAX=IMAX-1
      RJMAX=JMAX-1
      RKMAX=KMAX-1
      KPRT=RKMAX/10.0
      IF(KPRT.LE.20) KPRT=0
      DELR=RMAX/RIMAX
      DELTHA=THETAO/RJMAX
      DELT=TMAX/RKMAX
      DEN=D*SEL*FAR
      SLOPEM=BASEI/(ARAD-RHOO)
      DO 15 I=1,IMAX
      RI=I-1
      R=RI*DELR
      DO 14 J=1,JMAX
      RC(I,J,1)=0.0
      RC(I,J,2)=RC(I,J,1)
      IF(I.EQ.1) GO TO 14
      RJ=J-1
      THETA=RJ*DELTHA
      Y=R*SIN(THETA)
      X=R*COS(THETA)
      BASEIO=BASEI
```

```
      IF(X.LE.(ARAD-RHOO)) BASEIO=SLOPEM*X
      DELTA=(2.0*DEN*CBULK)/BASEIO
      IF(DELTA.LT.(X*TAN(THETAO))) GO TO 12
      ALPHA=BASEIO/DEN
      BETA=-BASEIO/(DEN*X*TAN(THETAO))
      GO TO 13
   12 RC(I,J,1)=1.0
      IF(Y.GE.DELTA) GO TO 29
      ALPHA=2.0*CBULK/DELTA
      BETA=-2.0*CBULK/(DELTA**2)
   13 RC(I,J,1)=(ALPHA*Y+((BETA/2.0)*(Y**2)))/CBULK
   29 RC(I,J,2)=RC(I,J,1)
      VR=U*(-THETAO*COS(THETA)+(SIN(THETAO)**2)*(SIN(THETA)+
     1THETA*COS(THETA))+SIN(THETAO)*COS(THETAO)*(COS(THETA)-
     2THETA*SIN(THETA)))/(SIN(THETAO)*COS(THETAO)-THETAO)
      VTHA=-U*(-THETAO*SIN(THETA)+THETA*(SIN(THETAO)**2)*
     1SIN(THETA)+SIN(THETAO)*COS(THETAO)*THETA*COS(THETA))/
     2(SIN(THETAO)*COS(THETAO)-THETAO)
      A(I,J)=(DELT/(4.0*DELR))*(VR-D/R)
      B(I,J)=DELT*VTHA/(4.0*R*DELTHA)
      E(I,J)=-D*DELT/(2.0*(DELR**2))
      F(I,J)=-D*DELT/(2.0*(R*DELTHA)**2)
   14 CONTINUE
   15 CONTINUE
      WSOR=1.5
      L=51
      DO 19 K=2,KMAX
      RK=K-1
      T=RK*DELT
      IF(K.NE.L.AND.K.NE.KMAX) GO TO 33
      PRINT 7,T
    7 FORMAT(# TIME = #,E20.13,# SECONDS #)
      PRINT 4
    4 FORMAT(#    RHO    (CM)      #,#        R (CM)        #,
     1# I (AMPS/CM**2) #)
   33 CONTINUE
      DO 18 M=1,200
      MCK=0
      DO 17 I=1,IMAX
      DO 16 J=1,JMAX
      IF(I.EQ.1) GO TO 28
      IF(J.NE.1) GO TO 20
   28 RC(I,J,2)=0.0
      RESID(I,J)=0.0
      GO TO 23
   20 IF(I.NE.IMAX) GO TO 21
      RC(I,J,2)=RC(I,J,1)
      RESID(I,J)=0.0
      GO TO 23
   21 IF(J.NE.JMAX) GO TO 22
      RESID(I,J)=((-(A(I,J)+E(I,J))*RC(I+1,J,1)-2.0*F(I,J)*RC(I,J-1,1)
     1+(1.0+2.0*F(I,J)+2.0*E(I,J))*RC(I,J,1)+(A(I,J)-E(I,J))*
     2RC(I-1,J,1)-(A(I,J)+E(I,J))*RC(I+1,J,2)-2.0*F(I,J)*
```

```
     3RC(I,J-1,2)+(A(I,J)-E(I,J))*RC(I-1,J,2))/
     4(1.0-2.0*E(I,J)-2.0*F(I,J)))-RC(I,J,2)
      RC(I,J,2)=RC(I,J,2)+WSOR*RESID(I,J)
      GO TO 23
   22 RESID(I,J)=((-(A(I,J)+E(I,J))*(RC(I+1,J,1)+RC(I+1,J,2))-
     1(B(I,J)+F(I,J))*(RC(I,J+1,1)+RC(I,J+1,2))+
     2(1.0+2.0*E(I,J)+2.0*F(I,J))*RC(I,J,1)+
     3(B(I,J)-F(I,J))*(RC(I,J-1,1)+RC(I,J-1,2))+
     4(A(I,J)-E(I,J))*(RC(I-1,J,1)+RC(I-1,J,2)))/
     5(1.0-2.0*E(I,J)-2.0*F(I,J)))-RC(I,J,2)
      RC(I,J,2)=RC(I,J,2)+WSOR*RESID(I,J)
   23 IF(RC(I,J,2).LT.0.0) RC(I,J,2)=0.0
      IF(RC(I,J,2).GT.1.0) RC(I,J,2)=1.0
      IF(ABS(RC(I,J,2)).LT.1.0E-20) GO TO 16
      IF(ABS(RESID(I,J)/RC(I,J,2)).GT.0.0001) MCK=1
   16 CONTINUE
   17 CONTINUE
      IF(MCK.EQ.1) GO TO 18
      DO 24 I=1,IMAX
      IF(K.NE.L.AND.K.NE.KMAX) GO TO 34
      RI=I-1
      R=RI*DELR
      IF(I.EQ.1) GO TO 25
      CURDEN=(DEN/(R*DELTHA))*CBULK*(RC(I,4,2)/3.0-
     13.0*RC(I,3,2)/2.0+3.0*RC(I,2,2)-11.0*RC(I,1,2)/6.0)
      GO TO 26
   25 CURDEN=0.0
   26 RHO=RHOO-U*T+R
      PRINT 5,RHO,R,CURDEN
    5 FORMAT(3E20.13)
   34 CONTINUE
      DO 27 J=1,JMAX
      RC(I,J,1)=RC(I,J,2)
   27 CONTINUE
   24 CONTINUE
      IF(K.EQ.L) L=L+50
      GO TO 19
   18 CONTINUE
      PRINT 6
    6 FORMAT(# THE SYSTEM DID NOT CONVERGE #)
      DO 31 I=1,IMAX
      DO 32 J=1,JMAX
      PRINT 100,I,J,RC(I,J,1),RC(I,J,2),RESID(I,J)
  100 FORMAT (2I5,3E15.8)
   32 CONTINUE
   31 CONTINUE
      GO TO 1000
   19 CONTINUE
 1000 CONTINUE
      STOP
      END
```

```
0: dsp "MASS
 TRANSFER IN A
 WEDGE"
1: wait 3000
2: dim A$[5]
3: flt 5
4: rad
5: enp "BULK
 CONC. (MOLES/
 CM↑3)",C
6: enp "DIFFUSIO
 N COEFFICIENT
 (CM↑2/SEC)",D
7: enp "BUBBLE
 RADIUS (CM)",R
8: enp "CONTACT
 ANGLE (RAD)",A
9: enp "RELEASE
 TIME (SEC)",T
10: enp "EQUIV./
 MOLE",S
11: enp "BASE
 CURRENT (AMPS/
 CM↑2)",I
12: R*sin(A)→B
13: prt "RADIUS
 OF BASE (CM)",B
14: B/T→U
15: prt "VELOCIT
 Y (CM/SEC)",U
16: U*R/D→P
17: prt "PECLET
 NUMBER",P
18: enp "FACTOR
 TO OBTAIN DELTA
  THETA ",E
19: 96487→F
20: ent "IS THE
 AXIS TO BE PLOT
 TED?",A$
21: if cap(A$)#"
 YES";gto 31
22: I+5e-4→Q
23: prnd(Q,-3)→Q
24: prt "IMAX
 (AMPS/CM**2)",Q
25: scl 0,.1,0,Q
26: prt "RMAX =
 0.1 CM"
27: axe 0,0,.005
 ,2e-4
28: axe 0,Q,.005
 ,Q
29: axe .1,0,.1,
 2e-4
30: pen
31: enp "TIME
 OF CURRENT DIST
 . (SEC)",r1
32: if .1>R;gto
 37
33: I/(R-B)*(.1-
 B)→r2
34: plt .1,r2,-2
35: plt B,0
36: gto 40
37: plt .1,I,-2
38: plt R,I
39: plt B,0
40: B-U*r1→r3
41: if r1=0;gto
 76
42: U*r1/500→r4
43: for N=1 to
 499
44: B-N*r4→r5
45: r5-r3→r6
46: (sin(A)-A*
 cos(A))/(sin(A)
 *cos(A)-A)→V
47: V*(r6-U*r1)→
 r7
48: r7*cos(A)→r9
49: r7*sin(A)→r8
50: 2*D*S*F*C/
 (I/(R-B)*r9)→r1
 0
51: if r10<r8;
 gto 57
52: r9*(I/(R-
 B))/(D*S*F)→r11
53: -r11/r8→r12
54: r11*r8+r12/
 2*r8↑2→r13
55: gto 57
56: C→r13
57: r13/C→r13
58: r6/(V↑2*(r6-
 U*r1)*rP*E)+
 A→r16
59: -r6/((A-r16)
 *rP*E*V)→r17
60: r17*cos(r16)
 →r18
61: r17*sin(r16)
 →r19
62: 2*D*S*F*C/
 (I/(R-B)*r18)→r
 20
63: if r20<r18*
 tan(A);gto 68
64: r18*(I/(R-
 B))/(D*S*F)→r21
65: -r21/(r17*
 sin(A))→r22
66: r21*r19+r22/
 2*r19↑2→r23
67: gto 69
68: C→r23
69: r23/C→r23
70: (r23-r13)*R/
 (r6*E)→r24
71: D*S*F*rP*C/
 R*(r13/r(#*(r6/
 R))+r24)→Y
72: r5→X
73: plt X,Y
74: next N
75: pen
76: plt r3,0,-2
77: plt 0,0,-1
78: ent "DO YOU
 HAVE POINTS TO
 PLOT?",A$
79: if cap(A$)#"
 YES";gto 89
80: enp "R VALUE
  (CM)",X
81: enp "I VALUE
  (AMPS/CM↑2)",Y
82: csiz 1,1,1.5
83: plt X,Y
84: cplt -.3,-.3
85: lbl "+"
86: dsp "PRESS
 CONTINUE FOR
 NEXT POINT"
87: stp
88: gto 80
89: end
*16099
```

Program I.2 Listing.

REFERENCES

1. C.L. Mantell, Electrochemical Engineering, McGraw Hill Book, New York (1960).
2. A.T. Kuhn, Industrial Electrochemical Processes, Elsevier Publishing Co., (1971).
3. Chemical and Engineering News, vol. 61, no. 9 (1983), p. 23.
4. C.L. Mantell, Batteries and Energy Systems, McGraw Hill Book, New York (1983).
5. Paul J. Sides, Ph.D. thesis, "Bubble Dynamics at Gas-Evolving Electrodes," Lawrence Berkeley Laboratory report LBL-11899, December 1980.
6. Wing Cheong Hui, M.S. thesis, "Electrolyte Gas Evolution in Forced Flow," Lawrence Berkeley Laboratory report LBL-11945, December 1980.
7. P. Cettou, "The First Generation of Bubbles at Gas Evolving Electrodes," Lawrence Berkeley Laboratory report LBL-13632, December, 1981.
8. F. Foerster, Trans. Am. Electrochem. Soc., 46 (1924), pp. 23-50.
9. N. Ibl, Chem. Ing. Techn., 35 (1963), pp. 353-361.
10. N. Ibl, E. Adam, J. Venczel, and E. Schalch, Chem. Ing. Techn., 43 (1971), pp. 202-215.
11. L.J.J. Janssen and J.G. Hoogland, Electrochimica Acta, vol. 15 (1970), pp. 1013-1023.
12. L.J.J. Janssen and J.G. Hoogland, Electrochimia Acta, vol. 18 (1973) pp. 543-550.

13. I. Rousar, J. Kacin, E. Lippert, F. Smirous, and V. Cezner, Electrochimica Acta, vol. 20 (1975), pp. 295-299.

14. Richard Alkire and Po-Yen Lu, J. Electrochem. Soc., vol. 126 (1979), pp. 2118-2124.

15. M.G. Fouad and G.H. Sedahmed, Electrochimica Acta, vol. 20 (1975), pp. 615-618.

16. J. Venezel, Thesis, Zurich (1961).

17. M.G. Fouad, G.H. Sedahmed, and H.A. El-Abd, Electrochimica Acta, vol. 18, (1973), pp. 279-281.

18. L.J.J. Janssen, Electrochimica Acta, vol. 23 (1978), pp. 81-86.

19. L.J.J. Janssen, and E. Barendrecht, Electrochimica Acta, vol. 24 (1979), pp. 693-699.

20. L.J.J. Janssen and S.J.D. van Stralen, Electrochimica Acta, vol. 26 (1981), pp. 1011-1022.

21. H. Hamzah and A.T. Kuhn, J. Appl. Electrochem., vol. 10 (1980), pp. 635-647.

22. I.V. Kadija and V.M. Nakic, J. Electroanal. Chem. Interf. Electrochem., vol. 34 (1972), pp. 15-19.

23. I.V. Kadija and V.M. Nakic, J. Electroanal. Chem. Interf. Electrochem., vol. 35 (1972), pp. 177-180.

24. I. Rousar and V. Cezner, Electrochimica Acta, vol. 20 (1975), pp. 289-293.

25. K. Stephan and H. Vogt, Electrochimica Acta, vol. 24 (1979), pp. 11-18.

26. N. Ibl, Electrochimica Acta, vol. 24 (1979), pp. 1105-1108.

27. T.R. Beck, J. Electrochem. Soc., vol. 116 (1969), pp. 1038-1041.

28. D.E. Westerheide and J.W. Westwater, A.I.Ch.E. Journal, vol. 7 (1961), pp. 357-362.

29. J.P. Glas and J.W. Westwater, Int. J. Heat Mass Transfer, vol. 7 (1964), pp. 1427-1443.

30. B. Kabanow and A. Frumkin, Zeitschrift fur Physikalische Chemie, vol. 165A (1933), pp. 433-452.

31. R. Darby and M. Haque, Chemical Engineering Science, vol. 28 (1973), pp. 1129-1138.

32. Huk Yuk Cheh, Ph.D. thesis, "On the Mechanism, of Electrolyte Gas Evolution," Lawrence Berkeley Laboratory report UCRL-17324, February 1967.

33. J.R. Selman, Ph.D. thesis, "Measurement and Interpretation of Limiting Currents," Lawrence Berkeley Laboratory report UCRL-20557, June 1971.

34. T. Mizushina, Adv. Heat Transfer, vol. 7 (1971), pp. 87-162.

35. J.R. Selman and C.W. Tobias, Advances in Chemical Engineering, vol. 10 (1978), pp. 211-318.

36. A.J. Bard and L.R. Faulkner, Electrochemical Methods Fundamentals and Applications, John Wiley and Sons, Inc., (1980).

37. R.A. Colclaser, Microelectronics: Processing and Device Design, John Wiley and Sons, Inc., (1980).

38. D.R. Coughanowr and L.B. Koppel, Process Systems Analysis and Control, McGraw-Hill Book Co., (1965), p. 120.

39. R.M. Gould and R.C. Alkire, J. Electrochem. Soc., vol. 126 (1979), pp. 2125-2133.

40. A.A. Wragg, Electrochimica Acta, vol. 13 (1968), pp. 2159-2165.

41. E.J. Fenech, M.S. thesis, "Correlation of Limiting Currents at Horizontal Electrodes under Free Convection Conditions," Lawrence Berkeley Laboratory report UCRL-3586, November 1956.

42. E.J. Fenech, Ph.D. thesis, "Ionic Mass Transport by Free Convection to Horizontal Electrodes," Lawrence Berkeley Laboratory report UCRL-9079, April 1960.

43. J. S. Turner, Buoyancy Effects In Fluids, Cambridge University Press (1973).

44. G. Whitney, Ph. D. Thesis (to be published), University of California, Berkeley.

45. J.S. Newman, Electrochemical Systems, Prentice-Hall, Inc., Englewood Cliffs, N.J., (1973).

46. V. Levich, "The Theory of Concentration Polarization," Acta Physicochimica U.R.S.S. 17 (1942), p. 257-307.

47. J.F. Padday, Surface and Colloid Science, vol. 1 (1969), pp. 39-251.

48. F. Bashforth and J.C. Adams, An Attempt to Test the Theory of Capillary Action, University Press, Cambridge (1883).

49. G. Dahlquist and A. Bjorck, Numerical Methods, Prentice-Hall, Inc., Englewood Cliffs, N.J., (1969).

50. E. Wacholder and D. Weihs, Chemical Engineering Science, vol. 27 (1972), pp. 1817-1828.

51. J. Happel and H. Brenner, Low Reynolds Number Hydrodynamics, Prentice-Hall, Englewood Cliffs, N.J., (1965).

52. F. White, Viscous Fluid Flow, McGraw-Hill Inc. (1974).

53. P. Moon and D. Spencer, Field Theory Handbook, Springer-Verlag (1961).

54. B.A. Finlayson, Nonlinear Analysis in Chemical Engineering, McGraw-Hill Inc. (1980).

55. G.K. Batchelor, An Introduction to Fluid Dynamics, Cambridge University Press (1979).

56. M. Van Dyke, "Perturbation Methods in Fluid Mechanics," The Parabolic Press, Stanford, California (1978).

57. J.M. McDonough and I. Catton, Int. J. Heat Mass Transfer, vol. 25, no. 8 (1982), pp. 1137-1146.

58. J.O. Wilkes and S.W. Churchill, A.I.Ch.E. Journal, vol. 12, no. 1, (1966), pp. 161-166.

59. N. Ibl, Electrochimica Acta, vol. 1, (1959), pp. 117-129.

60. J. Jorne and J.F. Louvar, J. Electrochem. Soc., vol. 127 (1980), pp. 298-303.

61. V.G. Levich, Physicochemical Hydrodynamics, Prentice-Hall, Inc., Englewood Cliffs, N. J. (1962).

This report was done with support from the Department of Energy. Any conclusions or opinions expressed in this report represent solely those of the author(s) and not necessarily those of The Regents of the University of California, the Lawrence Berkeley Laboratory or the Department of Energy.

Reference to a company or product name does not imply approval or recommendation of the product by the University of California or the U.S. Department of Energy to the exclusion of others that may be suitable.

TECHNICAL INFORMATION DEPARTMENT
LAWRENCE BERKELEY LABORATORY
UNIVERSITY OF CALIFORNIA
BERKELEY, CALIFORNIA 94720